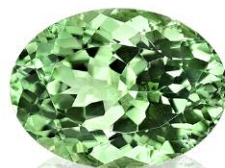


# GEMS & GEMOLOGY

SPRING 2019  
VOLUME LV

THE QUARTERLY JOURNAL OF THE GEMOLOGICAL INSTITUTE OF AMERICA



Method for Identifying Tourmaline Species  
Age Dating of Zircon Inclusions in Sapphire  
Ethiopia Field Report  
2019 Tucson Report



p. 3



p. 33



p. 135

## EDITORIAL

- 1 Studies on Tourmaline, Sapphire, Cultured Pearl, and a Reliquary of Legend...**  
*Duncan Pay*

## FEATURE ARTICLES

- 2 A New Method for Determining Gem Tourmaline Species by LA-ICP-MS**  
*Ziyin Sun, Aaron C. Palke, Christopher M. Breeding, and Barbara L. Dutrow*  
Presents a simplified but comprehensive classification of gem tourmaline species based on quantitative measurement of six common major elements.
- 18 U-Pb Ages of Zircon Inclusions in Sapphires from Ratnapura and Balangoda (Sri Lanka) and Implications for Geographic Origin**  
*Emilie Elmaleh, Susanne Theodora Schmidt, Stefanos Karampelas, Klemens Link, Lore Kiefert, Annette Süssenberger, and André Paul*  
Establishes a metamorphic origin for sapphire samples from these deposits, supported by their trace-element composition and inclusion characterization, including the age dating of zircon inclusions.
- 30 The Talisman of Charlemagne: New Historical and Gemological Discoveries**  
*Gerard Panczer, Geoffroy Riondet, Lauriane Forest, Michael S. Krzemnicki, Davy Carole, and Florian Faure*  
Reveals new details about this historical jewel and the results of its first gemological analysis.

## NOTES & NEW TECHNIQUES

- 47 Provenance Discrimination of Freshwater Pearls by LA-ICP-MS and Linear Discriminant Analysis (LDA)**  
*Artitaya Homkrajae, Ziyin Sun, Troy Blodgett, and Chunhui Zhou*  
Investigates trace-element chemistry of freshwater natural pearls from North America and China with LA-ICP-MS and uses LDA to identify their origins.
- 61 Pleochroism and Color Change in Faceted Alexandrite: Influence of Cut and Sample Orientation**  
*Karl Schmetzer*  
Shows how alexandrite's color and color change are affected by cut and the orientation of table facets.

## FIELD REPORTS

- 72 Land of Origins: A Gemological Expedition to Ethiopia**  
*Wim Verriest, Daniel Girma, Patcharee Wongrawang, Ungkhana Atikarnsakul, and Kevin Schumacher*  
Documents a visit to the sapphire, opal, and emerald mining and trading areas of Ethiopia.

## REGULAR FEATURES

- 29 The Dr. Edward J. Gübelin Most Valuable Article Award**

- 89 2019 G&G Challenge**

- 91 Lab Notes**

Largest diamond discovered in North America • Chatoyant quartz/tourmaline doublet • Faceted gahnospinel • Glass bangles resembling jade • Faceted parasite • Freshwater bead-cultured pearls with multiple features of interest • Color-change Burmese sapphire • CVD layer on natural diamond • Faint green HPHT synthetic diamonds • Paraíba-like synthetic sapphire

- 102 Diamonds from the Deep**

An exploration of diamond ages and what they reveal to scientists.

- 110 G&G Micro-World**

Condor agate from Argentina • "Double bubble" multiphase inclusion in beryl • Native copper inclusions in Indonesian purple chalcidony • Grandidierite inclusions in sapphires • Lazurite in spinel • Fossil insect in opal • Trapiche-like ruby from the Batakundi mine in Kashmir • Sapphire inclusion with rutile "silk" in Burmese star sapphire • Star-like growth in natural yellow sapphire • Quarterly Crystal: Orpiment in barite

- 118 Gem News International**

Tucson 2019 • Boulder opal mining • Brazilian alexandrite • Cat's-eye nephrite from Washington • Color-change pyrope garnet • Colombian emerald and Mozambican ruby • Colored stone trends • Granada Gallery • Gray spinel • Greenland ruby • Hand-carved cameos • Moonstone jewelry • Oregon sunstone • Potentate mine sapphire update • "Rainbow lattice" feldspar • Responsibly sourced gemstones • The Chinese and Japanese gem markets • Unusual and vibrant gems • Jeff Hapeman on cutting • Largest square cushion-cut tsavorite • Cutting in Idar-Oberstein • Designs by Derek Katzenbach, Jeffrey Bilgore, Paula Crevoshay • Responsible and sustainable practices • Buccellati Award • Orange sapphire with gold sheen • Colombian sapphire and trapiche emerald • CIBJO responsible sourcing book • Conference reports • E. Alan Jobbins (1925–2019)

## Editorial Staff

### Editor-in-Chief

Duncan Pay

### Managing Editor

Stuart D. Overlin  
soverlin@gia.edu

### Editor

Jennifer-Lynn Archuleta

### Associate Editor

Brooke Goedert

### Technical Editors

Tao Z. Hsu

tao.hsu@gia.edu

Jennifer Stone-Sundberg

jstone@gia.edu

## Production Staff

### Creative Director

Faizah Bhatti

### Production and Multimedia Specialist

Juan Zanahuria

### Photographer

Robert Weldon

### Editors, Lab Notes

Thomas M. Moses

Shane F. McClure

### Editors, Micro-World

Nathan Renfro

Elise A. Skalwold

John I. Koivula

### Editors, Gem News

Emmanuel Fritsch

Gagan Choudhary

Christopher M. Breeding

### Editorial Assistant

Erin Hogarth

### Contributing Editors

James E. Shigley

Raquel Alonso-Perez

Donna Beaton

### Editor-in-Chief Emeritus

Alice S. Keller

### Customer Service

Martha Erickson

(760) 603-4502

gangd@gia.edu

### Video Production

Larry Lavitt

Pedro Padua

Nancy Powers

Albert Salvato

Betsy Winans

## Editorial Review Board

### Ahmadjan Abduriyim

Tokyo, Japan

### Timothy Adams

San Diego, California

### Edward W. Boehm

Chattanooga, Tennessee

### James E. Butler

Washington, DC

### Alan T. Collins

London, UK

### John L. Emmett

Brush Prairie, Washington

### Emmanuel Fritsch

Nantes, France

### Eloise Gaillou

Paris, France

### Gaston Giuliani

Nancy, France

### Jaroslav Hyršl

Prague, Czech Republic

### Dorrit Jacob

Sydney, Australia

### A.J.A. (Bram) Janse

Perth, Australia

### E. Alan Jobbins

Caterham, UK

### Mary L. Johnson

San Diego, California

### Anthony R. Kampf

Los Angeles, California

### Robert E. Kane

Helena, Montana

### Stefanos Karpelas

Manama, Bahrain

### Lore Kiefert

Lucerne, Switzerland

### Ren Lu

Wuhan, China

### Thomas M. Moses

New York, New York

### Aaron Palke

Carlsbad, California

### Nathan Renfro

Carlsbad, California

### Benjamin Rondeau

Nantes, France

### George R. Rossman

Pasadena, California

### Andy Shen

Wuhan, China

### Guanghai Shi

Beijing, China

### James E. Shigley

Carlsbad, California

### Elisabeth Strack

Hamburg, Germany

### Nicholas Sturman

Bangkok, Thailand

### Fanus Viljoen

Johannesburg, South Africa

### Wuyi Wang

New York, New York

### Christopher M. Welbourn

Reading, UK

### J.C. (Hanco) Zwaan

Leiden, The Netherlands

### Subscriptions

Copies of the current issue may be purchased for \$29.95 plus shipping. Subscriptions are \$79.99 for one year (4 issues) in the U.S. and \$99.99 elsewhere. Canadian subscribers should add GST. Discounts are available for renewals, group subscriptions, GIA alumni, and current GIA students. To purchase print subscriptions, visit [store.gia.edu](http://store.gia.edu) or contact Customer Service. For institutional rates, contact Customer Service.

### Database Coverage

*Gems & Gemology's* impact factor is 1.844, according to the 2017 Thomson Reuters Journal Citation Reports (issued July 2018). *G&G* is abstracted in Thomson Reuters products (Current Contents: Physical, Chemical & Earth Sciences and Science Citation Index—Expanded, including the Web of Knowledge) and other databases. For a complete list of sources abstracting *G&G*, go to [gia.edu/gems-gemology](http://gia.edu/gems-gemology), and click on "Publication Information."

### Manuscript Submissions

*Gems & Gemology*, a peer-reviewed journal, welcomes the submission of articles on all aspects of the field. Please see the Author Guidelines at [gia.edu/gems-gemology](http://gia.edu/gems-gemology) or contact the Managing Editor. Letters on articles published in *G&G* are also welcome. Please note that Field Reports, Lab Notes, Gem News International, Micro-World, and Charts are not peer-reviewed sections but do undergo technical and editorial review.

### Copyright and Reprint Permission

Abstracting is permitted with credit to the source. Libraries are permitted to photocopy beyond the limits of U.S. copyright law for private use of patrons. Instructors are permitted to reproduce isolated articles and photographs/images owned by *G&G* for noncommercial classroom use without fee. Use of photographs/images under copyright by external parties is prohibited without the express permission of the photographer or owner of the image, as listed in the credits. For other copying, reprint, or republication permission, please contact the Managing Editor.

*Gems & Gemology* is published quarterly by the Gemological Institute of America, a nonprofit educational organization for the gem and jewelry industry.

Postmaster: Return undeliverable copies of *Gems & Gemology* to GIA, The Robert Mouawad Campus, 5345 Armada Drive, Carlsbad, CA 92008.

Our Canadian goods and service registration number is 126142892RT.

Any opinions expressed in signed articles are understood to be opinions of the authors and not of the publisher.

## About the Cover

The lead article in this issue presents a system for classifying tourmaline species based on LA-ICP-MS analysis of trace elements. The rings shown on the cover feature a 15.16 ct pink cushion-cut tourmaline (left) and a 10.23 ct oval cuprian elbaite (right). The loose tourmalines (left to right) are a 75.25 ct bicolor emerald cut from Mozambique, an 8.64 ct green oval from Namibia, a 4.61 ct cuprian elbaite oval from Mozambique, a 24.60 ct pink emerald cut from Nigeria, and a 3.20 ct Paraiba tourmaline trillion from Brazil. The rings and loose stones are courtesy of Omi Privé. Photo composite by Kevin Schumacher.

Printing is by L+L Printers, Carlsbad, CA.

GIA World Headquarters The Robert Mouawad Campus 5345 Armada Drive Carlsbad, CA 92008 USA

© 2019 Gemological Institute of America

All rights reserved.

ISSN 0016-626X



# Studies on Tourmaline, Sapphire, Cultured Pearl, and a Reliquary of Legend.....



Spring is always a time of renewal. For our industry, early February marks the Tucson gem shows, the first big event of the season, where buyers are tempted with colored gems of every type and price. Similarly, there is truly something for everyone in our Spring 2019 edition.

We begin with multicolored tourmalines; few gems encompass such a rich variety of colors. In our lead article, GIA's Ziyin Sun, Aaron Palke, and Christopher Breeding join Louisiana State University's Barbara Dutrow to present a simplified classification system for tourmaline species using laser ablation–inductively coupled plasma–mass spectrometry (LA-ICP-MS) analysis of major trace elements. *“A simplified classification system for tourmaline species using LA-ICP-MS...”*

Our second study unites researchers based in Switzerland, Bahrain, and Scotland. Age dating of sulfide inclusions in diamonds using radiogenic decay systems is well known, but for gemologists, applying similar analyses to zircon inclusions in corundum is an emerging practice. Lead author Emilie Elmaleh tells us more about the age and origin of sapphires from two Sri Lankan alluvial deposits.

Next, a team headed by Gerard Panczer of France's Claude Bernard University Lyon 1 contributes the first scientific, gemological analysis of the fascinating Talisman of Charlemagne. This historical, bejeweled container of holy relics—or reliquary—is a rare masterpiece of the goldsmith's art dating back to the ninth century.

The authors of our fourth paper use a combination of LA-ICP-MS and multivariate analysis to compare the trace-element concentrations of two groups of cultured freshwater pearls (one from China, one from the United States) with natural pearls found in the U.S. This study, by Artitaya Homkrajae and her GIA team, provides the prospect of greater confidence identifying pearls of freshwater origin.

In our fifth paper, regular contributor Karl Schmetzer investigates the color appearance of faceted alexandrite, where the quest for the best color change is complicated by this biaxial gem's inherent pleochroism. Through direct observation of synthetic alexandrite samples, he documents the impact of the inevitable multiple internal reflections on placement of a faceted gem's table facet and its perceived color change and pleochroism.

Our final paper is a field report on Ethiopia, a new land of opportunity for colored gems. The 2016 discovery of fine emerald at Shakiso in the southern part of the country, coupled with the 2017 news of sapphires from northern Tigray Province, prompted a 2018 GIA field expedition. Led by field gemologist Wim Vertriest, the group documented mining and processing, measured social impact, and collected samples for GIA's reference collection.

Our regular columns also provide plenty of interest. Our Lab Notes section features the largest diamond ever discovered in North America, Burmese color-change sapphire, and a synthetic diamond containing a CVD layer grown on natural diamond. In *Diamonds from the Deep*, Karen Smit and Steven Shirey examine fundamental questions around the ages of natural diamonds and the lessons we can draw from this information, while *Micro-World* offers a glimpse into the internal world of condor agate from Argentina, grandidierite inclusions in sapphire, and a fossil insect in opal. Our *Gem News International* section has more than 30 pages covering the 2019 Tucson shows, blending market insights with a fascinating display of gems from around the world.

As is customary, this issue contains the annual *G&G* Challenge (pages 89 and 90): We invite you to test your gemological knowledge and skills of recall in the 2019 quiz. Finally, congratulations to our 2018 Dr. Edward J. Gübelin Most Valuable Article Award winners: Please see page 29 for this announcement.

Welcome to the 2019 Spring edition of *Gems & Gemology*!

A handwritten signature in dark ink, appearing to read 'Duncan Pay'.

Duncan Pay | Editor-in-Chief | [dpay@gia.edu](mailto:dpay@gia.edu)

# A NEW METHOD FOR DETERMINING GEM TOURMALINE SPECIES BY LA-ICP-MS

Ziyin Sun, Aaron C. Palke, Christopher M. Breeding, and Barbara L. Dutrow

The gem world is rich with species of tourmaline such as the vivid greens of dravite, uvite, chromium-dravite, and vanadium-dravite; the pinks of elbaite and rossmanite; and the multicolored fluor-liddicoatite. To date, simple gemological tests to separate these various species, and many others of the tourmaline group, are lacking. Laser ablation–inductively coupled plasma–mass spectrometry (LA-ICP-MS) analysis is becoming a prevalent method to measure chemical composition in gemstones because it provides inexpensive, clean, fast, and largely nondestructive analyses. With adequate standards and calibration, this technique can quantitatively measure six common major elements in tourmaline (Na, Ca, Mg, Fe, Al, and Si) as well as trace elements (Cr, V). These data provide the basis for a simplified classification of gem tourmalines.

Analyses of 14 tourmalines by both electron probe microanalysis (EPMA) and LA-ICP-MS for major and minor elements demonstrates that an LA-ICP-MS system with proper calibration, standardization, and normalization is capable of accurate measurements of six major elements in tourmalines, generally within  $\pm 10\%$  error. While some volatile elements such as H, Li, B, and F cannot be measured reliably by this technique, a data reduction scheme can be implemented to calculate those elements based on select assumptions of concentrations of other major elements. Thus, LA-ICP-MS analysis is ideal for some tourmaline species determination in a gemological laboratory setting. The ability to provide a simple tourmaline species classification will enhance GIA identification reports and provide additional tools for identification.

**T**ourmaline has been a much sought-after gemstone since the late 1800s. The Chinese Dowager Empress Tz'u Hsi was especially fond of pink tourmaline, which led to a dramatic increase in mining of the San Diego County pegmatites in the late nineteenth and early twentieth centuries (Fisher, 2002). Tiffany & Co. gemologist George F. Kunz popularized the stone when he wrote about the tourmaline deposits of Southern California (Kunz, 1905; Fisher, 2002). Many sources have produced gem-quality tourmaline for the jewelry market, including the states of Maine (Simmons et al., 2005) and California (Fisher, 2011) in the U.S. as well as Brazil (Proctor, 1985a,b; Koivula and Kammerling, 1989), Madagascar (Dirlam et al., 2002), Afghanistan (Bowersox,

1985), Mozambique (Abduriyim and Kitawaki, 2005; Laurs et al., 2008), and Nigeria (Smith et al., 2001; Garba, 2003; Laurs, 2015; Olatunji and Jimoh, 2017).

Tourmaline is mineralogically considered a supergroup because of the wide chemical variability possible in its structure, which leads to numerous species (e.g., Henry et al., 2011; Dutrow and Henry, 2011; Hawthorne and Dirlam, 2011). Tourmaline has an idealized chemical formula of  $XY_3Z_6(T_6O_{18})(BO_3)_3V_3W$ . The most common constituents are:  $^{[9]}X = Na^{1+}, Ca^{2+}, K^{1+}, \square$  (vacancy);  $^{[6]}Y = Fe^{2+}, Mg^{2+}, Al^{3+}, Li^{1+}$ ;  $^{[6]}Z = Al^{3+}, Fe^{3+}, Mg^{2+}$ ;  $^{[4]}T = Si^{4+}, Al^{3+}$ ;  $^{[3]}B = B^{3+}$ ;  $V = OH^{1-}$  and  $O^{2-}$ ; and  $W = OH^{1-}, F^{1-}$ , and  $O^{2-}$  (Hawthorne and Henry, 1999; Henry et al., 2011). To date, 33 species have been described (table 1). Elbaite, the most common gem tourmaline species, also has the largest color range (red, pink, green, blue, orange, yellow, colorless, and bicolored; figures 1 and 2). Liddicoatite (figure 3) is another important species of gem-quality tourmaline (although the type specimen is fluor-liddicoatite).

See end of article for About the Authors and Acknowledgments.

GEMS & GEMOLOGY, Vol. 55, No. 1, pp. 2–17,  
<http://dx.doi.org/10.5741/GEMS.55.1.2>

© 2019 Gemological Institute of America



Figure 1. Bicolored elbaite tourmalines (5–8 ct) from the Himalaya mine in Southern California are set with yellow diamonds, tsavorites, and red-purple elbaite. These custom-made earrings, ring, and pendant are a gift to the GIA Museum in memory of Nicholas Scott Golden. Photo by Orasa Weldon.

Gem uvite is also known, commonly in shades of green, yellow, and brown (figure 4), as is an attractive orange gem dravite (figure 5).

In the gem and jewelry trade, tourmaline species are commonly determined visually based on their color rather than on accurate chemical analyses.



Figure 2. Elbaite tourmalines, species determined by LA-ICP-MS. Top row, left to right: 41.90 ct blue elbaite, 31.21 ct brownish orange elbaite, and 12.95 ct green elbaite. Middle row, left to right: 2.12 ct light blue cuprian elbaite, 8.15 ct red elbaite, 9.69 ct colorless elbaite, and 5.50 ct yellow elbaite. Bottom row: a 3.28 ct deep blue cuprian elbaite. Photo by Orasa Weldon, stones courtesy of the GIA Museum.

**TABLE 1.** IMA-CMNMC-approved tourmaline species (as of December 2017) from Henry and Dutrow (2018).

General formula	(X)	(Y) <sub>3</sub>	(Z) <sub>6</sub>	T <sub>6</sub> O <sub>18</sub>	(BO <sub>3</sub> ) <sub>3</sub>	(V) <sub>3</sub>	(W)
<b>Alkali group (23 species)</b>							
Subgroup 1	*R <sup>1+</sup>	R <sup>2+</sup> <sub>3</sub>	R <sup>3+</sup> <sub>6</sub>	R <sup>4+</sup> <sub>6</sub> O <sub>18</sub>	(BO <sub>3</sub> ) <sub>3</sub>	**S <sup>1-</sup> <sub>3</sub>	S <sup>1-</sup>
Dravite	Na	Mg <sub>3</sub>	Al <sub>6</sub>	Si <sub>6</sub> O <sub>18</sub>	(BO <sub>3</sub> ) <sub>3</sub>	(OH) <sub>3</sub>	(OH)
Fluor-dravite	Na	Mg <sub>3</sub>	Al <sub>6</sub>	Si <sub>6</sub> O <sub>18</sub>	(BO <sub>3</sub> ) <sub>3</sub>	(OH) <sub>3</sub>	(F)
Schorl	Na	Fe <sub>3</sub>	Al <sub>6</sub>	Si <sub>6</sub> O <sub>18</sub>	(BO <sub>3</sub> ) <sub>3</sub>	(OH) <sub>3</sub>	(OH)
Fluor-schorl	Na	Fe <sub>3</sub>	Al <sub>6</sub>	Si <sub>6</sub> O <sub>18</sub>	(BO <sub>3</sub> ) <sub>3</sub>	(OH) <sub>3</sub>	(F)
Tsilaisite	Na	Mn <sub>3</sub>	Al <sub>6</sub>	Si <sub>6</sub> O <sub>18</sub>	(BO <sub>3</sub> ) <sub>3</sub>	(OH) <sub>3</sub>	(OH)
Fluor-tsilaisite	Na	Mn <sub>3</sub>	Al <sub>6</sub>	Si <sub>6</sub> O <sub>18</sub>	(BO <sub>3</sub> ) <sub>3</sub>	(OH) <sub>3</sub>	(F)
Chromium-dravite	Na	Mg <sub>3</sub>	Cr <sub>6</sub>	Si <sub>6</sub> O <sub>18</sub>	(BO <sub>3</sub> ) <sub>3</sub>	(OH) <sub>3</sub>	(OH)
Subgroup 2	R <sup>1+</sup>	R <sup>1+</sup> <sub>1.5</sub> R <sup>3+</sup> <sub>1.5</sub>	R <sup>3+</sup> <sub>6</sub>	R <sup>4+</sup> <sub>6</sub> O <sub>18</sub>	(BO <sub>3</sub> ) <sub>3</sub>	S <sup>1-</sup> <sub>3</sub>	S <sup>1-</sup>
Elbaite	Na	Li <sub>1.5</sub> Al <sub>1.5</sub>	Al <sub>6</sub>	Si <sub>6</sub> O <sub>18</sub>	(BO <sub>3</sub> ) <sub>3</sub>	(OH) <sub>3</sub>	(OH)
Fluor-elbaite	Na	Li <sub>1.5</sub> Al <sub>1.5</sub>	Al <sub>6</sub>	Si <sub>6</sub> O <sub>18</sub>	(BO <sub>3</sub> ) <sub>3</sub>	(OH) <sub>3</sub>	(F)
Subgroup 3 (Y-Z order/disorder)	R <sup>1+</sup>	R <sup>3+</sup> <sub>3</sub> to R <sup>2+</sup> <sub>2</sub> R <sup>3+</sup> <sub>1</sub>	R <sup>3+</sup> <sub>4</sub> R <sup>2+</sup> <sub>2</sub> to R <sup>3+</sup> <sub>6</sub>	R <sup>4+</sup> <sub>6</sub> O <sub>18</sub>	(BO <sub>3</sub> ) <sub>3</sub>	S <sup>1-</sup> <sub>3</sub>	S <sup>2-</sup>
Oxy-dravite	Na	Al <sub>2</sub> Mg	Al <sub>5</sub> Mg	Si <sub>6</sub> O <sub>18</sub>	(BO <sub>3</sub> ) <sub>3</sub>	(OH) <sub>3</sub>	(O)
Oxy-schorl	Na	Fe <sup>2+</sup> <sub>2</sub> Al	Al <sub>6</sub>	Si <sub>6</sub> O <sub>18</sub>	(BO <sub>3</sub> ) <sub>3</sub>	(OH) <sub>3</sub>	(O)
Povondraite	Na	Fe <sup>3+</sup> <sub>3</sub>	Fe <sup>3+</sup> <sub>4</sub> Mg <sub>2</sub>	Si <sub>6</sub> O <sub>18</sub>	(BO <sub>3</sub> ) <sub>3</sub>	(OH) <sub>3</sub>	(O)
Bosiite	Na	Fe <sup>3+</sup> <sub>3</sub>	Al <sub>4</sub> Mg <sub>2</sub>	Si <sub>6</sub> O <sub>18</sub>	(BO <sub>3</sub> ) <sub>3</sub>	(OH) <sub>3</sub>	(O)
Chromo-alumino-povondraite	Na	Cr <sub>3</sub>	Al <sub>4</sub> Mg <sub>2</sub>	Si <sub>6</sub> O <sub>18</sub>	(BO <sub>3</sub> ) <sub>3</sub>	(OH) <sub>3</sub>	(O)
Oxy-chromium dravite	Na	Cr <sub>3</sub>	Cr <sub>4</sub> Mg <sub>2</sub>	Si <sub>6</sub> O <sub>18</sub>	(BO <sub>3</sub> ) <sub>3</sub>	(OH) <sub>3</sub>	(O)
Oxy-vanadium dravite	Na	V <sub>3</sub>	V <sub>4</sub> Mg <sub>2</sub>	Si <sub>6</sub> O <sub>18</sub>	(BO <sub>3</sub> ) <sub>3</sub>	(OH) <sub>3</sub>	(O)
Vanadio-oxy-chromium-dravite	Na	V <sub>3</sub>	Cr <sub>4</sub> Mg <sub>2</sub>	Si <sub>6</sub> O <sub>18</sub>	(BO <sub>3</sub> ) <sub>3</sub>	(OH) <sub>3</sub>	(O)
Vanadio-oxy-dravite	Na	V <sub>3</sub>	Al <sub>4</sub> Mg <sub>2</sub>	Si <sub>6</sub> O <sub>18</sub>	(BO <sub>3</sub> ) <sub>3</sub>	(OH) <sub>3</sub>	(O)
Maruyamaite	K	MgAl <sub>2</sub>	Al <sub>5</sub> Mg	Si <sub>6</sub> O <sub>18</sub>	(BO <sub>3</sub> ) <sub>3</sub>	(OH) <sub>3</sub>	(O)
Oxy-vanadium-dravite	Na	V <sub>3</sub>	V <sub>4</sub> Mg <sub>2</sub>	Si <sub>6</sub> O <sub>18</sub>	(BO <sub>3</sub> ) <sub>3</sub>	(OH) <sub>3</sub>	(O)
Subgroup 4	R <sup>1+</sup>	R <sup>1+</sup> R <sup>3+</sup> <sub>2</sub>	R <sup>3+</sup> <sub>6</sub>	R <sup>4+</sup> <sub>6</sub> O <sub>18</sub>	(BO <sub>3</sub> ) <sub>3</sub>	S <sup>1-</sup> <sub>3</sub>	S <sup>2-</sup>
Darrellhenryite	Na	LiAl <sub>2</sub>	Al <sub>6</sub>	Si <sub>6</sub> O <sub>18</sub>	(BO <sub>3</sub> ) <sub>3</sub>	(OH) <sub>3</sub>	(O)
Subgroup 5	R <sup>1+</sup>	R <sup>3+</sup> <sub>3</sub>	R <sup>3+</sup> <sub>6</sub>	R <sup>4+</sup> <sub>6</sub> O <sub>18</sub>	(BO <sub>3</sub> ) <sub>3</sub>	S <sup>2-</sup> <sub>3</sub>	S <sup>1-</sup>
Olenite	Na	Al <sub>3</sub>	Al <sub>6</sub>	Si <sub>6</sub> O <sub>18</sub>	(BO <sub>3</sub> ) <sub>3</sub>	(O) <sub>3</sub>	(OH)
Fluor-buergerite	Na	Fe <sup>3+</sup> <sub>3</sub>	Al <sub>6</sub>	Si <sub>6</sub> O <sub>18</sub>	(BO <sub>3</sub> ) <sub>3</sub>	(O) <sub>3</sub>	(F)
<b>Calcic group (6 species)</b>							
Subgroup 1	R <sup>2+</sup>	R <sup>2+</sup> <sub>3</sub>	R <sup>3+</sup> <sub>5</sub> R <sup>2+</sup> <sub>1</sub>	R <sup>4+</sup> <sub>6</sub> O <sub>18</sub>	(BO <sub>3</sub> ) <sub>3</sub>	S <sup>1-</sup> <sub>3</sub>	S <sup>1-</sup>
Uvite	Ca	Mg <sub>3</sub>	Al <sub>5</sub> Mg	Si <sub>6</sub> O <sub>18</sub>	(BO <sub>3</sub> ) <sub>3</sub>	(OH) <sub>3</sub>	(OH)
Fluor-uvite	Ca	Mg <sub>3</sub>	Al <sub>5</sub> Mg	Si <sub>6</sub> O <sub>18</sub>	(BO <sub>3</sub> ) <sub>3</sub>	(OH) <sub>3</sub>	(F)
Feruvite	Ca	Fe <sup>2+</sup> <sub>3</sub>	Al <sub>5</sub> Mg	Si <sub>6</sub> O <sub>18</sub>	(BO <sub>3</sub> ) <sub>3</sub>	(OH) <sub>3</sub>	(OH)
Subgroup 2	R <sup>2+</sup>	R <sup>1+</sup> <sub>2</sub> R <sup>3+</sup> <sub>1</sub>	R <sup>3+</sup> <sub>6</sub>	R <sup>4+</sup> <sub>6</sub> O <sub>18</sub>	(BO <sub>3</sub> ) <sub>3</sub>	S <sup>1-</sup> <sub>3</sub>	S <sup>1-</sup>
Fluor-liddicoatite	Ca	Li <sub>2</sub> Al	Al <sub>6</sub>	Si <sub>6</sub> O <sub>18</sub>	(BO <sub>3</sub> ) <sub>3</sub>	(OH) <sub>3</sub>	(F)
Subgroup 3	R <sup>2+</sup>	R <sup>2+</sup> <sub>3</sub>	R <sup>3+</sup> <sub>6</sub>	R <sup>4+</sup> <sub>6</sub> O <sub>18</sub>	(BO <sub>3</sub> ) <sub>3</sub>	S <sup>1-</sup> <sub>3</sub>	S <sup>2-</sup>
Lucchesiite	Ca	Fe <sup>2+</sup> <sub>3</sub>	Al <sub>6</sub>	Si <sub>6</sub> O <sub>18</sub>	(BO <sub>3</sub> ) <sub>3</sub>	(OH) <sub>3</sub>	(O)
Subgroup 4	R <sup>2+</sup>	R <sup>2+</sup> <sub>3</sub>	R <sup>3+</sup> <sub>6</sub>	R <sup>4+</sup> <sub>5</sub> R <sup>3+</sup> <sub>1</sub> O <sub>18</sub>	(BO <sub>3</sub> ) <sub>3</sub>	S <sup>1-</sup> <sub>3</sub>	S <sup>1-</sup>
Adachiite	Ca	Fe <sup>2+</sup> <sub>3</sub>	Al <sub>6</sub>	Si <sub>5</sub> AlO <sub>18</sub>	(BO <sub>3</sub> ) <sub>3</sub>	(OH) <sub>3</sub>	(OH)
<b>X-site vacant group (4 species)</b>							
Subgroup 1	□***	R <sup>2+</sup> R <sup>3+</sup> <sub>3</sub>	R <sup>3+</sup> <sub>6</sub>	R <sup>4+</sup> <sub>6</sub> O <sub>18</sub>	(BO <sub>3</sub> ) <sub>3</sub>	S <sup>1-</sup> <sub>3</sub>	S <sup>1-</sup>
Magnesio-foitite	□	Mg <sub>2</sub> Al	Al <sub>6</sub>	Si <sub>6</sub> O <sub>18</sub>	(BO <sub>3</sub> ) <sub>3</sub>	(OH) <sub>3</sub>	(OH)
Foitite	□	Fe <sup>2+</sup> <sub>2</sub> Al	Al <sub>6</sub>	Si <sub>6</sub> O <sub>18</sub>	(BO <sub>3</sub> ) <sub>3</sub>	(OH) <sub>3</sub>	(OH)
Subgroup 2	□	R <sup>1+</sup> R <sup>3+</sup> <sub>2</sub>	R <sup>3+</sup> <sub>6</sub>	R <sup>4+</sup> <sub>6</sub> O <sub>18</sub>	(BO <sub>3</sub> ) <sub>3</sub>	S <sup>1-</sup> <sub>3</sub>	S <sup>1-</sup>
Rossmannite	□	LiAl <sub>2</sub>	Al <sub>6</sub>	Si <sub>6</sub> O <sub>18</sub>	(BO <sub>3</sub> ) <sub>3</sub>	(OH) <sub>3</sub>	(OH)
Subgroup 3	□	R <sup>1+</sup> R <sup>3+</sup> <sub>2</sub>	R <sup>3+</sup> <sub>6</sub>	R <sup>4+</sup> <sub>6</sub> O <sub>18</sub>	(BO <sub>3</sub> ) <sub>3</sub>	S <sup>1-</sup> <sub>3</sub>	S <sup>2-</sup>
Oxy-foitite	□	Fe <sup>2+</sup> <sub>2</sub> Al	Al <sub>6</sub>	Si <sub>6</sub> O <sub>18</sub>	(BO <sub>3</sub> ) <sub>3</sub>	(OH) <sub>3</sub>	(O)

\*R is a generic designation of a cation of the indicated charge.

\*\*S is a generic designation of an anion of the indicated charge.

\*\*\*X-site vacancy □



Figure 3. Liddicoatite tourmaline, species determined by LA-ICP-MS. Top, left to right: 7.54 ct purple-red liddicoatite, 3.57 ct purple-red liddicoatite, and 4.60 ct purple-red liddicoatite, all courtesy of the GIA Museum. Bottom row, left and right: 3.80 and 4.14 ct pear-shaped greenish blue cuprian liddicoatite, courtesy of Hubert Gesser at Hubert Inc. Bottom row, center: 3.16 ct bluish green cuprian liddicoatite, courtesy of John R. Evans. Photo by Orasa Weldon.

However, tourmaline color is not species-specific (Dutrow, 2018). For example, a green tourmaline can be a dravite, uvite, chromium-dravite, vanadium-dravite, a vanadio-oxy-chromium dravite, or another

Figure 4. Uvite tourmaline, classified by LA-ICP-MS. Top row, left to right: 10.36 ct green uvite, 8.32 ct brownish orange uvite, and 13.31 ct green uvite. Bottom row, left to right: 4.87 ct green uvite, 5.63 ct green uvite, and 3.78 ct green uvite. Photo by Orasa Weldon, stones courtesy of the GIA Museum.

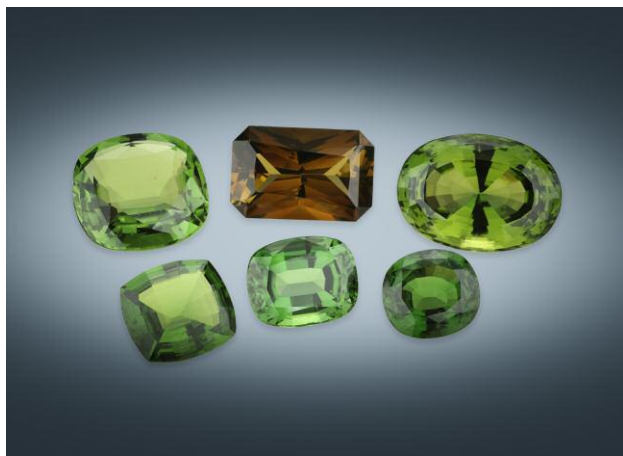


Figure 5. Dravite tourmaline, classified by LA-ICP-MS. Left to right: 0.33 ct orange dravite, 0.51 ct orange dravite, 0.69 ct orange dravite, and 0.68 ct orange dravite. Photo by Orasa Weldon, stones courtesy of the GIA Museum.

species. Much of the brown and yellow tourmaline on the market is sold as dravite or uvite but could be elbaite. Many color-zoned tourmalines are labeled as elbaite or liddicoatite but may contain several different species. In many cases, it would be impossible for a person, even an experienced tourmaline dealer, to accurately distinguish different species with similar color hue and saturation, such as the red elbaite and red rossmanite in figure 6, the green elbaite and

Figure 6. Left to right: 4.80 ct red elbaite, 8.15 ct red elbaite, and 2.76 ct red rossmanite, all classified by LA-ICP-MS. Photo by Orasa Weldon, stones courtesy of the GIA Museum.







Figure 7. A 4.83 ct green elbaite (left) and a 5.63 ct green uvite (right), species determined by LA-ICP-MS. Photo by Orasa Weldon, stones courtesy of the GIA Museum.

green uvite in figure 7, and the cuprian (Cu-bearing) liddicoatite and cuprian elbaite in figure 8. Cuprian elbaite was discovered in the 1980s, whereas cuprian liddicoatite was only recently reported (Katsurada and Sun, 2017). While elbaite is the most common gem-quality tourmaline, non-elbaite tourmalines can have added value due to their rarity and novelty. And, as noted in the section below, stones similar to tourmaline may be intermixed. These market factors point to a demand for gemological laboratories to

Figure 8. Cuprian liddicoatite and cuprian elbaite, species determined by LA-ICP-MS. Top row, left and right: 3.80 ct and 4.14 ct greenish blue cuprian liddicoatite, courtesy of Hubert Gesser at Hubert Inc. Top row, center: 3.16 ct bluish green cuprian liddicoatite, courtesy of John R. Evans. Bottom row from left to right: 2.59 ct and 2.12 ct greenish blue cuprian elbaite, courtesy of the GIA Museum. Photo by Orasa Weldon.



provide reliable tourmaline-species identification services.

The classification of tourmaline species was problematic until Hawthorne and Henry (1999) provided a systematic classification scheme. They modified the “50% rule” for ternary solid solutions and eased the determination of species by developing simple graphical representations. This classification scheme was further updated and refined by Henry et al. (2011), whose revised guidelines divided the supergroup into primary and secondary groups. However, the proper use of this classification scheme demands a precise and accurate chemical analysis.

A variety of analytical methods have been applied to measure tourmaline chemistry (e.g., Henry and Dutrow, 1990, 2001; Abduriyim et al., 2006; Tiepolo et al., 2006; Breeding and Shen, 2008; Okrusch et al., 2016; McMillan et al., 2017; Marger et al., 2017; Shinjo et al., 2017). In fact, a preliminary method to use LA-ICP-MS data to analyze gem tourmaline was

## In Brief

- Gem tourmaline species cannot be determined visually in the gem and jewelry trade based on their color and appearance.
- With adequate standards and calibration, LA-ICP-MS can quantitatively measure six common major elements in tourmaline (Na, Ca, Mg, Fe, Al, and Si), allowing for species classification.
- LA-ICP-MS provides inexpensive, clean, fast, and largely nondestructive analyses for tourmaline species classification. Even large, complex jewelry pieces can be easily analyzed with good precision and accuracy.

proposed by Breeding and Shen (2008). However, electron probe microanalysis (EPMA) is the most widely accepted method to determine tourmaline species because it is capable of accurately and precisely measuring major and minor element chemistry even though it cannot determine directly transition metal valence or H, Li, or B values. Unfortunately, EPMA is expensive and time consuming. Most gemological laboratories do not possess the instruments and cannot justify the cost of outsourcing this analysis. Therefore, EPMA is not a practical everyday tool for a gemological laboratory. LA-ICP-MS, on the other hand, is a common analytical tool in many gemological labs due to the ease of analysis and the minimal sample preparation required.

Here we present a comprehensive method for using LA-ICP-MS analyses to accurately determine most tourmaline species. With this method we produce LA-ICP-MS data for major and minor element concentrations in tourmaline that closely match the values determined by EPMA. Consequently, it is possible for a gemological laboratory equipped with an LA-ICP-MS system to provide accurate species determinations using a simplified classification that does not distinguish between fluor-, oxy-, or hydroxy-tourmaline species. Gemological laboratories such as GIA's can now offer species identification for gem-quality tourmaline.

## MATERIALS AND METHODS

**Samples.** To develop a method for species identification by LA-ICP-MS, samples from a variety of chemical compositions were selected. Eight tourmaline samples—GIA-T1, T2, T3, T4, T5, T6, T7, and T8 (table 2, figure 9)—were obtained from the GIA Museum for this study. The samples were mounted in epoxy and polished (figure 9). Additionally, six samples of various compositions were obtained for analysis by both EPMA and LA-ICP-MS (table 2, BD-S1 to BD-S6; figure 10). These samples were billets, analyzed by LA-ICP-MS, from which the thin sections were made for the corresponding EPMA analyses.

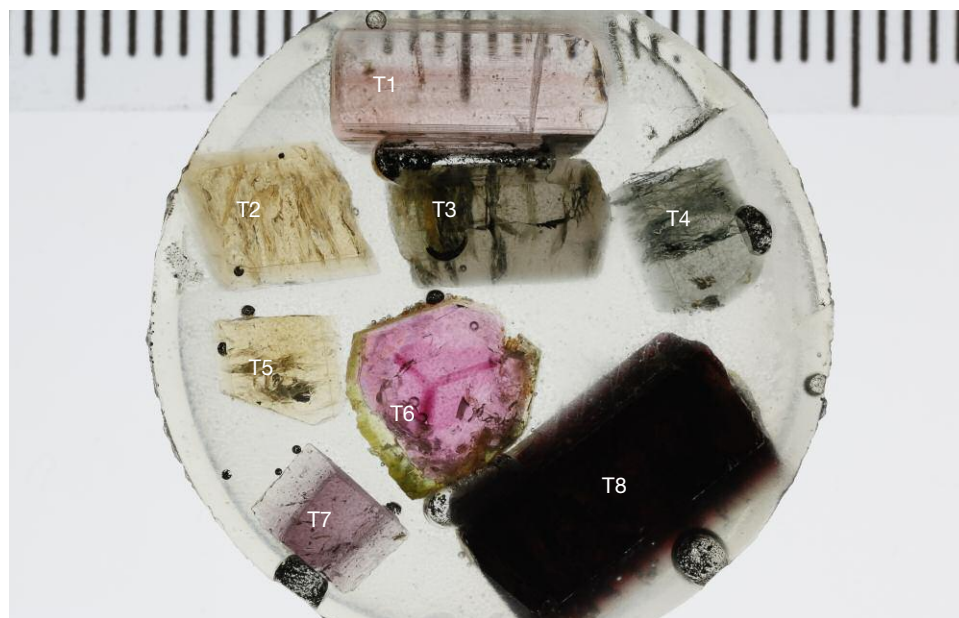
**LA-ICP-MS.** For this study we used a Thermo Fisher iCAP Qc ICP-MS, coupled with a New Wave Research

**TABLE 2.** Samples used for tourmaline species determination.

Sample no.	Description
GIA <sup>a</sup> -T1	Light pink elbaite; unknown geographic origin
GIA-T2	Orange dravite; unknown geographic origin
GIA-T3	Brown dravite; unknown geographic origin
GIA-T4	Gray dravite; unknown geographic origin
GIA-T5	Orange dravite; unknown geographic origin
GIA-T6	Watermelon elbaite; unknown geographic origin
GIA-T7	Pink elbaite; unknown geographic origin
GIA-T8	Black liddicoatite; unknown geographic origin
BD <sup>b</sup> -S1	Black oxy-schorl in granitic rock; Czech Republic
BD-S2	Dark bluish dravite coexisting with phlogopite and corundum; Badakhshan, Afghanistan
BD-S3	Pink elbaite with gray fibers; Cruzeiro mine, Brazil (see Dutrow and Henry, 2000)
BD-S4	Black schorl in quartz symplectite; Larsemann Hills, Antarctica (donated by Ed Grew)
BD-S5	Cluster of small reddish brown uvite crystals; Brumado, Brazil
BD-S6	Cluster of small light green uvite crystals; Brumado, Brazil

<sup>a</sup>GIA samples obtained from the GIA Museum, Carlsbad  
<sup>b</sup>BD samples obtained from Barbara Dutrow

UP-213 laser ablation unit with a frequency-quintupled Nd:YAG laser (213 nm wavelength) running at 4 ns pulse width. Ablation was achieved using a 55  $\mu\text{m}$  diameter laser spot size, a fluence (energy density) of approximately 10–12  $\text{J}/\text{cm}^2$ , and a 15 Hz repetition rate. Argon was used as nebulizer gas (0.73 L/min),



*Figure 9. Eight tourmaline samples, GIA-T1 to GIA-T8, used for this study (see table 2). The scale bar is in 1 mm increments. Photo by Aaron Palke.*

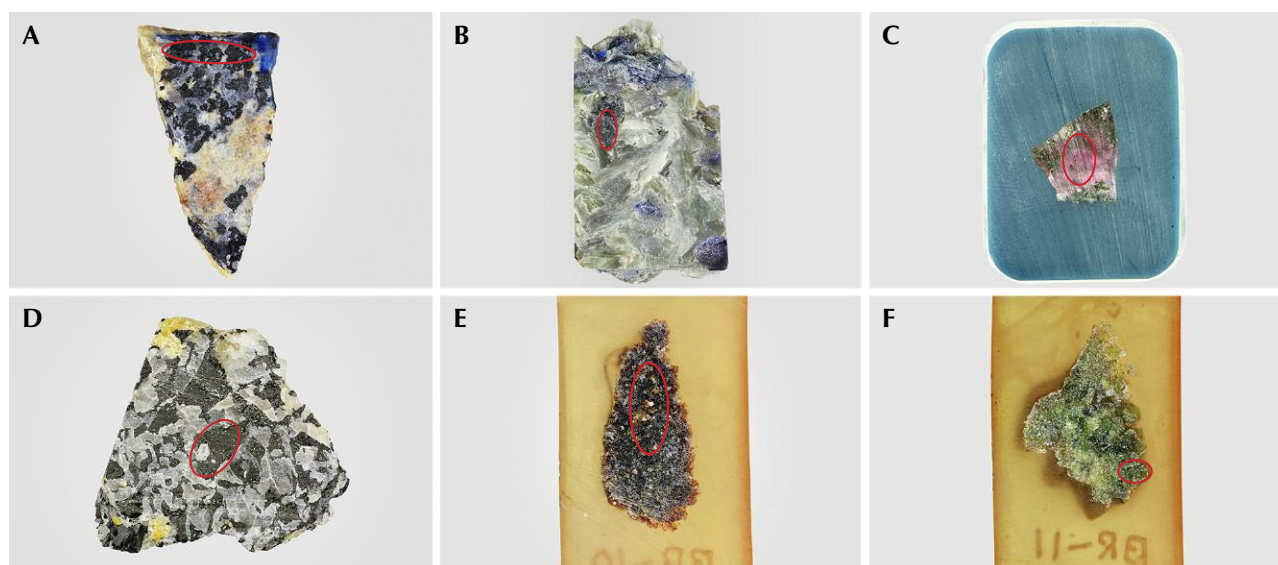


Figure 10. Optical scans of sample chips used for both LA-ICP-MS and EPMA. A: Oxy-schorl (BD-S1) from the Czech Republic. B: Blue dravite (BD-S2) from Badakhshan, Afghanistan. C: Pink elbaite (BD-S3) from the Cruzeiro mine in Minas Gerais, Brazil. D: Schorl (BD-S4) from Larsemann Hills, Antarctica. E: Uvite (BD-S5) from Brumado, Brazil. F: Uvite (BD-S6) from Brumado, Brazil (see table 2). The red circle in each photo denotes the area selected for chemical analysis. Photos by Ziyin Sun.

auxiliary gas (0.8 L/min), and cooling gas (14 L/min). Helium, used as part of a carrier gas, has a flow rate of 0.8 L/min. Argon and helium gas flow, torch position, sampling depth, and lens voltage were optimized to achieve maximum sensitivity (counts per concentration) and low oxide production rates ( $^{232}\text{Th}^{16}\text{O}/^{232}\text{Th} < 1\%$ ). Ablated material was vaporized, atomized, and ionized by a plasma power of 1550 W. Data acquisition was performed in time-resolved mode. The dwell time of each isotope measured was 0.01 second except  $^{27}\text{Al}$  and  $^{28}\text{Si}$ , which were measured for 0.005 second. Gas background was measured for 20 seconds, while the dwell time of each laser spot was 40 seconds. Only the second half (20-second ablation) of the laser profile was used to calculate concentration, which eliminates surface contamination.  $^{29}\text{Si}$  was used as an internal standard. GSD-1G, GSE-1G (U.S. Geological Survey), and NIST 610 were used as external standards.  $^{23}\text{Na}$ ,  $^{24}\text{Mg}$ ,  $^{27}\text{Al}$ ,  $^{29}\text{Si}$ ,  $^{43}\text{Ca}$ , and  $^{57}\text{Fe}$  (the six major elements for species classification in gem tourmaline; see discussion below), along with other isotopes of trace elements, were selected for analyses. All isotopes were standardized using all three standards. Note that F, OH, and O cannot be analyzed by LA-ICP-MS and must be calculated. Internal standardization of data was initially processed by Qtegra software version 2.4 before proceeding with our normalization method (see the “Calculation Method for LA-ICP-MS Raw Data” section below).

A 10  $\mu\text{m}$  diameter laser spot was used to mark four corners of a square area on the samples before performing EPMA analysis in the center of the area. After EPMA analysis, a 55  $\mu\text{m}$  diameter laser spot was applied in the center of the same area to obtain the LA-ICP-MS results, which ensured the same regions of the tourmalines were analyzed by both methods.

**EPMA.** To obtain precise and accurate major and minor element chemistry for verification and validation of the LA-ICP-MS approach, six tourmaline samples were quantitatively analyzed by wavelength-dispersive spectrometry.

The samples in figures 9 and 11 (see Appendix 1 at [www.gia.edu/gems-gemology/spring-2019-new-method-identifying-gem-tourmaline-appendix-1](http://www.gia.edu/gems-gemology/spring-2019-new-method-identifying-gem-tourmaline-appendix-1)) were analyzed at the California Institute of Technology on a JEOL JXA-8200 electron microprobe with an accelerating voltage of 15 kV and 20 nA current with a defocused beam of 10 micrometers. Standards employed were forsterite (Mg), fayalite (Fe), Mn olivine (Mn), phlogopite (F), albite (Na, Si), microcline (K), and anorthite (Ca). Analytical precision is estimated to be  $\pm 1\%$  relative for the major elements and  $\pm 5\%$  for the minor elements. Normalization procedures followed those suggested for EPMA by Henry et al. (2011). For Li-rich samples, Li was estimated based on the method described by Pesquera et al. (2016).

COMPARISON OF LA-ICP-MS AND EPMA ANALYSES

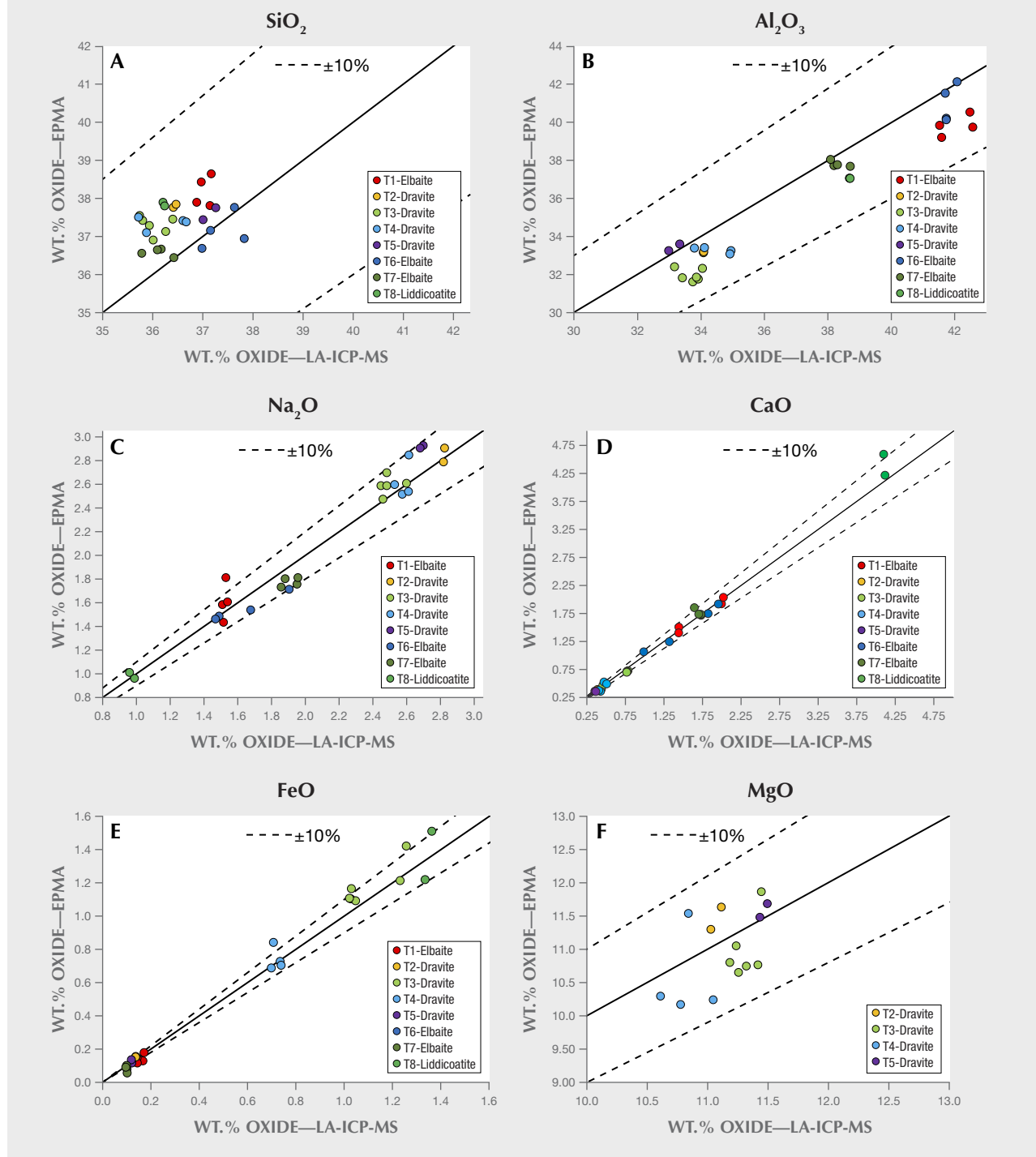


Figure 11. Comparison between LA-ICP-MS and EPMA analyses for Si, Al, Na, Ca, Fe, and Mg. In each plot, the black dashes represent the boundary of  $\pm 10\%$  error. Each colored dot represents a single analysis. The vertical axis represents the value obtained from EPMA, while the horizontal axis represents the value obtained from LA-ICP-MS. The closer the dot is to the solid black middle line, the better the agreement between EPMA and LA-ICP-MS data.

Although analyses could be further normalized to 15 YZT cations, that method is not performed here because of the uncertainty in the LA-ICP-MS data for Li.

The samples in figures 10 and 12 (see Appendix 2 at [www.gia.edu/gems-gemology/spring-2019-new-method-identifying-gem-tourmaline-appendix-2](http://www.gia.edu/gems-gemology/spring-2019-new-method-identifying-gem-tourmaline-appendix-2)) were analyzed on the JEOL 8230 electron microprobe at Louisiana State University. Analyses were conducted at an accelerating potential of 15 kV and 5–15 nA using a 5–10 micrometer spot size. Several elements were analyzed but were present in trace amounts or below detection limits. Those are shown in the tables. Well-characterized natural minerals were used as standards, including andalusite (Al), diopside (Ca, Mg, Si), fayalite (Fe), chromite (Cr), kaersutite (Ti), rhodonite (Mn), willemite (Zn), albite (Na), sanidine (K), and apatite or fluor-phlogopite (F). Several well-characterized tourmalines served as secondary standards to ensure consistency among analyses. Analytical precision is estimated to be  $\pm 1\%$  relative for the major elements and  $\pm 5\%$  for the minor elements. Eight to twelve points were analyzed per sample to test for homogeneity and obtain a representative analysis (see Appendix 5 at [www.gia.edu/gems-gemology/spring-2019-new-method-identifying-gem-tourmaline-appendix-5](http://www.gia.edu/gems-gemology/spring-2019-new-method-identifying-gem-tourmaline-appendix-5)). For unzoned crystals, the composition reported is the average from the points for that sample. For zoned crystals, average chemical analyses represent each distinct zone. The number of analyses per sample are given in the tables (again, see Appendix 2).

**Calculation Method for LA-ICP-MS Raw Data.** Tourmaline compositions are based on the calculation method from Henry et al. (2011) and Clark (2007), with modifications based on the additional limitations of LA-ICP-MS. LA-ICP-MS analysis for tourmaline provides an incomplete chemical characterization because critical light elements (H and F) and the oxidation states of transition elements (e.g., Fe and Mn) cannot be determined. While Li can be measured by LA-ICP-MS, we were unable to produce good tourmaline stoichiometry with our data when directly measuring Li. This is likely due to significant differential fractionation of Li between the glass standards and tourmaline. Such differential fractionation is a known problem for volatile light elements such as Li (Gaboardi and Humayun, 2009). Calculating tourmaline species from LA-ICP-MS data requires the following assumptions:

1. Three boron cations per formula (i.e., no tetrahedral B).
2. The sum of Y-, Z-, and T-sites equals 15 cations per formula. If Li is present, it is calculated to make up for site deficiency.
3. The V- and W-sites are fully occupied by hydroxyl groups, although additional data reduction could produce the oxy species.
4. Iron and manganese are divalent.

Consequently, the fluor- and oxy-tourmaline species cannot be determined. Future work will characterize oxy species. A full and detailed description of the formula and procedures for the calculation method is presented in Appendix 3 ([www.gia.edu/gems-gemology/spring-2019-new-method-identifying-gem-tourmaline-appendix-3](http://www.gia.edu/gems-gemology/spring-2019-new-method-identifying-gem-tourmaline-appendix-3)).

For clarity, a brief overview of the calculation method is presented here. Before the LA-ICP-MS analysis is performed, the correct concentration of the internal standard  $^{29}\text{Si}$  is unknown, and therefore the concentrations for the elements obtained initially are not correct on an absolute ppm scale. However, the concentrations of the various elements are all correct relative to each other because all elements are referenced to the concentration of Si. All of the major elements except for Li and B are converted into atomic proportions to determine the stoichiometric tourmaline formulae. The assumptions described above provide sufficient constraints so that a simple set of mathematical formulae can be used to determine the number of each cation per formula unit (see Appendix 3). Once these data are determined, the elements can be assigned to each of the specific tourmaline crystallographic sites outlined in Henry et al. (2011). Further, the total number of each cation on each site will determine the species of the tourmaline analyzed in most instances. With disordering in the oxy-species tourmalines, however, the exact formula is less certain. The more detailed and complete steps required for site assignments and species identification are provided online in Appendixes 4 and 5.

## RESULTS AND DISCUSSION

**Strengths of the Method.** The method has three main strengths. First, Si is used as an internal standard (Okrusch et al., 2016). Elements with similar atomic masses are assumed to fractionate similarly. Consequently, the use of Si as an internal standard means short- and long-term fractionation is less problematic when measuring major elements with similar

COMPARISON OF LA-ICP-MS AND EPMA ANALYSES

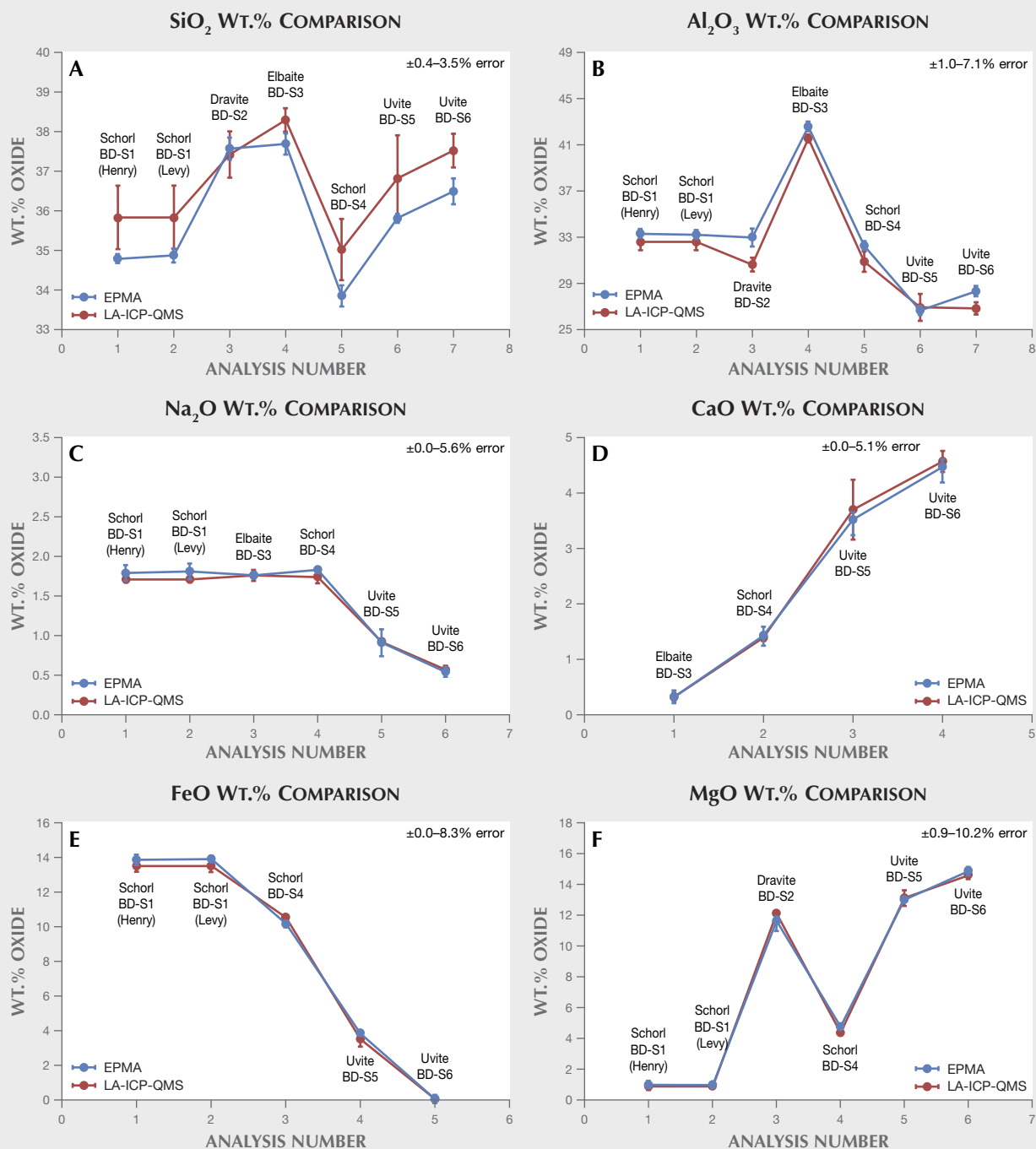


Figure 12. Comparison of EPMA and LA-ICP-MS measurements for Si, Al, Na, Ca, Fe, and Mg. In each graph, the blue trace represents the value obtained from EPMA. Each error bar, representing standard deviations, is calculated based on a large number of analyses (the number of analyses for each sample is shown in Appendix 5). The red trace represents the value obtained from LA-ICP-MS. Overlap of the red and blue solid lines shows better agreement between EPMA and LA-ICP-MS data. EPMA analyses for BD-S1 (schorl) were performed by both Henry and Levy.

masses (Na, Mg, Al, Ca, and Fe) in tourmaline (e.g., Chen, 1999).

Second, three samples (GSD-1G, GSE-1G, and NIST 610) are used as external standards. It is optimal to select standards in which the elements being analyzed are at similar or higher concentrations than in the unknowns. The concentration ranges of Na, Mg, Al, Si, Ca, and Fe in GSD-1G and GSE-1G are similar to the concentration ranges of those elements in most tourmaline species.

Third, the procedure uses an optimized normalization method to post-process data. Typically, the value used for the internal standard concentration is derived from an external measurement such as EPMA (method 1). In this study, an internal standard concentration for  $^{29}\text{Si}$  is estimated and the data is renormalized to 100 wt.% to account for deviations from the initial Si value (method 2). A comparison between methods 1 and 2 using the data from eight GIA stones (GIA-T1 to GIA-T8) demonstrates excellent results. With method 1, the difference is within 3% relative for Na, Mg, Al, Si, Ca, and Fe (2.27% for Na, 2.91% for Mg, 2.27% for Al, 2.27% for Si, 2.27% for Ca, and 2.46% for Fe). These data further support the accuracy of our method. Not requiring a predetermined Si value from EPMA for internal standardization of LA-ICP-MS makes the method most suitable for tourmaline species determinations in gemological laboratories that are only equipped with LA-ICP-MS.

**Simplified Tourmaline Species Classification for LA-ICP-MS Processed Data.** The species classification presented here is a simplified version of the one presented in Henry et al. (2011), due to the limitations of LA-ICP-MS analysis. The inability to measure F or transition metal oxidation states by LA-ICP-MS does not allow determination of the V-site and W-site occupancy; we therefore cannot determine the fluor or oxy species. For example, fluor-elbaite would be elbaite in our simplified classification (table 1 and Appendix 3). Further, the assumption that all iron is divalent precludes determination of ferric iron-dominant species (table 1) such as povondraite and potassium-povondraite. Although olenite, tsilaisite, and adachiite can be determined by LA-ICP-MS, to the authors' knowledge they have not been observed as gem-quality specimens. LA-ICP-MS measurements are not sufficiently precise (compared to EPMA analysis) to accurately separate hydroxyl- from oxy-tourmaline species.

Consideration of these limitations provides the following 11 tourmaline species. If the data falls out-

side these simplified classification categories, the tourmaline is assigned to alkali subgroups 3, 4, and 5, or calcic subgroups 3 and 4, or vacant subgroup 3 (Henry et al., 2011; table 1). None of these tourmaline species are considered in our method, as they are rarely encountered as gem-quality specimens. This simplified tourmaline classification is also illustrated using ternary plots in box A. Vanadium-dravite was redefined by Bosi et al. (2013) as oxy-vanadium-dravite. The following formulae for the species are hypothetical:

- |                      |   |
|----------------------|---|
| 1. Dravite           | $^x\text{Na}^y\text{Mg}_3^z\text{Al}_6^t\text{Si}_6\text{O}_{18}(\text{BO}_3)_3(\text{OH})_3(\text{OH})$                      |
| 2. Vanadium-dravite  | $^x\text{Na}^y\text{Mg}_3^z\text{V}_6^t\text{Si}_6\text{O}_{18}(\text{BO}_3)_3(\text{OH})_3(\text{OH})$                       |
| 3. Chromium-dravite  | $^x\text{Na}^y\text{Mg}_3^z\text{Cr}_6^t\text{Si}_6\text{O}_{18}(\text{BO}_3)_3(\text{OH})_3(\text{OH})$                      |
| 4. Schorl            | $^x\text{Na}^y\text{Fe}^{2+}_3\text{Al}_6^t\text{Si}_6\text{O}_{18}(\text{BO}_3)_3(\text{OH})_3(\text{OH})$                   |
| 5. Elbaite           | $^x\text{Na}^y(\text{Li}_{1.5}\text{Al}_{1.5})^z\text{Al}_6^t\text{Si}_6\text{O}_{18}(\text{BO}_3)_3(\text{OH})_3(\text{OH})$ |
| 6. Uvite             | $^x\text{Ca}^y\text{Mg}_3^z(\text{MgAl}_5)^t\text{Si}_6\text{O}_{18}(\text{BO}_3)_3(\text{OH})_3(\text{OH})$                  |
| 7. Feruvite          | $^x\text{Ca}^y\text{Fe}^{2+}_3(\text{MgAl}_5)^t\text{Si}_6\text{O}_{18}(\text{BO}_3)_3(\text{OH})_3(\text{OH})$               |
| 8. Liddicoatite      | $^x\text{Ca}^y(\text{Li}_2\text{Al})^z\text{Al}_6^t\text{Si}_6\text{O}_{18}(\text{BO}_3)_3(\text{OH})_3(\text{OH})$           |
| 9. Foitite           | $^x\text{Ca}^y(\text{Fe}^{2+}_2\text{Al})^z\text{Al}_6^t\text{Si}_6\text{O}_{18}(\text{BO}_3)_3(\text{OH})_3(\text{OH})$      |
| 10. Magnesio-foitite | $^x\text{Ca}^y(\text{Mg}_2\text{Al})^z\text{Al}_6^t\text{Si}_6\text{O}_{18}(\text{BO}_3)_3(\text{OH})_3(\text{OH})$           |
| 11. Rossmanite       | $^x\text{Ca}^y(\text{LiAl}_2)^z\text{Al}_6^t\text{Si}_6\text{O}_{18}(\text{BO}_3)_3(\text{OH})_3(\text{OH})$                  |

**Comparison of LA-ICP-MS and EPMA Data.** Eight gem-quality tourmaline rough samples, GIA-T1 to GIA-T8 (see table 2 and figure 9) were tested initially. The agreement between EPMA and LA-ICP-MS analyses using the method described in this article was generally very good (figure 11). The error for major elements Si, Al, Na, Ca, Fe, and Mg was generally within 5–10%. Al values were systematically higher by LA-ICP-MS, while Si was generally slightly lower by LA-ICP-MS than EPMA. LA-ICP-MS measurements of Fe were generally within 10% at higher concentrations, but the difference was greater at low concentrations due to lower precision of EPMA in this range (<0.2 wt.% oxide; see figure 11E). The full chemical composition of these eight tourmaline samples is shown in Appendix 1.

Six additional tourmaline samples (table 2, BD-S1 to BD-S6; figure 10) were analyzed by both EPMA and LA-ICP-MS, with the results shown in figure 12. The difference between EPMA and LA-ICP-MS for Si, Al, Na, Ca, Fe, and Mg was within 3.5%, 7.5%, 6%, 5.5%, 8.5%, and 10.5%, respectively. The more detailed data comparison (including other trace elements) is shown in Appendix 2.

Overall, the comparison of EPMA and LA-ICP-MS data demonstrates that LA-ICP-MS analysis can measure major and minor elements with sufficient accuracy to determine tourmaline species.

## BOX A: FLOWCHART OF THE SIMPLIFIED TOURMALINE SPECIES CLASSIFICATION

The ternary plots shown in figure A-1 demonstrate how the nine tourmaline species described above are determined. Fluor or oxy species are not included in the flowchart. The Ca-Na-vacancy ternary plot establishes the dominance of the X-site in tourmaline (top row), which is the first step of species classification. The Al-Cr-V ternary plot determines the dominance of the Z-site (middle row), which narrows down the results and provides further discrimination. The Li-Fe-

Mg ternary plot indicates the dominance of the Y-site and finally assigns the tourmaline to one of nine species (bottom row).

Detailed species classification criteria are shown in Appendix 5. An updated set of Al-Cr-V and Al-Cr-Fe ternary diagrams to establish species was generated by Henry and Dutrow (2018) for sodic oxy-tourmalines that contain significant amounts of Cr, V, and Fe<sup>3+</sup>. Future work will characterize oxy species by LA-ICP-MS.

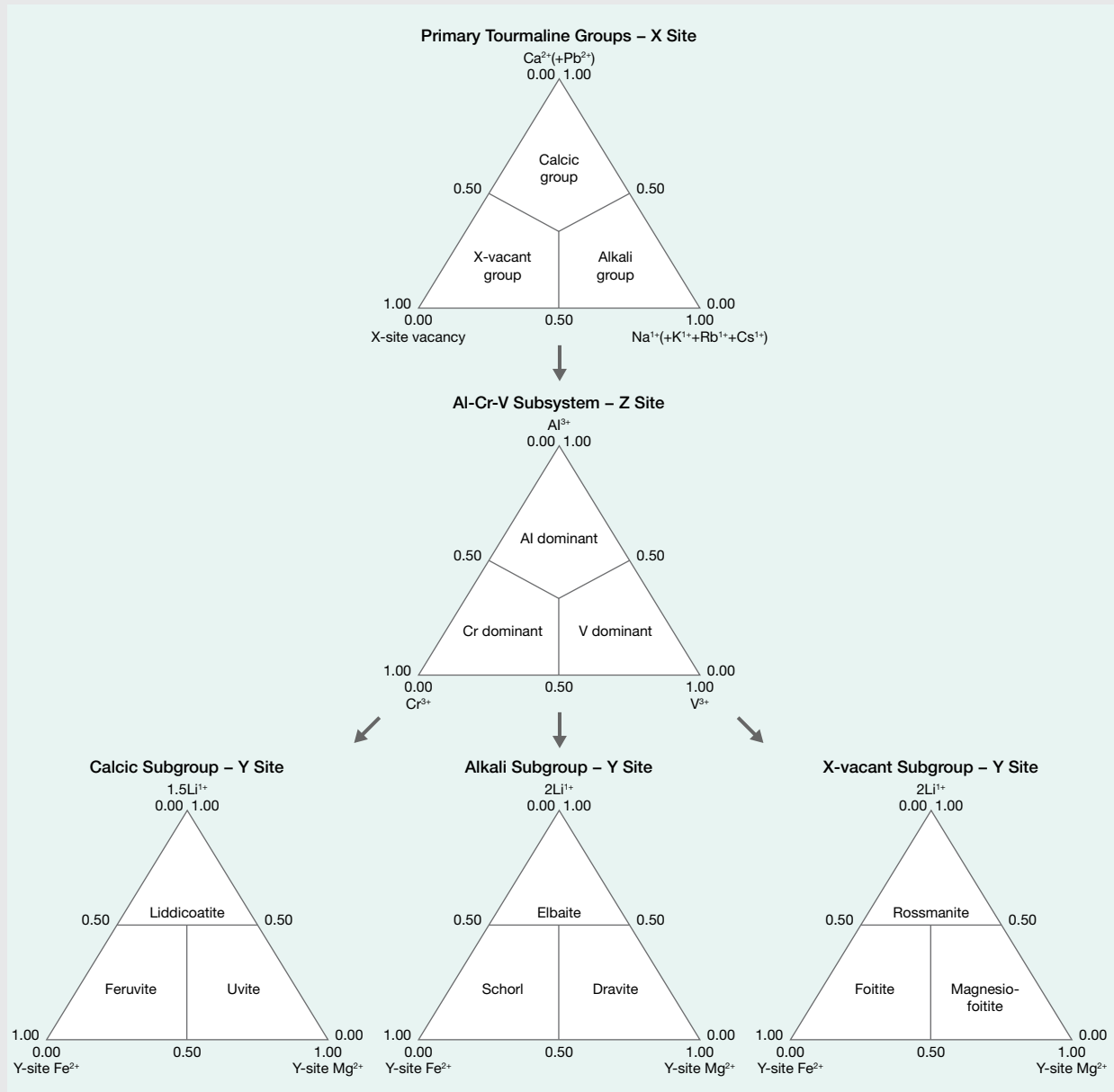


Figure A-1. This flowchart illustrates the use of ternary plots to classify tourmaline species. Modified after Henry et al. (2011).



## BOX B: TOURMALINE ANALYSIS AT GIA

**From Client Stone to Certificate: GIA Procedures for Tourmaline Species Classification.** A bicolored tourmaline ring (see figure 1) demonstrates how jewelry is handled and analyzed at GIA laboratories. This same procedure was used to analyze the tourmalines in the bracelet shown in figure 13 and to detect two imitation stones.

**Analytical Procedure.** The bicolored tourmaline ring was wiped cleaned to remove liquid and dust. It was secured with BlueTac in an orientation allowing access to the stone's girdle (figure B-1A) and placed inside the sample chamber (figure B-1B). The ring was carefully placed to make sure that no part of it extended above the top of the sample chamber (figure B-1B). The sample chamber was put back under the laser and purged for 20 minutes before ablating (figure B-1C to B-1E) to minimize the background signal and fractionation. Three craters were ablated on the girdle of the stone (figure B-1F). The diameter of the round craters (laser spots) was approximately 55  $\mu\text{m}$ , smaller in that of human hair—effectively invisible to the unaided eye and difficult to see

with a 10 $\times$  triplet loupe. The amount of tourmaline powder ablated from the three spots is minimal and does not result in any noticeable weight loss, demonstrating that the method is minimally destructive and does not affect the appearance of the stone. The ablated material was then transported via argon and helium carrier gases to the plasma to be ionized (figure B-1G). The gaseous ions were deflected to pass through a quadrupole mass analyzer to be separated according to their mass-to-charge ratio, until they finally reached the detector (figure B-1H). The LA-ICP-MS system used by GIA is shown in figure B-1I.

**Data Process and Species Classification.** After analysis, the LA-ICP-MS data was renormalized to calculate site assignment, which was further used for species classification (Appendixes 3 and 4). The data of each stone (table 3) was saved in GIA's colored stone database for rechecking and placed in corresponding tourmaline ternary classification plots (e.g., figure B-2) to provide a good visual representation for gemologists.

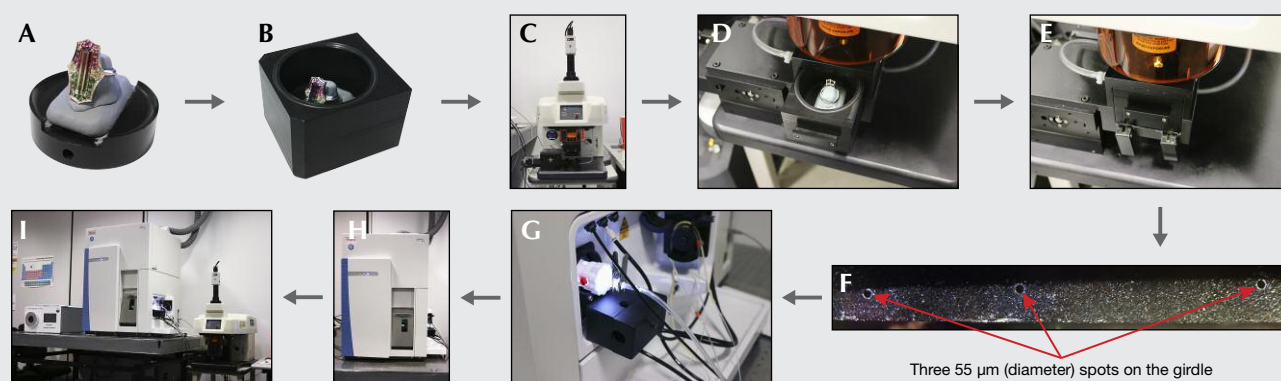


Figure B-1. This flowchart shows how a tourmaline ring was analyzed by LA-ICP-MS at GIA. Photos by Ziyin Sun.

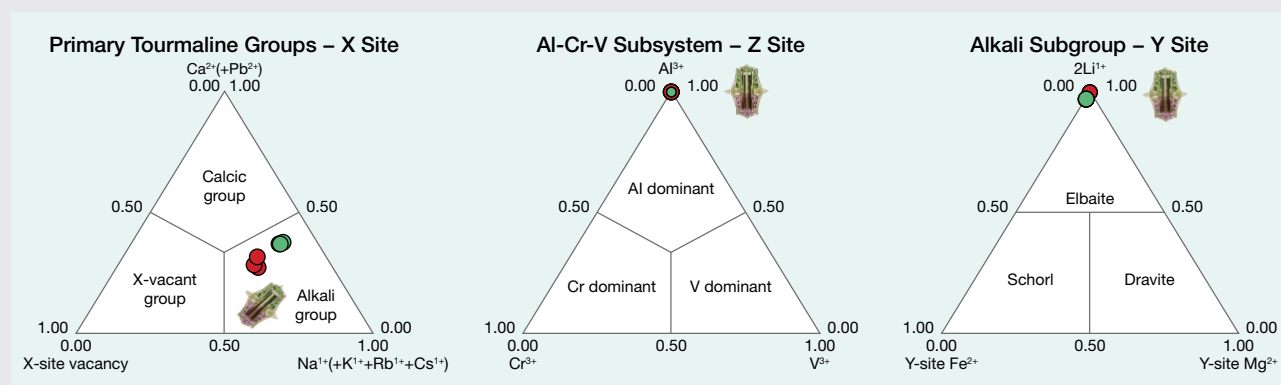


Figure B-2. Left: Ternary system for the primary tourmaline groups based on the dominant occupancy of the X-site. The tourmaline center stone on the ring belongs to the alkali primary group, the first step of species classification. Center: Ternary diagram for the Al-V-Cr subsystem for the dominant occupancy of the Z-site.  $\text{Al}^{3+}$  is the dominant trivalent cation on the Z-site. Right: Ternary dravite-schorl-elbaite subsystem based on the dominant occupancy of the Y-site.  $\text{Li}^+$  is the dominant monovalent cation on the Y-site. The species of tourmaline for both the red and the green color zoning in the ring is elbaite.

**TABLE 3.** Chemical composition and site distribution of the tourmaline ring by LA-ICP-MS.

Spot name	Red color zoning			Green color zoning		
	SP1	SP2	SP3	SP1	SP2	SP3
<b>Obtained and normalized from LA-ICP-MS<sup>a</sup> (ppmw)</b>						
Li (calculated)	10326	10777	10929	10746	10512	10501
B (calculated)	34645	34688	34666	34462	34424	34439
Na	11032	10736	10632	11364	11530	11438
Mg	0.84	0.40	0.37	95.12	100	99.93
Al	220647	215788	214760	211493	213978	214202
Si	177573	181361	181391	179520	177221	177407
K	71.09	bdl	69.74	30.09	59.73	39.93
Ca	9586	9886	10844	12311	12465	12270
Ti	10.72	10.74	9.20	115	116	119
V	0.23	0.21	0.26	0.54	0.48	0.72
Cr	bdl	bdl	bdl	bdl	bdl	bdl
Mn <sup>2+</sup>	1915	1924	2179	4977	5152	5002
Fe <sup>2+</sup>	19.25	bdl	18.29	3420	3563	3359
Cu	1.20	1.84	2.15	0.65	0.61	0.64
Zn	1.39	0.99	1.64	122	119	125
Rb	bdl	bdl	0.36	bdl	bdl	bdl
Cs	bdl	bdl	0.57	bdl	bdl	bdl
Ba	bdl	0.04	bdl	bdl	bdl	bdl
Pb	65.57	64.31	73.46	66.81	63.47	66.76
<b>Atoms per formula unit, 27 O + 4 OH anions normalization</b>						
B-site: B (total)	3.000	3.000	3.000	3.000	3.000	3.000
<b>B-site total</b>	<b>3.000</b>	<b>3.000</b>	<b>3.000</b>	<b>3.000</b>	<b>3.000</b>	<b>3.000</b>
T-site: Si (total)	5.919	6.038	6.042	6.016	5.945	5.949
T-site: Al	0.081	0.000	0.000	0.000	0.055	0.051
<b>T-site total</b>	<b>6.000</b>	<b>6.038</b>	<b>6.042</b>	<b>6.016</b>	<b>6.000</b>	<b>6.000</b>
Z-site: Al	6.000	6.000	6.000	6.000	6.000	6.000
Z-site: Cr <sup>3+</sup>	0.000	0.000	0.000	0.000	0.000	0.000
Z-site: V <sup>3+</sup>	0.000	0.000	0.000	0.000	0.000	0.000
Z-site: Mg <sup>2+</sup>	0.000	0.000	0.000	0.000	0.000	0.000
<b>Z-site total</b>	<b>6.000</b>	<b>6.000</b>	<b>6.000</b>	<b>6.000</b>	<b>6.000</b>	<b>6.000</b>
Y-site: Al	1.574	1.478	1.447	1.377	1.417	1.425
Ti	0.000	0.000	0.000	0.002	0.002	0.002
Y-site: V <sup>3+</sup>	0.000	0.000	0.000	0.000	0.000	0.000
Y-site: Cr <sup>3+</sup>	0.000	0.000	0.000	0.000	0.000	0.000
Fe <sup>2+</sup>	0.000	0.000	0.000	0.058	0.060	0.057
Mn <sup>2+</sup>	0.033	0.033	0.037	0.085	0.088	0.086
Y-site: Mg <sup>2+</sup>	0.000	0.000	0.000	0.004	0.004	0.004
Zn	0.000	0.000	0.000	0.002	0.002	0.002
Cu	0.000	0.000	0.000	0.000	0.000	0.000
Li	1.393	1.452	1.473	1.457	1.427	1.425
<b>Y-site total</b>	<b>3.000</b>	<b>2.962</b>	<b>2.958</b>	<b>2.984</b>	<b>3.000</b>	<b>3.000</b>
Ca	0.224	0.231	0.253	0.289	0.293	0.288
Pb	0.000	0.000	0.000	0.000	0.000	0.000
Ba	0.000	0.000	0.000	0.000	0.000	0.000
Na	0.449	0.437	0.433	0.465	0.473	0.469
K	0.002	0.000	0.002	0.001	0.001	0.001
Rb	0.000	0.000	0.000	0.000	0.000	0.000
Cs	0.000	0.000	0.000	0.000	0.000	0.000
X-site vacancy	0.325	0.332	0.312	0.245	0.233	0.242
<b>X-site total</b>	<b>1.000</b>	<b>1.000</b>	<b>1.000</b>	<b>1.000</b>	<b>1.000</b>	<b>1.000</b>
<b>V+W-site: OH</b>	<b>4.000</b>	<b>4.000</b>	<b>4.000</b>	<b>4.000</b>	<b>4.000</b>	<b>4.000</b>
<b>Species</b>	<b>Elbaite</b>	<b>Elbaite</b>	<b>Elbaite</b>	<b>Elbaite</b>	<b>Elbaite</b>	<b>Elbaite</b>

<sup>a</sup>If normalized data is greater than or equal to 100 ppmw, it is rounded to zero decimal places. If normalized data is less than 100 ppmw, it is rounded to two decimal places. bdl = below detection limit.



Figure 13. This rainbow-colored tourmaline bracelet was examined for identification and species classification at GIA's Carlsbad laboratory. The tourmaline species ranged from red-pink elbaites and orange dravites to green-blue elbaites and violet-purple liddicoatites. Stones 12 and 13 were citrines that had been set between the two orange dravites. Photo by Robison McMurtry.

## CONCLUSIONS

Comparing LA-ICP-MS data to highly precise and accurate EPMA data for major elements on our samples demonstrated that some tourmaline species can be determined solely by LA-ICP-MS. The new method described here (1) allows for inexpensive, clean, fast, and largely nondestructive analysis of tourmaline gemstones by LA-ICP-MS and (2) uses this data to determine a general species. The method is suitable for gemological laboratories equipped only with LA-ICP-MS. Many large complex jewelry pieces, such as the rainbow tourmaline bracelet in figure 13, mounted with 33 square step-cut stones, can be easily analyzed with good precision and accuracy. As shown

here, the method permits the identification of imitations that are intermingled with the tourmalines.

LA-ICP-MS is generally chosen to measure minor or trace elements and is considered less accurate due to interferences and matrix effects that cannot be corrected entirely. With carefully chosen internal standards and further development of external standards, however, our LA-ICP-MS method can produce data comparable to EPMA measurements of the same gem tourmaline samples. The ability to accurately measure the range of chemical compositions found in gem tourmaline using LA-ICP-MS allows GIA to help the colored stone industry better understand the varieties of tourmaline being bought and sold.

### ABOUT THE AUTHORS

Mr. Sun is a research associate, and Dr. Palke and Dr. Breeding are senior research scientists, at GIA in Carlsbad, California. Dr. Dutrow is the Williams Distinguished Alumni professor at Louisiana State University in Baton Rouge.

### ACKNOWLEDGMENTS

The authors thank Professor Darrell Henry, Nele Muttik, and Elizabeth Levy (Louisiana State University, Baton Rouge) for assistance in EPMA. Professor Ed Grew (University of Maine, Orono) is thanked for his donation of the tourmaline specimen to author BD. The authors thank Chi Ma of Caltech for assistance with

EPMA measurements. Terri Ottaway, curator of the GIA Museum, is kindly thanked for providing gem-quality tourmaline from GIA's Gübelin Gem Collection for chemical analysis and photography. We are deeply grateful to Orasa Weldon for her beautiful photographs for the article. Bruce Fry is greatly thanked for sharing his enormous tourmaline collection with us for chemical analysis and photography. Many thanks are owed to GIA's Dino DeGhionno, Shane McClure, Nathan Renfro, Yusuke Katsurada, David Nelson, Troy Ardon, Robert Weldon, Robison McMurtry, Jonathan Muyal, and Tao Hsu. Portions of this study benefited from National Science Foundation funding to Barbara Dutrow and Darrell Henry (grant number EAR-1551434).

## REFERENCES

- Abduriyim A., Kitawaki H. (2005) Gem News International: Cu- and Mn-bearing tourmaline—More production from Mozambique. *G&G*, Vol. 41, No. 4, pp. 360–361.
- Abduriyim A., Kitawaki H., Furuya M., Schwarz D. (2006) "Paraíba"-type copper-bearing tourmaline from Brazil, Nigeria, and Mozambique: Chemical fingerprinting by LA-ICP-MS. *G&G*, Vol. 42, No. 1, pp. 4–21, <http://dx.doi.org/10.5741/GEMS.42.1.4>
- Bosi F., Reznitskii L.Z., Sklyarov E.V. (2013) Oxy-vanadium-dravite,  $\text{NaV}_3(\text{V}_4\text{Mg}_2)(\text{Si}_6\text{O}_{18})(\text{BO}_3)_3(\text{OH})_5\text{O}$ : Crystal structure and redefinition of the "vanadium-dravite" tourmaline. *American Mineralogist*, Vol. 98, pp. 501–505, <http://dx.doi.org/10.2138/am.2013.4243>
- Bowersox G.W. (1985) A status report on gemstones from Afghanistan. *G&G*, Vol. 21, No. 4, pp. 192–204, <http://dx.doi.org/10.5741/GEMS.21.4.192>

- Breeding C.M., Shen H. (2008) Quantitative major element chemical analysis using LA-ICP-MS: Gemstone feldspar and tourmaline. Poster Session: Environmental, Geochemical Applications. 2008 Winter Conference on Plasma Spectrochemistry. Temecula, California, January 7–12.
- Chen Z. (1999) Inter-element fractionation and correction in laser ablation inductively coupled plasma mass spectrometry. *Journal of Analytical Atomic Spectrometry*, Vol. 14, No. 12, pp. 1823–1828, <http://dx.doi.org/10.1039/A903272J>
- Clark C.M. (2007) Tourmaline: Structure formula calculations. *The Canadian Mineralogist*, Vol. 45, No. 2, pp. 229–237, <http://dx.doi.org/10.2113/gscanmin.45.2.229>
- Dirlam D.M., Laurs B.M., Pezzotta F., Simmons W.B. (2002) Liddicoatite tourmaline from Anjanabonoina, Madagascar. *G&G*, Vol. 38, No. 1, pp. 28–53, <http://dx.doi.org/10.5741/GEMS.38.1.28>
- Dutrow B.L. (2018) Tourmaline: A gemstone's guide to geologic evolution of the earth's crust. *G&G*, Vol. 54, No. 3, pp. 256–257.
- Dutrow B.L., Henry D.J. (2000) Complexly zoned fibrous tourmaline, Cruzeiro mine, Minas Gerais, Brazil: a record of evolving magmatic and hydrothermal fluids. *The Canadian Mineralogist*, Vol. 38, No. 1, pp. 131–143, <http://dx.doi.org/10.2113/gscanmin.38.1.131>
- Dutrow B.L., Henry D.J. (2011) Tourmaline: A geologic DVD. *Elements*, Vol. 7, No. 5, pp. 301–306, <http://dx.doi.org/10.2113/gselements.7.5.301>
- Fisher J. (2002) Gem and rare-element pegmatites of Southern California. *Mineralogical Record*, Vol. 33, No. 5, p. 363.
- (2011) Mines and minerals of the Southern California pegmatite province. *Rocks & Minerals*, Vol. 86, No. 1, pp. 14–35, <http://dx.doi.org/10.1080/00357529.2011.537167>
- Gaboardi M., Humayun M. (2009) Elemental fractionation during LA-ICP-MS analysis of silicate glasses: implications for matrix-independent standardization. *Journal of Analytical Atomic Spectrometry*, Vol. 24, No. 9, pp. 1188–1197, <http://dx.doi.org/10.1039/b900876d>
- Garba I. (2003) Geochemical discrimination of newly discovered rare-metal bearing and barren pegmatites in the Pan-African (600 ± 150 Ma) basement of northern Nigeria. *Applied Earth Science*, Vol. 112, No. 3, pp. 287–292, <http://dx.doi.org/10.1179/037174503225011270>
- Hawthorne F.C., Dirlam D.M. (2011) Tourmaline the indicator mineral: From atomic arrangement to Viking navigation. *Elements*, Vol. 7, No. 5, pp. 307–312, <http://dx.doi.org/10.2113/gselements.7.5.307>
- Hawthorne F.C., Henry D.J. (1999) Classification of the minerals of the tourmaline group. *European Journal of Mineralogy*, Vol. 11, No. 2, pp. 201–215, <http://dx.doi.org/10.1127/ejm/11/2/0201>
- Henry D.J., Dutrow B.L. (1990) Ca substitution in Li-poor aluminous tourmaline. *The Canadian Mineralogist*, Vol. 28, No. 1, pp. 111–124.
- (2001) Compositional zoning and element partitioning in nickeloan tourmaline from a metamorphosed karstbauxite from Samos, Greece. *American Mineralogist*, Vol. 86, No. 10, pp. 1130–1142, <http://dx.doi.org/10.2138/am-2001-1002>
- (2012) Tourmaline at diagenetic to low-grade metamorphic conditions: Its petrologic applicability. *Lithos*, Vol. 154, pp. 16–32, <http://dx.doi.org/10.1016/j.lithos.2012.08.013>
- (2018) Tourmaline studies through time: contributions to scientific advancements. *Journal of Geosciences*, Vol. 63, No. 2, pp. 77–98, <http://dx.doi.org/10.3190/jgeosci.255>
- Henry D.J., Novák M., Hawthorne F.C., Ertl A., Dutrow B.L., Uher P., Pezzotta F. (2011) Nomenclature of the tourmaline-super-group minerals. *American Mineralogist*, Vol. 96, No. 5–6, pp. 895–913, <http://dx.doi.org/10.2138/am.2011.3636>
- van Hinsberg V.J., Henry D.J., Dutrow B.L. (2011) Tourmaline as a petrologic forensic mineral: A unique recorder of its geologic past. *Elements*, Vol. 7, No. 5, pp. 327–332, <http://dx.doi.org/10.2113/gselements.7.5.327>
- Koivula J.I., Kammerling R.C., Eds. (1989) Gem News: Paraíba tourmaline update. *G&G*, Vol. 25, No. 4, pp. 248–249.
- Kunz G.F. (1905) Gems, Jewelers' Materials, and Ornamental Stones of California. Bulletin No. 37, California State Mining Bureau, San Francisco.
- Laurs B.M. (2015) "Ruby"-red tourmaline from Nigeria. *The Journal of Gemmology*, Vol. 34, No. 7, pp. 569–570.
- Laurs B.M., Zwaan J.C., Breeding C.M., Simmons W.B., Beaton D., Rijdsdijk K.F., Befi R., Falster A.U. (2008) Copper-bearing (Paraíba-type) tourmaline from Mozambique. *G&G*, Vol. 44, No. 1, pp. 4–30, <http://dx.doi.org/10.5741/GEMS.44.1.4>
- McMillan N., Curry J., Dutrow B.L., Henry D.J. (2017) Lithologic determination of tourmaline based on laser-induced breakdown spectroscopy: an alternative approach to provenance studies. Tourmaline 2017 International Symposium, Bystrice nad Pernštejnem, Czech Republic, June 23–28.
- Marger K., Baumgartner L.P., Putlitz B., Dutrow B.L., Bouvier A.S., Vennemann T., Henry D.J., Dini A. (2017) Tourmaline reference material for oxygen isotope analysis by SIMS. Tourmaline 2017 International Symposium, Bystrice nad Pernštejnem, Czech Republic, June 23–28.
- Okrusch M., Ertl A., Schüssler U., Tillmanns E., Brätz H., Bank H. (2016) Major- and trace-element composition of Paraíba-type tourmaline from Brazil, Mozambique and Nigeria. *The Journal of Gemmology*, Vol. 35, No. 2, pp. 120–139.
- Olatunji A.S., Jimoh O.R. (2017) Major oxides geochemistry of tourmaline from selected gem-mineral deposits in southwestern Nigeria. *Asia Pacific Journal of Energy and Environment*, Vol. 3, No. 1, pp. 7–20.
- Pesquera A., Gil-Crespo P.P., Torres-Ruiz F., Torres-Ruiz J., Roda-Robles E. (2016) A multiple regression method for estimating Li in tourmaline from electron microprobe analyses. *Mineralogical Magazine*, Vol. 80, No. 6, pp. 1129–1133, <http://dx.doi.org/10.1180/minmag.2016.080.046a>
- Proctor K. (1985a) Gem pegmatites of Minas Gerais, Brazil: the tourmalines of the Araçuaí districts. *G&G*, Vol. 21, No. 1, pp. 3–19, <http://dx.doi.org/10.5741/GEMS.21.1.3>
- (1985b) Gem pegmatites of Minas Gerais, Brazil: the tourmalines of the Governador Valadares district. *G&G*, Vol. 21, No. 2, pp. 86–104, <http://dx.doi.org/10.5741/GEMS.21.2.86>
- Shinjo R., Kinjo K., Nakashima K., Imaoka T. (2017) Development of boron isotopic analysis of tourmaline by LA-MC-ICP-MS and its application to natural samples. Tourmaline 2017 International Symposium, Bystrice nad Pernštejnem, Czech Republic, June 23–28.
- Simmons W.B., Laurs B.M., Falster A.U., Koivula J.I., Webber K.L. (2005) Mt. Mica: A renaissance in Maine's gem tourmaline production. *G&G*, Vol. 41, pp. 150–163.
- Smith C.P., Bosshart G., Schwartz D. (2001) Gem News International: Nigeria as a new source of copper-manganese-bearing tourmaline. *G&G*, Vol. 37, No. 3, pp. 239–240.
- Tiepolo M., Bouman C., Vannucci R., Schwieters J. (2006) Laser ablation multicollector ICPMS determination of  $\delta^{11}\text{B}$  in geological samples. *Applied Geochemistry*, Vol. 21, No. 5, pp. 788–801, <http://dx.doi.org/10.1016/j.apgeochem.2006.02.014>

# U-Pb AGES OF ZIRCON INCLUSIONS IN SAPPHIRES FROM RATNAPURA AND BALANGODA (SRI LANKA) AND IMPLICATIONS FOR GEOGRAPHIC ORIGIN

Emilie Elmaleh, Susanne Theodora Schmidt, Stefanos Karampelas, Klemens Link, Lore Kiefert, Annette Süssenberger, and André Paul

Five sapphires from the secondary placer deposits of Ratnapura and Balangoda in Sri Lanka were classified as being of metamorphic/metasomatic/non-basalt-related origin based on trace-element analysis (LA-ICP-MS) and inclusion characterization. Two sapphires—one from each deposit—contained suitable zircon inclusions that were dated using the LA-ICP-MS method. They yielded U-Pb ages of approximately 549 Ma. The results suggest that the zircon enclosed in the sapphires probably formed in a high-temperature event at the end of the Precambrian granulite facies metamorphism of the ancient Gondwana continent and that this event coincides with the crystallization of the sapphires. The metamorphic character of these sapphires is confirmed from the trace-element composition as well as the solid- and liquid-phase inclusions.

Blue sapphire is one of the most appreciated gemstones, and its geographic-geological origin significantly affects its value. Most gem-quality sapphires are found in secondary placer deposits worldwide, and little is known about their crystallization in the geological environment. Although the geological context of gem-quality sapphires from secondary deposits is unknown, studying their geochemistry and the type of inclusions in combination with dating zircon inclusions could increase our understanding of their geological formation and geographic origin.

Zircon is probably the most powerful chronometer, since it can record peak temperature(s) but will generally survive post-cooling history (for a summary of zircon and its use as a geochronometer, see Hancher and Hoskin, 2003). Two independent clocks or radiogenic U-decay lines record the time elapsed starting with the crystallization of zircon. Complications arise if the zircon inclusion is zoned, displaying multiple growth events at different times. For

example, a zircon in a granitic magma chamber may have grown continuously during magmatic crystallization pulses, as indicated by oscillatory zoning (fine growth bands best viewed with cathodoluminescence), and then be eroded and washed into a sediment that is metamorphosed to high-grade metamorphic conditions. New zircon growth may occur around the former magmatic zircon under favorable conditions. The new zircon may recrystallize homogeneously, reflecting the metamorphic event of its formation. In the latter case, the U-Pb clock will be reset and the U-Pb dating of this inclusion in sapphire will provide age information about the crystallization event of the sapphire. In the case of dating an inherited detrital zircon—normally in the center of the crystal—the maximum age of sapphire crystallization obtained may be close to the actual crystallization age or a considerable interval away. Zircon inclusions are often reported from gem-quality sapphires (Coenraads et al., 1990; Sutherland et al., 1998a, 1998b, 2008, 2015; Link, 2015; Zeug et al., 2017). Zircon in sapphire has been dated in alkaline basalts of Australia's Central Province by Coenraads et al. (1990); from the Mercaderes–Rio Mayo area in southwest Colombia, related to northern Miocene Andean uplift and volcanism (Sutherland et al.,


See end of article for About the Authors and Acknowledgments.

GEMS & GEMOLOGY, Vol. 55, No. 1, pp. 18–28,

<http://dx.doi.org/10.5741/GEMS.55.1.18>

© 2019 Gemological Institute of America

**TABLE 1.** Characteristic gemological parameters of sapphires from Ratnapura and Balangoda, Sri Lanka.

Sample number	Form	Color	Weight (ct)	Dimensions (mm)	UV reaction
SASLR016 (Ratnapura)	 Rough with two polished windows	Light blue	1.323	8.72 × 2.8 × 5.28	SW: None LW: Weak orange
SASLR017 (Ratnapura)	 Rough with two polished windows	Light blue	1.235	7.86 × 2.36 × 6.66	SW: Weak yellowish (unpolished zone) LW: Very strong orange
SASLR019 (Ratnapura)	 Rough with two polished windows	Very light blue	1.321	6.9 × 3.7 × 5.3	SW: Weak yellowish LW: Strong orange
<b>SASLR050_01<sup>a</sup></b> (Ratnapura)	 Rough with two polished windows	Milky white to light purple-blue	2.218	13.84 × 2.32 × 5.9	SW: Weak yellowish LW: Weak orange
<b>SASLA01</b> (Balangoda)	 Rough	Violet to dark blue	n.d. <sup>b</sup>	n.d.	n.d.

<sup>a</sup>Samples in bold type contain dated zircon inclusions.

<sup>b</sup>n.d. = not determined

2008); from the New England sapphire fields in Australia (Abduriyim et al., 2012); from the Lava Plains area of northeast Australia, related to a complex interplay between initial metasomatized mantle involvement with infiltrations of felsic and mafic melts into the crustal levels (Sutherland et al., 2015); from the alkali basalt-related placers at Primorye in Russia (Akinin et al., 2017); and from Mogok and Madagascar (Link, 2015, 2016).

This study reports on the gemological and geochemical characteristics of Sri Lankan sapphires from the secondary deposits of Balangoda and Ratnapura, as well as the results of U-Pb dating of zircon inclusions in establishing some characteristic parameters for sapphire from these deposits. The sapphires were characterized by a combination of classical gemological methods such as solid and fluid inclusion study, polarized ultraviolet/visible/near-infrared absorption (UV-Vis-NIR) spectroscopy, Fourier-transform infrared (FTIR) spectroscopy, Raman spectroscopy, and geochemical methods such as laser ablation-inductively coupled plasma-mass spectrometry (LA-ICP-MS) for trace-element analysis and U-Pb dating.

## MATERIALS AND METHODS

Five rough sapphires (table 1) from the secondary placer deposits of Ratnapura and Balangoda were selected from the Gübelin Reference Stone Collection at the Gübelin Gem Lab (GGL). Samples SASLR016, SASLR017, SASLR019, and SASLA01 were acquired by GGL at the Ratnapura gem market in May 2005, while SASLR050\_01 was purchased directly at the Marapona mine in the mining area of Ratnapura in February 2009. One sapphire from Balangoda (SASLA01, violet to dark blue) and one from Ratnapura (SASLR050\_01, milky white to light purple-blue) presented zircon inclusions (>30 µm) suitable for U-Pb dating using LA-ICP-MS (table 1).

The sapphires were studied using a standard gemological microscope at GGL, and their specific fluorescence characteristics were monitored in a dark room (using 3 W lamps emitting 365 nm long-wave and 254 nm short-wave UV). Specific gravity was measured using the hydrostatic method. Mineral inclusions were identified using a Renishaw Raman 1000 spectrometer with an Ar<sup>+</sup> laser and a wavelength of 514 nm (without the use of a polarizer), connected

to a Leica DMLM optical microscope. The laser excitation used was from 10 to 15 mW, in confocal mode, with 20 to 50× magnification, from 200 to 2000 cm<sup>-1</sup> (three cycles with an acquisition time from 10 to 30 seconds). Rayleigh scattering was blocked by a holographic notch filter, and the backscattered light was dispersed on an 1800 groove/mm holographic grating with a 50 micron slit width (approximately 1.5 cm<sup>-1</sup> spectral resolution). The system was calibrated using a diamond and its single characteristic first-order band at 1331.8 cm<sup>-1</sup>, which designates its normal mode of vibration, usually referred to as LO=TO mode (longitudinal optical = transversal optical). LO and TO have the same frequency due to the high symmetry of the diamond lattice (Nasdala et al., 2005). UV-Vis-NIR absorption spectra were collected

## In Brief

- Sapphires from the secondary placer deposits of Balangoda and Ratnapura in Sri Lanka were gemologically classified as being of metamorphic/metasomatic/non-basalt-related origin.
- Dated zircon inclusions yielded U-Pb ages of approximately 549 Ma. The zircons probably formed in a high-temperature metamorphic event at the end of the Precambrian granulite facies metamorphism of the ancient continent of Gondwana.
- The sapphires probably crystallized during or at the end of this granulite facies metamorphism and are younger than sapphires from Madagascar.

in the range between 250 and 1000 nm using a Varian Cary 5000 UV-Vis-NIR spectrophotometer with diffraction grating polarizers. We used a data sampling interval and spectral bandwidth of 0.5 nm and a scan rate of 150 nm/min. FTIR absorption spectra were acquired from 6000 to 400 cm<sup>-1</sup> using a Varian 640 spectrometer with a resolution of 4 cm<sup>-1</sup> and 200 scans and a diffuse reflectance (DRIFT) accessory as the beam condenser. Trace-element analysis (Mg, Ti, V, Cr, Fe, and Ga) was performed on a Perkin Elmer ELAN DRC-e single collector quadrupole mass spectrometer combined with a 193 nm ESI Excimer gas laser ablation system. A set of three single-spot analyses (120 µm diameter) was collected on each sample using a laser frequency of 10 Hz, an ablation time of 50 seconds, and a laser energy of 6.2 J/cm<sup>2</sup>. The mass spectrometer performance was optimized to maximum intensities at U/Th ratios of ~1 and ThO/Th less than 0.3 using 16.25 liters per minute Ar plasma

gas, 0.88 L/min argon as nebulizer gas, and 1 L/min helium as sample gas. Multi-element NIST610 was used as the glass standard for external calibration; internal calibration was done by normalizing to 100% cations of stoichiometric corundum. The data reduction was carried out using an in-house spreadsheet following Longerich et al. (1996).

Zircon inclusions were carefully localized and cut with a special saw using a fine cord as a cutting blade. This cutting method allowed us to obtain the largest possible surface of the zircon crystals. Sapphires were embedded into a special epoxy to avoid degassing under vacuum. The zircons reached up to 120 µm in size. Cathodoluminescence images of zircon inclusions were obtained at the University of Geneva, with a JEOL JSM7001F scanning electron microscope. Acceleration voltage was 15 kV, probe current was 3.2 nA, and emission current was approximately 90 µA. Cathodoluminescence imaging is a powerful tool in identifying multiple growth zones in zircon related to different crystallization pulses during magmatic or metamorphic events.

The Raman spectrum of the dated zircon SASLR050\_01 was obtained at the University of Geneva using a confocal LABRAM spectrometer equipped with a green 532.12 nm Nd-YAG laser coupled to a charge-coupled device (CCD) detector and an optical microscope (Olympus BX51, 100× objective lens). The system was calibrated using a diamond and its single characteristic first-order band at 1331.8 cm<sup>-1</sup>. The parameters were: a spot diameter of 2.5 µm, a depth resolution of 5 µm, and a spatial resolution of <10 µm<sup>3</sup>. A laser power of 10 mW was used. The spectrum was acquired in the range from 200 to 1700 cm<sup>-1</sup> in three cycles with an acquisition time of 30 seconds.

U-Pb dating of zircon inclusions was carried out on an Element XR sector field ICP-MS (Thermo Fisher Scientific) interfaced to an UP 193-FX ArF 193 nm excimer ablation system (New Wave Research) at the University of Lausanne. Two spot analyses (diameter <25 µm) were carried out on one zircon inclusion in sample SASLA01 from Balangoda, and three spots were measured on two zircon inclusions in SASLR050\_1 from Ratnapura. The zircon samples GJ1 (<sup>206</sup>Pb/<sup>238</sup>U age 609.7 ± 1.8 Ma; Jackson et al., 2004) and Plešovice (<sup>206</sup>Pb/<sup>238</sup>U age 337.13 ± 1.8 Ma; Sláma et al., 2008) were used as external and secondary reference, respectively. The dwell time was 10 ms for <sup>207</sup>Pb, 8 ms for <sup>208</sup>Pb, 8 ms for <sup>235</sup>U, and 5 ms for all other masses. Laser pulse duration was approximately 5 ns, with a repetition rate of five pulses per

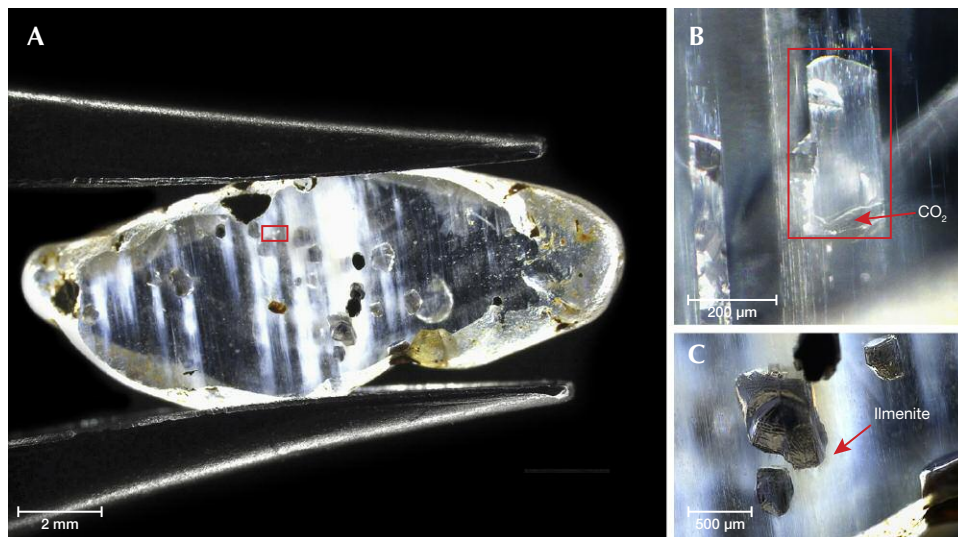


Figure 1. Sapphire SASLR050\_01 from Ratnapura (A) showed an abundance of inclusions such as CO<sub>2</sub> (B) and ilmenite (C).

second. The data reduction was done with LAMTRACE, a Lotus 1-2-3 spreadsheet written by Simon Jackson of Macquarie University in Sydney.

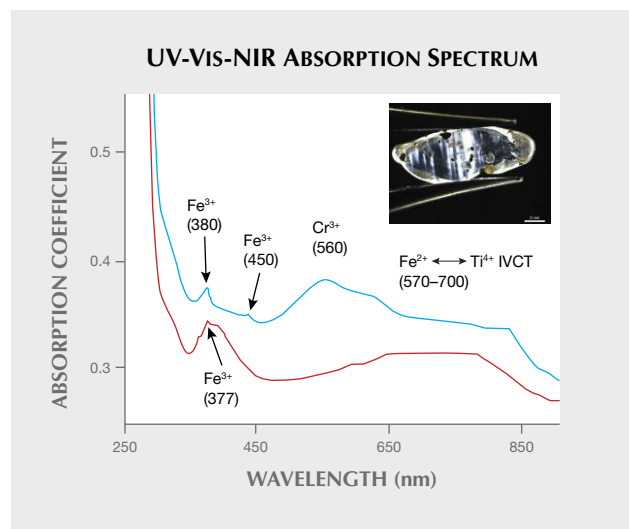
### GEMOLOGICAL PROPERTIES AND SPECTROSCOPY

Five rough to partially cut sapphires were selected from the Ratnapura and Balangoda deposits in Sri Lanka (figure 1A and table 1). They ranged in color from bluish white to blue and dark blue. Under short- and long-wave UV, they displayed a weak to strong reaction with yellow to orange colors. Their UV-Vis-NIR spectra showed a similar band distribution. In a representative UV-Vis-NIR spectrum of the sapphire from Ratnapura (SASLR050\_01), the absorption bands at 377, 380, and 450 nm (Ferguson and Fielding, 1971; Schwarz et al., 2000, 2008) are attributed to Fe<sup>3+</sup> (figure 2). In addition, the Cr<sup>3+</sup> absorption band was present at 560 nm (Schwarz et al., 2008). This sample also showed the broad Fe<sup>2+</sup>→Ti<sup>4+</sup> intervalence charge transfer band between 570 and 700 nm that is responsible for the blue color. We did not observe the pronounced band at around 800 nm, often attributed to the Fe<sup>2+</sup>→Fe<sup>3+</sup> intervalence charge transfer, ruling out a possible basalt-related origin (Schwarz et al., 2000; Kan-Nyunt et al., 2013; Emmett et al., 2017). Bands due to artifacts are also observed around 550 nm as well as at 600 nm due to Wood's anomaly, and at around 800 nm due to detector change.

**Solid- and Liquid-Phase Inclusions.** The Ratnapura samples contained abundant inclusions (figure 1), and a summary is given in table 2 for both deposits. The

importance of mineral inclusions and their link to the genesis of sapphire deposits has been emphasized by many studies, such as De Maesschalck and Oen (1989), Beran and Rossman (2006), Palanza et al. (2008), and Khamloet et al. (2014). FTIR analysis of samples from Ratnapura revealed hematite, carbon-

Figure 2. The UV-Vis-NIR absorption spectrum of sapphire SASLR050\_01 from Ratnapura shows absorption peaks characteristic for designated elements, the Fe<sup>3+</sup> bands at 377/388 nm and 450 nm, and the absorption band typical for Cr<sup>3+</sup> at 560 nm and the Fe<sup>2+</sup>-Ti<sup>4+</sup> intervalence charge transfer band (IVCT) between 570 and 700 nm. The two lines correspond to the fast ray (n<sub>e</sub>, in red) and the slow ray (n<sub>o</sub>, in blue) in corundum. The absorption coefficient  $\alpha = 2.303 A/d$ , where  $A$  is absorption and  $d$  is thickness in mm.





**TABLE 2.** Type of inclusions in Sri Lankan sapphire, as identified by FTIR and Raman spectroscopy.

Deposit	Hematite (FTIR)	Carbonate (FTIR)	Kaolinite (FTIR)	Boehmite (FTIR)	Ilmenite (Raman)	Zircon (Raman)	Spinel (Raman)	Graphite (Raman)	Apatite (Raman)	CO <sub>2</sub> fluid inclusion (FTIR and Raman)
Ratnapura	Present	Present	Present	Present	Present	Present	Present	Present	Present	Present
Balangoda	Present	Not identified	Present	Not identified	Not identified	Present	Not identified	Not identified	Present	Not identified

ate, kaolinite, boehmite, and CO<sub>2</sub> inclusions (figure 1B), which confirm the observations of De Maesschalck and Oen (1989) for Ratnapura. Zircon, apatite, spinel, ilmenite (figure 1C), and graphite were identified by Raman spectroscopy. Spinel, ilmenite, and CO<sub>2</sub> inclusions point to a medium- to high-grade metamorphic host rock. According to Beran and Rossman (2006), kaolinite-group minerals are the most common phases in turbid parts of corundum. Rakotondrazafy et al. (2008) observed the occurrence of quartz-free, kaolinite-bearing rocks hosting veins of sapphire in Andilamena, Madagascar. The occurrence of kaolinite might be related to the mineral paragenesis of the host rock, or it could reflect a late, low-temperature event after the formation of the sapphire.

**Raman Spectrum of Dated Zircon Inclusion.** The Raman spectrum of the dated zircon inclusion SASLA01 (Balangoda) in figure 3 indicates the main band positions for the molecular vibrational modes. The spectrum displays the typical  $\nu_3$  band near 1006 cm<sup>-1</sup>, which is considered to reflect the anti-symmetric stretching of the SiO<sub>4</sub> group (Dawson et al., 1971).

Its position near 1006 cm<sup>-1</sup> demonstrates the well-crystallized nature of this zircon crystal (Davies et al., 2015). The  $\nu_2$  band at 440 and 356 cm<sup>-1</sup> is related to bending vibration around the SiO<sub>4</sub> groups (Dawson et al., 1971). The  $\nu_1$  band near 973 cm<sup>-1</sup> is caused by the Si-O symmetric stretching band (Dawson et al., 1971). Generally, all of these bands are quite sharp—the  $\nu_2$  band at 356 cm<sup>-1</sup> has a FWHM of 13.6, and the  $\nu_3$  band near 1006 cm<sup>-1</sup> has a FWHM of 8.8—which is characteristic for crystalline material (Davies et al., 2015).

**Trace-Element Chemistry.** Trace-element geochemistry, in particular the elements Fe, Ti, Ga, Cr, Mg, and V, is used for discriminating the geographic origin and/or type of sapphire deposit—i.e., metamorphic, non-basalt-related versus basalt-related (e.g., Sutherland et al., 1998a,b, 2002; Schwarz et al., 2000, 2008; Saminpanya et al., 2003; Abduriyim and Kitawaki, 2006; Peucat et al., 2007; Giuliani et al., 2014). The results of the discriminating elements and ratios used in figure 4 are given in table 3.

The Fe content of the sapphires from Ratnapura ranges from 286 to 1213 ppmw, Ga content from 20

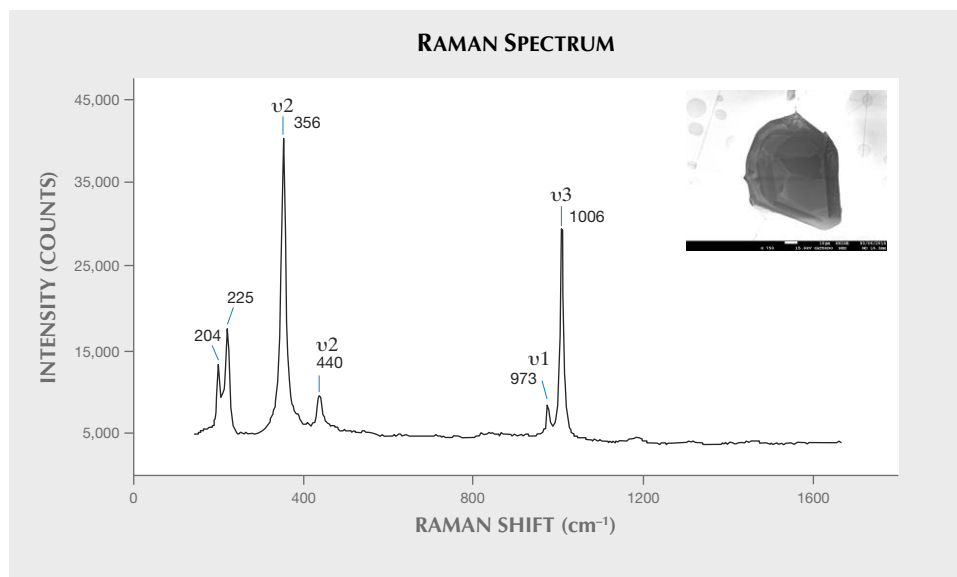


Figure 3. The Raman spectrum of a dated zircon inclusion in sample SASLA01 from Balangoda shows bands characteristic for well-crystallized zircon.

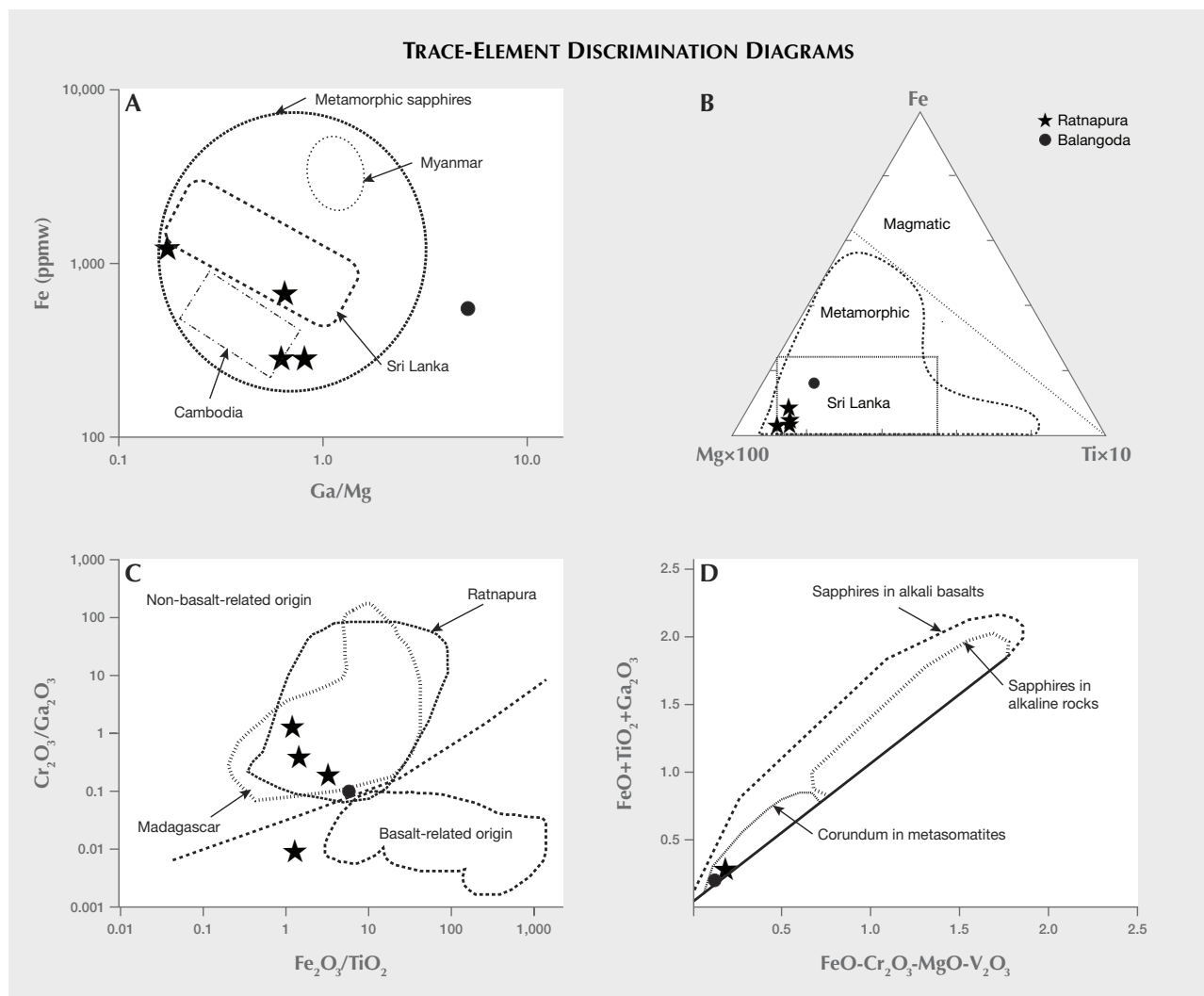


Figure 4. Trace-element discrimination diagrams for magmatic and metamorphic sapphires with the location of the analyzed gemstones. A and B: Compositional fields according to Peucat et al. (2007). C: Compositional fields according to Abduriyim and Kitawaki (2006). D: Compositional fields according to Giuliani et al. (2014).

to 99 ppmw, and Cr content from 2 to 102 ppmw. Ti shows a large variation from 92 to 253 ppmw, while V content measured between 14 and 70 ppmw. For the Balangoda sample, the following concentrations were obtained: 514 ppmw Fe, 110 ppmw Ga, 17 ppmw Cr, 42 ppmw Ti, and 6 ppmw V. These values lie within the range reported by Abduriyim and Kitawaki (2006).

The Ga/Mg ratio has been applied to classify metamorphic and magmatic deposits (Peucat et al., 2007). The value is generally high for magmatic and basalt-hosted sapphires (10 or much higher) and low for metamorphic and metasomatic ones (10 or much lower). Sapphires from Ratnapura display Ga/Mg ratios of 0.18 to 0.84 (table 3), coinciding with the value of 0.6 reported for a blue sapphire from Ratnapura by

Peucat et al. (2007). The Ga/Mg value of the sapphire from Balangoda was determined to be 5.03 (table 3). Both values lie within the range indicated for metamorphic sapphire. In figure 4A, Fe (ppmw) is plotted versus the Ga/Mg ratio and the field for metamorphic sapphire occurrences is outlined. Values for both analyzed deposits are located well within the field defined by Peucat et al. (2007) for metamorphic sapphires from Sri Lanka. In the Fe-(Ti × 10)-(Mg × 100) ternary diagram (figure 4B), the sapphires plot in the field for metamorphic sapphires, as well as in the area characteristic for Sri Lankan sapphires defined by Schwarz et al. (2008). In the Cr<sub>2</sub>O<sub>3</sub>/Ga<sub>2</sub>O<sub>3</sub> versus Fe<sub>2</sub>O<sub>3</sub>/TiO<sub>2</sub> diagram (Abduriyim and Kitawaki, 2006), three samples from Ratnapura plot within the com-

**TABLE 3.** Main discriminant elements (in ppmw) for Sri Lankan sapphires, as determined by ICP-MS analysis.

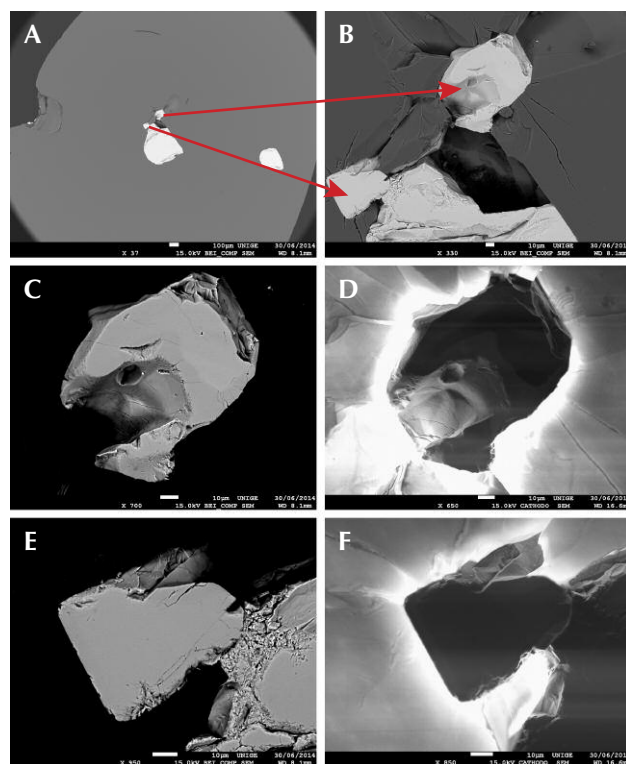
Sample number	Ti	V	Cr	Fe	Ga	Mg	Ga/Mg	Cr <sub>2</sub> O <sub>3</sub> /Ga <sub>2</sub> O <sub>3</sub>	Fe <sub>2</sub> O <sub>3</sub> /TiO <sub>2</sub>	TiO <sub>2</sub> /Ga <sub>2</sub> O <sub>3</sub>	Fe <sub>2</sub> O <sub>3</sub> /Cr <sub>2</sub> O <sub>3</sub>
SASLR016 (Ratnapura)	193	14	5	1213	20	114	0.18	0.27	4.84	11.86	205.4
SASLR017 (Ratnapura)	253	70	102	673	99	149	0.67	1.12	2.05	3.17	5.8
SASLR019 (Ratnapura)	92	16	2	286	46	55	0.84	0.04	2.4	2.45	163.5
SASLR050_01 (Ratnapura)	197	24	37	692	84	129	0.66	0.48	2.7	2.89	16.3
SASLA01 (Balangoda)	42	6	17	514	110	22	5.03	0.17	9.4	0.48	26.6

positional field for a non-basalt-related origin and another plots outside the field. The Balangoda sample plots within the Ratnapura field (figure 4C). When the samples are displayed in the FeO + TiO<sub>2</sub> + Ga<sub>2</sub>O<sub>3</sub> versus FeO-Cr<sub>2</sub>O<sub>3</sub>-MgO-V<sub>2</sub>O<sub>3</sub> diagram (Giuliani et al., 2014), they lie at the lower end of the field, characteristic for corundum in metasomatites (figure 4D).

**U-Pb Dating of Zircon Inclusions.** In characterizing the Sri Lankan sapphires (Elmaleh, 2015), one sample from Ratnapura (SASLR050\_01, figure 5) and one from Balangoda (SASLA01, figure 6) provided zircon inclusions ranging up to 120 μm in size that were suitable for dating with conventional LA-ICP-MS. Under the scanning electron microscope, the backscattered images of the polished surface of sapphire SASLR050\_01 (figure 5, A and B) are shown with its zircon inclusions observed in backscattered and cathodoluminescence mode (figure 5, C–F). The dated zircon inclusion in sapphire SASLA01 is shown in figure 6 in the scanning electron microscope (left), under cathodoluminescence (center), and with the craters of the LA-ICP-MS measurement (right). It showed sector zoning under cathodoluminescence and a small overgrowth along the rim that could not be dated due to its size of 10 μm (figure 6, center). Radial cracks around zircon inclusions were observed in the host sapphire of both deposits (figure 5, D and F). During cooling and decompression of the host rock, the zircon inclusion expands more rapidly than the enclosing sapphire crystal, resulting in stress along the wall and the formation of cracks in the host sapphire (Noguchi et al., 2013). Crack formation due to heating is considered very unlikely since the samples were purchased at the mine as rough sapphires and from reputable sources (at the mine or near the mine). In addition, the presence of inclusions such as kaolinite and boehmite, which degrade at relatively low temperatures, is a strong indication that the samples are unheated. In the concordia

diagram for the zircon inclusion in the Balangoda sapphire (SASLA01; see figure 7, left, and table 4 for results of zircon dating), the axes are defined by the

Figure 5. Sapphire SASLR050\_01 viewed with SEM as backscattered image (COMP, left column) or under cathodoluminescence (CATHODO, right column). A and B: Polished surface with zircon inclusions, and a close-up of the zone with the zircons. C and E: Zircons as backscattered images. D and F: Zircons from images C and E under cathodoluminescence. Both zircons show sector zoning that is known from metamorphic rocks and radial cracks emanating from the borders of the crystal into the sapphire.



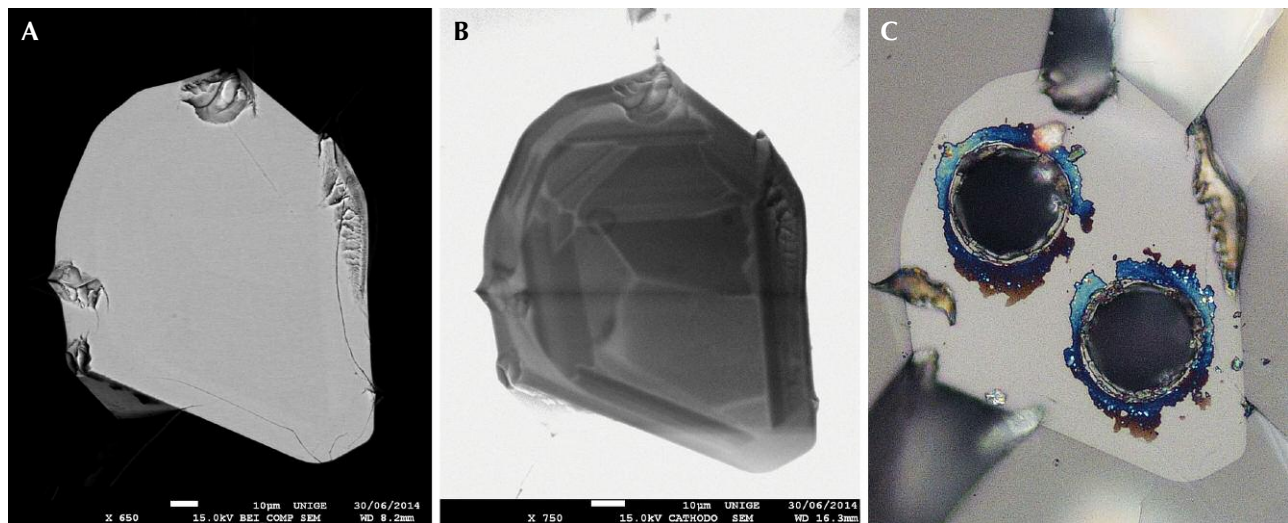
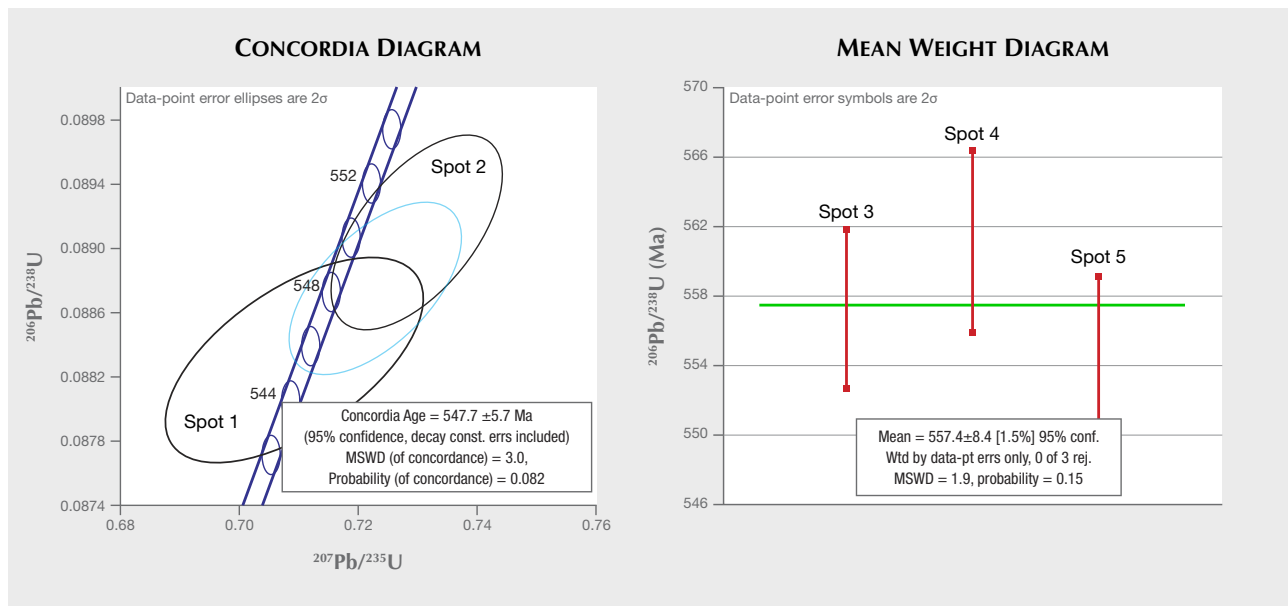


Figure 6. Sapphire SASLA01 from Balangoda contained a zircon inclusion, shown under SEM as backscattered image (left); under cathodoluminescence (center), displaying sector zoning that is typical in metamorphic rocks and a 10 µm overgrowth; and in reflected polarized light (right), with two ablation craters from ICP-MS analysis.

ratios of the radiogenic daughter Pb isotopes ( $^{206}\text{Pb}$  and  $^{207}\text{Pb}$ ) to their corresponding parent U isotopes ( $^{236}\text{U}$  and  $^{235}\text{U}$ ). At time zero, when the two U-Pb clocks were set or when the zircon formed, there was no radiogenic Pb in the zircon. Once the zircon was below

a critical temperature, radiogenic Pb ( $^{206}\text{Pb}$  and  $^{207}\text{Pb}$ ) would accumulate due to the decay of  $^{236}\text{U}$  and  $^{235}\text{U}$ . The ratios of  $^{207}\text{Pb}/^{235}\text{U}$  and  $^{206}\text{Pb}/^{238}\text{U}$  would increase with time, and by analyzing the appropriate isotopic ratios one can determine the age of the zircon inclu-

Figure 7. Left: concordia diagram for the zircon inclusion in sapphire SASLA01 from Balangoda. The two black ellipsoids represent two individual laser spot ages, while the blue ellipsoid is the calculated average concordia age. The concordia is drawn as a band depicting the uranium decay constant uncertainty and includes small ellipsoids; each concordia age tick represents one million years with its respective uncertainty. Right: Mean weight diagram for the zircon in sapphire SASLR050\_01 from Ratnapura. The three red vertical bars represent individual  $^{206}\text{Pb}/^{238}\text{U}$  ages in Ma with their associated uncertainty; the green horizontal line is the calculated mean age for the three values.



**TABLE 4.** Results of LA-ICP-MS and U-Pb dating for zircons in Sri Lankan sapphire.

Sample number	$^{206}\text{Pb}/^{238}\text{U}$		$^{207}\text{Pb}/^{235}\text{U}$		$^{207}\text{Pb}/^{206}\text{Pb}$		$^{206}\text{Pb}/^{238}\text{U}$		$^{207}\text{Pb}/^{235}\text{U}$		$^{207}\text{Pb}/^{206}\text{Pb}$	
	Ratio	$1\sigma^a$ (%)	Ratio	$1\sigma$ (%)	Ratio	$1\sigma$ (%)	Age (Ma)	$2\sigma$ (Ma)	Age (Ma)	$2\sigma$ (Ma)	Age (Ma)	$2\sigma$ (Ma)
SASLA01, sp 1 (Balangoda)	0.0883	0.59	0.7093	2.5	0.059	1.79	545.3	6.1	544.3	21.0	568.0	78
SASLA01, sp 2 (Balangoda)	0.0891	0.55	0.7299	1.6	0.0595	1.31	550.1	5.8	556.5	13.3	584.0	58
SASLR050_01, sp 3 (Ratnapura)	0.0903	0.43	0.7184	1.05	0.0584	0.96	557.3	4.6	549.7	8.4	544.0	42
SASLR050_01, sp 4 (Ratnapura)	0.0909	0.49	0.7165	0.7	0.0581	0.73	561.1	5.2	548.6	6.3	532.0	32
SASLR050_01, sp 5 (Ratnapura)	0.0898	0.47	0.7172	0.7	0.0587	0.65	554.1	5.0	549.0	6.2	554.0	28

<sup>a</sup> $\sigma$  = standard deviation

sion using the established equation with the decay constant for the corresponding decay series (e.g., Harley and Kelly, 2007). Two analyses were obtained on the same zircon inclusion (figure 5, right, with the ablation craters of sample SASLA01), and the Pb/U ratios (figure 7, left) correspond to a concordia age of  $547.7 \pm 5.7$  Ma (table 4).

A weighted mean diagram (figure 7, right) is used to determine the mean age from U-Pb analysis of the zircons in sapphire SASLR050\_01 from Ratnapura, since the analyses plot in the conventional concordia diagram above the concordia line. This may be related to an excess of radiogenic  $^{206}\text{Pb}$  or a loss of  $^{238}\text{U}$ . The younger range of uncertainty is then applied to approximate the crystallization age of zircon. In other words, the obtained age of 557 Ma should be reduced by the uncertainty of approximately 8.4 Ma, resulting in an age of approximately 549 Ma (table 4).

In summary, the U-Pb zircon ages obtained for the sapphires from Ratnapura and Balangoda show a similar crystallization age of around 549 Ma and are therefore probably related to the same metamorphic event (Elmaleh, 2015; Elmaleh et al., 2015a,b; Schmidt et al., 2017).

**Geological Considerations: Time of Sapphire Crystallization.** The Ratnapura and Balangoda deposits are located in the Highland Complex of Sri Lanka. The Highland Complex is part of an extensive Precambrian granulite belt of the ancient Gondwana continent related to the Pan-African evolution and comprising the Kerala Khondalite Belt in southern India, Madagascar, Mozambique, and Tanzania as well as the Lütz-Holm Bay area in Antarctica (Baur et al., 1991; Dissanayake and Chandrajith, 1999). Baur et al. (1991) systematically analyzed zircons of

the Central Highland in the granulite facies formation and concluded that localized charnockitization or the local influx of  $\text{CO}_2$ -enriched fluids are responsible for the granulite facies metamorphism. The main phase of granulite facies metamorphism is bracketed between approximately 660 Ma and 550 Ma and related to the Pan-African orogeny (Baur et al., 1991; Dissanayake and Chandrajith, 1999). In addition, Baur et al. (1991) record in their zircon population a younger event at  $547 \pm 35$  Ma, which they assign to a high-grade regional metamorphic event at the end of the granulite facies metamorphism. In a zircon inclusion in a pink sapphire of Madagascar, Link (2015) reports an age of  $652 \pm 41$  Ma and relates it to the Pan-African tectonic-metamorphic event, which occurred within a time window of 730–550 Ma (Black and Liegeois, 1993). This would indicate an earlier crystallization event of zircon in sapphire from Madagascar than from Sri Lanka, in line with the time windows for the regional high-grade metamorphic events in the respective areas.

Unfortunately, placer deposits do not provide sufficient information about the geological background. Nevertheless, the obtained ages for the zircons probably correspond to this granulite facies event. Evidence for a granulite facies metamorphism and a possible charnockitization comes also from the homogenization temperatures from primary  $\text{CO}_2$ -fluid inclusions in sapphire suggesting temperatures of  $>630^\circ\text{C}$  and pressures of 5.5 kbar, as reported from Balangoda by De Maesschalck and Oen (1989). The zircon in our sample from Balangoda displayed a small overgrowth that could not be dated, but could reflect a metamorphic event at the end of the granulite facies metamorphism or a post-metamorphic or post-tectonic event, which would make it younger than the dated core.

The sapphires probably crystallized during or at the end of the granulite facies metamorphism.

## CONCLUSIONS

The trace-element composition of the Sri Lankan sapphire samples, the presence of CO<sub>2</sub> inclusions, the radial cracks around the zircon inclusions, and the obtained zircon ages of approximately 549 Ma all support a metamorphic origin related to granulite facies metamorphism or a later metamorphic or magmatic event. The zircons probably crystallized during or at the end of the Precambrian granulite facies metamorphism of Gondwana related to the Pan-African evolution. They are younger than the zircons in sapphire from the Pan-African rocks of Madagas-

car. The zircon probably formed when the sapphire crystallized or shortly before. The determined ages of the zircon inclusions coincide or nearly coincide with the age of the sapphire crystallization within the host rock.

Dating zircon inclusions in individual sapphires using high-resolution SIMS, TIMS, or SHRIMP methods, detailed cathodoluminescence imaging, and characterization by Raman spectroscopy does increase our understanding of sapphire formation. However, it would be desirable to study sapphire and its geological context at the extraction site as well as investigate the pressure-temperature-time (*P-T-t*) conditions of sapphire formation directly on sapphire occurrences in high-grade metamorphic rocks.

### ABOUT THE AUTHORS

Ms. Elmaleh ([emilie\\_el@hotmail.com](mailto:emilie_el@hotmail.com)) is a former master's student at the University of Geneva, now responsible for quality management in an asbestos laboratory in Geneva. Dr. Schmidt (corresponding author, [susanne.schmidt@unige.ch](mailto:susanne.schmidt@unige.ch)) teaches metamorphic petrology and optical mineralogy at the University of Geneva. Dr. Karamelas is research director at the Bahrain Institute for Pearls & Gemstones in Manama, Kingdom of Bahrain. During this study, he was research scientist at the Gübelin Gem Lab in Lucerne, Switzerland. Mr. Link is head of development, and Dr. Kiefert is chief gemologist, at the Gübelin Gem Lab. Dr. Süssenberger is a postdoctoral research assistant at the University of Geneva studying metamorphic processes. Dr. Paul is a postdoctoral research assistant at the Grant Institute in Edinburgh investigating B isotope systematics.

### ACKNOWLEDGMENTS

This paper is part of the master's thesis of Emilie Elmaleh at the University of Geneva under the Joint Geneva and Lausanne School of Earth Sciences (ELSTE), supervised by Susanne Theodora Schmidt and Stefanos Karamelas. Ms. Elmaleh thanks the "Bourse August Lombard" at the University of Geneva and the Gübelin Gem Lab for financial support. We are also thankful to the Gübelin Gem Lab for making available its vast sapphire collection. This work would not have been possible without the excellent sample preparation by Jean-Marie Boccard at the University of Geneva. We also acknowledge the help of Agathe Martignier at the SEM facility at the University of Geneva and Federico Galster for support at the ICP-MS facilities at the University of Lausanne. We thank Sam Carmalt for correcting the English of our manuscript. The manuscript profited from a fruitful discussion with Joshua Davis and Jörn-Fredrik Wotzlaw (University of Geneva), as well as the helpful suggestions from three anonymous reviewers.

## REFERENCES

- Abduriyim A., Kitawaki H. (2006) Determination of the origin of blue sapphire using laser ablation inductively coupled plasma mass spectrometry (LA-ICP-MS). *The Journal of Gemmology*, Vol. 30, pp. 23–36, <http://dx.doi.org/10.15506/joG.2006.30.1.23>
- Abduriyim A., Sutherland F.L., Belousov E.A. (2012) U–Pb age and origin of gem zircon from the New England sapphire fields, New South Wales, Australia. *Australian Journal of Earth Sciences*, Vol. 59, No. 7, pp. 1067–1081, <http://dx.doi.org/10.1080/08120099.2012.724031>
- Akinin V.V., Vysotskiy S.V., Coble M., Aseeva A.V. (2017) U–Pb age and geochemistry of zircon inclusions in sapphire: Alkali basaltic source of gems in placers of Primorye. *Doklady Earth Sciences*, Vol. 476, No. 2, pp. 1173–1176, <http://dx.doi.org/10.1134/S1028334X17100129>
- Baur N., Kröner A., Liew T.C., Todt W., Williams I.S., Hofmann A.W. (1991) U–Pb isotopic systematics of zircons from prograde and retrograde transition zones in high-grade orthogneisses, Sri Lanka. *Journal of Geology*, Vol. 99, No. 4, pp. 527–545, <http://dx.doi.org/10.1086/629515>
- Beran A., Rossman G.R. (2006) OH in naturally occurring corundum. *European Journal of Mineralogy*, Vol. 18, No. 4, pp. 441–447, <http://dx.doi.org/10.1127/0935-1221/2006/0018-0441>
- Black R., Liegeois J.-P. (1993) Cratons, mobile belts, alkaline rocks and continental lithospheric mantle: The Pan-African testimony. *Journal of the Geological Society*, Vol. 150, No. 1, pp. 89–98, <http://dx.doi.org/10.1144/gsjgs.150.1.0088>
- Coenraads R.R., Sutherland F.L., Kinny P.D. (1990) The origin of sapphires: U–Pb dating of zircon inclusions sheds new light. *Mineralogical Magazine*, Vol. 54, pp. 113–122, <http://dx.doi.org/10.1180/minmag.1990.054.374.13>
- Davies J., Stern R., Heaman L., Rojas X., Walton E. (2015) Resolving oxygen isotopic disturbance in zircon: A case study from the low δ<sup>18</sup>O Scourie dikes, NW Scotland. *American Mineralogist*, Vol. 100, No. 8–9, pp. 1952–1966, <http://dx.doi.org/10.2138/am-2015-5221>
- Dawson P., Hargreave M.M., Wilkinson G.R. (1971) The vibrational spectrum of zircon (ZrSiO<sub>4</sub>). *Journal of Physics C, Solid State Physics*, Vol. 4, No. 2, pp. 240–256, <http://dx.doi.org/10.1088/0022-3719/4/2/014>
- De Maesschalck A.A., Oen I.S. (1989) Fluid and mineral inclusion

- in corundum from gem gravels in Sri Lanka. *Mineralogical Magazine*, Vol. 53, No. 373, pp. 539–545, <http://dx.doi.org/10.1180/minmag.1989.053.373.04>
- Dissanayake C.B., Chandrajith R. (1999) Sri Lanka-Madagascar Gondwana linkage: Evidence for a Pan-African mineral belt. *Journal of Geology*, Vol. 107, No. 2, pp. 223–235, <http://dx.doi.org/10.1086/314342>
- Elmaleh E. (2015) Blue Sapphires from Madagascar, Sri Lanka, Tanzania and Burma (Myanmar): Gemological, Chemical, Spectroscopic Characterization and Dating of Zircon Inclusions. Master's thesis, University of Geneva, 425 pp.
- Elmaleh E., Karamelas S., Schmidt S.T., Galster F. (2015a) Zircon inclusions in blue sapphire. *34th International Gemmological Conference*, Vilnius, Lithuania, August 26–30, pp. 51–52.
- Elmaleh E., Schmidt S.T., Karamelas S., Galster F. (2015b) Characterization of sapphire from Madagascar, Sri Lanka, Tanzania and Burma. *13th Swiss Geoscience Meeting*, Basel, November 20–21, p. 127.
- Emmett J.L., Dubinsky E.V., Hughes R., Scarratt K. (2017) Chapter 4: Color, Spectra & Luminescence. In R. Hughes, Ed., *Ruby & Sapphire: A Gemmologist's Guide*. RWH Publishing, pp. 90–148.
- Ferguson J., Fielding P.E. (1971) The origins of the colours of natural yellow, green, and blue sapphires. *Chemical Physics Letters*, Vol. 10, No. 3, pp. 262–265, <http://dx.doi.org/10.1071/CH9721371>
- Giuliani G., Caumon G., Rakotosamizanany S., Ohnenstetter D., Rakotondrazafy M. (2014) Classification chimique des corindons par analyse factorielle discriminante: application à la typologie des gisements de rubis et saphirs. *Revue de l'Association Française de Gemmologie*, Vol. 188, pp. 14–22.
- Hanchar J.M., Hoskin P.W.O., Eds. (2003) *Zircon*. Reviews in Mineralogy and Geochemistry, Vol. 53, Mineralogical Society of America, p. 500, <http://dx.doi.org/10.1515/9781501509322>
- Jackson S.E., Pearson N.J., Griffin W.L., Belousova E.A. (2004) The application of laser ablation-inductively coupled plasma-mass spectrometry to in situ U–Pb zircon geochronology. *Chemical Geology*, Vol. 211, No. 1–2, pp. 47–69, <http://dx.doi.org/10.1016/j.chemgeo.2004.06.017>
- Kan-Nyunt H.P., Karamelas S., Link K., Thu K., Kiefert L., Hardy P. (2013) Blue sapphires from the Baw Mar mine in Mogok. *G&G*, Vol. 49, No. 4, pp. 223–232, <http://dx.doi.org/10.5741/GEMS.49.4.223>
- Khamloet P., Pisutha-Arnond V., Sutthirath C. (2014) Mineral inclusions in sapphire from the basalt-related deposit in Bo Phloi, Kanchanaburi, western Thailand: indication of their genesis. *Russian Geology and Geophysics*, Vol. 55, No. 9, pp. 1087–1102, <http://dx.doi.org/10.1016/j.rgg.2014.08.004>
- Link K. (2015) Age determinations of zircon inclusions in faceted sapphires. *Journal of Gemmology*, Vol. 34, No. 8, pp. 692–700.
- (2016) Gem Notes: New age data for blue sapphire from Mogok, Myanmar. *The Journal of Gemmology*, Vol. 35, No. 2, pp. 107–109.
- Longerich P.H., Jackson E.S., Günther D. (1996) Inter-laboratory note. Laser ablation inductively coupled plasma mass spectrometric transient signal data acquisition and analyte concentration calculation. *Journal of Analytical Atomic Spectrometry*, Vol. 11, No. 9, pp. 899–904, <http://dx.doi.org/10.1039/JA9961100899>
- Nasdala L., Hofmeister W., Harris J.W., Glinnemann J. (2005) Growth zoning and strain patterns inside diamond crystals as revealed by Raman maps. *American Mineralogist*, Vol. 90, No. 4, pp. 745–748, <http://dx.doi.org/10.2138/am.2005.1690>
- Noguchi N., Abduriyim A., Shimizu I., Kamegata N., Odake S., Kagi H. (2013) Imaging of internal stress around a mineral inclusion in a sapphire crystal: Application of micro-Raman and photoluminescence spectroscopy. *Journal of Raman Spectroscopy*, Vol. 44, No. 1, pp. 147–154, <http://dx.doi.org/10.1002/jrs.4161>
- Palanza V., Di Martino D., Paleari A., Spinolo G., Prospero L. (2008) Micro-Raman spectroscopy applied to the study of inclusions within sapphire. *Journal of Raman Spectroscopy*, Vol. 39, No. 8, pp. 1007–1011, <http://dx.doi.org/10.1002/jrs.1939>
- Peucat J.J., Ruffault P., Fritsch E., Bouhnik-Le Coz M., Simonet C., Lasnier B. (2007) Ga/Mg ratio as a new geochemical tool to differentiate magmatic from metamorphic blue sapphires. *Lithos*, Vol. 98, No. 1–4, pp. 261–274, <http://dx.doi.org/10.1016/j.lithos.2007.05.001>
- Rakotondrazafy A.F.M., Giuliani G., Fallick A.E., Ohnenstetter D., Andriamamonjy A., Rakotosamizanany S., Ralantoarison Th., Razatseheno M., Offant Y., Garnier V., Maluski H., Dunai-gre C., Schwarz D., Mercier A., Ratrimo V., Ralison N. (2008) Gem corundum deposits in Madagascar: a review. *Ore Geology Reviews*, Vol. 34, No. 1–2, pp. 134–154, <http://dx.doi.org/10.1016/j.oregeorev.2007.05.001>
- Saminpanya S., Manning D.A.C., Droop G.T.R., Henderson C.M.B. (2003) Trace elements in Thai gem corundums. *Journal of Gemmology*, Vol. 28, pp. 399–415.
- Schmidt S.T., Elmaleh E., Karamelas S., Link K., Kiefert L., Süssnerberger A., Paul A. (2017) U–Pb ages of zircon inclusions in sapphire from Ratnapura and Balangoda (Sri Lanka). *Annual Meeting of the Geological Society of America 2017*, October 22–25, Seattle, Abstract 172–13.
- Schwarz D., Kanis J., Schmetzer K. (2000) Sapphires from Antsirana Province, northern Madagascar. *G&G*, Vol. 36, No. 3, pp. 216–233, <http://dx.doi.org/10.5741/GEMS.36.3.216>
- Schwarz D., Pardieu V., Saul J.M., Schmetzer K., Laurs B.M., Giuliani G., Klemm L., Malsy A.-K., Erel E., Hauzenberger C., Du Toit G., Fallick A.E., Ohnenstetter D. (2008) Rubies and sapphires from Winza, central Tanzania. *G&G*, Vol. 44, No. 4, pp. 322–347, <http://dx.doi.org/10.5741/GEMS.44.4.322>
- Sláma J., Košler J., Condon D.J., Crowley J.L., Gerdes A., Hanchar J.M., Horstwood M.S.A., A. Morris G.A., Nasdala L., Norberg N., Schaltegger U., Schoene B., Tubrett M.N., Whitehouse M.J. (2008) Plešovice zircon—A new natural reference material for U–Pb and Hf isotopic microanalysis. *Chemical Geology*, Vol. 249, No. 1–2, pp. 1–35, <http://dx.doi.org/10.1016/j.chemgeo.2007.11.005>
- Sutherland F.L., Hoskin P.W.O., Fanning C.M., Coenraads R.R. (1998a) Models of corundum origin from alkali basalt terrains: a reappraisal. *Contributions to Mineralogy and Petrology*, Vol. 133, No. 4, pp. 356–372, <http://dx.doi.org/10.1007/s004100050458>
- Sutherland F.L., Schwarz D., Jobbins E.A., Coenraads R.R., Webb G. (1998b) Distinctive gem corundum suites from discrete basalt fields: a comparative study of Barrington, Australia, and West Pailin, Cambodia, gemfields. *Journal of Gemmology*, Vol. 26, No. 2, pp. 65–85, <http://dx.doi.org/10.15506/joG.1998.26.2.65>
- Sutherland F.L., Graham I.T., Pogson R.E., Schwarz D., Webb G.B., Coenraads R.R., Fanning C.M., Hollis J.D., Allen T.C. (2002) The Tumbaramba Basaltic Gem Field, New South Wales: in relation to sapphire-ruby deposits of eastern Australia. *Records of the Australian Museum*, Vol. 54, No. 2, pp. 215–248, <http://dx.doi.org/10.3853/j.0067-1975.54.2002.1358>
- Sutherland F.L., Duroc-Danner J.M., Meffre S. (2008) Age and origin of gem corundum and zircon megacrysts from the Mercaderes–Rio Mayo area, South-west Colombia, South America. *Ore Geology Reviews*, Vol. 34, No. 1–2, pp. 155–168, <http://dx.doi.org/10.1016/j.oregeorev.2008.01.004>
- Sutherland F.L., Coenraads R.R., Abduriyim A., Meffre S., Hoskin P.W.O., Giuliani G., Beattie R., Wührer R., Sutherland G.B. (2015) Corundum (sapphire) relationships, Lava Plains gem fields, NE Australia: Integrated mineralogy, geochemistry, genesis and geographical typing. *Mineralogical Magazine*, Vol. 79, No. 3, pp. 545–581, <http://dx.doi.org/10.1180/minmag.2015.079.3.04>
- Zeug M., Vargas A.I.R., Nasdala L. (2017) Spectroscopic study of inclusions in gem corundum from Mercaderes, Cauca, Colombia. *Physics and Chemistry of Minerals*, Vol. 44, No. 3, pp. 221–233, <http://dx.doi.org/10.1007/s00269-016-0851-4>

# The Dr. Edward J. Gübelin Most Valuable Article AWARD

## First Place

### THE COLOR ORIGIN OF GEM DIASPORE: CORRELATION TO CORUNDUM

WINTER 2018

Che Shen and Ren Lu

**Che Shen** is a graduate student at the Gemmological Institute, China University of Geosciences in Wuhan. In 2018, he was a research intern at the Gemmological Institute of America in Carlsbad, California. **Ren Lu** is a distinguished professor at the Gemmological Institute, China University of Geosciences in Wuhan. He received his PhD from the University of California, Davis.



Che Shen



Ren Lu

## Second Place

### GEMOLOGICAL CHARACTERISTICS OF SAPPHIRES FROM YOGO GULCH, MONTANA

SUMMER 2018

Nathan D. Renfro, Aaron C. Palke, and Richard B. Berg

**Nathan Renfro** is manager of colored stones identification at GIA in Carlsbad, California. He earned a bachelor's degree in geology from Appalachian State University in Boone, North Carolina. **Aaron Palke** is a senior research scientist, also at GIA in Carlsbad. He holds a PhD in geology from Stanford University. **Richard Berg** is research professor and curator emeritus of the Mineral Museum at Montana Technological University in Butte. He earned his PhD at the University of Montana.



Nathan Renfro



Aaron Palke



Richard Berg

## Third Place

### NATURAL-COLOR GREEN DIAMONDS: A BEAUTIFUL CONUNDRUM

SPRING 2018

Christopher M. Breeding, Sally Eaton-Magaña, and James E. Shigley

**Christopher M. Breeding** is a senior research scientist and manager at GIA in Carlsbad, where he investigates origin of color in diamond and other gems. Dr. Breeding, who is a co-editor of *G&G's* Gem News International section, holds a PhD in geology from Yale University. **Sally Eaton-Magaña** is a senior research scientist at GIA in Carlsbad, where she investigates the physics of natural, treated, and synthetic diamonds. Dr. Eaton-Magaña received her PhD in chemical engineering from Case Western Reserve University in Cleveland, Ohio. **James E. Shigley** is distinguished research fellow at GIA in Carlsbad. He is the author of numerous articles on diamonds and colored gemstones. Dr. Shigley holds a PhD from Stanford University.



Christopher Breeding



Sally Eaton-Magaña



James Shigley

Many thanks to all the readers who voted. In addition to our winning authors, we congratulate **Cristina Grossi of Milan**, whose name was randomly drawn from the entries to win a one-year subscription to *G&G*.



# THE TALISMAN OF CHARLEMAGNE: NEW HISTORICAL AND GEMOLOGICAL DISCOVERIES

Gerard Panczer, Geoffray Riondet, Lauriane Forest, Michael S. Krzemnicki, Davy Carole, and Florian Faure

The gem-bearing reliquary known as the Talisman of Charlemagne is closely associated with the history of Europe. Its legend follows such figures as Charlemagne, Napoleon I, Empress Josephine, Hortense de Beauharnais, Napoleon III, and Empress Eugénie. This study provides new historical information collected in France, Germany, and Switzerland about the provenance of this exceptional jewel, which contains a large glass cabochon on the front, a large blue-gray sapphire on the back, and an assortment of colored stones and pearls. The first scientific gemological analysis of this historical piece, carried out on-site at the Palace of Tau Museum in Reims, France, has made it possible to identify the colored stones and offer insight into their possible geographic origins. Based on our data and comparison with similar objects of the Carolingian period, we propose that the blue-gray sapphire is of Ceylonese (Sri Lankan) origin, that the garnets originate from India or Ceylon, and that most of the emeralds are from Egypt except for one from the Habachtal deposit of Austria. The estimated weight of the center sapphire is approximately 190 ct, making it one of the largest known sapphires as of the early seventeenth century.

The Talisman of Charlemagne is a sumptuous jewel that has passed through the centuries. At various times it has been said to contain fragments of the hair of the Virgin Mary and a remnant of the True Cross. It is therefore a reliquary, a container in which sacred relics are kept. Its globular shape resembles that of a pilgrim's small bottle or eulogy ampulla, which were filled with earth or liquid from a holy place (Gaborit-Chopin and Taburet, 1981; Scordia, 2012). The talisman's romantic fate is intertwined with many historical figures involved in its passage through Germany, France, and Switzerland. This first gemological characterization was conducted during two rounds of analysis, lasting one day each, in May 2017 and June 2018.

## HISTORICAL BACKGROUND

**Origin of the Talisman of Charlemagne.** As the origin of the reliquary has been lost in the mists of time since the Carolingian period, it is difficult to specify the circumstances of its creation. Charlemagne died in the imperial capital of Aachen (known as Aix-la-

Chapelle in French) on February 28, 814 CE. Since the emperor did not leave specific instructions, his entourage decided to bury him in Aachen Cathedral (Minois, 2010). The talisman was believed to have been suspended from a necklace worn on Charlemagne's body in his tomb, though it has not been possible to prove this. Eginhard (770–840 CE), in his biography *Vita Karoli Magni* (*The Life of Charlemagne*), written shortly after the emperor's death, does not mention the reliquary. While the talisman's characteristics are slightly different from the works that can be dated with certainty to the reign of Charlemagne, considering the shape of the jewel and its typical Carolingian goldsmithery (gold buttons, palmettes, filigree, and *repoussé* work), the experts on this period, De Montesquiou-Fezensac (1962) and Gaborit-Chopin and Taburet (1981), attested with confidence a dating to the middle to late ninth century (i.e., just after the reign of Charlemagne, excluding any forgery).

The exhumation of Charlemagne conducted in the year 1000 by Otto III, the Holy Roman Emperor, was chronicled by Thietmar, bishop of Merseburg around 1012–1018:

Ignoring the exact place where the bones of Emperor Charles lay, [Otto III] secretly broke the ornamental tiling of the church where they were supposed to be,

See end of article for About the Authors and Acknowledgments.

GEMS & GEMOLOGY, Vol. 55, No. 1, pp. 30–46,  
<http://dx.doi.org/10.5741/GEMS.55.1.30>

© 2019 Gemological Institute of America



Figure 1. Details of two engravings, published by Gerhard Altzenbach (left, British Museum, Q5.375, 1664) and from Jacobus Harrewijn (right, 1711), both representing the treasury of Aachen Cathedral. A stylized Talisman of Charlemagne appears in the center, as number 15 (left engraving) and number 11 (right engraving). Represented on the right engraving: (4) a piece of the rope with which Jesus was bound, (5) a piece of the Holy Cross, (6) a statue of the Virgin Mary, (10) a portrait of the Virgin Mary according to St. Lucas, (11) hairs of the Virgin Mary, (12) the right arm of Charlemagne, (16) St. Charlemagne's bust, (17) his hunting horn and sword, and (18) relics of the sanctuary.

then dug until discovering them in a royal sarcophagus. He took for himself the golden cross that hung around the corpse's neck and a part of his not yet putrefied clothes; after which he put everything back in place with the utmost respect. (Thietmar of Merseburg, 2001)

This text is too imprecise to establish a link with the reliquary. The body of Charlemagne was exhumed again in 1166 for his canonization by order of the Holy Roman Emperor Frederick Barbarossa (Gobry, 1997). Once again, no information was given about a reliquary.

The list of relics of Aachen was mentioned in manuscripts written circa 1200, based on original documents from the ninth century. While the original documents have been lost, some elements of these secondary sources have been copied in more recent manuscripts deposited at the Berlin State Library and the University of Bonn in Germany (Quix, 1840; Schiffers, 1937). We find in particular the mention of the hair of the Virgin Mary.

The booklet of the relics of Aachen (Montesquiou-Fezensac, 1962), *Heiltumsbüchlein* in German, was produced circa 1520. Intended for the pilgrims, it is more accurate and does mention a reliquary: *Quoddam cleinodium, continens de capillis et lacte beatae Mariae Virginis* ("A precious jewel, container of hairs and milk of the Saint Virgin Mary"). This brief description of the "precious jewel"

could correspond to the Charlemagne reliquary, during a period when the preserved relics were much more important than the reliquary itself.

It was not until the seventeenth century that engravings of the reliquary began to appear. One of the first was by Abraham Hogenberg, in Noppius (1632), in which the talisman was shown with the other relics from the treasury of Aachen Cathedral. The engraving is accompanied by the words *Capilli B. virginis Mariae*: "the hair of the Virgin Mary." Later engravings of the relics, especially by the engravers Gerhard Altzenbach (1664) and Jacobus Harrewijn (1771), were reproduced in various works during the seventeenth and eighteenth centuries. On all of these engravings the talisman is stylized, with a center stone surrounded alternately by four faceted stones and four cabochons (figure 1). Pearls, which appeared in later engravings between each stone pair, are not visible. Pöllnitz (1736) also gave an illustrated representation. Subsequent descriptions are more precise, as in de Barjolé (1786), who notes: "The hair of the Blessed Virgin. They are enshrined in a Golden Reliquary, lined with precious stones."

**Early Nineteenth Century: From the Reliquary to the "Talisman of Charlemagne."** During the French Revolution (1789–1799), the relics from Aachen Cathedral were taken to the German city of Paderborn.

After the revolution, Aachen became the administrative headquarters of the Roer department in 1802 and acquired French status. Relics that had been displaced in 1794 were restored to Aachen Cathedral (Kleinclausz, 2005). Napoleon, crowned emperor on May 18, 1804, considered himself the heir to Charlemagne and decided to visit the tomb of his great predecessor. Empress Josephine preceded him to Aachen in July 1804. In August, Marc-Antoine Berdolet, nominated bishop of Aachen by Napoleon two years earlier, offered the emperor the reliquary (Minois, 2010). Newspapers of the time such as the *Moniteur*, the *Gazette de France*, and the *Journal du Commerce* attest to this gift, as does a message written

## In Brief

- The Talisman of Charlemagne is a sumptuous jewel covered in gemstones and dating to the middle to late ninth century, just after the reign of Charlemagne.
- Using portable spectroscopy equipment, the authors characterized the 29 gemstones and propose that all but one of the almandine-pyrope garnets originated from southern India or Ceylon, while all but one of the emeralds were from Egypt and the sapphires were from Ceylon.
- The substitution of the front center gemstone by the cobalt-doped glass cabochon probably occurred in the late eighteenth century and certainly before 1843.
- The center sapphire has an estimated weight of 190 ct and can be considered the largest sapphire used in European jewelry during the Early to High Medieval period.

by the bishop and addressed to the empress dated 23rd Thermidor, year XII (i.e., August 11, 1804). An excerpt reveals the presence of

a small round reliquary made of pure gold adorned with stones, the bulb of which contains relics, and the large stones in the middle contain a small cross made of the wood from the holy cross. These two small reliquaries were found around the neck of St. Charlemagne when his body was exhumed from his sepulcher in 1166, and history tells us that Charlemagne was accustomed to wear these same relics during battles. (Lohmann, 1924)

This message suggests that at the time the talisman preserved several relics.

From this point on, the relevant texts no longer mention the Virgin Mary's hair in the reliquary. It is therefore possible that between 1801 and 1804 the bishop had removed all or part of the relic and re-

placed it with a small wooden cross consisting of two fragments—supposedly from the True Cross—fastened by a thread. An examination carried out in the 1960s by Bernard Gomond, a specialist in ornamental trimmings, identified the thread as raw Tussar silk from India, used between the late eighteenth and late nineteenth centuries.

The rest of the reliquary's history is much more precise. After her divorce from Napoleon, Josephine de Beauharnais remained its custodian (Ollivier, 1897). The talisman was her personal property and not part of the crown jewels of France. At Josephine's death in 1814, her daughter, Hortense de Beauharnais, inherited the talisman. Hortense's memoirs, written during exile after the fall of the Empire, described the reliquary:

My mother had gone to take the waters at Aachen.... The Emperor, on his arrival in the city, was received with the greatest enthusiasm. The city was grateful to him for having brought back the relics which, since Charlemagne, had made the glory of Aix-la-Chapelle. The chapter and the city believed they could not better prove their gratitude than to offer to the one whom they regarded as a new Charlemagne an object which had belonged to their glorious founder. It was a talisman that Charlemagne always wore in combat and that was still found at his collar when his tomb was opened in the year.... I still possess all these objects.

Besides being Napoleon's stepdaughter, Hortense was also the emperor's sister-in-law following her marriage to Louis Bonaparte, king of Holland (r. 1806–1810). As such, she became the guardian of the Napoleonic legacy.

At the Arenenberg estate on Lake Constance in Switzerland, Hortense received many visitors, including Alexandre Dumas père (Baylac, 2016). In his 1833 book *Impressions de voyage en Suisse*, which includes historical chronicles, a journey log, and ethnological considerations, the great writer describes the reliquary. This is the first known use of the term *talisman* for this object:

It is now the Talisman of Charlemagne; this talisman has quite a story; lend your ear. When the tomb in which the great Emperor had been buried was opened at Aachen, his skeleton was clothed in his Roman clothes, and his talisman, which made him victorious, was suspended from his neck. This talisman was a piece of the True Cross sent to him by the Empress. It was enclosed in an emerald, and this emerald was suspended by a chain to a large ring of gold. The citizens of Aix-la-Chapelle gave it to Napoleon when he entered their city, and Napoleon, in 1813, tied this chain round the neck of Queen Hortense, confessing to her that, the day of Austerlitz and of Wagram, he had carried it on his breast, as Charlemagne had done nine hundred years ago.



*Figure 2. Felix Cottreau's 1834 portrait of Hortense de Beauharnais, wearing the talisman with the front side facing out. This scene put the spotlight on the talisman, which most certainly was never modified to be worn as a cloak clasp. Courtesy of Napoleon Museum Thurgau.*

This romantic description of the talisman by Dumas contributed to its mystery and notoriety. Nineteenth-century texts on the origin of the talisman must be regarded with caution, but these beliefs about the amulet were shared by the imperial family (Paléologue, 1928).

The Napoleon Museum in the castle of Arenenberg preserves an 1834 portrait by Felix Cottreau of Queen Hortense “wearing” the reliquary as a cloak clasp (figure 2). Instead of the chain we know today, the reliquary

depicted on this painting is connected to several elements, including two ovals adorned with gems and a cloak clasp, a clothing fastener commonly used in the eighteenth and nineteenth centuries in place of buttons. These elements are most certainly the fruits of the artist's imagination, since no other representation or description of the talisman reports that it was modified to be worn as a cloak clasp, and since the present-day regular chain appears in the previous seventeenth and eighteenth centuries engravings (again, see figure 1).

**The Talisman of Charlemagne from Napoleon III to Today.** Queen Hortense passed down the Arenenberg estate and its possessions to her son Prince Louis Napoleon Bonaparte, the future Napoleon III. Sentenced to life imprisonment following his failed coup attempt in 1836, he was a prisoner at Fort de Ham in the Somme until 1846. After selling the Arenenberg castle in 1843, he also sought to sell precious objects such as the reliquary. In a letter to his first cousin, Prince Jerome Napoleon, he valued the reliquary at 150,000 francs (Guériot, 1933), though the sale did not go through (Maison, 1991). A drawing of the reliquary signed by Prince Louis Napoleon (figure 3) dates from this period. The text above the drawing is a rewritten copy of the 1804 description by Berdolet, the Bishop of Aachen. Below the talisman is an updated characterization of the center stone as a “rough sapphire” with a “very light color,” as translated below:

Talisman of Charlemagne, which antique dealers believe was sent to Charlemagne by the Empress Irene [of Constantinople, 752–803 CE]. This talisman was given to the Emperor Napoleon at Aix la Chapelle by the Clergy as attested by the above copy of the Bishop's letter. The middle stone is a rough sapphire and has a very light color.

A year later, an engraving of the reliquary appeared in the newspaper *L'Illustration* (“Talisman de Charlemagne,” 1844). The article contained inaccurate rumors that had been circulating since the beginning of the nineteenth century, namely that Charlemagne “constantly wore” the talisman and that the Abbasid caliph Harun al-Raschid had given it to him:

The drawing above represents, in its natural size, an object of immense interest, both archeologically and religiously. It was the talisman that Charlemagne constantly wore on him, which was found hanging around his neck when his sepulcher was opened in 1166, and which was given to Emperor Napoleon by the clergy of Aix-la-Chapelle on the 23rd Thermidor Year XII... At the end of the eighth century, there were only two great sovereigns in the world, Charlemagne and Haroun-al-Raschid... it was offered with the keys of the holy sepulcher.

The exchange of diplomatic gifts with the East was a common practice in the Carolingian period. Charlemagne and the caliph are said to have exchanged several ambassadors, but no archival source authenticates the gift of this jewel. Nevertheless, several newspapers reproduced this account and the engraving, including the *Illustrated London News* in 1845 and *The New Illustrated* in 1866. A more complete article was written by Sir Martin Conway for *The Antiquaries Journal* in 1922.

Prince Louis Napoleon became Emperor Napoleon III and grew attached to the talisman, keeping it until his death in 1873. During the Second French Empire, from 1852 to 1870, it resided in his room in the Tuileries Palace (Clouzot, 1925). A reliquary box was even made for it in 1855 by the Parisian goldsmith Froment-Meurice. In 1866, Charles Clément, deputy curator at the Louvre, appraised the reliquary at the emperor's request. His appraisal indicated that three stones were missing: one emerald and two pearls (Taralon, 1966). That same year, the note was reproduced with engravings (realized from three photos taken in 1866 and provided by Napoleon III) by the German historian and archaeologist Ernst Aus'm Weerth (1866; see figure 4, bottom):

This reliquary, preserved in the Treasury of Aachen, was offered by the city of Aix-la-Chapelle with other relics to Emperor Napoleon I during the coronation. He then presented it to Empress Josephine. At her death it passed to Queen Hortense, and now belongs to her [Josephine's] grandson Napoleon [III]. Two large sapphire cabochons, one oval and the other square, enclose a cross made of wood of the true cross; it is only seen on the side of the oval sapphire. It is invisible on the side of the rough cabochon.

At the fall of the Second French Empire in 1870, the talisman's pedigree remained unclear. Some believe it was hidden in a subterranean passage connecting the two houses of Baugrand, the crown jeweler, in Etretat (Lindon, 1949). According to the Duke of Alba, the empress handed the talisman to a Dr. Conneau, who hid it in a wall of his house. The doctor was later able to return it to the empress in England. Napoleon III was known to keep it in his bedroom while in exile (Anceau, 2008). A painting by George Goodwin Kilburne depicts this room, where the emperor met his death in 1873. The painting's precision makes it possible to identify certain details such as the reliquary box crafted in 1855 by Froment-Meurice. Empress Eugénie, the widow of Napoleon III, resisted the solicitations of Kaiser William II to return it to Aachen (Maison, 1991). Moved by the fire of the Cathedral of Reims during World War I, she donated it before her death to the Archbishop of Reims, Cardinal Luçon, on the advice of Dom Cabrol, Abbot of Farnborough (Taralon, 1966). In *Paléologue* (1928), she recounts this episode:

This talisman, I held it as the apple of my eyes; I had it near my bed while I was giving birth to the Imperial Prince. But since 1879, since I no longer have a direct heir, a question arose for me, a question which troubled me very much: After my death, what would become of the relic? Many times, under one pretext or another,



Figure 3. A drawing believed to be from 1843 or 1844, showing the front of the reliquary, with a copy of the description by Berdolet, the Bishop of Aachen (1804), and an inscription by Prince Louis Napoleon (later Napoleon III). Courtesy of Napoleon Museum Thurgau.

the Archbishop of Cologne and the Chapter of Aix-la-Chapelle had begged me to restore it to the Carolingian treasury: I had obstinately refused. Then, in my lifetime, I thought of giving it to Pope Leo XIII, in memory

of Pope Leo III, by whom Charles was crowned emperor, in the basilica of St. Peter, in front the tomb of the Apostles, Christmas night 800... But I have reflected that sooner or later the people of Cologne and

Aix-la-Chapelle would obtain from an accommodating Pope the restitution of the jewel; for strictly, theologically, there is no prescription for relics... So I was very perplexed when the war of 1914 broke out. The horror of the bombardment of Reims suddenly illuminated me. One fine morning I exclaimed: "It is at Reims that I shall leave the Talisman of Charlemagne, and it will be the punishment for the barbarians!" I had, beside me, the person most capable of advising me in this respect, the very erudite Abbé de Farnborough, Dom Cabrol. He studied the legal means to accomplish the donation and managed to find formulae such that in no event could the French government, the Archbishop of Reims or even the Holy See ever remove the Talisman from the reliquary of our kings. Cardinal Luçon having acquiesced in all the clauses, Dom Cabrol handed over to him last Sunday the famous pendant.

The reliquary was turned over to Cardinal Luçon by Dom Cabrol on November 30, 1919, according to Daudet (1922) in *L'inconnue*. With the gift, the following statement was issued:

The formal wish of the Empress is to give to the Cathedral of Reims, in reparation for the outrages it suffered during the war 1914–1918, of this relic and the reliquary which contains it, so that they remain forever the property of the church of Reims, with the duty for the Archbishop of Reims to take whatever measures he deems necessary to achieve this end.

The empress died the following year in Madrid. In her will, she bequeathed 100,000 francs for the reconstruction of the Cathedral of Reims. In 1927, the reliquary became the property of the Diocesan Association of Reims. It was classified as a historical monument in 1962 and deposited five years later in the treasury of the Palace of Tau in Reims, where it remains on permanent display. In 1964, the famous goldsmiths Lucien and Jean-Claude Toulouse restored the talisman under the supervision of Jean Taralon, General Inspector of Historical Monuments. During the restoration, two missing pearls and one emerald were replaced, as indicated by Taralon (1966). All known photos of the talisman taken thereafter, by Henri Graindorge (1964), Hélène Guillot (1964), Claude François Garnier (1965), and Louis André and Denis Cailleaux (1985), present the talisman in its current form and with the same small chain (seen in figures 3 and 4). Unfortunately, the only photographs from before the restoration, taken in 1866 and circa 1915 by Henri Deneux, lack sufficient resolution to show the missing stones.

## METHODS OF ANALYSIS

It is only rather recently that items of historical jewelry have been analyzed on-site using spectroscopic methods that are portable and compact (Häberli, 2010;

Barone et al., 2014; Jeršek and Kramar, 2014; Reiche et al., 2014; Farges et al., 2015). Often these are the only analytical methods possible when cultural treasures cannot be moved from their location, such as a museum or historical site. The drawback is that the results are not as complete as those that could be obtained in the laboratory or on uncut stones.

For the Talisman of Charlemagne, we used conventional gemological tools: electronic balance, microscope, polariscope, and ultraviolet lamp. Due to the stones' size and position in the setting, their refractive indices could not be determined. To gain additional data, we further analyzed the talisman using portable spectroscopic techniques, namely Raman scattering and visible/near-infrared (Vis-NIR) optical absorption spectroscopy at room temperature. We used two compact Raman spectrometers (Ocean Optics QE 65000) with 532 and 785 nm laser excitation. The absorption spectrum in the visible to near-infrared range (400–1000 nm) was recorded with an Ocean Optics USB2000 spectrometer. A Niton XL3T GOLDD+ portable X-ray fluorescence (XRF) analyzer was used to estimate the chemical composition (elements heavier than Na) of the various gemstones using a 3 mm collimator. The predefined "mining" setup mode and the NIST610 and 612 glass standards were used as references to control the calibration. It must be mentioned that quantification of Mg by XRF can be challenging, as its detection limit is quite high. The average detection limits of the analyzed elements were: 6500 ppmw Mg, 2500 ppmw Al, 1500 ppmw Si, 110 ppmw Ca, 100 ppmw Co, 85 ppmw Mn, 60 ppmw Ti, 45 ppmw Ba, 35 ppmw Cr, 35 ppmw Fe, 35 ppmw V, 20 ppmw Au, 10 ppmw Pb, 5 ppmw Y, 5 ppmw Ga, and 3 ppmw Rb.

## RESULTS OF THE ANALYSIS

**Macroscopic Observations.** The talisman is a gold reliquary, in the form of a eulogy ampulla, composed of two circular parts joined together by a band of gold. It measures 6.5 cm wide, 7.3 cm tall, and 3.50 cm in thickness (the thickest point at the centers of the two center stones). The surface includes filigree and *re-poussé* work. Its total mass is 160.45 g (an estimated 7 g from the chain). The front side is dominated by a large bluish cabochon surrounded by nine colored stones (numbered V1 to V9 in figure 4) alternating with eight pearls. This is the face most often seen in artistic representations of the talisman. It is also the face that reveals by magnifying effect through the cabochon the supposed fragments of the True Cross mounted in the shape of a cross. The reverse side



Figure 4. Left to right: Present-day photos of the front, back, and side of the talisman (top) compared with engravings (bottom) from Ernst Aus'm Weerth (1866). V1, V3, V5, V7, V9, S1, S3, S7, S9, P1, and P9: pyrope-almandine garnet. S5: grossular garnet. V2, V4, V6, V8, S2, S4, S6, and S8: emerald. P2, P4, P6, and P8: sapphire. P3, P5, and P7: amethyst. A pearl is set between each colored gemstone. Photos by G. Panczer.

shows a large bluish gray polished stone with a “sugarloaf” shape, again surrounded by nine colored stones (S1 to S9 in figure 4) alternating with pearls. The side of the talisman is also set with nine colored stones, numbered P1 to P9. The small stones are mainly polished as cabochons and have various shapes such as oval, round, diamond, pear, or free-form. Only two stones are faceted: Dark red S1 on the back has four facets, while violet P3 on the side

has an oval table. Most of the green stones present polished natural prism faces. All the pearls have the peculiarity of being drilled. Their original setting consisted of a gold crimp pushed inside the drill hole. This is the case for all the pearls except the one between P3 and P4, which presents a bezel setting and has a clearly visible drill hole. We presume that this is one of the two replacement pearls that were added with an emerald during the restoration of the talis-





Figure 5. Reflected light (left) and transmitted light (right) reveal an abundance of bubbles in the glass cabochon. In both photos, the wooden cross and the silk thread are clearly visible. Photos by G. Panczer.

man in 1964 (Taralon, 1966). The second replacement pearl is on the front of the talisman, located between V8 and V9 (figure 4). It was missing on the photo presented in the report of Taralon (1966) and appears much whiter than the others.

**Microscopic Observations.** Observation of the center cabochon on the front of the talisman revealed the presence of numerous bubbles, which are characteristic for artificial glass. In addition, the sacral relic was clearly visible when viewed in transmitted light

Figure 6. A composite image from four magnified photos of the large center sapphire (38 × 32 mm) on the back of the reliquary, seen through a trinocular microscope in transmitted light. Photos by G. Panczer and M.S. Krzemnicki.



(figure 5). This relic consists of two fragments of wood tied together in the shape of a cross. The center stone on the back of the talisman (figure 6) contained numerous fissures (visible in brightfield illumination through the cabochon), unaltered healing fissures, and parallel tubes of fluid inclusions and brown inclusions (possibly mica). No needles could be observed in the large center stone. The smaller colored stones set in the talisman are relatively opaque and did not reveal characteristic inclusions. The green stones have a characteristic hexagonal prismatic shape and fingerprint textures that indicate beryl.

**Spectroscopic Results. Sapphires.** The gray to bluish stones (P2, P4, P6, and P8) were identified by Raman spectroscopy as corundum with various background fluorescence levels (P6 and P8). The polished center sapphire on the back of the talisman was also unambiguously identified by its Raman spectrum as corundum. XRF analysis revealed weak amounts of Fe (565 ppm), Ti (116 ppm), and Ga (68 ppm), while Cr was not detected (table 1). This center sapphire showed an absorption spectrum (figure 7) typical for

**TABLE 1.** Trace-element concentration (XRF) of the talisman's center sapphire and four small sapphires (average of P2, P4, P6, and P8).

	Center sapphire		Small sapphires	
	Avg. (4 spots)	Standard deviation	Avg. (4)	Standard deviation
Fe	565	66	817	220
Ti	116	16	153	40
Ga	68	6	64	14
Cr	bdl	—	bdl	—
Mg	bdl	—	bdl	—
V	bdl	—	bdl	—

*bdl = below detection limit*

**TABLE 2.** Trace-element concentrations (ppmw) of seven of the talisman's eight emeralds compared to those of other beryls from early deposits (Habachtal, first to thirteenth century CE; Djebel Zabara, first century BCE to sixth century CE; Swat, first century BCE to third century CE; and Panjshir, thirteenth century BCE).

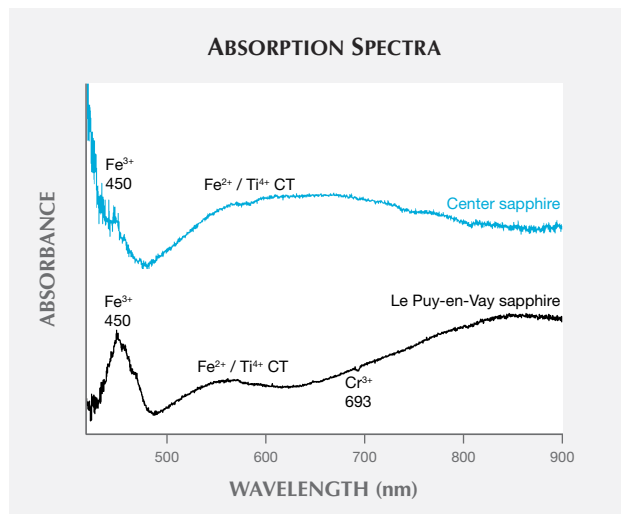
Source	Talisman of Charlemagne		Habachtal (Austria)		Djebel Zabara (Egypt)		Swat (Pakistan)		Panjshir (Afghanistan)	
	This work	Standard dev.	Calligaro et al. (2000)	Auriscichio et al. (2018)	Calligaro et al. (2000)	Auriscichio et al. (2018)	Calligaro et al. (2000)	Auriscichio et al. (2018)	Calligaro et al. (2000)	Auriscichio et al. (2018)
Number of samples	7		13	3	6	2	4	3	5	3
Analytical technique	XRF		PIXE	EPMA	PIXE	EPMA	PIXE	EPMA	PIXE	EPMA
Fe	4518 (958)		4000	3316	4600	6024	6230	10390	2080	1632
Cr	3689 (1672)		1390	945	2600	3224	5930	6635	2650	1458
V	454 (324)		170	145	330	300	320	433	970	1774
Ti	76 (75)		30	4	7	60	10	40	12	120
Rb	10 (5)		18	n.m.	24	14	6	3	30	33

*n.m.* = not measured

metamorphic sapphires (Smith, 2010), with a broad absorption band (550–700 nm) assigned to Fe<sup>2+</sup>/Ti<sup>4+</sup> intervalence charge transfer and a very small absorption peak at 450 nm caused by the presence of some trivalent iron (Fe<sup>3+</sup>). For comparison, figure 7 also shows a typical absorption spectrum for basaltic sapphire from Le Puy-en-Velay in the Haute-Loire region of France, a potential source of sapphires for European medieval jewelry. Its spectrum exhibits a very different absorption behavior, with a marked Fe<sup>3+</sup> peak at 450 nm and a general increase in absorption toward the near-infrared range, a pattern very char-

acteristic for such basaltic sapphires (Fritsch and Mercer, 1993; Krzemnicki et al., 1996). Based on this, we conclude that the sapphire in this talisman is of metamorphic origin. Moreover, we did not observe a Cr<sup>3+</sup> emission line at 693 nm. This was confirmed by the total absence of red fluorescence under long-wave UV illumination (365 nm). We could not record the absorption spectrum of the other sapphires because of their small size and their position in the setting. Their chemical composition was similar to that of the main center sapphire (table 1).

Figure 7. The absorption spectrum of the talisman's center sapphire, obtained with diffuse reflectance, compared to that of a representative sapphire from Le Puy-en-Velay in the Haute-Loire region of France. Here, CT represents charge transfer.



*Emeralds.* The Raman spectra of the green beryls on the front (V2, V4, V6, and V8) and back (S2, S4, S6, and S8) exhibited an intense background fluorescence that did not allow the detection of characteristic vibration modes. XRF analyses were conducted on all beryls except V2 and S2, for which the setting was too close to the stone's surface. The chemical results corresponded to beryl, and a high average Cr content confirmed that they are emeralds (table 2).

*Garnets.* Raman spectrometry is well suited for identifying members of the garnet group (Pinet and Smith, 1994; Kolesov and Geiger, 1998). Most of the talisman's small red stones (V and S, numbers 1, 3, 5, 7, and 9) show characteristic spectra of the almandine-pyrope solid solution series (Fe,Mg)<sub>3</sub>Al<sub>2</sub>(SiO<sub>4</sub>)<sub>3</sub> with a major Fe-rich almandine component (figure 8). Only brownish red S5, on the back of the talisman, appears to be an almandine-grossular garnet (figures 4 and 8) and V1 a Mg-rich pyrope-almandine. Beside those two garnets, XRF analyses confirm that the others presented an Alm<sub>91-46</sub>Py<sub>0-42</sub>Gr<sub>4-27</sub>Sp<sub>1-6</sub> compositional range of the continuous series (table 3).

**TABLE 3.** Composition of garnets in the Talisman of Charlemagne, as determined by XRF analysis.

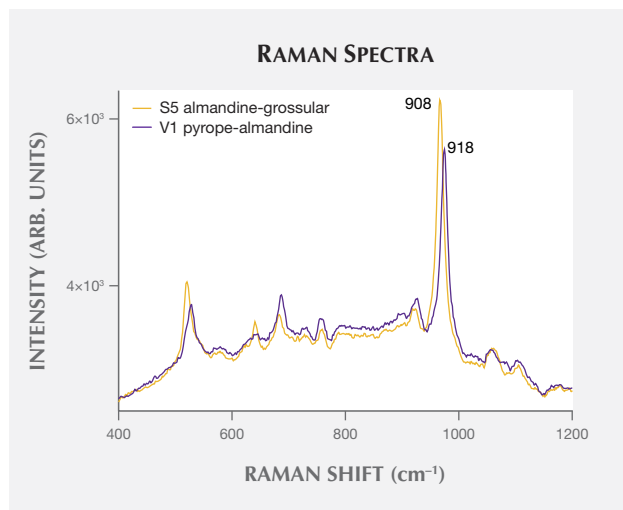
	Almandine (mol.%)	Pyrope (mol.%)	Spessartine (mol.%)	Grossular (mol.%)	Cr (ppmw)	Standard deviation	Y (ppmw)	Standard deviation
S7	91	0	4	4	53	66	450	23
V3	72	16	6	5	815	76	613	26
S5	70	0	3	27	216	60	6	5
S3	55	33	2	10	bdl	—	53	8
S9	48	37	2	13	158	54	15	5
S1	47	41	1	11	155	51	8	4
V7	46	40	1	12	164	45	bdl	—
V5	46	42	2	11	369	48	8	4
V9	41	47	2	10	bdl	—	12	5
V1	29	55	1	16	402	43	67	7

bdl = below detection limit

*Amethysts.* The Raman spectra of the violet stones (P3, P5, and P7; not shown) identified them as amethyst quartz.

*Glass Cabochon.* Under 785 nm excitation, the center cabochon on the front side reveals a broad intense luminescence band at a Raman shift of 1375  $\text{cm}^{-1}$ , which corresponds to an 880 nm fluorescence band (figure 9). When excited with a solid state 532 nm laser, its spectrum was dominated by broad Raman bands and Q2 and Q3 modes (again, see figure 9) characteristic of partially depolymerized sodic glass (Raffaëly et al., 2008).

Figure 8. Raman spectra (785 nm excitation) of the representative pyrope-almandine garnet V1 (purple line) and the almandine-grossular garnet S5 (orange line) in the talisman.



The absorption spectrum of the glass cabochon showed characteristic absorption bands (542, 597, and 644 nm) of divalent cobalt  $\text{Co}^{2+}$  (Lima et al., 2012) and a transmission domain at 480 nm, which explains the cabochon's blue color (figure 10). As cobalt is a very strong chromophore and the cabochon's color is not very saturated, it is not surprising that the Co concentration was below the detection limit of XRF while the chemical composition was 81 wt.%  $\text{SiO}_2$ , 10 wt.%  $\text{PbO}$ , 7 wt.%  $\text{K}_2\text{O}$ , and 2 wt.%  $\text{CaO}$ . Under long-wave UV illumination (365 nm), it exhibited intense blue fluorescence, which could be caused by  $\text{Bi}^{3+}$  traces (Xu et al., 2012).

*Pearls.* The pearls' composition did not present any Mn and Ba traces; both were below the XRF limit of detection.

*Gold Setting and Chain.* XRF analysis of the gold setting showed that the jewel is made of nearly pure gold: 92.5 wt.% Au, 5 wt.% Ag, and 2.1 wt.% Cu, which corresponds to 22K gold. The chain composition is quite different: 77.1 wt.% Au, 20.8 wt.% Ag, and 1.1 wt.% Cu, which corresponds to 18K gold.

## INTERPRETATIONS AND DISCUSSION

Because the talisman's gems have different cuts, we can speculate that they were recovered from various ornaments or jewels. The fact that the pearls all have drill holes corroborates this hypothesis. However, the very basic styles of the different cuts allow us to suggest, as Taralon (1966) and as Gaborit-Chopin and Taburet (1981) did, that the setting of these gemstones is contemporaneous with the reliquary and thus probably from the ninth century (except for two

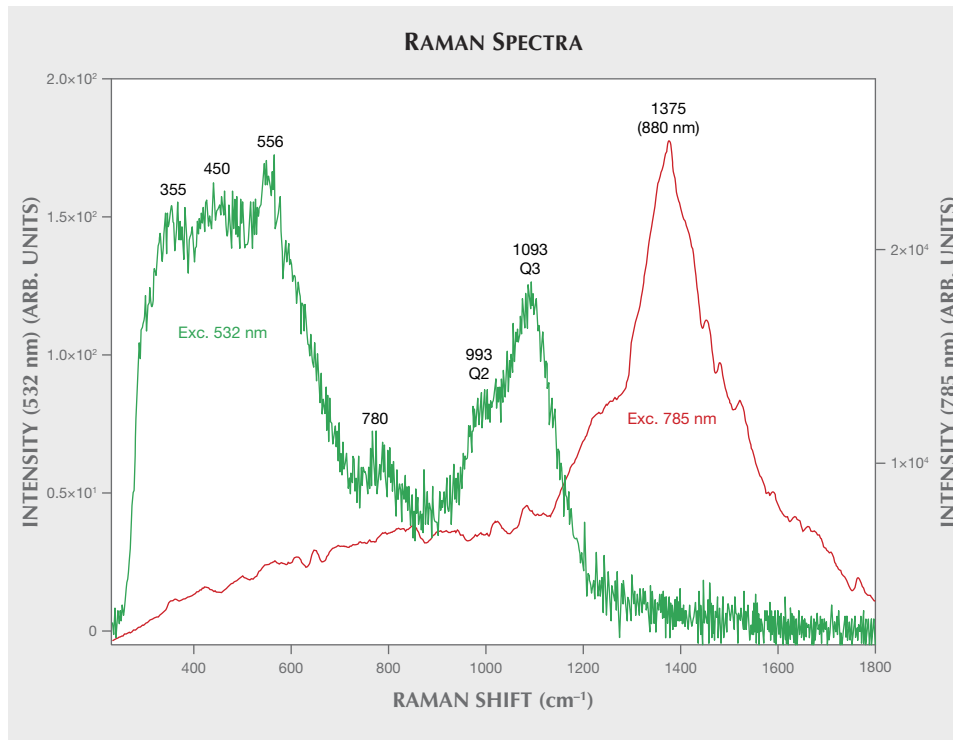
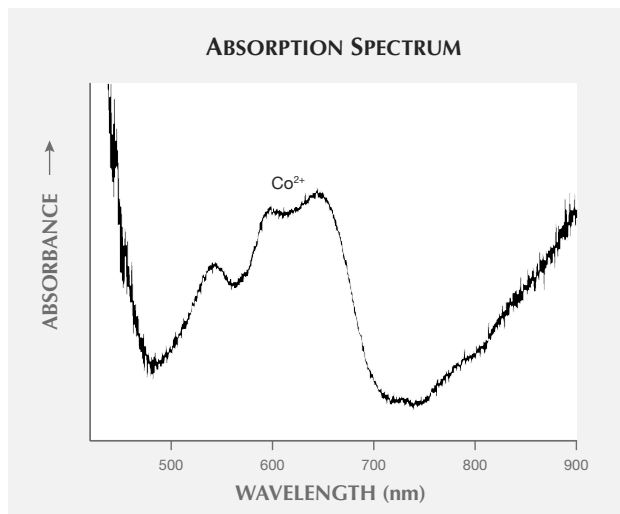


Figure 9. Under 532 nm laser excitation, the glass cabochon exhibits characteristic Raman bands of partially depolymerized glass. Under 785 nm excitation, a strong fluorescence conceals the Raman spectrum. Qn species are  $[SiO_4]$  tetrahedra with n bridging oxygen; Q2 has two non-bridging oxygen and Q3 has one non-bridging oxygen.

pearls and one emerald that were replaced during restoration in 1964).

The gold setting of the talisman is composed of nearly pure gold, as it was worked during the Middle Ages and antiquity, while the chain corresponds to a more recent alloy. According to several authors (Taralon, 1966; Gaborit-Chopin and Taburet, 1981;

Figure 10. The glass cabochon's absorption spectrum shows the characteristic  $Co^{2+}$  bands at 542, 597, and 644 nm.



Scordia, 2012), the gold cable-type chain with thick round links we know today was likely added during the nineteenth century. They claim that the change had been made before the 1843 or 1844 drawing signed by Prince Louis Napoleon and the newspaper article from *L'illustration*. Indeed, the different representations of the reliquary since this date shows a comparable chain. The painting by Felix Cottreau (1834) is not taken into account because its representation of the reliquary was modified for artistic reasons. On the older engravings of the seventeenth and eighteenth centuries, a chain is also visible. If that model is not very different from the current model, we cannot prove with certainty that the chain has been changed. The reliquary could have originally been suspended from a leather or fabric cord (Taralon, 1966; Scordia, 2012).

Concerning the pearls, the absence of Mn and Ba traces indicates a marine origin. The fact that they are all drilled confirms they were recycled from antique jewels (earring or necklace), which was commonplace.

**Assumptions About the Geologic Origin of the Colored Gemstones. Sapphires.** For the center sapphire, the inclusions do not allow an unambiguous geographical origin determination. But since the absorption spectrum we obtained corresponds to that of a sapphire of metamorphic origin, and due to the

nature of some of its inclusions, notably the elongated parallel fluid tubes and the resorbed brownish mica flakes (Hughes, 2017), it is reasonable to suggest a Ceylonese origin. Furthermore, the negligible amount of Fe, Ti, Ga, and Cr (below the XRF detection limit) and lack of fluorescence was consistent with the data of Halicki (2013) for Sri Lankan sapphire. Similar grayish blue stones are known in Sri Lanka today and would usually be heat-treated to improve their color. A French origin can be excluded, as sapphires from the Haute-Loire region are of magmatic (basaltic) origin (figure 7). A Ceylonese origin would also be consistent with other sapphires set in objects of the Carolingian period (700–1100 CE), such as those of Charlemagne’s ninth-century ewer (Caplan and Notari, 2015), the Golden Tabernacle (Superchi, 1988), and the eleventh-century Crown of Cunegonde (Gübelin, 1988). The sapphires around the talisman as well as the large sapphire are characterized by a similar gray-blue to blue-gray color. In the case of the smaller sapphires, however, the impossibility of performing optical absorption spectroscopy means their origin remains unknown.

**Garnets.** In attempting to identify the origin of the garnets, the authors referred to the classification of Gilg et al. (2010) and Schmetzer et al. (2017). These

authors classified ancient Greek, Roman, and Early Medieval garnet-bearing jewels according to five main type clusters, based on their chemical composition, and related to this the calculated percentages of the different pure end members of the pyrospite and ugrandite garnets as well as their chromium and yttrium content. Raman peak positions and chemical signatures (a major almandine component with relatively high Y concentration) indicate that almost all of the garnets set in the talisman correspond to cluster A (historical garnets originating from southern India or Sri Lanka in the Middle Ages) as described by Gilg et al. (2010) and Schmetzer et al. (2017). We therefore assume they originated from southern India or Ceylon. Garnet V1 with its different chemical composition might be of a different origin, presumably corresponding to a Bohemian garnet (cluster E, chromium-rich pyrope), a provenance also encountered in European jewelry of that period.

**Emeralds.** The emeralds set on the talisman all present the same characteristic chemical signature, with an average of 0.68 wt.%  $\text{Fe}_2\text{O}_3$ , 0.57 wt.%  $\text{Cr}_2\text{O}_3$ , and 0.07 wt.%  $\text{V}_2\text{O}_3$ , except for emerald S6 (figure 4) and its lower contents (0.58 wt.%  $\text{Fe}_2\text{O}_3$ , 0.18 wt.%  $\text{Cr}_2\text{O}_3$ , and 0.03 wt.%  $\text{V}_2\text{O}_3$ ). These values can be compared with the data collected for emeralds from

## Timeline of the Talisman of Charlemagne

**742:** Birth of Charlemagne (Charles the Great or Charles I), King of the Franks and ruler of the Carolingian Empire.

**801:** According to legend, the talisman is a gift from Abbasid Caliph Harun al-Rashid to Charlemagne.

**January 28, 814:** Charlemagne dies at the age of 72 in Aix-la-Chapelle. It is said that the talisman was suspended from his neck in his tomb.



**1000:** First exhumation of Charlemagne’s body. No description of the talisman is mentioned.

**1166:** Second exhumation on the occasion of his canonization by Antipope Paschal III.

**12th or 13th Century:** A manuscript mentions a reliquary with a strand of hair of the Virgin Mary as part of the Aix-la-Chapelle treasury.

**17th Century:** The first engravings of the stylized reliquary, with a central stone surrounded alternately by four faceted stones and four cabochons, appear with the other relics from the treasury of the Cathedral of Aachen. One of the oldest is made by Abraham Hogenberg in the book *Aachener Chronik* by Johannes Noppius in 1632, accompanied by the words: *Capilli B. virginis Mariae* (the hair of the Virgin Mary).

**August 1804:** Marc-Antoine Berdolet, Bishop of Aix-la-Chapelle, gives the reliquary to Josephine de Beauharnais, who precedes the arrival of Napoleon on an imperial visit. From this date there is no longer any mention of the Virgin Mary’s hair in the reliquary. It is therefore possible that all or part of the relic were removed to add two pieces of wood presented as the True Cross of Christ.



**December 1809:** Josephine is divorced by Napoleon, but continues to be the owner of the reliquary. Therefore it is not part of the crown jewels of France.

**May 29, 1814:** At the death of Josephine, her daughter, Hortense de Beauharnais, inherits the reliquary. It will stay with Napoleon’s stepdaughter for the rest of her life, even during her exile in Arenenberg on the shores of Lake Constance.



historical mines worldwide such as Habachtal, Austria (first to thirteenth century CE); Swat, Pakistan (first century BCE to third century CE); Panjshir, Afghanistan (thirteenth century BCE); and Djebel Zabara, Egypt (first century BCE to sixth century CE); see Giuliani et al. (2000), Calligaro et al. (2000), Groat et al. (2014), and Aurisicchio et al. (2018). Table 2 compares the results of XRF analyses from this study with the results of Calligaro et al. (2000) by proton-induced X-ray emission (PIXE) and of Aurisicchio et al. (2018) by electron probe microanalyzer (EPMA). We assumed that the potential presence of very tiny inclusions did not interfere with the emerald composition results from the other studies. The composition of the emeralds in the talisman does not appear to correspond to those of Habachtal, which have a much higher Cr and V concentration (table 2). The chemical values are comparable to those of Djebel Zabara, which have very similar Cr and V values. Compared with the talisman, emeralds from Pakistan present a much higher amount of Cr, while those from Afghanistan much higher V. As an exception, emerald S6 shows a chemical composition (4049 ppm Fe, 1201 ppm Cr, 189 ppm V, 15 ppm Rb, and Ti below the detection limit) similar to those of emeralds from Habachtal. This emerald could be the one that was replaced by Taralon during the restoration of 1964. Unfortunately, the three 1866 photos

do not represent the back face of the talisman where this emerald is located.

Our conclusion is consistent with Giuliani et al. (2000), who investigated emeralds set in jewelry prior to 1545 and found that they originated either from Habachtal or early Egyptian mines. The fact that the chemical signature of seven of our studied emeralds corresponded with Egyptian origin and one with Austrian provenance, suggests that the emeralds of the talisman were extracted much before the sixteenth century. Yet the basic fashioning of the emeralds, in the form of simply polished prismatic crystal fragments or as cabochons, is in our opinion a good indication that these stones are at least contemporary with the reliquary (Gaborit-Chopin and Taburet, 1981). We therefore assume that most of the emeralds of the talisman originate from Egypt (except emerald S6, see above) and not from Austria, as often expected for historical emeralds of this age.

*Amethysts.* The origin of the amethysts in the talisman is unknown. A number of quartz deposits in the crystalline massifs of Saxony were already known and exploited by the Middle Ages (Scordia, 2012). At the same time, the recycling of even older (ancient) amethysts, originating from Egyptian mines such as those of Wadi el-Hudi, southeast of Aswan, could be a possibility in this context (Liszka, 2018).

**1832:** In his book *Impressions de voyage en Suisse*, Alexandre Dumas mentions the reliquary and calls it a "talisman." This is the first time the term is used to describe it.



**1834:** Felix Cottreau's portrait, housed in the Napoleon Museum Thurgau, of Queen Hortense bearing the reliquary.



**October 5, 1837:** When Queen Hortense dies, she passes down the Arenenberg estate to her son, Prince Louis Napoleon (later Napoleon III).

**1843:** Prince Louis Napoleon, heavily indebted, sells the property of Arenenberg and seeks to sell the reliquary. The drawing of the reliquary signed by Prince Louis Napoleon could date from this period.

**1844:** An engraving of the reliquary appears in the newspaper *L'Illustration*.

**1855:** A reliquary box is made for the talisman by Parisian goldsmith Froment-Meurice.

**1866:** Charles Clément, deputy curator at the Louvre, appraises the reliquary accompanied by an engraving by the German historian and archaeologist Ernst Aus'm Weerth.



**1919:** Napoleon III's widow, Empress Eugénie, moved by the fire of the Cathedral of Reims, donates the talisman to the Archbishop of Reims.



**1960s:** First expert examination is carried out by Bernard Gomond.

**1962:** The talisman is classified as a historical monument and deposited in the treasury of the Palace of Tau.

**Characterization of the Center Sapphire.** The basic polishing and fashioning of the large center sapphire strongly suggests that it is contemporaneous with the reliquary. It could, however, be a recycled stone from an antique jewel. The presence of unaltered inclusions indicates that no heat treatment was applied to improve its clarity and color. Its shape is slightly trapezoidal, broader at its base. Its dimensions are 41 mm long × 25–29 mm wide. Its approximate depth can be estimated as 16 mm, since the total thickness of the sapphire and glass cabochon is 35 mm, and we can assume that the space between the two stones is less than 1.5 mm keeping the wooden cross relic fixed in place. Based on these measurements, we estimate the weight of the center sapphire as approximately 190 ct (38 grams). To our knowledge, the center sapphire of the Talisman of Charlemagne is the largest sapphire used in European jewelry during the Early to High Medieval period. For comparison, the historic Grand Sapphire of Louis XIV weighs 135 ct or 27 grams (Farges et al., 2015).

**Possible Substitution with the Blue Glass Cabochon.**

As indicated earlier, various descriptions of the main center stones have been recorded. The 1844 newspaper article in *L'Illustration* mentions two sapphires: "This talisman is a gold reliquary, round, encrusted on the surface with precious stones and whose middle is composed of two superimposed raw sapphires which contain a piece of the True Cross." Charles Clément, deputy curator at the Louvre, also notes the presence of two sapphires, one "square cabochon. Big coarse cabochon weak stone of imperfect color" and one "oval cabochon. Big sapphire perfect in water and size, pale blue..." (Aus'm Weerth, 1866). Other descriptions, which are probably much less reliable, indicate gems other than sapphire. Lucien Daudet in *L'inconnue* (1922) describes an aquamarine: "The relic known as the Talisman of Charlemagne is a piece of the True Cross enclosed in a great aquamarine." Alexandre Dumas père mentions an emerald as the major stone of the talisman in his 1833 book *Impressions de voyage en Suisse*, as does Augustus C. Hamlin (1884).

The substitution of a large gem by an oval glass cabochon is attested to by Taralon (1966), based on his description of the gold setting, his sketchings, and his own photographs taken during the talisman restoration and compared to 1866 photographs. The main argument is that the glass cabochon does not match the shape of the bezel setting, which was similar to the shape on the back (see figure 4), and therefore was roughly forced into the talisman (Taralon, 1966; Scor-

dia, 2012). Furthermore, the perfect oval shape and polishing of the glass cabochon as well as its composition (Co-doped lead glass with a high amount of potassium flux) are similar to that of blue potassium-rich smalt glass developed during the sixteenth century and generally used from the eighteenth century (Boon et al., 2001). Based on these factors, we can hypothesize that the glass cabochon was created during the eighteenth or nineteenth century.

Several hypotheses of substitution are therefore possible. Taralon (1966) mentions a possible incident when the relics were relocated from Aachen to Paderborn during the French Revolution. However, comparison between the present talisman with the 1834 portrait of Queen Hortense (figure 2), the circa 1843 drawing (figure 3), and the 1866 engravings (figure 4) indicates that the oval cabochon was already in place around 1843 and thus before 1866, with its present-day dimensions and appearance. Therefore, we believe that the 1844 indication of two superimposed raw sapphires ("Talisman de Charlemagne," 1844; Aus'm Weerth, 1866) is a mistake due to gemological confusion by nonspecialists who described the talisman from engravings and were seeking a sensational story. The substitution of the front center gemstone (which could have been another large sapphire) by the glass cabochon, therefore, probably occurred at the end of the eighteenth century and certainly before 1843.

**CONCLUSIONS**

This study combined gemological analysis carried out at the Palace of Tau in Reims with thorough historical research in order to unravel mysteries surrounding the Talisman of Charlemagne. Alexandre Dumas's romantic description of the talisman in 1833 contributed to its mystery and notoriety.

The first engravings of the reliquary did not appear until the seventeenth century. However, its typical medieval goldsmithery strongly suggests a dating at least as early as the late ninth century. At the time it was part of the treasury of Aachen Cathedral and was said to contain hair from the Virgin Mary. The replacement of the hair with splinters allegedly from the True Cross probably occurred at the beginning of the nineteenth century and was very likely contemporaneous with the setting of the glass cabochon. Only then did it become known as the Talisman of Charlemagne. It then passed through the hands of Napoleon I; Josephine de Beauharnais and her daughter, Hortense de Beauharnais; and Napoleon III and his wife Empress Eugénie. The empress donated it to

the Archbishop of Reims, where it became a permanent exhibit at the Palace of Tau Museum in Reims.

Gemological examination by the present authors has made it possible to propose the geographic origin of the colored stones. Most of the garnets appear to come from southern India or from Ceylon, except one garnet of presumably Bohemian origin. The large blue-gray sapphire in the center is assumed, based on its inclusions and spectral features, to originate from Ceylon. The emeralds probably originate from Djebel Zabara, Egypt, except for one that is presumably from the Habachtal region of Austria. With this interpretation of our data, we suggest that emeralds from Egypt

have entered the trade along ancient trade routes since at least the Middle Age (i.e., prior middle to late ninth century, when the Talisman of Charlemagne was made), if not even earlier. The substitution of the large gemstone in the front by a glass cabochon probably would have occurred at the end of the eighteenth century and certainly before 1843. The center sapphire's weight is estimated at approximately 190 ct (38 grams), which represents a substantial portion of the reliquary's total weight of 163 grams. This sapphire, having undergone no treatments such as heating, is to our knowledge one of the largest used in historical jewelry before the seventeenth century.

#### ABOUT THE AUTHORS

Dr. Panczer is a professor of physics of geomaterials at the Institute of Light and Matter, UMR5306 at Claude Bernard University Lyon 1, responsible for the DUGEM, Diplôme Universitaire de Gemmologie. Mr. Riondet is an antiquarian and gemologist in Lyon specializing in antique jewels and an expert at the Court of Appeal. Mrs. Forest is a jewelry expert assessor at GGTL, Liechtenstein. Dr. Kizemnicki is director of the Swiss Gemmological Institute SSEF and assistant professor in mineralogy at Basel University. Dr. Carole is researcher and XRF specialist at the Multimaterial and Interfaces Laboratory, UMR 5615 in Lyon 1. Mr. Faure is an independent jewelry trader and gemologist.

#### ACKNOWLEDGMENTS

We warmly thank Henry Papounaud, past curator of the jewelry department of the Palace of Tau Museum, as well as Jean-

Marc Bouré, administrator, and Anne-Sophie Daumont, cultural mediation manager for allowing us to conduct gemmological analyses on the Talisman of Charlemagne. Our thanks also go to Christina Egli, curator at the Napoleon Museum Thurgau at the Arenenberg castle in Salenstein, Switzerland, for granting permission to reproduce the drawing of the reliquary signed by Prince Louis Napoleon and Felix Cottreau's portrait of Queen Hortense wearing the jewel. Lastly, we thank Lydwine Scordia (University of Rouen) for kindly sending her publication cited in this work, as well as Romain Bertrand (AFG Lyon), a lapidary in Villefranche-sur-Saone, for providing sapphire samples from Le Puy-en-Velay. Finally, we would like to thank Nicholas Blanchart (ILM, Lyon) for the English corrections. The CECOMO platform of optical spectrometry (Lyon 1 University) provided the analytical equipment.

#### REFERENCES

- Anceau E. (2008) *Napoléon III*. Tallandier Ed., Paris [in French].
- Aurisicchio C., Conte A.M., Medeghini L., Ottolini L., De Vito C. (2018) Major and trace element geochemistry of emerald from several deposits: Implications for genetic models and classification schemes. *Ore Geology Reviews*, Vol. 94, pp. 351–366, <http://dx.doi.org/10.1016/j.oregeorev.2018.02.001>
- Aus'm Weerth E. (1866) Karl des Grossen ehemals und jetzt in Aachen befindliche Reliquien und Reliquiare [Charlemagne's relics and reliquaries formerly and now in Aachen]. In *Jahrbücher des Vereins von Allerthumsfreunden in Rheinlande*, Vol. 39-40, pp. 265–272, <https://archive.org/stream/bonnerjahrbcher39bonngoog#page/n275/mode/2up>
- de Barjolé M. (1786) *Lettres sur la ville et les eaux d'Aix-la-Chapelle* [Letters on the city and waters of Aachen]. Amsterdam [in French].
- Barone G., Bersani D., Crupi V., Longo F., Longobardo U., Lottici P.P., Aliatis I., Majolino D., Mazzoleni P., Raneria S., Venuti V. (2014) A portable versus micro-Raman equipment comparison for gemmological purposes: the case of sapphires and their imitations. *Journal of Raman Spectroscopy*, Vol. 45, No. 11-12, pp. 1309–1317, <http://dx.doi.org/10.1002/jrs.4555>
- Baylac M.-H. (2016) *Hortense de Beauharnais*. Perrin, Paris.
- Boon J.J., Keune K., van der Weerd J., Geldof M., Mensch K., Bryan S., van Asperen de Boer J.R.J. (2001) Imaging microspectroscopic, secondary ion mass spectrometric and electron microscopic studies on discoloured and partially discoloured smalt in cross-sections of 16th century paintings. *Chimia*, Vol. 55, No 11, pp. 952–960.
- Calligaro T., Dran J.-C., Poirot J.-P., Querrée G., Salomon J., Zwaan J.C. (2000) PIXE/PIGE characterisation of emeralds using an external micro-beam. *Nuclear Instruments and Methods in Physics Research Section B: Beam Interactions with Materials and Atoms*, Vol. 161-163, pp. 769–774, [http://dx.doi.org/10.1016/S0168-583X\(99\)00974-X](http://dx.doi.org/10.1016/S0168-583X(99)00974-X)
- Caplan C., Notari F. (2015) Sous l'œil du gemmologue. Analyse de sept objets du trésor [Under the eye of the gemologist. Analysis of seven treasury objects]. In P.A. Mariaux, Ed., *L'abbaye de Saint-Maurice d'Agaune, 515–2015*. Infolio, Gollion, pp. 415–423 [in French].
- Clouzot H. (1925) *Des Tuileries à Saint-Cloud*. Payot Ed., Paris [in French].
- Daudet L. (1922) *L'inconnue. La vraie vie de l'impératrice Eugénie* [The Unknown: The Real Life of Empress Eugenie]. Flammarion, Paris [in French].
- Dumas A. (1833) *Impressions de voyage en Suisse* [Impressions of Travel in Switzerland]. Charpentier & Dumont, Paris [in French].
- Eginhard (770–840?) *Vita Karoli Magni* (The Life of Charlemagne).



- Translated from Latin by S.E. Turner in 1880, Harper & Brothers, New York.
- Farges F., Panczer G., Benbalagh N., Riondet G. (2015) The Grand Sapphire of Louis XIV and the "Ruspoli" sapphire: Historical and gemological discoveries. *G&G*, Vol. 51, No. 4, pp. 392–409, <http://dx.doi.org/10.5741/GEMS.51.4.392>
- Fritsch E., Mercer M. (1993) Letters: Blue color in sapphire caused by Fe<sup>2+</sup>/Fe<sup>3+</sup> intervalence charge transfer. *G&G*, Vol. 29, No. 3, pp. 151, 226.
- Gaborit-Chopin D., Taburet E. (1981) *Objets d'art du moyen âge* [*Objects of art from the Middle Ages*]. Editions de la Réunion des musées nationaux, Paris [in French].
- Gilg H.A., Gast N., Calligaro T. (2010) Vom Karfunkelstein. [From escarbuncle stone] In L. Wamser, Ed., *Karfunkelstein und Seide*. Ausstellungskataloge der Archäologischen Staatssammlung (München), Vol. 37, pp. 87–100 [in German].
- Giuliani G., Chaussidon M., Schubnel H.-J., Piat D.H., Rollion-Bard C., France-Lanord C., Giard D., de Narvaez D., Rondeau B. (2000) Oxygen isotopes and emerald trade routes since Antiquity. *Science*, Vol. 287, pp. 631–633.
- Gobry I. (1997) *Frédéric Barberousse: Une épopée du Moyen Age*. Tallandier Ed., Paris [in French].
- Groat L.A., Giuliani G., Marshall D., Turner D.J. (2014) Emerald. In L.A. Groat, Ed., *Geology of Gem Deposits*, 2nd ed. Mineralogical Association of Canada. pp. 135–174.
- Gübelin E. (1988) The jewels of the Bavarian Crown. In M. Superchi, Ed., *Gemmologia Europa II: European Gemmologists on Treasures of the World*. CIGEM, Milan, pp. 114–145.
- Guériot P. (1933) *Napoléon III*, Vol. 1. Payot Ed., Paris [in French].
- Häberli S. (2010) Edelsteine, gut und bö: Edelsteine, Gläser und Perlen an oberrheinischen Goldschmiedewerken des 13.–16. Jahrhunderts [Gems, good and evil: precious stones, glasses and pearls on the Upper Rhine goldsmith's workshops of the 13th–16th centuries]. Unpublished PhD thesis, University of Berne, Switzerland.
- Halicki P. (2013) Part I: Chemical characterisation of gem-quality sapphires from metamorphic and magmatic host rocks: a LA-ICP-MS study. Master thesis, University Basel, Switzerland, 180 pp.
- Hamlin A.C. (1884) *Leisure Hours Among the Gems*. J.R. Osgood and Co, Boston, p. 299.
- Hughes R.W. (2017) *Ruby & Sapphire: A Gemologist's Guide*. Lotus RWH Publishing, Bangkok, 816 pp.
- Jeršek M., Kramar S. (2014) Raman microspectroscopy of gemstones from a chalice made in 1732. *Journal of Raman Spectroscopy*, Vol. 45, No. 11–12, pp. 1000–1005, <http://dx.doi.org/10.1002/jrs.4560>
- Kleinclausz A. (2005) *Charlemagne*. Tallandier, Paris [in French].
- Kolesov B.A., Geiger C.A. (1998) Raman spectra of silicate garnets. *Physics and Chemistry of Minerals*, Vol. 25, No. 2, pp. 142–151, <http://dx.doi.org/10.1007/s002690050097>
- Krzemnicki, M.S., Hänni H.A., Guggenheim R., Mathys D. (1996) Investigations on sapphires from an alkali basalt, SW-Rwanda. *Journal of Gemmology*, Vol. 25, No. 2, pp. 90–106.
- Lima A., Medici T., Pires de Matos A., Verità M. (2012) Chemical analysis of 17th century Millefiori glasses excavated in the Monastery of Sta. Clara-a-Velha, Portugal: comparison with Venetian and façon-de-Venise production. *Journal of Archaeological Science*, Vol. 39, No. 5, pp. 1238–1248, <http://dx.doi.org/10.1016/j.jas.2012.01.006>
- Lindon R. (1949) *Étretat, son histoire, ses légendes* [Étretat, its history, its legends]. Les Éditions de minuit, Paris.
- Liszka K. (2018) Site 4 at Wadi el-Hudi: A lost amethyst mining settlement. *Egyptian Archaeology*, Vol. 51, pp. 36–40.
- Lohmann F. (1924) Die Lösung der Frage über die Verluste des Aachener Domschatzes in französischer Zeit. [The solution of the question about the losses of the Aachen cathedral treasury in French time]. *Zeitschrift des Aachener Geschichtsvereins*, Vol. 46, pp. 285–290.
- Maison F. (1991) Le Talisman de Charlemagne et l'impératrice Eugénie. *Nouveaux cahiers du Second Empire*, Vol. 28, pp. 44–46.
- Minois G. (2010) *Charlemagne*. Perrin, Paris [in French].
- de Montesquiou-Fezensac, B. (1962) Le Talisman de Charlemagne. In *Art de France, Revue annuelle de l'art ancien et moderne*, Vol. 2, pp. 66–76.
- Noppius J. (1632) *Aachener Chronik*. Cologne [in German]
- Ollivier E. (1897) *L'Empire libéral: récits et souvenirs*. Vol. 1. Garnier Frères, Paris, p. 55.
- Paléologue M. (1928) *Les Entretiens de l'impératrice Eugénie* [Interviews with Empress Eugénie]. Plon, Paris.
- Pinet M., Smith D.C. (1994) Raman microspectrometry of garnets X<sub>3</sub>Y<sub>2</sub>Si<sub>3</sub>O<sub>12</sub>: II. The natural aluminian series pyrope-almandine-spessartine. *Schweizerische Mineralogische und Petrographische Mitteilungen*, Vol. 74, No. 2, pp. 161–179.
- Pöllnitz C.-L. (1736) *Amusemens des eaux d'Aix-la-Chapelle: ouvrage utile à ceux qui vont y prendre les bains, ou qui font l'usage de ses eaux* [Amusements of the Waters of Aix-la-Chapelle: A Useful Work for Those Who Will Take Baths, or Who Make Use of Its Waters]. Chez Pierre Mortier, Amsterdam.
- Quix C. (1840) *Geschichte der Stadt Aachen mit einem Codex Diplomaticus Aquensis* [History of the City of Aachen with a Codex Diplomaticus Aquensis]. Hensen & Co. Publisher, Aachen.
- Raffaëly L., Champagnon B., Ollier N., Foy D. (2008) IR and Raman spectroscopies, a way to understand how the Roman window glasses were made? *Journal of Non-Crystalline Solids*, No. 354, No. 2–9, pp. 780–786, <http://dx.doi.org/10.1016/j.noncrysol.2007.07.077>
- Reiche I., Pages-Camagna S., Lambacher L. (2014) *In situ* Raman spectroscopic investigations of the adorning gemstones on the reliquary *Heinrich's Cross* from the treasury of Basel Cathedral. *Journal of Raman Spectroscopy*, Vol. 35, No. 8–9, pp. 719–725, <http://dx.doi.org/10.1002/jrs.1197>
- Salet F. (1966) Le "Talisman de Charlemagne." *Bulletin Monumental*, Vol. 124, No. 4, pp. 425–426.
- Schiffers H. (1937) *Aachener Heiligtumsfahrt. Reliquien, Geschichte, Brauchtum* [Aachen Sanctuary Walk. Relics, History, Customs]. Johannes Volk Ed., Aachen.
- Schmetzer K., Gilg H.A., Schüssler U., Panjikar J., Calligaro T., Périn P. (2017) The linkage between garnets found in India at the Arikamedu archaeological site and their source at the Garibpet deposit. *The Journal of Gemmology*, Vol. 35, No. 7, pp. 598–638, <http://dx.doi.org/10.15506/JoG.2017.35.7.598>
- Scordia L. (2012) Le talisman de Charlemagne: l'empire d'un objet précieux [The talisman of Charlemagne: the empire of a precious object]. In Magali Coumert, Marie-Céline Isaïa, Klaus Krönert, Sumi Shimahara (dir.), *Mélanges Michel Sot, L'écriture de l'histoire*, Université Paris Sorbonne, Paris. Histoire et historiographie au Moyen Âge. Pups, Paris [in French].
- Smith C.P. (2010) Inside sapphires. *Rapaport Diamond Report*, No. 33, p. 7.
- Superchi M. (1988) Volvinio's altar gems in St. Ambrose's, Milan. In M. Superchi, Ed., *Gemmologia Europa II: European Gemmologists on Treasures of the World*. CIGEM, Milan, pp. 72–99.
- Talisman de Charlemagne (1844) *L'illustration*, Vol. 4, No. 94, December 14, p. 240 [in French].
- Taron J. (1966) Note technique sur le Talisman de Charlemagne. *Les Monuments historiques de la France*, No. 1–2, pp. 24–43.
- Thietmar of Merseburg (2001) *Ottoman Germany: The Chronicon of Thietmar of Merseburg (975–1018)*. D.A. Warner, Ed. and transl., Manchester Medieval Sources, Manchester University Press, UK.
- Xu W., Peng M., Ma Z., Dong G., Qiu J. (2012) A new study on bismuth doped oxide glasses. *Optics Express*, Vol. 20, No. 14, pp. 15692–15702, <https://doi.org/10.1364/OE.20.015692>

# PROVENANCE DISCRIMINATION OF FRESHWATER PEARLS BY LA-ICP-MS AND LINEAR DISCRIMINANT ANALYSIS (LDA)

Artitaya Homkrajae, Ziyin Sun, Troy Blodgett, and Chunhui Zhou

This study investigates trace-element concentrations of 225 freshwater pearl samples using laser ablation–inductively coupled plasma–mass spectrometry (LA-ICP-MS) and subsequent statistical analysis using linear discriminant analysis (LDA). The samples consisted of three types: non-bead-cultured pearls (NBC) grown in China, natural pearls found in the United States, and cultured pearls (bead and non-bead) grown in the United States. By capturing variations in trace-element concentrations simultaneously through multivariate analysis, these supplementary techniques assist in identifying freshwater pearl origins with a greater degree of confidence.

With more than 300 native mussel species, the rivers and lakes of the United States have produced countless prized natural freshwater pearls over the centuries (Haag, 2012). America’s rich freshwater pearling and shelling heritage has been recorded in the literature over the years. Natural pearls discovered in these waters have exhibited a wide range of shapes, colors, and surface characteristics (Kunz and Stevenson, 1908; Sweaney and Latendresse, 1984; Strack, 2006; Haag, 2012; Hsu et al., 2016). Overharvesting in the past by the shelling industry, dam construction, water pollution, siltation, and the introduction of non-native mussel species have damaged the habitat and shortened the lifespans of the indigenous mussels. Approximately 70% of the mussels are extinct, endangered, or of special concern (U.S. Fish & Wildlife Service, 2018). Wild mussels are still harvested under license in the states of Kentucky, Alabama, and Tennessee, and the shelling in-

dustry is heavily regulated (Watters et al., 2009; Hsu et al., 2016). Nevertheless, pearl production is currently very limited in the United States.

By contrast, the dominant source of freshwater cultured pearls—bead cultured and non-bead cultured (NBC)—is China, which developed NBC pearl cultivation during the 1990s in order to satisfy global demand for high-quality, affordable pearls. There are thousands of freshwater pearling farms in China; Zhuji, in Zhejiang Province, accounts for 85% of the total production (China Gems, 2019). The rest of the culturing operations are mainly situated in the southeastern part of China. *Hyriopsis* species mollusks are extensively used to culture Chinese freshwater pearls. The gemological characteristics of these pearls, as well as the culturing techniques applied, have been reported on previously (Scarratt et al., 2000; Akamatsu et al., 2001; Hua and Gu, 2002; Fiske and Shepherd, 2007). Freshwater NBC pearls are intentionally cultured without a solid shell bead nucleus, using just a piece of mantle tissue (epithelial cells) from donor mussels transplanted into a living host mussel. The grafted tissue later develops into a pearl sac and secretes calcium carbonate (nacre) as well as organic matter and water to form a pearl.

Real-time microradiography (RTX) and X-ray computed microtomography ( $\mu$ -CT) are efficient techniques used by gemological laboratories to analyze a pearl’s internal structure and determine whether it is natural or cultured (Karampelas et al., 2010, 2017; Krzemnicki et al., 2010). Most freshwater NBC pearls have distinct internal structures that can easily be identified by microradiography: twisted voids and elongated linear features in their center (Scarratt et al., 2000; Sturman, 2009). Nevertheless, some NBC pearls are challenging to accurately identify, as they contain small central growth features similar to those in some natural pearls. The identification can be further complicated if any drill holes are present or the pearls are mounted in jewelry, as these may cause the masking or removal of critical evidence.

See end of article for About the Authors and Acknowledgments.

GEMS & GEMOLOGY, Vol. 55, No. 1, pp. 47–60,  
<http://dx.doi.org/10.5741/GEMS.55.1.47>

© 2019 Gemological Institute of America



Figure 1. Representative freshwater pearl samples from the three sources studied: American natural pearls (top left), Chinese cultured pearls (center), and American cultured pearls (top right). Photo by Diego Sanchez.

Freshwater mussels are sedentary filter-feeders, and trace-element variability in such an organism can provide revealing information about their growth environment (Grabarkiewicz and Davis, 2008). The purpose of this study is to perform a preliminary investigation of the trace-element concentrations of natural pearls from North America and NBC pearls from China using laser ablation–inductively coupled plasma–mass spectrometry (LA-ICP-MS) and linear discriminant analysis (LDA) to separate these pearls by geographic origin, growth environment conditions, and mollusk species. LA-ICP-MS has become an important tool for gemstone identification due to its high spatial resolution, rapid and direct chemical analysis, and ultra-high sensitivity when measuring a wide range of elements (Abduriyim and Kitawaki, 2006). LDA is a type of multivariate analysis that can distinguish one class of object from another by applying weighted coefficients of multiple parameters—such as trace elements—to multiple functions representing each group such as USA-NAT, USA-CUL, and CH-NBC, potentially enhancing the benefits of the LA-ICP-MS analysis. This technique has already been applied to determine the country of origin of various gemstones (Blodgett and Shen, 2011; Pornwilard et al., 2011; Shen et al., 2013; Giuliani et al., 2014; Luo et al., 2015).

To augment the study, we also included a unique group of American freshwater cultured pearls. While not a major source for the pearl market, these serve as

interesting samples since they were grown in very specific conditions in Kentucky Lake in the state of Tennessee. Washboard (*Megaloniaias nervosa*) is a major mussel species used to culture American pearls. The culturing period takes three to five years, and the pearls were typically harvested in the autumn months of the year (Hsu et al., 2017). Thus their chemical compositions were expected to be more homogenous than those of the other sample bases.

## MATERIALS AND METHODS

For LA-ICP-MS analysis, we selected 74 American natural (designated here as USA-NAT), 75 American cultured (USA-CUL), and 76 Chinese NBC freshwater pearls, all of various shapes, colors, and sizes (figure 1). Each loose pearl was analyzed in two or three spots (table 1). The variability of trace-element concentration in relation to the pearls' color was not considered in this study. All the American pearls were purchased from the American Pearl Company, Inc. (Nashville, Tennessee) and were claimed to be known samples from their collections (Hsu et al., 2017). These cultured pearls were reportedly grown in Kentucky Lake and harvested during different years. For the natural pearls reportedly collected from North American lakes and rivers, however, there is no exact record of the location, time, or mollusk species in which the pearls were formed. The Chinese pearls, mainly harvested from *Hyriopsis* mollusks, belong to the GIA research collection and were

**TABLE 1.** Freshwater pearls examined in this study.

Sample	Number	Weight range (ct)	Number of spots tested with LA-ICP-MS
American natural pearls (USA-NAT)	74	0.43–8.82	207
American cultured pearls (USA-CUL)			
• Non-bead cultured	61	0.26–4.35	168
• Bead cultured	14	2.43–8.16	42
Chinese non-bead-cultured pearls (CH-NBC)	76	1.39–5.65	213
Total	225		630

purchased from various sources over many years.

To confirm each pearl's identity before the chemical analysis, we examined their internal structures using RTX. The natural pearls showed a variety of structures that consisted mainly of concentric growth arcs following the pearl shape, with and without a dark organic spot in the center. Nine samples showed a questionable void structure that could be considered indicative of NBC pearl formation, though they resembled the other pearls in the group and most experienced pearl testers would consider their internal structures natural rather than NBC. The American NBC pearls revealed distinctive structures expected for this type of pearl. The majority exhibited relatively large void structures, some of which also contained small granular features. Some of the void features tended to be long and thin, appearing "linear" in form. The bead-cultured pearls showed bead nuclei with various shapes that related directly to their external appearance. The majority of the Chinese NBC samples had characteristic "twisted" void-like or elongated linear structures typical of freshwater NBC pearls. However, seven of them did not show any clear indication of a cultured origin because the evidence was entirely removed by the drilling process, leaving only the outer growth arcs, which are less diagnostic.

A MatriX-FocalSpot Verifier PF-100 X-ray fluorescence unit (100 kV and 3.2 mA excitation) equipped with a Canon EOS REBEL T4i DSLR camera (five-second exposure, F5.0, ISO 12800) was used to confirm the pearls' growth environment (either saltwater or freshwater) prior to advanced analysis. Most of the samples tested in the X-ray fluorescence unit showed moderate to strong greenish yellow fluorescence when exposed to X-rays due to the presence of trace amounts of manganese (Mn) (Hänni et

al., 2005; Kessrapong et al., 2017), confirming their freshwater origin. Moreover, some freshwater pearls also exhibited an orange reaction, which is probably related to Mn<sup>2+</sup> in calcite composition and has been reported in freshwater pearls (Habermann et al., 2001; Dumańska-Słowik et al., 2008).

**LA-ICP-MS.** A Thermo Fisher Scientific iCAP Qc ICP-MS, coupled with a New Wave Research UP-213 laser ablation unit with a frequency-quintupled Nd:YAG laser (213 nm wavelength) running at 4 ns pulse width, was used for this study in GIA's Carlsbad laboratory. Ablation was achieved using a 55 µm diameter laser spot size, a fluence (energy density) of approximately 10–12 J/cm<sup>2</sup>, and a 15 Hz repetition rate. <sup>43</sup>Ca was used as an internal standard, with a value of 400,400 ppmw calculated and rounded from pure calcium carbonate (CaCO<sub>3</sub>). U.S. Geological Survey (USGS) pressed powder pellet carbonate standards (microanalytical reference materials MACS-1 and MACS-3) were used as matrix-matched external

## In Brief

- Pearl identification is still carried out primarily by observing and interpreting the internal structural results obtained from various X-ray techniques.
- Trace-element chemistry can be used to differentiate pearls formed in different environments.
- In the absence of definitive structural indicators, the combination of LA-ICP-MS and LDA can assist in identifying freshwater pearls with a greater degree of confidence.

standards to minimize errors caused by matrix effects (Jochum et al., 2012). Argon was used as nebulizer gas (0.73 L/min), auxiliary gas (0.8 L/min), and cooling gas (14 L/min). Helium, used as part of the carrier gas, had a flow rate of 0.8 L/min. Argon and helium gas flow, torch position, sampling depth, and lens voltage were optimized for maximum sensitivity (counts per concentration) and low oxide production rates (<sup>232</sup>Th<sup>16</sup>O/<sup>232</sup>Th <1%). Ablated material was then vaporized, atomized, and ionized by a plasma powered at 1550 W. Twenty-three different isotopes of interest were selected (table 2). When ablating a calcium carbonate matrix, interferences in the forms of molecules and ions with multiple charges produced by matrix compounds and a gas blank may produce inaccurate results (Jochum et al., 2012).

## BOX A: CHOOSING AN APPROPRIATE STATISTICAL MODEL FOR PREDICTING UNKNOWN SAMPLES

Selecting an appropriate prediction model may depend on many factors, such as the data type, the availability of training data, and the data distribution. For some data sets, no prior knowledge is available about the possible classes you wish to predict. When no training classes are available, cluster analysis which uses unsupervised learning can be applied (Hastie et al. 2008). Data can be continuous—as is the case for trace elements—or discrete, such as yes or no responses in a survey. Logistic regression is a good statistical tool for analyzing discrete data. For continuous data with known classes, there are a number of analytical tools available. LDA is a common statistical model and closely related to principle component analysis (PCA) and factor analysis. All look for linear combinations of variables that best explain the data (Martinez and Kak, 2001). LDA specifically models the differences between the classes while PCA does not;

PCA is a better choice for distinguishing between classes when the class means are similar and there are large differences in variance. Quadratic discriminate analysis (QDA) can be used to draw nonlinear boundaries between classes, but like any other nonlinear fit, the data density needs to be high enough to prevent overtuning the model to a data scattering where no solid relationships really exist. QDA is only viable in situations where the ratio of the sample size to the variable count is large (Hastie et al., 2008). Logistic regression does not have as many assumptions and restrictions as discriminant analysis and therefore tends to be more universal. However, when discriminant analysis' assumptions are met, the LDA model tends to perform better than logistic regression (Hastie et al., 2008). Regularized discriminant analysis (RDA) is best for sample distributions that are strongly ellipsoidal (Friedman, 1989).

Table 2 shows major interferences of each isotope related to matrix and gas blank and indicates the minimum required mass resolving power (MRP) necessary for a particular mass being analyzed to make a separation from the corresponding interferences (table 2, column 6). The unit we used has two resolution modes: normal and high. Normal-resolution mode has a peak width of 0.7 atomic mass units (amu), which results in a 57 MRP at atomic mass 40 and a 429 MRP at atomic mass 300. High-resolution mode has a peak width of 0.3 amu, yielding a 133 MRP at atomic mass 40 and a 1000 MRP at atomic mass 300. If a required MRP for the separation of isotopes (table 2, column 6) is smaller than the MRP applied by LA-ICP-MS (table 2, column 7), the interferences related to the isotopes can be resolved. It is obvious that the MRP required for the separation of elements cannot be achieved with either resolution mode for almost all selected isotopes except  $^{60}\text{Ni}$ . As a result, the analysis of isotopes with high interference signals (table 2, column 5) as discriminators must be carefully avoided. To optimize the signals, measurements were performed in high-resolution mode for  $^{43}\text{Ca}$  and with normal resolution for other isotopes.

Data acquisition was performed in time-resolved mode. Dwell time for each isotope was 0.01 second. The gas background was measured for 20 seconds, while the dwell time of each laser spot was 40 seconds. To eliminate surface contamination, only the second half (20-second ablation time) of the laser profile was used in the calculations. Data was processed

by Qtegra software. The LA-ICP-MS method was created to ensure the reproducibility of measurements and in order to be applicable for pearl identification submissions received by the laboratory. LA-ICP-MS is a quasi-nondestructive technique where the resulting tiny laser ablation spots are rarely visible without magnification. Further consideration is given to the position of analysis, which is usually carried out in an inconspicuous place that does not affect the visual appearance of the pearls (near the drill hole, the tapered end of a drop, or the flat base of a button). The round crater (laser spot) measures approximately 55  $\mu\text{m}$  in diameter. The amount of nacre ablated from the two or three laser spots applied to each pearl is minimal and does not result in any noticeable weight loss.

**LDA Methods.** There are many statistical methods available that can model data in order to make predictions about unknown samples. Choosing the appropriate model depends on the type of data sought, whether or not information from *training classes*<sup>1</sup> is available, and the data's distribution (see box A). In this study, LDA was appropriate for origin determination of the three freshwater pearl types because the densities of the sample clusters with respect to various element concentrations have an approximately normal distribution. Cross-validation testing in-

<sup>1</sup>In this context, *training classes* are composed of samples sorted into specific categories that the statistical model is working to predict.

**TABLE 2.** Interferences of molecules and multiply charged ions on isotopes of interest.

Isotope	Atomic mass-ionic charge ratio of isotope	Interference in calcium carbonate (stalagmite)	Atomic mass-ionic charge ratio of interference	Interference in percentage of total counts	Required MRP to separate	MRP applied by LA-ICP-MS	Able to resolve from interference?
<sup>7</sup> Li <sup>+</sup>	7.016004	<sup>14</sup> N <sup>++</sup>	7.001537	>10%	485	10	No
<sup>11</sup> B <sup>+</sup>	11.009305	<sup>22</sup> Ne <sup>++</sup>	10.995693	1%–10%	809	16	No
<sup>23</sup> Na <sup>+</sup>	22.989770	<sup>46</sup> Ca <sup>++</sup>	22.976846	<1%	1779	33	No
<sup>24</sup> Mg <sup>+</sup>	23.985042	<sup>48</sup> Ca <sup>++</sup>	23.976267	>10%	2733	34	No
<sup>31</sup> P <sup>+</sup>	30.973762	<sup>15</sup> N <sup>16</sup> O <sup>+</sup>	30.995024	1%–10%	1457	44	No
		<sup>14</sup> N <sup>17</sup> O <sup>+</sup>	31.002206	1%–10%	1089	44	No
<sup>39</sup> K <sup>+</sup>	38.963707	<sup>38</sup> Ar <sup>1</sup> H <sup>+</sup>	38.970557	1%–10%	5688	56	No
<sup>43</sup> Ca <sup>+</sup>	42.958767	<sup>86</sup> Kr <sup>++</sup>	42.955305	<1%	12409	143	No
<sup>44</sup> Ca <sup>+</sup>	43.955481	<sup>40</sup> Ar <sup>4</sup> He <sup>+</sup>	43.964986	<1%	4624	63	No
		<sup>12</sup> C <sup>16</sup> O <sub>2</sub> <sup>+</sup>	43.989830	<1%	1280	63	No
		<sup>15</sup> N <sup>16</sup> O <sub>2</sub> <sup>+</sup>	46.989939	1%–10%	1230	67	No
<sup>47</sup> Ti <sup>+</sup>	46.951764	<sup>14</sup> N <sup>16</sup> O <sub>2</sub> <sup>1</sup> H <sup>+</sup>	47.000729	1%–10%	959	67	No
		<sup>12</sup> C <sup>16</sup> O <sup>18</sup> O <sup>1</sup> H <sup>+</sup>	47.001900	1%–10%	936	67	No
<sup>53</sup> Cr <sup>+</sup>	52.940654	<sup>40</sup> Ar <sup>13</sup> C <sup>+</sup>	52.965738	>10%	2111	76	No
		<sup>40</sup> Ca <sup>13</sup> C <sup>+</sup>	52.965946	>10%	2093	76	No
<sup>55</sup> Mn <sup>+</sup>	54.938050	<sup>40</sup> Ar <sup>15</sup> N <sup>+</sup>	54.962492	1%–10%	2248	78	No
<sup>57</sup> Fe <sup>+</sup>	56.935399	<sup>40</sup> Ca <sup>16</sup> O <sup>1</sup> H <sup>+</sup>	56.965331	>10%	1902	81	No
<sup>59</sup> Co <sup>+</sup>	58.933200	<sup>43</sup> Ca <sup>16</sup> O <sup>+</sup>	58.953682	>10%	2877	84	No
		<sup>40</sup> Ca <sup>18</sup> O <sup>1</sup> H <sup>+</sup>	58.969576	>10%	1620	84	No
<sup>60</sup> Ni <sup>+</sup>	59.930791	<sup>44</sup> Ca <sup>16</sup> O <sup>+</sup>	59.950396	>10%	58	84	Yes
<sup>63</sup> Cu <sup>+</sup>	62.929601	<sup>27</sup> Al <sup>36</sup> Ar <sup>+</sup>	62.949084	1%–10%	3230	90	No
		<sup>23</sup> Na <sup>40</sup> Ar <sup>+</sup>	62.952153	1%–10%	2790	90	No
<sup>66</sup> Zn <sup>+</sup>	65.926037	Interference-free	–	–	–	–	–
<sup>69</sup> Ga <sup>+</sup>	68.925581	<sup>29</sup> Si <sup>40</sup> Ar <sup>+</sup>	68.938878	>10%	5184	98	No
		<sup>138</sup> Ba <sup>++</sup>	68.952911	>10%	2522	98	No
<sup>88</sup> Sr <sup>+</sup>	87.905614	<sup>176</sup> Yb <sup>++</sup>	87.971284	<1%	1339	126	No
		<sup>176</sup> Lu <sup>++</sup>	87.971341	<1%	1337	126	No
<sup>89</sup> Y <sup>+</sup>	88.905848	Interference-free	–	–	–	–	–
<sup>95</sup> Mo <sup>+</sup>	94.905841	Interference-free	–	–	–	–	–
<sup>137</sup> Ba <sup>+</sup>	136.905821	Interference-free	–	–	–	–	–
<sup>139</sup> La <sup>+</sup>	138.906348	Interference-free	–	–	–	–	–
<sup>208</sup> Pb <sup>+</sup>	207.976636	Interference-free	–	–	–	–	–

Modified after Jochum et al. (2012).

Following the trial (test) work, these were considered the elements most likely to assist in separating the different types of freshwater pearls in this study.

Rows highlighted in gray are the elements selected as “good discriminators.”

<sup>43</sup>Ca<sup>+</sup> was measured under high-resolution mode. Everything else was measured under normal resolution mode. <sup>60</sup>Ni<sup>+</sup> was the only isotope LA-ICP-MS could resolve from interferences.

volved removing each sample from the aforementioned classes, training the LDA on the remaining samples, and then applying the LDA prediction on the removed sample. This robustness test yielded prediction rates only slightly lower than focusing the LDA with all available samples and then predicting to which class those same samples belong, indicating that the LDA method had sufficient training samples to maintain high prediction rates if additional pearls with the same origins were added. Pairwise analysis was applied, similar to the study by Luo et al. (2015),

because otherwise the discriminant functions will change as more classes are added. Elements useful for the separation of two classes may not be useful for a third or fourth class. The authors introduced a decision tree to allow for the additional sophistication of classifying unknown samples as “undetermined” if there are contradictory results between pairwise tests or if unknown samples fall far from the clusters of known samples analyzed. However, no unknown samples were run in this experiment. In developing the LDA model, we collected multiple

spots of chemical analysis for each pearl. Each spot was treated as a separate sample unit. The number of pearls and associated spots for each type of pearl are shown in table 1.

Pairwise LDA formulas were developed in which two functions are formulated: Each function computes a score for each pearl type. The higher score indicates a sample's pearl type. When running a pairwise LDA, a cross-validation method is applied to test the robustness of the model, whereby each pearl sample is classified by the functions derived from every other pearl sample. To make a final prediction, we constructed a simple *decision tree*<sup>2</sup> that merged the pairwise results into a single final result. If two out of three pairwise tests yielded the same result, then that "consensus" result became the final prediction. For example, if 1 vs. 2 = 2, and 1 vs. 3 = 1, and 2 vs. 3 = 2, then the predicted result would be "2." If no pearl types are selected twice, then the prediction becomes a fourth class: "undetermined." Note that in this study, an "undetermined" result was considered an incorrect prediction.

## LA-ICP-MS AND LDA RESULTS

Chemical data recorded for the 22 elements selected are shown in table 3. The three types of freshwater pearls showed similar Ca concentrations. Of the trace elements analyzed, Na, Mn, Sr, and Ba were found to be useful discriminators based on careful examination of data with standard chemistry plots. <sup>23</sup>Na<sup>+</sup> and <sup>88</sup>Sr<sup>+</sup> had major interferences that were less than 1% of total counts, while <sup>55</sup>Mn<sup>+</sup> had major interferences between 1% and 10% of total counts and <sup>137</sup>Ba<sup>+</sup> had no major interference (see table 2, highlighted gray). Li, Na, Mg, Mn, Sr, and Ba have been proven to be useful discriminators when identifying marine aragonites (otolith) (Veinott and Porter, 2005; Sturgeon et al., 2005; Lara et al., 2008). However, Li and Mg both had interferences greater than 10% of the total counts (see table 2) and thus could not be corrected sufficiently by subtracting only the gas blank. Therefore, they were not used in the method because of the limitations of the instrument.

Seven of the USA-NAT samples contained Mn contents of less than 100 ppmw, which is unusual for freshwater pearls. Mn is generally above 100 ppmw in freshwater pearls and shells, but is low or even ab-

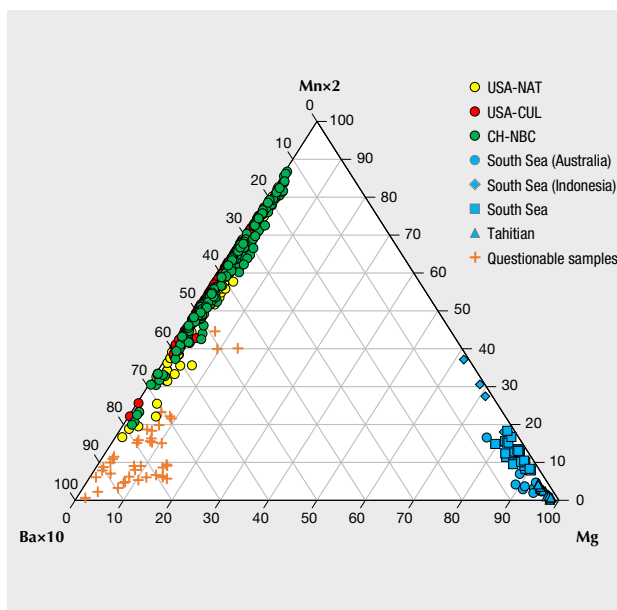


Figure 2. This ternary diagram of the relative percentages of Ba, Mg, and Mn shows clear separation between freshwater and saltwater pearls. All the questionable samples plotted alongside the freshwater pearls, indicating a likely freshwater rather than saltwater origin.

sent in saltwater material. The low Mn content of the seven samples suggests that they could be saltwater pearls. To verify the growth environment of these questionable samples, three extra spots were tested on each sample; the results are presented in table 4. All questionable samples contained low Sr (<1100 ppmw), low Na (<2100 ppmw), and high Ba (>30 ppmw), which is the opposite of the trace element results that were documented on known saltwater origin pearls from the *Pinctada maxima* mollusk (Scarratt et al., 2012; Sturman et al., 2016). A ternary diagram of Ba, Mg, and Mn (figure 2) was used to plot all studied freshwater and known saltwater pearls for better clarification. Moreover, additional groups of South Sea and Tahitian pearls that were analyzed by the same method used for the freshwater pearls were included in the diagram for supporting information. All the questionable samples plotted alongside the freshwater pearls, which showed that the samples likely have a freshwater rather than saltwater origin.

A chemical plotting method was used to plot the chemistry. The nine categories listed in table 5 represent different chemical ranges that were defined according to the concentrations of Sr and Ba. In order to reduce the overlapping areas among the three groups as much as possible, the boundaries of each

<sup>2</sup>A *decision tree* is a flowchart tool where each starting node is a test on an attribute, each branch is an outcome of the test, and each leaf (or final node) is a class.

**TABLE 3.** LA-ICP-MS chemical composition ranges of American and Chinese freshwater pearls studied (in ppmw).

Elements	USA-NAT			USA-CUL			CH-NBC		
	Maximum	Minimum	Average	Maximum	Minimum	Average	Maximum	Minimum	Average
Li	4.16	bdl	0.052	2.53	bdl	0.10	0.85	bdl	0.013
B	10.8	bdl	3.93	14.4	1.51	4.03	14.2	1.09	4.50
Na	2300	460	1710	2300	1050	1850	2870	879	2146
Mg	908	12.1	50.0	376	22.2	38.0	108	7.82	33.4
P	3260	bdl	251	693	bdl	230	315	bdl	207
K	162	bdl	9.49	518	bdl	8.04	64.6	bdl	10.7
Ca	422,000	384,000	407,000	427,000	359,000	407,000	441,000	324,000	403,000
Ti	bdl	bdl	bdl	58.8	bdl	0.48	1.23	bdl	0.018
Cr	24.7	bdl	0.13	5.38	bdl	0.048	2.24	bdl	0.026
Mn	2860	10.1	732	4080	667	1910	3330	185	856
Fe	973	126	319	1120	231	290	456	254	356
Co	0.50	bdl	0.13	0.43	bdl	0.11	0.81	0.082	0.16
Ni	134	bdl	1.15	184	bdl	1.39	1.94	0.40	0.71
Cu	8.52	bdl	0.71	9.77	bdl	0.32	0.73	bdl	0.25
Zn	3.92	bdl	0.55	8.24	bdl	0.86	4.32	bdl	0.88
Ga	22.6	1.20	5.03	45.5	3.29	13.0	17.4	0.44	5.67
Sr	1280	150	382	707	346	505	986	238	470
Y	0.13	bdl	0.004	0.52	bdl	0.009	0.12	bdl	0.004
Mo	0.14	bdl	0.010	0.18	bdl	0.023	0.17	bdl	0.013
Ba	441	23.8	111	1360	82.6	300	324	11.1	112
La	0.25	bdl	0.006	0.93	bdl	0.010	0.29	bdl	0.009
Pb	0.21	bdl	0.017	1.27	bdl	0.017	0.83	bdl	0.027

Detection limits: Li (0.027–0.26), B (0.23–0.63), Na (0.73–40.5), Mg (0.015–0.096), P (2.83–27.2), K (1.40–1.02), Ca (15.7–75.4), Ti (0.13–0.36), Cr (0.16–0.59), Mn (0.10–1.04), Fe (1.26–3.37), Co (0.009–0.023), Ni (0.026–6.36), Cu (0.024–0.43), Zn (0.097–0.56), Ga (0.013–0.84), Sr (0.014–0.14), Y (0.001–0.003), Mo (0.004–0.027), Ba (0.005–0.14), La (0.001–0.031), Pb (0.004–0.16).

bdl: below detection limit.

If the value is larger than or equal to 1, we use three significant figures. For example, 3260, 908, 24.7, and 1.15.

If the value is smaller than 1 and larger than or equal to 0.01, we use two significant figures. For example, 0.50 and 0.023.

If the value is smaller than 0.01, we use one significant figure. For example, 0.006.

All data in this article is presented by following the significant figure rule.

category were determined based on the analytical data and authors' experience. This method is modified based on geographic origin plots for sapphires used internally by GIA (A. Palke, pers. comm., 2018). Mn-Na corresponding chemical plots were constructed for each Ba-Sr category (figure 3). These categories showed it was easy to separate the USA-CUL pearls from the USA-NAT and CH-NBC pearls. In the low Ba, low Sr category (figure 3A), all USA-CUL pearls were off the plot, which left only two groups (USA-NAT and CH-NBC). In the high Ba, high Sr category (figure 3B), the majority of USA-CUL pearls were in the plot, while a high proportion of pearls from the other two groups were off the plot. Aside

from these results, partial separation may also be made using the high Ba, medium Sr (figure 3H) and medium Ba, medium Sr (figure 3I) categories.

The Mn concentrations were high in all the USA-CUL samples, with none less than 650 ppmw. The USA-CUL samples all had Sr or Ba contents greater than 340 and 80 ppmw, respectively. These samples are easier to identify through the narrower range in trace elements, because they were farmed from a single location and mollusk species. The USA-NAT and CH-NBC both showed many overlapping trace elements, most likely because the natural pearls formed in many mussel species spread across a large geographic footprint in North America. In the case



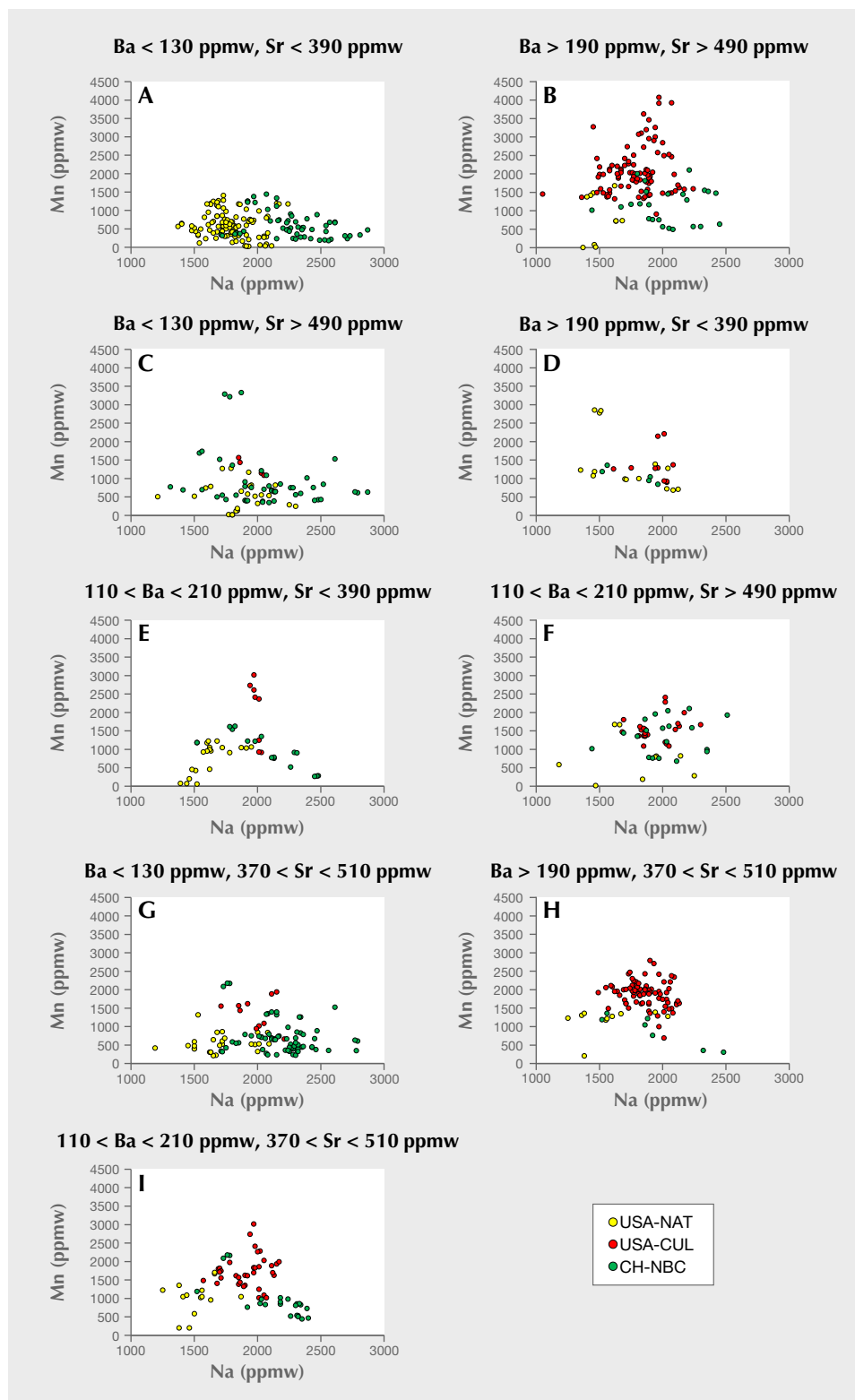


Figure 3. Mn vs. Na plots for the three freshwater pearl groups in each Ba-Sr category, modified from selective chemistry plots for the geographic origin of corundum.

of the Chinese pearls, the samples were obtained from different pearl dealers who no doubt acquired them from different culturing areas, also distributed

over a wide geographic area. Nonetheless, they did reveal a degree of separation when specific parameters were applied. Of the samples studied, only the

**TABLE 4.** LA-ICP-MS trace-element results (in ppmw) on questionable pearl samples.

Sample	Li	B	Na	Mg	P	K	Mn	Fe	Zn	Sr	Ba
NAT-EB2 SP1	bdl	2.36	2070	47.7	362	8.28	90.3	262	2.40	172	54.7
NAT-EB2 SP2	bdl	2.90	2020	47.9	368	7.81	64.3	265	2.22	170	47.1
NAT-EB2 SP3	bdl	0.91	1980	32.2	240	8.70	54.1	329	1.33	144	43.9
NAT-EB2 SP4	bdl	0.72	1960	31.8	253	7.55	48.9	330	1.31	151	48.6
NAT-EB2 SP5	bdl	0.79	1930	33.6	257	6.19	49.2	327	1.36	153	51.7
NAT-USA5 SP1	bdl	2.62	2060	133	243	15.6	42.1	291	0.93	332	70.2
NAT-USA5 SP2	bdl	2.65	1900	134	252	14.3	44.5	298	0.98	342	72.2
NAT-USA5 SP3	bdl	2.36	2110	135	263	13.9	42.2	296	0.99	355	75.7
NAT-USA5 SP4	bdl	0.54	1850	96.4	192	19.8	24.7	328	0.61	333	78.1
NAT-USA5 SP5	bdl	bdl	1780	103	190	11.3	26.6	330	0.66	319	72.3
NAT-USA5 SP6	bdl	bdl	1800	112	192	10.9	28.0	328	0.56	300	66.8
NAT-USA12 SP1	bdl	4.19	1460	89.2	165	117	83.3	279	0.42	546	210
NAT-USA12 SP2	bdl	4.07	1470	73.0	116	162	22.7	290	0.84	511	192
NAT-USA12 SP3	bdl	4.47	1370	56.0	99.2	21.4	10.1	288	0.47	780	303
NAT-USA12 SP4	bdl	bdl	1900	77.5	225	7.03	260	331	0.26	277	56.9
NAT-USA12 SP5	bdl	bdl	1930	176	230	bdl	260	327	0.51	274	60.1
NAT-USA12 SP6	bdl	bdl	1910	105	230	bdl	223	332	bdl	272	56.5
NAT-USA21 SP1	bdl	3.35	1920	28.1	229	7.02	28.4	349	1.28	212	27.9
NAT-USA21 SP2	bdl	3.22	1930	27.6	225	5.10	29.6	359	1.35	204	27.6
NAT-USA21 SP3	bdl	3.58	1910	24.1	216	4.04	32.9	347	1.40	201	26.9
NAT-USA21 SP4	bdl	0.54	1910	29.6	270	9.36	11.4	334	3.32	230	31.4
NAT-USA21 SP5	bdl	0.42	1910	32.3	266	7.72	15.5	302	2.93	230	32.2
NAT-USA21 SP6	bdl	0.53	1940	30.4	262	8.20	18.0	329	2.92	237	33.2
NAT-USA26 SP1	bdl	4.97	1770	70.0	253	18.9	21.4	385	0.99	896	77.1
NAT-USA26 SP2	bdl	5.37	1800	67.9	262	19.8	15.3	378	0.95	944	84.0
NAT-USA26 SP3	bdl	4.87	1800	66.4	259	16.0	19.8	377	1.28	905	75.6
NAT-USA26 SP4	bdl	1.73	2030	83.0	207	7.65	17.8	327	1.70	632	43.7
NAT-USA26 SP5	bdl	1.47	1990	84.5	207	6.64	17.2	329	1.64	623	44.3
NAT-USA26 SP6	bdl	1.54	2000	93.9	204	5.68	16.6	327	1.64	621	45.5
NAT-ANP14 SP1	bdl	8.11	1440	30.7	bdl	bdl	73.3	269	bdl	346	168
NAT-ANP14 SP2	bdl	5.92	1390	27.9	bdl	bdl	81.9	259	bdl	348	168
NAT-ANP14 SP3	bdl	7.09	1520	25.9	bdl	bdl	62.8	264	bdl	341	190
NAT-ANP14 SP4	bdl	bdl	1620	31.8	273	14.5	68.6	313	0.24	346	121
NAT-ANP14 SP5	bdl	bdl	1630	30.3	274	13.5	71.1	309	0.25	337	113
NAT-ANP14 SP6	bdl	bdl	1590	28.0	273	12.8	70.8	309	0.26	328	106
NAT-HS2 SP1	bdl	2.81	1840	97.7	313	26.7	127	261	1.71	1000	79.4
NAT-HS2 SP2	bdl	2.53	1830	99.7	311	27.5	118	256	0.93	1020	75.8
NAT-HS2 SP3	bdl	bdl	1810	82.6	227	29.9	76.7	327	0.59	964	76.5
NAT-HS2 SP4	bdl	bdl	1850	97.4	234	18.3	70.9	329	0.36	1000	70.1
NAT-HS2 SP5	bdl	0.47	1780	104	254	21.2	51.8	327	0.26	1020	93.7

*bdl = below detection limit*

USA-NAT samples (14%) had both Na contents of less than 2000 ppmw and Mn contents of less than 320 ppmw. USA-NAT samples showed Sr concentrations below 230 ppmw (9%) and Mn concentrations below 180 ppmw (10%). Only CH-NBC samples (31%) had Na concentrations over 2300

ppmw. None of the other sample groups showed these concentrations.

In general, the American samples showed Na levels lower than 2000 ppmw (USA-NAT 85% and USA-CUL 73%), while 69% of Chinese samples were higher than this amount. For the USA-CUL

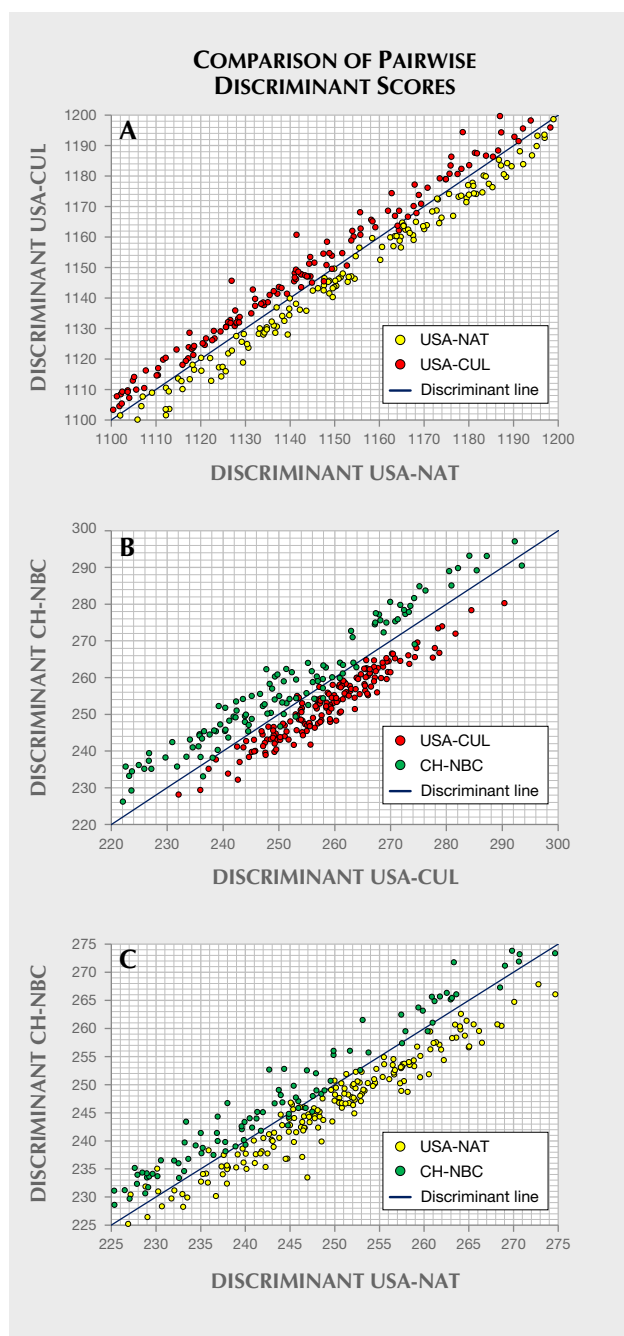


Figure 4. These three plots compare pairwise discriminant scores between American natural and American cultured samples (4A), Chinese NBC and American cultured samples (4B), and Chinese NBC and American natural samples (4C). For a pairwise LDA analysis, two discriminant functions are produced using a combination of the following elements:  $^{23}\text{Na}$ ,  $^{39}\text{K}$ ,  $^{44}\text{Ca}$ ,  $^{55}\text{Mn}$ ,  $^{57}\text{Fe}$ , and  $^{88}\text{Sr}$ . Applying the chemical concentrations for each sample into each of the two functions produces two scores, one representing each group. For each sample in the pairwise plots, the x-axis represents the score for one group and the y-axis represents the score for the other. In general, the relatively higher score indicates to which group the sample belongs. For example, samples from the CH-NBC group in figure 4B have a higher CH-NBC score in the y-axis direction relative to its USA-CUL score in the x-axis direction. The blue line separates the prediction of the two groups. The area above the blue line predicts that the sample belongs to the group on the y-axis; below the blue line predicts that the sample belongs to the group on the x-axis.

samples, 73% showed high Mn (>1000 ppmw) and Ba (>200 ppmw). Conversely, 82% of USA-NAT and 75% of CH-NBC samples showed low Mn (<1500 ppmw) and Ba (<200 ppmw). Sr concentration was high (>400 ppmw) in 88% of the USA-CUL samples, low (<400 ppmw) in 68% of the USA-NAT samples, and medium (300 to 600 ppmw) in 77% of the CH-NBC samples. All the percentages reported are based on the numbers of samples studied, rather than the number of analyzed spots.

The chemical characteristics of the freshwater pearl samples enabled a relatively well-defined separation to be carried out using the LDA application we developed. A combination of the following elements was found to be most useful for the separation of the different groups:  $^{23}\text{Na}$ ,  $^{39}\text{K}$ ,  $^{44}\text{Ca}$ ,  $^{55}\text{Mn}$ ,  $^{57}\text{Fe}$ , and  $^{88}\text{Sr}$ . For a pairwise LDA model, two discriminant functions were constructed and predicted two scores, one for each group. In general, the higher score indicated to which group the sample belonged. A model that predicts 100% places all samples correctly into the known groups. For the pair USA-NAT vs. USA-CUL, the (non-cross-validated) discriminant scores are plotted in figure 4A with the overall trend for USA-NAT samples to have higher USA-NAT discriminant scores relative to USA-CUL scores and with USA-CUL samples showing the opposite trend. Although the separation between the two groups looks small, 92.6% of the cross-validated grouped cases were correctly predicted. Thus, the model is a very good predictor, with the cross-validation test confirming the model's statistical validity. For the USA-CUL vs. CH-NBC and USA-NAT vs. CH-NBC pairs, the cross-validated prediction rates were 87.7% and 87.6%, respectively (figures 4B and 4C). The percentage of all the samples correctly predicted by the final decision tree step into the three known groups was over 85%. There are a number of factors such as varying species, location, and environment that could be contributing

**TABLE 5.** Sample categories defined by Ba and Sr concentration ranges (in ppmw<sup>a</sup>).

Category	Ba range	Sr range	Corresponding plot
Low Ba, Low Sr	Ba<130	Sr<390	Figure 3A
High Ba, High Sr	Ba>190	Sr>490	Figure 3B
Low Ba, High Sr	Ba<130	Sr>490	Figure 3C
High Ba, Low Sr	Ba>190	Sr<390	Figure 3D
Medium Ba, Low Sr	110<Ba<210	Sr<390	Figure 3E
Medium Ba, High Sr	110<Ba<210	Sr>490	Figure 3F
Low Ba, Medium Sr	Ba<130	370<Sr<510	Figure 3G
High Ba, Medium Sr	Ba>190	370<Sr<510	Figure 3H
Medium Ba, Medium Sr	110<Ba<210	370<Sr<510	Figure 3I

<sup>a</sup>A 20 ppmw overlapping area was defined between each adjacent category to account for analytical error.

Pearls showing chemistry within the overlapping areas were included in plots in figure 3.

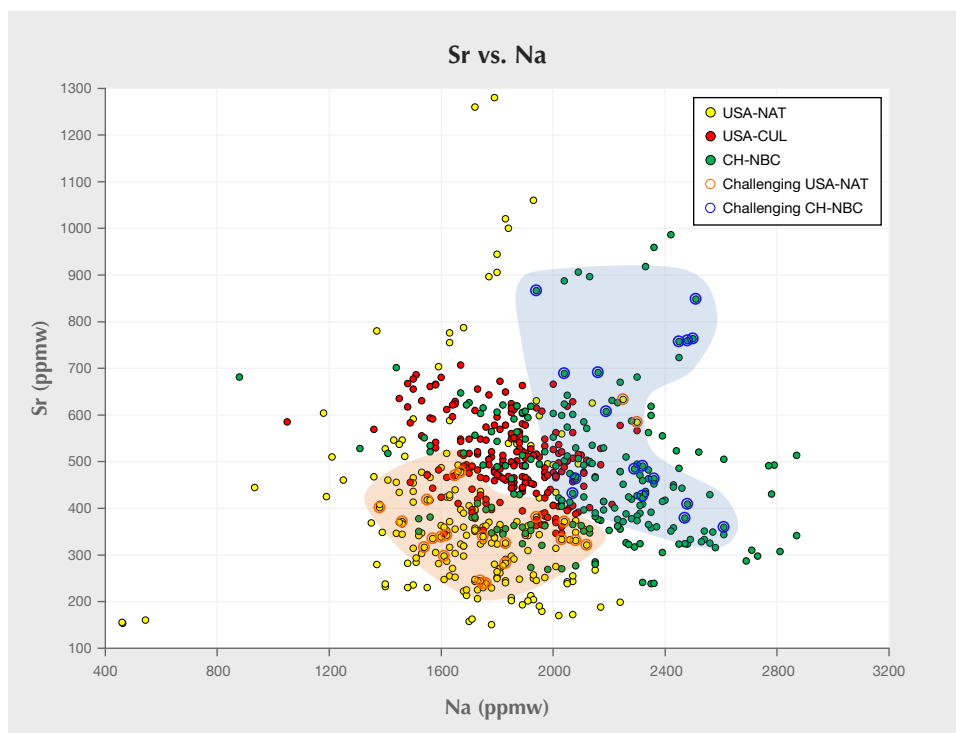
to the variance in sample chemistry, making the task of predicting these groups correctly more difficult. Despite such potential sources of variance, the LDA empirically predicts much better than chance. So at least for the samples tested, there are tendencies in chemistry that can be applied broadly to China, for example, that do not apply to the United States. Nevertheless, collections of samples that better represent any important factors contributing to the vari-

ance can lead to models that accommodate the influence of those additional factors, thereby improving upon the current prediction rates.

Lastly, the chemical plots comparing Sr and Na contents (figure 5) revealed a large number of USA-NAT and CH-NBC samples that exhibited challenging internal growth structures and were difficult to identify with X-ray techniques, thus separating them from the other sample groups. All the measurement spots of the studied samples are displayed in the plot, and concentrations of Sr and Na of these specific samples are shown in table 6. The LDA method correctly discriminated 60% and 70% of these challenging USA-NAT and CH-NBC samples, respectively (again, see table 6, column 4).

## CONCLUSIONS

From the findings of this preliminary study, we propose that the combination of trace-element information provided by LA-ICP-MS and subsequent application of LDA has the potential to classify freshwater pearls from different sources with relatively reliable accuracy. This method can be a useful aid in identifying freshwater pearls exhibiting challenging internal growth structures. The samples studied here were not collected directly from the mollusks (but



*Figure 5. The chemical plot of Sr vs. Na contents shows that a large number of American natural (orange shaded area) and Chinese NBC (blue shaded area) samples exhibited challenging internal growth structures and were difficult to identify using X-ray techniques, thus separating them from the other sample groups.*

**TABLE 6.** Na and Sr concentrations (in ppmw) of challenging American natural and Chinese NBC samples.

USA-NAT				CH-NBC			
Sample	Na <sup>a</sup>	Sr <sup>a</sup>	LDA <sup>b</sup>	Sample	Na <sup>a</sup>	Sr <sup>a</sup>	LDA <sup>b</sup>
NAT-TR1 SP1	1670	477	USA-NAT	NBC-CH5 SP1	2510	848	CH-NBC
NAT-TR1 SP2	1650	470	USA-NAT	NBC-CH5 SP2	1940	866	CH-NBC
NAT-TR3 SP1	2080	331	USA-CUL	NBC-CH9 SP1	2070	432	CH-NBC
NAT-TR3 SP2	2030	333	USA-CUL	NBC-CH9 SP2	2080	463	CH-NBC
NAT-TR3 SP3	2120	321	USA-CUL	NBC-CH12 SP1	2610	359	CH-NBC
NAT-TR4 SP1	1750	239	USA-NAT	NBC-CH12 SP2	2470	379	CH-NBC
NAT-TR4 SP2	1760	239	USA-NAT	NBC-CH15 SP1	2480	409	USA-CUL
NAT-TR4 SP3	1740	244	USA-NAT	NBC-CH15 SP2	2320	426	USA-CUL
NAT-MIX1 SP1	1550	418	USA-NAT	NBC-CH16 SP1	2480	759	CH-NBC
NAT-MIX1 SP2	1610	297	USA-NAT	NBC-CH16 SP2	2500	763	CH-NBC
NAT-USA1 SP1	2040	371	USA-CUL	NBC-CH16 SP3	2450	757	CH-NBC
NAT-USA1 SP2	1940	381	USA-CUL	NBC-CH35 SP1	2290	484	CH-NBC
NAT-USA2 SP1	2250	633	CH-NBC	NBC-CH35 SP2	2320	490	CH-NBC
NAT-USA2 SP2	2300	584	CH-NBC	NBC-CH35 SP3	2360	463	CH-NBC
NAT-USA17 SP1	1620	342	USA-NAT	NBC-CHRB3 SP1	2190	607	CH-NBC
NAT-USA17 SP2	1600	338	USA-NAT	NBC-CHRB3 SP2	2160	691	USA-CUL
NAT-USA17 SP3	1570	335	USA-NAT	NBC-CHRB3 SP3	2040	689	USA-CUL
NAT-USA18 SP1	1460	371	USA-NAT				
NAT-USA18 SP2	1380	401	USA-NAT				
NAT-USA18 SP3	1540	316	USA-NAT				
NAT-ANP04 SP1	1750	339	USA-NAT				
NAT-ANP04 SP2	1830	325	USA-NAT				
NAT-ANP04 SP3	1830	282	USA-NAT				

<sup>a</sup>Plotted in figure 5.<sup>b</sup>LDA-predicted results. Gray shading indicates challenging samples that were not correctly discriminated.

were supplied by reliable sources), and we cannot pinpoint the exact locations within the sources. The trace-element variations nonetheless corresponded to the geographic location, water environment, and mollusk species in which the pearls formed, and the results confirmed a degree of variation among sources.

To improve the usefulness of this technique to laboratory gemologists, we intend to study additional known samples from various geographic locations so that a large and dependable data set can be developed. The data may be further enhanced by narrowing down the recorded sources, as the results on the group of USA-CUL samples included in this work proves, by collecting pearls directly from specific localities, harvest seasons, and mollusk species, whether they be natural pearls from Tennessee and

Colorado in the United States, Scotland, or Germany, or NBC pearls from China, Japan, Thailand, or Vietnam, among other possibilities.

Pearl identification is still carried out primarily by observing and interpreting the structural results obtained from various X-ray techniques, and our method can only be used to support those results. Yet in cases where all the structural evidence has been destroyed by the drilling process or where the structure is so subjective that different opinions exist within the same laboratory, let alone between different laboratories, the combination of LA-ICP-MS and LDA may be the only way to reach a conclusion other than undeterminable. The only other possible aid to identification in the most challenging of cases is DNA testing, and this is another area of ongoing research for GIA and other institutes.

## ABOUT THE AUTHORS

Ms. Homkrajae is a senior staff gemologist in pearl identification, Mr. Sun is a research associate, and Dr. Blodgett is a research scientist at GIA in Carlsbad, California. Dr. Zhou is a research scientist and the manager of pearl identification at GIA in New York.

## ACKNOWLEDGMENTS

The authors wish to thank Gina Latendresse of the American Pearl Company, Inc. for providing the American pearl samples and information on them. Dr. Aaron Palke at GIA Carlsbad is kindly thanked for his guidance in helping us establish and standardize the method of making selective pearl chemical plots in dif-

ferent chemical ranges. We are deeply grateful to Dr. Zhongxing Chen at Harvard University's Department of Earth and Planetary Sciences for providing valuable advice to optimize LA-ICP-MS instrumental conditions, and sharing expertise in analyzing marine aragonites. Assistance from Daniel Girma at GIA's New York laboratory in finalizing the analytical procedure is greatly appreciated. Joyce WingYan Ho and Sally Chan Shih, also of GIA in New York, are thanked for their assistance with the examination of the internal structures and carrying out X-ray fluorescence analysis on the samples. Lastly, we thank Nicholas Sturman at GIA Bangkok for his helpful and constructive feedback.

## REFERENCES

- Abduriyim A., Kitawaki H. (2006) Applications of laser ablation-inductively coupled plasma-mass spectrometry (LA-ICP-MS) to gemology. *G&G*, Vol. 42, No. 2, pp. 98–118, <http://dx.doi.org/10.5741/GEMS.42.2.98>
- Akamatsu S., Li T.Z., Moses T.M., Scarratt K. (2001) The current status of Chinese freshwater cultured pearls. *G&G*, Vol. 37, No. 2, pp. 96–113, <http://dx.doi.org/10.5741/GEMS.37.2.96>
- Blodgett T.A., Shen A.H. (2011) Application of discriminant analysis in gemology: Country-of-origin separation in colored stones and distinguishing HPHT-treated diamonds. *G&G*, Vol. 47, No. 2, p. 145.
- China Gems (2019) Current status and development of the pearl industry, <https://mp.weixin.qq.com/s/IdSPt0KRmhvPKg4kKeBRrQ> [in Chinese].
- Dumańska-Słowik M., Heflik W., Natkaniec-Nowak L., Sikorska M., Weselucha-Birczyńska A. (2008) Cultured freshwater pearls from the Yangtze River (China); characterisation by optical microscopy, scanning electron microscopy, cathodoluminescence, electron microprobe analysis, and Raman spectroscopy. *The Australian Gemmologist*, Vol. 23, No. 7, pp. 290–299.
- Fiske D., Shepherd J. (2007) Continuity and change in Chinese freshwater pearl culture. *G&G*, Vol. 43, No. 2, pp. 138–145, <http://dx.doi.org/10.5741/GEMS.43.2.138>
- Friedman J.H. (1989) Regularized discriminant analysis. *Journal of the American Statistical Association*. Vol. 84, No. 405, pp. 165–175.
- Giuliani G., Caumon G., Rakotosamizany S., Ohnenstetter D., Rakotondrazafy M. (2014) Classification chimique des corindons par analyse factorielle discriminante: application à la typologie des gisements de rubis et saphirs. *Revue de l'Association Française de Gemmologie*, No. 188, pp. 14–22.
- Grabarkiewicz J.D., Davis W.S. (2008) An Introduction to Freshwater Mussels as Biological Indicators: Including Accounts of Interior Basin, Cumberlandian, and Atlantic Slope Species. United States Environmental Protection Agency, Washington, DC, <http://dx.doi.org/10.13140/2.1.3580.2405>
- Haag W.R. (2012) *North American Freshwater Mussels: Natural History, Ecology, and Conservation*. Cambridge University Press, Cambridge, UK.
- Habermann D., Banerjee A., Meijer J., Stephan A. (2001) Investigation of manganese in salt-and freshwater pearls. *Nuclear Instruments and Methods in Physics Research Section B: Beam Interactions with Materials and Atoms*, Vol. 181, No. 1-4, pp. 739–743, [http://dx.doi.org/10.1016/S0168-583X\(01\)00353-6](http://dx.doi.org/10.1016/S0168-583X(01)00353-6)
- Hänni H.A., Kiefert L., Giese P. (2005) X-ray luminescence, a valuable test in pearl identification. *The Journal of Gemmology*, Vol. 29, No. 5/6, pp. 325–329.
- Hastie T., Tibshirani R., Friedman J. (2009) *The Elements of Statistical Learning: Data Mining, Inference, and Prediction*, 2nd ed. Springer-Verlag, New York, 745 pp., <https://www.springer.com/us/book/9780387848570>
- Hsu T., Zhou C., Homkrajae A., Ho J.W.Y., Yazawa E., Padua P. (2016) Freshwater pearling in Tennessee. *GIA Field Report*, <https://www.gia.edu/gia-news-research/freshwater-pearling-tennessee>
- Hsu T., Zhou C., Homkrajae A., Ho J.W.Y., Yazawa E., Padua P. (2017) The lure of American freshwater pearls: Revisiting the Latendresse family. *GIA Field Report*, <https://www.gia.edu/gia-news-research/lure-american-freshwater-pearls-revisiting-latendresse-family>
- Hua D., Gu R. (2002) Freshwater pearl culture and production in China. *Aquaculture Asia*, Vol. 7, No. 1, pp. 6–8.
- Jochum K.P., Scholz D., Stoll B., Weis U., Wilson S.A., Yang Q., Schwalb A., Börner N., Jacob D.E., Andreae M.O. (2012) Accurate trace element analysis of speleothems and biogenic calcium carbonates by LA-ICP-MS. *Chemical Geology*, Vol. 318, pp. 31–44, <http://dx.doi.org/10.1016/j.chemgeo.2012.05.009>
- Karampelas S., Michel J., Zheng-Cui M., Schwarz J.-O., Enzmann F., Fritsch E., Leu L., Krzemnicki M.S. (2010) X-ray computed microtomography applied to pearls: Methodology, advantages, and limitations. *G&G*, Vol. 46, No. 2, pp. 122–127, <http://dx.doi.org/10.5741/GEMS.46.2.122>
- Karampelas S., Al-Alawi A.T., Al-Attawi A. (2017) Real-time micro-radiography of pearls: A comparison between detectors. *G&G*, Vol. 53, No. 4, pp. 452–456, <http://dx.doi.org/10.5741/GEMS.53.4.452>
- Kessrapong P., Lawanwong K., Sturman N. (2017) *Pinctada maculata* (pipi) bead-cultured blister pearls attached to their shells. *GIA Research News*, April 25, <https://www.gia.edu/gia-news-research/pinctada-maculata-bead-cultured-blister-pearls-shells>
- Krzemnicki M., Friess D., Chalus P., Hänni H.A., Karampelas S. (2010) X-ray computed microtomography: Distinguishing natural pearls from beaded and non-beaded cultured pearls. *G&G*, Vol. 46, No. 2, pp. 128–134, <http://dx.doi.org/10.5741/GEMS.46.2.128>
- Kunz G.F., Stevenson C.H. (1908) *The Book of the Pearl*. The Century Co., New York, pp. 485–513.
- Lara M.R., Jones D.L., Chen Z., Lamkin J.T., Jones C.M. (2008) Spatial variation of otolith elemental signatures among juvenile gray snapper (*Lutjanus griseus*) inhabiting southern Florida waters. *Marine Biology*, Vol. 153, No. 3, pp. 235–248, <http://dx.doi.org/10.1007/s00227-007-0799-5>
- Luo Z., Yang M., Shen A.H. (2015) Origin determination of dolomite-related white nephrite through iterative-binary linear discriminant analysis. *G&G*, Vol. 51, No. 3, pp. 300–311, <http://dx.doi.org/10.5741/GEMS.51.3.300>

- Martinez A.M., Kak A.C. (2001) PCA versus LDA. *IEEE Transactions on Pattern Analysis and Machine Intelligence*, Vol. 23, No. 2, pp. 228–233, <https://ieeexplore.ieee.org/document/908974>
- Pornwilard M.-M., Hansawek R., Shiowatana J., Siripinyanond A. (2011) Geographical origin classification of gem corundum using elemental fingerprint analysis by laser ablation-inductively coupled plasma-mass spectrometry. *International Journal of Mass Spectrometry*, Vol. 306, No. 1, pp. 57–62, <http://dx.doi.org/10.1016/j.ijms.2011.06.010>
- Scarratt K., Moses T.M., Akamatsu S. (2000) Characteristics of nuclei in Chinese freshwater cultured pearls. *G&G*, Vol. 36, No. 2, pp. 98–109, <http://dx.doi.org/10.5741/GEMS.36.2.98>
- Scarratt K., Bracher P., Bracher M., Attawi A., Safar A., Saeseaw S., Homkrajae A., Sturman N. (2012) Natural pearls from Australian *Pinctada maxima*. *G&G*, Vol. 48, No. 4, pp. 236–261, <http://dx.doi.org/10.5741/GEMS.48.4.236>
- Shen A., Blodgett T., Shigley J. (2013) Country-of-origin determination of modern gem peridot from LA-ICPMS trace-element chemistry and linear discriminant analysis (LDA). *Geological Society of America Abstracts with Programs*, Vol. 45, No. 7, p. 525.
- Strack E. (2006) *Pearls*. Rühle-Diebener-Verlag, Stuttgart, Germany, pp. 232–251.
- Sturgeon R.E., Willie S.N., Yang L., Greenberg R., Spatz R.O., Chen Z., Sciver C., Clancy V., Lam J. W., Thorrold S. (2005) Certification of a fish otolith reference material in support of quality assurance for trace element analysis. *Journal of Analytical Atomic Spectrometry*, Vol. 20, No. 10, pp. 1067–1071, <http://dx.doi.org/10.1039/b503655k>
- Sturman N. (2009) The microradiographic structures on non-bead cultured pearls. GIA Thailand, Bangkok, November 21, [www.giathai.net/pdf/The\\_Microradiographic\\_structures\\_in\\_NBCP.pdf](http://www.giathai.net/pdf/The_Microradiographic_structures_in_NBCP.pdf)
- Sturman N., Bergman J., Poli J., Homkrajae A., Manustrong A., Somsa-ard N. (2016) Bead-cultured and non-bead cultured pearls from Lombok, Indonesia. *G&G*, Vol. 52, No. 3, pp. 288–297, <http://dx.doi.org/10.5741/GEMS.52.3.288>
- Sweaney J.L., Latendresse J.R. (1984) Freshwater pearls of North America. *G&G*, Vol. 20, No. 3, pp. 125–140, <http://dx.doi.org/10.5741/GEMS.20.3.125>
- U.S. Fish & Wildlife Service (2018) Endangered species: America's mussels: Silent sentinels, <https://www.fws.gov/midwest/endangered/clams/mussels.html>
- Veinott G., Porter R. (2005) Using otolith microchemistry to distinguish Atlantic salmon (*Salmo salar*) parr from different natal streams. *Fisheries Research*, Vol. 71, No. 3, pp. 349–355, <http://dx.doi.org/10.1016/j.fishres.2004.09.004>
- Watters G.T., Hoggarth M.A., Stansbery D.H. (2009) *The Freshwater Mussels of Ohio*. The Ohio State University Press, Columbus.

For online access to all issues of GEMS & GEMOLOGY from 1934 to the present, visit:

[gia.edu/gems-gemology](http://gia.edu/gems-gemology)



# PLEOCHROISM AND COLOR CHANGE IN FACETED ALEXANDRITE: INFLUENCE OF CUT AND SAMPLE ORIENTATION

Karl Schmetzer

The color appearance of faceted gemstones is a complex subject, and the challenges are increased if the material is biaxial and pleochroism is added to the considerations. For alexandrite in particular, the quest for a beautiful cut gem is further intensified by efforts to achieve the “best” color change. As an optically biaxial material, alexandrite possesses three different vibration directions X, Y, and Z. These are parallel to the three crystallographic axes a, b, and c, each of which has a distinct pleochroic color.

The present study seeks to evaluate the effect of various factors on color and color change using two groups of faceted synthetic alexandrites of comparable sizes and cuts with table facets oriented perpendicular to one of the three crystallographic axes. If the faceted gemstones are examined in transmitted light in immersion with a polarizer between the sample and the observer, the basic pleochroic colors can be separated and seen individually. For the synthetic alexandrites, if the faceted gemstones are examined in reflected light, this study demonstrates that the mixing of the three colors X + Y + Z, caused by multiple reflections of light within the faceted stones, greatly diminishes the role of table facet orientation on the quality of color and color change in well-cut gems. Likewise, for other biaxial stones it is expected that the effects of pleochroism will also be reduced in faceted stones to some extent.

Alexandrite, the chromium-bearing variety of chrysoberyl, shows distinct pleochroism and a signature color change between daylight (or daylight-equivalent fluorescent light) and incandescent light, referred to as the alexandrite effect. A similar color change is also observed for other varieties of gem minerals such as garnet, sapphire, spinel, kyanite, fluorite, and diaspore (Bosshart et al., 1982; Gübelin and Schmetzer, 1982; Schmetzer et al., 2009).

Chrysoberyl, belonging to the orthorhombic crystal system, is birefringent and optically biaxial. If unpolarized light enters a birefringent crystal, the beam is split into two polarized waves in all directions not parallel to an optic axis. These two waves leave the crystal in polarized form and can be separated, and seen individually, by rotating a polarizer (i.e., a polarizing filter) located between the sample and the observer. The optically biaxial nature of chrysoberyl further means that the optical indicatrix has three different vibration directions X, Y, and Z, which are

parallel to the three crystallographic axes a, b, and c (Bloss, 1961; Wahlstrom, 1969; Kerr, 1977). In the three vibration directions, light can be differentially absorbed, and an absorption spectrum can be measured for each direction. These three directions thus generate three basic pleochroic colors (Burns, 1993; Schmetzer and Bosshart, 2010; Schmetzer et al., 2012, 2013; Sun et al., 2017; see also Devouard and Notari, 2009).

In views parallel to one of the three a, b, or c<sup>1</sup> crystallographic axes in alexandrite, two vibration directions and two of the three basic colors are always present simultaneously, i.e., X + Y, X + Z, or Y + Z (figure 1). Stated otherwise, the color seen with the unaided eye when looking parallel to any of the three crystallographic axes is always a mixture of two of the X, Y, and Z basic color components (Schmetzer and Bosshart, 2010; Schmetzer and Malsy, 2011).

The specific colors observed (and the spectra produced) are in turn dependent in large part on the concentrations of color-causing trace elements and the

See end of article for About the Author and Acknowledgments.

GEMS & GEMOLOGY, Vol. 55, No. 1, pp. 61–71,  
<http://dx.doi.org/10.5741/GEMS.55.1.61>

© 2019 Gemological Institute of America

<sup>1</sup>The present study refers to parameters based on the traditionally used morphological cell with a = 4.42, b = 9.33, c = 5.47 and X || a, Y || b, Z || c.



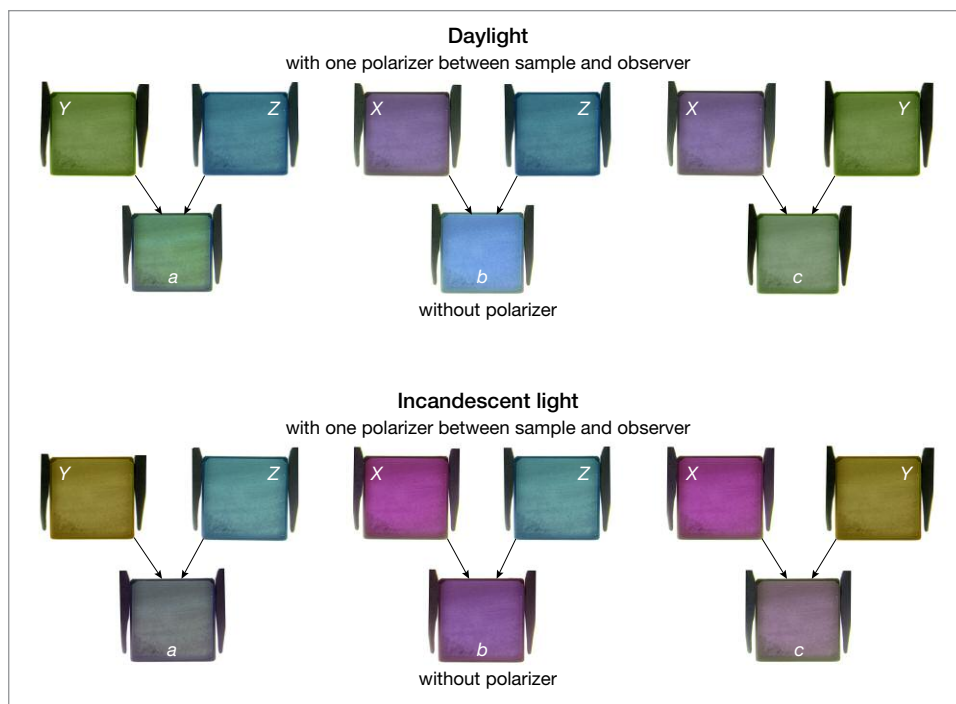


Figure 1. Color of a synthetic Czochralski-grown alexandrite cube with edge lengths of 9.0 to 9.2 mm, shown in daylight and incandescent light. In a view parallel to one of the crystallographic axes *a*, *b*, and *c*, the color is always a mixture of two of the three basic components *X*, *Y*, and *Z*, which can be separated and observed individually by using a polarizer (polarizing filter) between the sample and the observer.

All photos and drawings are by the author.

path length of light through the crystal. Principal trace elements affecting color in alexandrite are chromium, vanadium, and iron. Variations in path length result in the optical phenomenon referred to in gemology as the Usambara effect, with color changing or shifting as the path length increases (Halvorsen and Jensen, 1997; Halvorsen, 2006).

The color impressions just described, based on visual appearance and examination, have also been evaluated and verified through colorimetric measurement of natural alexandrite crystals, natural alexandrite cubes, and synthetic alexandrite cubes with different trace-element contents (Schmetzer and Bosshart, 2010; Schmetzer and Malsy, 2011; Schmetzer et al., 2012, 2013). For instance, colorimetric measurements using oriented cubes of synthetic alexandrite with edge lengths from 2 to 10 mm (Schmetzer et al., 2013) demonstrated that, regardless of size, for all three different orientations parallel to the *a*-, *b*-, and *c*-axes, changing between daylight and incandescent light resulted in a respective increase or decrease in blueness and redness (the alexandrite effect). With increasing cube size, a color shift was visible. The larger the cube, the redder the alexandrite appeared in both daylight and incandescent light (the Usambara effect).

The foregoing optical characteristics and phenomena have long spawned efforts to ascertain preferred orientations for fashioned alexandrines (and pleochroic materials more broadly). For alexandrite

in particular, the goal of gem cutters and merchants for decades has been the “best” color change, defined as a green or bluish green to blue-green purple in daylight and a red-purple or reddish purple to purple color in incandescent light. Conventional wisdom among cutters has traditionally held that this favored color change is obtained if the table facet is oriented perpendicular to the *b*-axis (Fischer, 1954). In practical terms, however, cutting in such a direction could prove problematic at times on account of the cyclic twinning commonly seen in natural alexandrines.

The above-noted work with oriented crystals and cubes has also lent scientific support to the traditional understanding, concluding on the basis of visual inspection in transmitted light and colorimetric measurements that the “best” and most highly desired color change between daylight and incandescent light was observed in a direction of view parallel to the *b*-axis (Schmetzer and Bosshart, 2010; Schmetzer and Malsy, 2011; Schmetzer et al., 2012).

Hughes (2014) described pleochroism using a simplified theoretical model for light behavior in optically biaxial faceted gemstones. That model was based upon a single light beam entering the crystal perpendicular to the table facet. If the table facet were oriented perpendicular to one of the crystallographic axes, that beam would be split into two of the three basic components *X*, *Y*, and *Z*. If next reflected from pavilion facets, the light beam would travel through the crystal in a direction parallel to

**TABLE 1.** Properties of synthetic alexandrites.

Growth method	No.	Orientation of seed	Orientation of table facet	Cut	Size (mm)	Weight (ct)	Color observed through table facet in reflected light	
							Daylight	Incandescent light
Flux growth by Creative Crystals Inc. (San Ramon, California) <sup>a</sup>	1		a (100)	Step cut	8.7 × 7.8 × 7.8	5.11	Green	Red-purple
	2	b (010)	b (010)	Step cut	9.1 × 8.6 × 8.2	5.83	Intense blue-green	Intense purple
	3		c (001)	Step cut	8.3 × 8.1 × 7.0	4.42	Green	Red-purple
HOC growth by V.V. Gurov (Novosibirsk, Russia) <sup>b</sup>	4		a (100)	Oval mixed	8.0 × 6.0 × 4.2	1.63	Blue-green	Purple
	5	b (010)	b (010)	Oval mixed	8.1 × 6.1 × 4.2	1.74	Blue-green	Purple
	6		c (001)	Oval mixed	8.1 × 6.0 × 4.1	1.66	Blue-green	Purple

<sup>a</sup>See Schmetzer et al. (2012)<sup>b</sup>See Schmetzer et al. (2013)

another of the three crystallographic axes and, consequently, would contain the third basic color component. After another reflection at the pavilion, the light leaving the faceted gemstone would be a mixture of all three components X, Y, and Z.

Hughes (2014) further noted that, depending on the cut of the sample, the light path length could vary based on whether the beam entered the faceted gemstone near the center of the table facet or near the girdle. Hence, the mixture of light reflected from different pavilion facets would show different percentages of X, Y, and Z, thereby generating different colors. Unfortunately, however, no faceted biaxial gemstones with known orientations were presented to support the theoretical model.

More recently, Sun et al. (2017) both inspected visually and measured colorimetrically a solely Cr-bearing Czochralski-grown synthetic alexandrite cuboid with edges between 2.65 and 3.18 mm and also calculated colorimetric data maps detailing color, chroma, chroma difference, hue angle difference, and color difference for wafers in various orientations and with path lengths between 1 and 25 mm. One point explicitly highlighted was that areas with large values for hue angle difference or color difference did not necessarily show the “best” orientation for the desired color change.

Maps of colorimetric data were likewise calculated for faceted alexandrites. Based upon the general considerations of Hughes (2014) for optically biaxial gemstones, Sun et al. computed parameters for color and color change for a hypothetical faceted stone with a 10 mm light path length. Using preferred ranges for hue angle for daylight versus incandescent light and large chroma values for both light sources for alexandrite, these authors tried to find the “best” orientation of the table facet or, in their own words, to “orient a stone along the ‘best’ direction.” It was concluded “that pleochroism in a faceted gemstone serves to

smear out the “best” direction for color change.” Furthermore, it was found “that stones cut with their table to culet direction oriented perpendicular to the b-axis show the best color change, while orientation parallel to the b-axis produces weaker color change” (Sun et al., 2017; Z. Sun pers. comm., 2018).<sup>2</sup>

Again, however, no faceted stones were examined and compared with the results obtained by theoretical calculations of colorimetric parameters.

Thus, with regard to faceted alexandrites found in the trade, the current situation remains one where questions abound. Due to differences in trace-element content, sample orientation, size, and cut, numerous parameters exist that might influence color and color change. The present study therefore attempts to address queries involving the influence of these factors using carefully prepared samples of faceted material.

## SAMPLES

The high value of facet-quality natural alexandrite material renders it nearly impossible to obtain suitable rough for cutting several small samples with different known orientations from the same large rough crystal. Hence, the present study was performed with synthetic gem material. Two groups of three samples each were cut from two synthetic crystals. An overview is provided in table 1.

One group consisted of three samples cut from a flux-grown synthetic alexandrite produced by Creative Crystals Inc. in San Ramon, California (see Schmetzer et al., 2012). The crystal was grown with a seed oriented parallel to *b* (010), and square or almost square

<sup>2</sup>Sun et al. (2017) presented results using the cell applied for crystal structure refinement in 1962 with *a* = 9.404, *b* = 5.476, *c* = 4.427 and X || *c*, Y || *a*, Z || *b*. For comparison purposes, those results have been converted to correspond with the morphological cell used here. See again footnote 1.

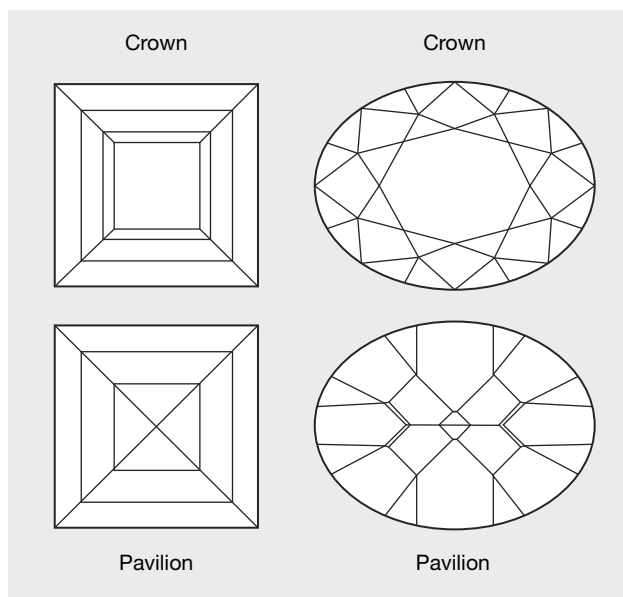


Figure 2. Diagram showing the cuts of the two groups of synthetic alexandrites examined in this study. Three samples were faceted with a simple step cut (emerald cut) with a nearly square table and three rows of facets on both the crown and the pavilion (left). The other three samples were faceted with an oval brilliant cut on the crown and a mixed cut (brilliant and step) on the pavilion (right).

table facets were cut parallel to either  $a$  (100),  $b$  (010), or  $c$  (001). Simple step cuts (emerald cuts) were fashioned with a table facet, three rows of crown facets, and three rows of pavilion facets (figure 2). Sizes ranged from  $8.3 \times 8.1 \times 7.0$  mm to  $9.1 \times 8.6 \times 8.2$  mm.

The other group comprised three synthetic alexandrites faceted from a crystal grown by the HOC technique in Novosibirsk, Russia, by V.V. Gurov (see Schmetzer et al., 2013). Starting with pieces sawn from the rough crystal, likewise produced with a seed parallel to  $a$  (010), table facets were again oriented parallel to either  $a$  (100),  $b$  (010), or  $c$  (001). An oval brilliant cut was used for the crown, with a mixed cut of brilliant and step facets for the pavilion (figure 2). Sizes spanned from  $8.0 \times 6.0 \times 4.2$  mm to  $8.1 \times 6.1 \times 4.2$  mm.

Within each group, the identical cuts and similar dimensions enabled a direct comparison of the influence of cut orientation upon color and color change.

## CHEMICAL PROPERTIES

The flux method employed by Creative Crystals for the alexandrites examined here used a series of several sequential growth cycles. As a result, the amount of chromium and iron, the principal color-

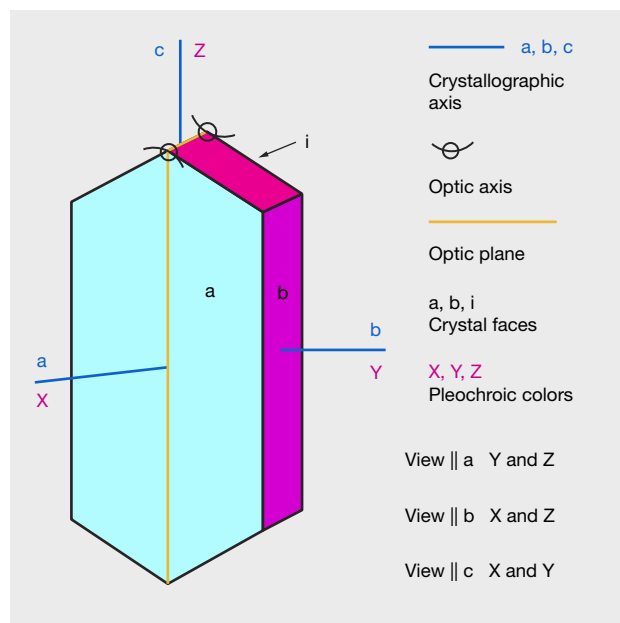
causing trace elements in these samples, incorporated in each growth layer was variable. Mean values ranged from 0.18 to 0.26 wt.%  $\text{Cr}_2\text{O}_3$  and from 0.86 to 1.14 wt.%  $\text{Fe}_2\text{O}_3$ . Vanadium contents were approximately 0.01 wt.%  $\text{V}_2\text{O}_3$  (Schmetzer et al., 2012).

The synthetic alexandrites grown by the HOC technique, in contrast, were more homogeneous in chemical composition, with chromium measuring from 0.30 to 0.43 wt.%  $\text{Cr}_2\text{O}_3$  and vanadium ranging from 0.07 to 0.14 wt.%  $\text{V}_2\text{O}_3$ . Iron levels were at 0.01 wt.%  $\text{Fe}_2\text{O}_3$  or below (Schmetzer et al., 2013).

## VERIFICATION OF SAMPLE ORIENTATION

The orientation of the table facets, which were cut according to morphological features of the rough gem alexandrites, was verified by ascertaining the positions of the optic axes in each stone. The optic axes lie in the optic plane, which in chrysoberyl is the  $ac$ -plane, and the  $c$ -axis is located exactly between the two optic axes (figure 3). The  $b$ -axis is perpendicular

Figure 3. Schematic diagram demonstrating the orientation of the optic plane and the two optic axes relative to the crystallographic axes  $a$ ,  $b$ , and  $c$  in alexandrite. The optic plane with both optic axes is the  $ac$ -plane. The three basic vibration directions  $X$ ,  $Y$ , and  $Z$ , which also represent the three basic color components, are oriented parallel to the  $a$ -,  $b$ -, and  $c$ -axes. In views parallel to one of the crystallographic axes, two basic vibrations and their color components are always present.



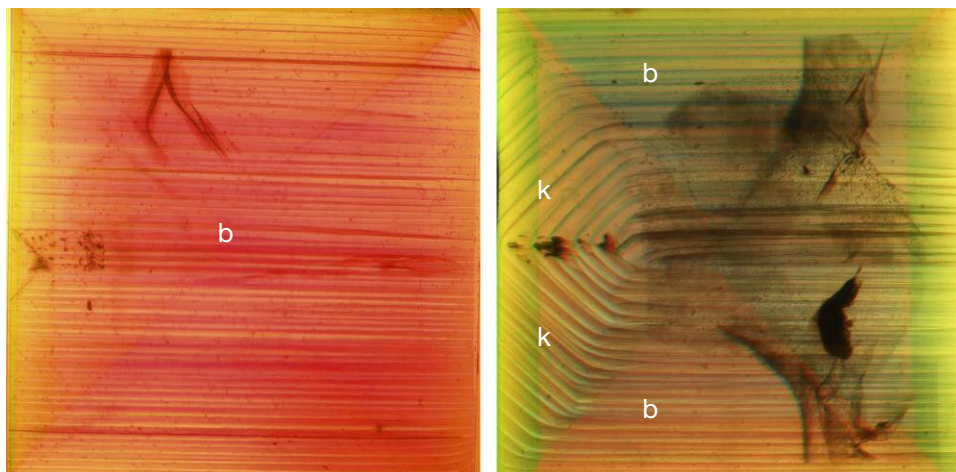


Figure 4. In faceted alexandrites produced using the flux method by Creative Crystals Inc., growth planes parallel to the pinacoid  $b$  (010) and the prism  $k$  (021) are observed in the immersion microscope. The  $b$ -axis runs north-south in both examples. These growth structures aid in locating the positions of the  $b$ -axis and the optic plane. Viewed in immersion with polarized light, field of view  $7.5 \times 7.5$  mm.

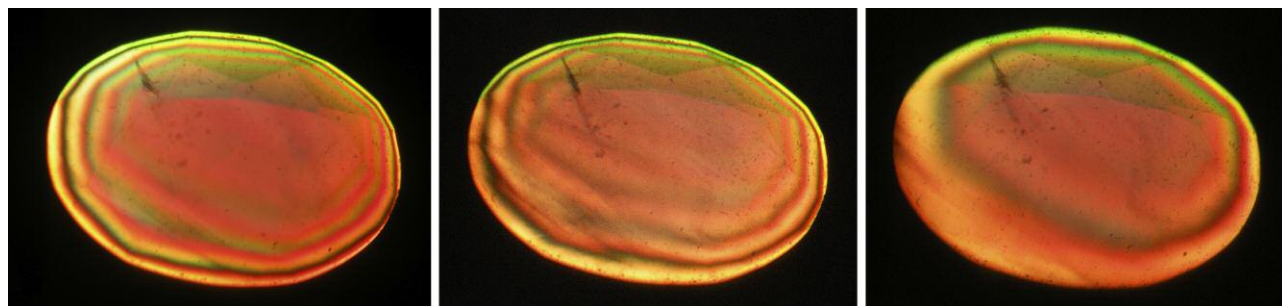
to the optic plane. Consequently, by viewing in a direction parallel to the optic plane and rotating a sample about the  $b$ -axis, both optic axes may be brought parallel to the direction of view.

In applying this information to the flux material grown by Creative Crystals, the task was aided by growth planes visible in immersion parallel to the seed (010) and, in one sample, additional growth planes parallel to the prism  $k$  (021) (figure 4). By using that insight (in conjunction with the observed pleochroism; see below), it was possible with reasonable ease to find the  $b$ -axis of the crystals and to use that axis for rotation in the immersion microscope. In so doing, an interference pattern consisting of several rings would be obtained if an optic axis were slightly inclined to the direction of view. Tilting the faceted alexandrite toward a position in which the optic axis was parallel to the direction of view would then move the interference rings toward the center

of the sample. The positions of both optic axes in the optic plane of the gemstone could thus be located, leading directly to the positions of the crystallographic axes  $a$ ,  $b$ , and  $c$  and making apparent the orientation of the table facet relative to the crystallographic axes. The practical measurements were made by means of two- and three-axial sample holders with attached dials to measure angles. For all three step-cut samples, the deviation of the table facets from the intended orientation was below  $5^\circ$ .

The same procedure was applied for the three oval samples cut from a crystal grown by the HOC technique. Because these crystals, in general, did not show distinct growth planes, finding the proper orientation for the sample in the immersion microscope with the  $b$ -axis as the rotation axis was somewhat more time consuming. However, after locating both optic axes through observation of interference patterns (figure 5), the positions of the three crystallo-

Figure 5. Interference figures of an  $8 \times 6$  mm faceted alexandrite grown by the HOC technique in Novosibirsk, Russia. In all three images, the optic axis is inclined to the direction of view. Tilting the crystal toward a position in which the angle between the optic axis and the direction of view is decreased (shown from left to right) moves the interference rings toward the center of the sample. Upon rotating the crystal about the  $b$ -axis, both optic axes can be observed. The locations of both optic axes determine the positions of the optic plane and of the  $a$ - and  $c$ -axes. With this information, the angle between the table facet and the relevant crystallographic axis can be verified. Viewed in immersion with crossed polarizers.



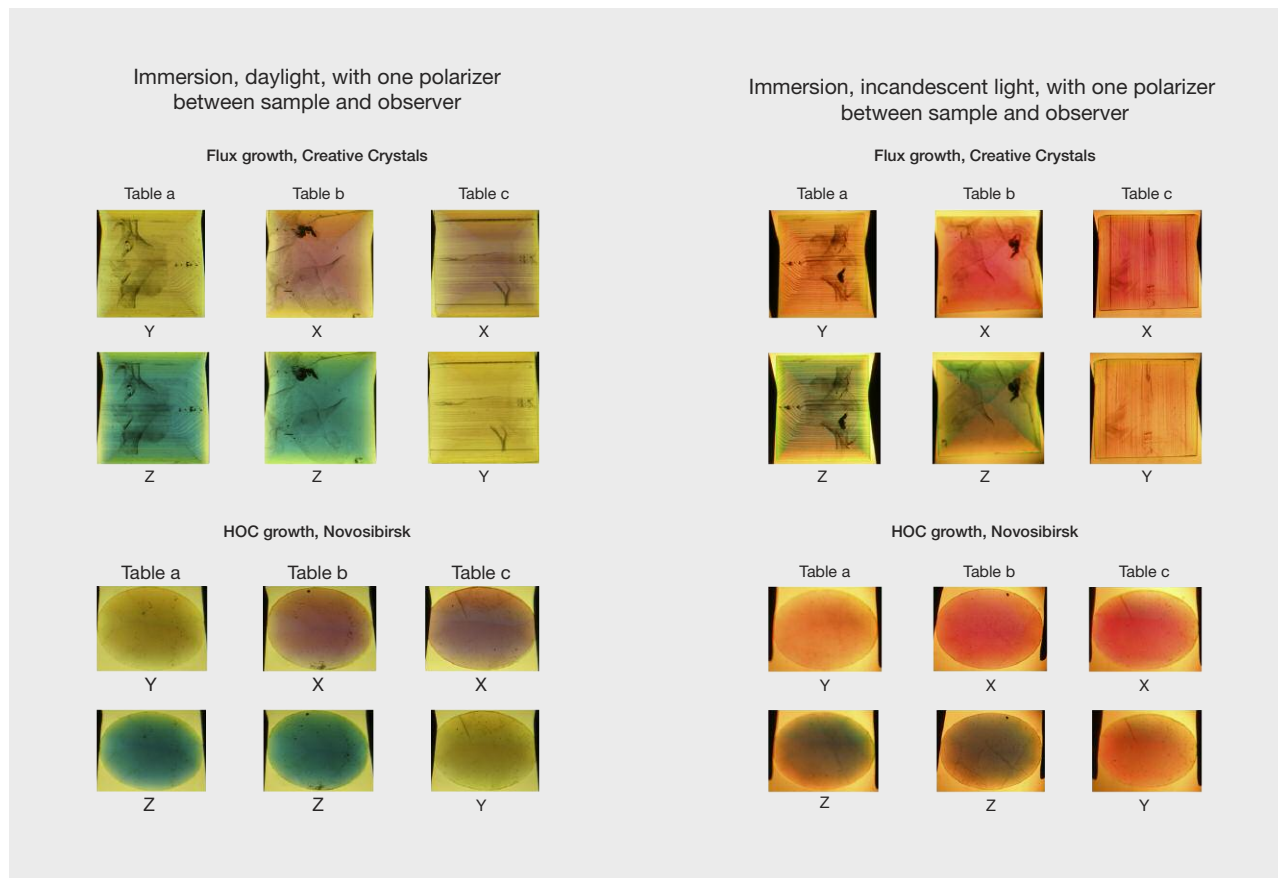


Figure 6. Pleochroism in faceted alexandrites cut with table facets perpendicular to the three crystallographic axes *a*, *b*, and *c*, in daylight (left) and incandescent light (right). The three basic colors of X, Y, and Z are observed by using a rotatable polarizer between the sample and the observer. The colors seen are nearly identical for all six alexandrite samples, regardless of differences in cuts and sizes. Use of immersion liquid reduces the influence of reflections from the facets. Field of view  $7.5 \times 7.5$  mm (flux-grown samples) and  $8 \times 6$  mm (HOC-grown samples).

graphic axes were determined, and the inclination of the table facet to the relevant crystal axis was measured. It was again found that the deviation of the table facets from the intended orientation was below  $5^\circ$  for all three mixed-cut gemstones.

### COLOR BEHAVIOR OF FACETED GEMSTONES IN TRANSMITTED LIGHT

As noted at the outset, unpolarized white light in birefringent chrysoberyl crystals is split into two polarized waves, which can in turn be separated and seen individually by rotating a polarizer placed between the sample and the observer. For purposes of evaluating this phenomenon in faceted alexandrites in transmitted light, the samples were observed in immersion. By doing so, reflection of light at the pavilion facets and the corresponding mixing of dif-

ferent color components could be largely avoided. The only minor side effect of the methodology was a slight shift in color toward yellow on account of the immersion liquid.

All six oriented samples displayed the pleochroic behavior and colors commonly seen in alexandrites of similar size in both daylight and incandescent light, as follows (figure 6):

**Daylight:** X || *a* = violet-purple, Y || *b* = yellow-orange, Z || *c* = intense blue-green

**Incandescent light:** X || *a* = reddish purple, Y || *b* = orange, Z || *c* = green

The results were consistent with the established orientation of the table facets of the six samples as described above. The colors of X, Y, and Z observed visually were almost identical for the different sam-

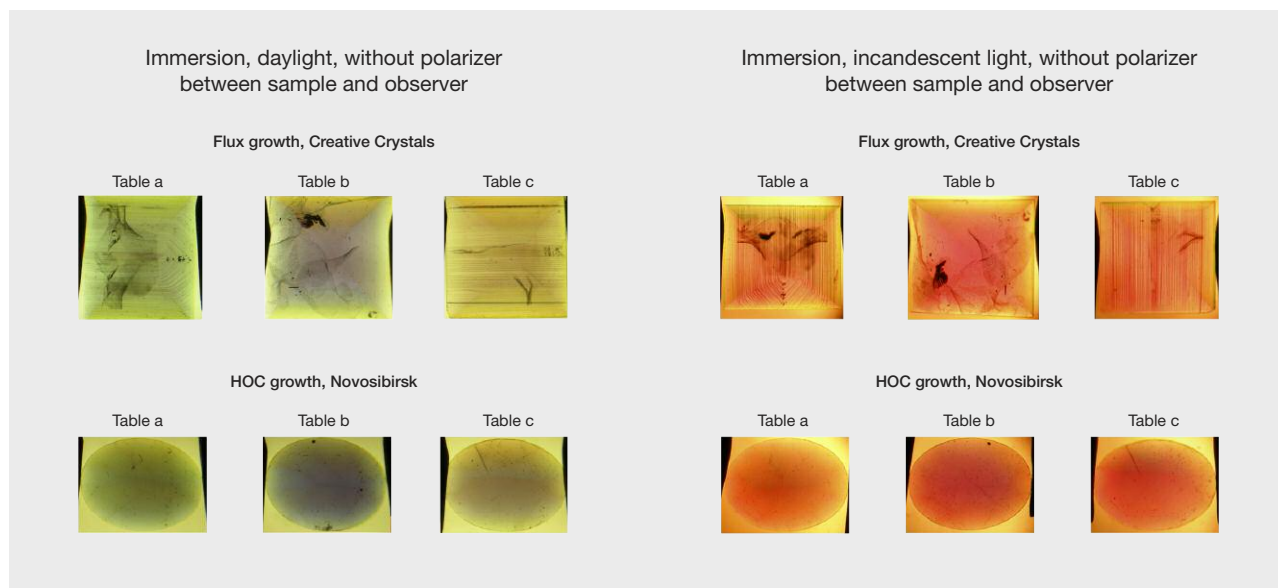


Figure 7. Pleochroism in faceted alexandrites cut with table facets perpendicular to the three crystallographic axes *a*, *b*, and *c*, in daylight (left) and incandescent light (right). The different colors are observed in views parallel to the crystallographic axes without using a polarizer. The colors seen are nearly identical for all six alexandrites, regardless of differences in cuts and sizes. Use of immersion liquid reduces the influence of reflections from the facets. Field of view approximately  $7.5 \times 7.5$  mm (flux-grown samples) and  $8 \times 6$  mm (HOC-grown samples).

ples of each group (flux-grown and HOC-grown synthetic alexandrites), with no distinct differences. Likewise demonstrated was the effect of differences in light path length and stone thickness, insofar as a fading of the color from the center of the table (or the culet) to the girdle was seen, especially in the step-cut samples grown by Creative Crystals.

Still in transmitted light but without a polarizer, two of the three basic colors previously separated by means of the filter were mixed in each direction of view. In all three directions, a color change between daylight and incandescent light was perceived (figure 7):

**Daylight:** view || *a* = green, view || *b* = blue-violet, view || *c* = greenish yellow

**Incandescent light:** view || *a* = red-purple, view || *b* = reddish purple, view || *c* = red-purple

Again, no distinct differences were seen when comparing samples with the table facets in the same orientation, regardless of the cut.

Thus, to summarize, in transmitted light and especially in immersion, it was possible to observe different colors in views parallel to one of the three crystallographic axes and, by means of a polarizer, to separate the three basic colors of *X*, *Y*, and *Z*.

## COLOR BEHAVIOR OF FACETED GEMSTONES IN REFLECTED LIGHT

Turning to the scenario in reflected light, the impression was one of a mixture of all three color components. To evaluate the general underpinnings of this situation, the simplified model presented by Hughes (2014) for biaxial gemstones in general was applied to the synthetic alexandrites examined.

With regard to the samples faceted with a relatively simple step cut (emerald cut), and by neglecting the refraction of light entering the crown facets and assuming a pavilion angle (the angle between the table and a pavilion facet) of  $45^\circ$ , a similarly simplified model for the path of light could be drawn. An example is given in figure 8 for an alexandrite cut with the table facet perpendicular to the *b*-axis. Unpolarized white light entering the sample at (1) through the table and crown facets would travel along the *b*-axis and split in the sample into *X* and *Z* color components. After reflection at the pavilion, light would travel along the *c*-axis, with *X* and *Y* color components. After a further reflection at the opposite side of the pavilion, the light beam would again travel along the *b*-axis. Light leaving the sample at (3) would thus contain *X*, *Y*, and *Z* color components. Reversing the scheme, light entering the

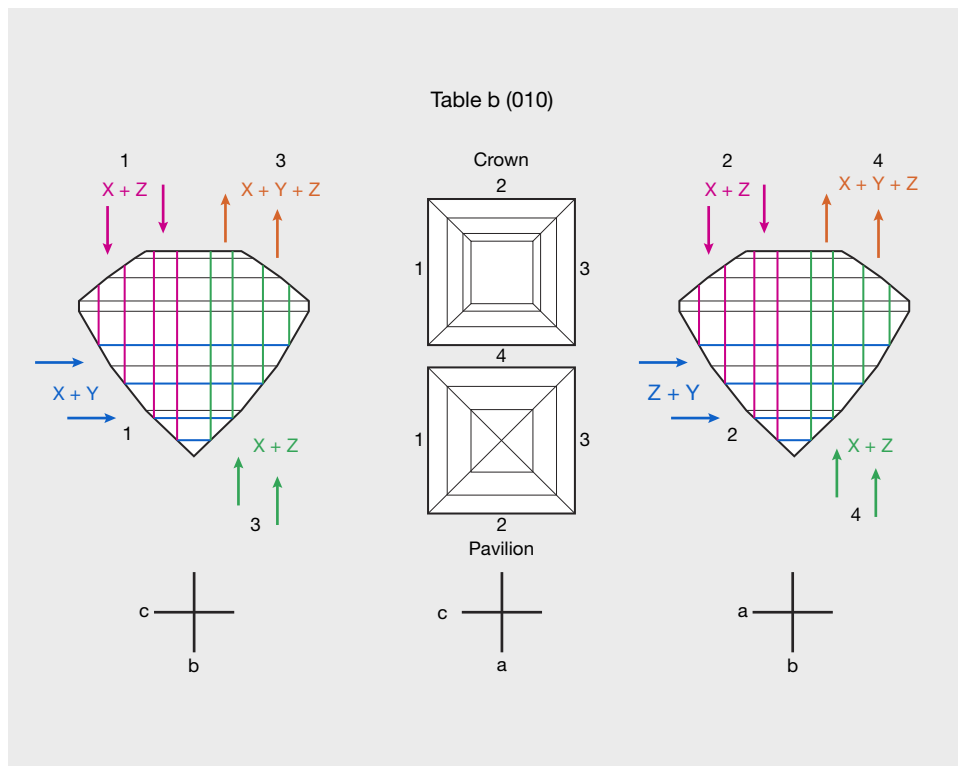


Figure 8. Schematic representation of simplified light paths through a faceted bi-axial alexandrite cut with a table facet perpendicular to the *b*-axis. Views perpendicular to the table facet—i.e., parallel to the *b*-axis (center) and parallel to the table facet (right and left); *a*, *b* and *c* represent the directions of the crystallographic axes. Light entering the crown at (1) is reflected at pavilion facets at (1) and (3), leaving the crown at (3). Light entering the crown at (2) is reflected at pavilion facets at (2) and (4), leaving the crown at (4). Light is absorbed along the different light paths, and a complex mixture of the three basic color components *X*, *Y*, and *Z* exits the crown of the gemstone.

sample at (3) would traverse along analogous paths, leaving the sample at (1). Light paths are not shown for this example.

If the starting point is shifted by 90°, light entering the sample at (2) through the table and crown facets would travel along the *b*-axis and split in the sample into *X* and *Z* color components. After reflection at the pavilion, the beam would travel along the *a*-axis, with *Y* and *Z* color components. Following a second reflection opposite, the beam would return to traveling along the *b*-axis. Upon exit at (4), the light would consist of two polarized waves with each wave showing *X*, *Y*, and *Z* color components. A reversed scenario for light entering at (4) would display a similar route, leaving the sample at (2). Again, light paths are not shown for this example.

Hence, application of the simplified model reveals that for each light path just described, the beam leaving the sample at the table or crown facets would have *X*, *Y*, and *Z* color components. If the simplifying assumptions are removed from the equation, light entering the alexandrite would be refracted at the crown facets, and the beam traveling through the sample would be reflected at facets with pavilion angles other than 45° (figure 9). For example, the three pavilion angles of the step-cut alexandrines examined here measured 62°, 54°, and 42°, respectively. The actual behavior in the faceted step-cut alexandrines

would therefore entail a far more diverse collection of beams, path lengths, and oblique directions through the sample. Such oblique directions, in turn, would alter the absorptions and corresponding mixtures of *X*, *Y*, and *Z* color components present in each beam exiting from the faceted gemstone. As a result, the light leaving the sample would show a more complex mixture of *X*, *Y*, and *Z* components than calculated on the basis of the simplified model.

Analogous theoretical considerations would pertain for samples cut with the table facets in other directions (i.e., perpendicular to the *a*- and *c*-axes). Similarly pertinent, if the cut is more complicated, such as that of the three HOC alexandrines with an oval brilliant-cut crown and a mixed-cut pavilion, more reflections would be generated, with light passing through the samples in an even greater number of different directions.

The foregoing theories suggesting extensive color mixing were tested on a practical basis using the six faceted samples in both daylight and incandescent light. The alexandrines of the two groups were placed table-up on a grooved plastic stone tray, which made it possible to view all six simultaneously while the light of a single lamp was reflected from their table facets. As such, the color impression given by each of the samples was quite similar, notwithstanding the different cut orientations for the table facets. This

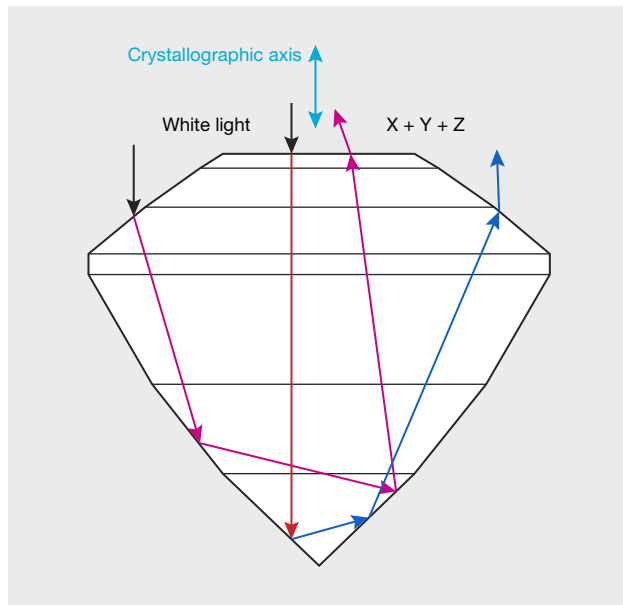


Figure 9. Schematic representation of light paths through a faceted biaxial alexandrite. Light is refracted at the crown facets and reflected from the pavilion facets. If the table facet is oriented perpendicular to a crystal axis, only the beam shown in red would consist of just two color components. All light beams inclined to this beam would be composed of all three color components X, Y, and Z. Therefore, light traveling through the faceted sample leaves the gemstone as a complex mixture of the X, Y, and Z color components.

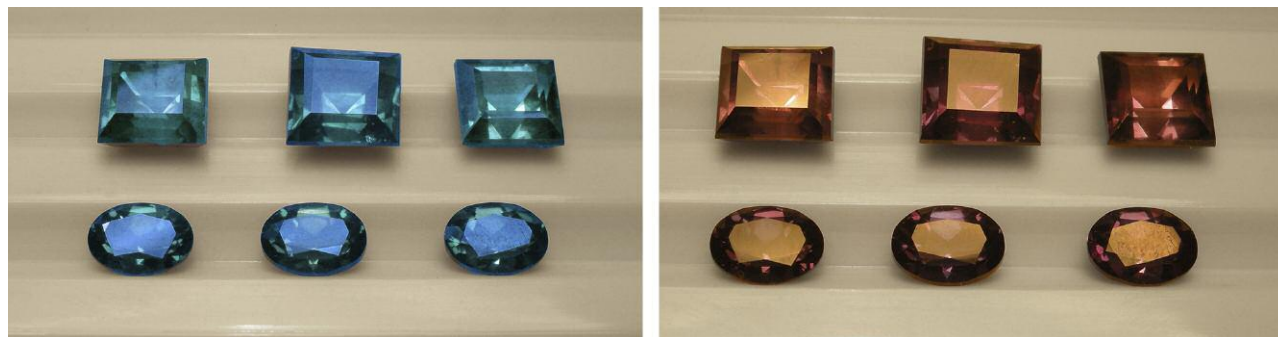
similarity thus corroborated the mixing of all three colors in faceted stones due to multiple reflections.

More specifically, with respect to the three step-cut alexandrites, some minor differences in color could be discerned. In daylight, the sample cut with the table facet perpendicular to the b-axis was blue-green, while the other two were less blue, more green, or even slightly yellowish green (figure 10). In incandescent light, the sample with the table perpendicular to the b-axis was intense purple, while the two other two were less intensely colored, somewhat more reddish purple or red-purple.

When using the stone tray arrangement, the colors of the three samples with a more complex cut and a greater number of crown and pavilion facets were equivalent to each other in daylight and incandescent light. No visual color differences were observed. Moreover, if the alexandrites were placed on a glass plate, with several light sources illuminating them from different directions through the table and crown facets, or if the alexandrites were observed in diffused daylight, the differences in visual impression for even the step-cut samples became almost indistinguishable.

The divergence of the above results from the colors calculated by Sun et al. (2017) for alexandrites of various orientations are potentially explained by the simplifications employed for the model used there. In particular, the calculations neglected refraction of light at the crown facets, reflection of light from pavilion facets at angles of other than  $45^\circ$ , and especially multiple reflections from light entering the stone at directions oblique to the table facet. As a consequence, oblique directions of travel were not taken into account, yet these contribute significantly to the lively appearance of a faceted gemstone. It would be interesting to see if an augmented, more

Figure 10. The six examined alexandrites in daylight (left) and incandescent light (right). These images have been corrected to represent the colors perceived by the eye. The samples, faceted with tables perpendicular to the a-, b-, and c-axes, are positioned face-up on a grooved plastic tray and illuminated with a light source placed directly above. The step-cut stones in the top row are in the range of 8 to 9 mm; the oval samples in the bottom row are approximately  $8 \times 6$  mm.





complex model incorporating a more realistic group of reflections and light paths within the sample would yield a closer approximation of reality.

In summary, the practical observations in the present study indicate that the cut and the orientation of the table facets play some role in achieving the desired colors in daylight or incandescent light. Nonetheless, all three simple step-cut alexandrites showed the “desired” color change. For samples with a more complex cut, such as a brilliant or mixed cut with numerous reflecting pavilion facets, the orientation of the table facet in such alexandrites is an almost negligible factor in determining color and color change.

## CONCLUSIONS

Examination of two groups of faceted synthetic alexandrites with three known specific orientations of the table facets confirmed the general applicability of widely held tenets regarding color in the gemstone and also showed that as the cuts become more complex, such considerations have a diminishing effect on the actual appearance. In alexandrite, the three main color components of X, Y, and Z are quite different, but their visual impact can depend heavily on the viewing scenario.

When faceted samples are observed in transmitted light, with or without the use of a polarizer, distinct color differences dependent on the orientation of the table facets can be perceived. Conversely, in reflected light, the color differences become less discernible. More particularly, the differences are weaker in samples with a simple step cut and nearly nonexistent with a complex cut.

Thus, to summarize the progression in moving from basic cases to the more complicated (see also Schmetzer et al., 2013):

- Cubes of different sizes viewed in transmitted light parallel to the a- and c-axes are green or even slightly yellowish green in daylight and red-purple or reddish purple in incandescent light. Cubes viewed parallel to the b-axis are more blue-green, blue, or even violet in daylight and more purple or purplish violet in incandescent light. In other words, parallel to the a- and c- axes there is a stronger yellow component in daylight and a stronger red component in incandescent light, while parallel to the b-axis there is a stronger blue component in both daylight and incandescent light.

- Faceted alexandrites with a simple cut such as a step cut exhibit, when viewed in reflected light, behavior similar to that of the cubes, albeit potentially weaker. Those with table facets perpendicular to the a- and c-axes are green or even slightly yellowish green in daylight and red-purple or reddish purple in incandescent light. Those with table facets perpendicular to the b-axis are more blue-green, blue, or even violet in daylight and more purple or purplish violet in incandescent light. The differences diminish with multiple light sources at a variety of angles, or with diffused light.
- Faceted alexandrites with a complex cut—such as a modern brilliant or mixed cut—display, when viewed in reflected light, almost no discernible color difference dependent upon table facet orientation.

The faceted samples studied here also demonstrated the interrelated effect of trace-element concentration and light path length. To wit, although the flux-grown alexandrites were larger than those grown by the HOC technique, the intensity of their colors was similar because the sum of color-inducing trace elements in the HOC material—primarily chromium and vanadium—was approximately double that in the flux material. The longer light path lengths in the three larger flux-grown samples (between 7.0 and 8.2 mm from table to culet) broadly compensated for the higher concentration of chromium and vanadium in the smaller HOC-grown synthetic alexandrites (between 4.1 and 4.2 mm from table to culet). Any influence on coloration from the iron measured in the flux-grown samples was minimal.

All six samples would be classified as showing the “desired” alexandrite color-change effect from daylight to incandescent light. In general, due to the mixing of colors by light traveling through the samples in different directions, alexandrites with appropriate sizes having the necessary amounts of color-causing trace elements, especially chromium or both chromium and vanadium, display good or at least acceptable color change regardless of cut orientation. For the synthetic alexandrite studied here, the risk of an unfavorable orientation of the table facet—again for stones of adequate sizes and concentrations of trace elements—is negligible. For other biaxial stones, it is expected that the effects of pleochroism in faceted stones will be reduced to some extent.

#### ABOUT THE AUTHOR

Dr. Schmetzer is an independent researcher living in Petershausen, near Munich, Germany.

#### ACKNOWLEDGEMENTS

Numerous rough and faceted synthetic alexandrites produced by Creative Crystals Inc. and by V.V. Gurov were provided by David Patterson (San Ramon, California) and V.V. Gurov (Novosibirsk, Russia) for previous studies (see Schmetzer et al., 2012, 2013). The present work was likewise based on these samples.

#### REFERENCES

- Bloss F.D. (1961) *An Introduction to the Methods of Optical Crystallography*. Holt, Rinehart and Winston, New York, 294 pp.
- Bosshart G., Frank E., Hänni H.A., Barot N. (1982) Blue colour-change kyanite from East Africa. *Journal of Gemmology*, Vol. 18, No. 3, pp. 205–212.
- Burns R.G. (1993) *Mineralogical Applications of Crystal Field Theory*, 2nd ed. Cambridge University Press, Cambridge, UK, 551 pp.
- Devouard B., Notari F. (2009) The identification of faceted gemstones: From the naked eye to laboratory techniques. *Elements*, Vol. 5, No. 3, pp. 163–168, <http://dx.doi.org/10.2113/gselements.5.3.163>
- Fischer W. (1954) *Praktische Edelsteinkunde*, 2nd ed. Verlag Gustav Feller-Nottuln, Kettwig, Germany, pp. 94–96.
- Gübelin E., Schmetzer K. (1982) Gemstones with alexandrite effect. *G&G*, Vol. 18, No. 4, pp. 197–203, <http://dx.doi.org/10.5741/GEMS.18.4.197>
- Halvorsen A. (2006) The Usambara effect and its interaction with other colour change phenomena. *Journal of Gemmology*, Vol. 30, No. 1/2, pp. 1–21.
- Halvorsen A., Jensen B.B. (1997) A new colour-change effect. *Journal of Gemmology*, Vol. 25, No. 5, pp. 325–330.
- Hughes R.W. (2014) Pleochroism in faceted gems: An introduction. *G&G*, Vol. 50, No. 3, pp. 216–226, <http://dx.doi.org/10.5741/GEMS.50.3.216>
- Kerr P.F. (1977) *Optical Mineralogy*, 4th ed. McGraw-Hill, New York, 492 pp.
- Schmetzer K., Bosshart G. (2010) Colorimetric data of Russian alexandrite and yellowish green to green chrysoberyl. In K. Schmetzer, Ed., *Russian Alexandrites*. Schweizerbart Science Publishers, Stuttgart, pp. 107–120.
- Schmetzer K., Malsy A.-K. (2011) Alexandrite and colour-change chrysoberyl from the Lake Manyara alexandrite-emerald deposit in northern Tanzania. *Journal of Gemmology*, Vol. 32, No. 5-8, pp. 179–209.
- Schmetzer K., Bernhardt H.-J., Bosshart G., Hainschwang T. (2009) Colour-change garnets from Madagascar: Variation of chemical, spectroscopic and colorimetric properties. *Journal of Gemmology*, Vol. 31, No. 5-8, pp. 235–282.
- Schmetzer K., Bernhardt H.-J., Hainschwang T. (2012) Flux-grown synthetic alexandrites from Creative Crystals Inc. *Journal of Gemmology*, Vol. 33, No. 1-4, pp. 49–81.
- Schmetzer K., Bernhardt H.-J., Balmer W.A., Hainschwang T. (2013) Synthetic alexandrites grown by the HOC method in Russia: Internal features related to the growth technique and colorimetric investigation. *Journal of Gemmology*, Vol. 33, No. 5-6, pp. 113–129.
- Sun Z., Palke A.C., Moyal J., McMurtry R. (2017) How to facet gem-quality chrysoberyl: Clues from the relationship between color and pleochroism, with spectroscopic analysis and colorimetric parameters. *American Mineralogist*, Vol. 102, No. 8, pp. 1747–1758.
- Wahlstrom E.E. (1969) *Optical Crystallography*, 4th ed. New York, John Wiley and Sons, 489 pp.

# LAND OF ORIGINS: A GEMOLOGICAL EXPEDITION TO ETHIOPIA

Wim Vertriest, Daniel Girma, Patcharee Wongrawang, Ungkhana Atikarnsakul, and Kevin Schumacher



Figure 1. The GIA field expedition team on the way to the Ethiopian opal mines near Wegel Tena. Photo by Wim Vertriest.

Although Ethiopia is considered the cradle of mankind and the land of origins, gemstones never played a significant role in its long history and rich culture. Only in the last decade did Ethiopia emerge in the gem trade, with the discovery of large opal deposits near the town of Wegel Tena (Rondeau et al., 2010). When the first high-quality emeralds from Shakiso in southern Ethiopia reached the mar-

ket in the fall of 2016, GIA's Carlsbad and Bangkok labs conducted a joint preliminary study (Renfro et al., 2017). And in February 2017, GIA received news of a sapphire discovery near Aksum in northern Tigray Province (Vertriest et al., 2017).

With all of this new material reaching the market, GIA collaborated with the Ethiopian Ministry of Mines, Petroleum and Natural Gas in Addis Ababa to set up an expedition to the sapphire, opal, and emerald sources. In March 2018, a team of four GIA gemologists and videographers traveled to Ethiopia to visit its gem sources. The first target was the sapphire deposit in the north, followed by the opal mines in the central highlands. The last area visited

---

See end of article for About the Authors and Acknowledgments.

GEMS & GEMOLOGY, Vol. 55, No. 1, pp. 72–88,

<http://dx.doi.org/10.5741/GEMS.55.1.72>

© 2019 Gemological Institute of America



Figure 2. Map of Ethiopia indicating its main gem sources: sapphire near the town of Aksum, opal in the central highlands surrounding Wegel Tena, and emeralds in the southern jungles near Shakiso.

was near Shakiso to witness the developing emerald mines. During the expedition (figure 1), we documented mining techniques, social impact, material processing, natural challenges, and limitations. We also collected samples at the mines and nearby markets in accordance with GIA's sampling protocols. These samples are now part of GIA's reference collection and used for origin determination, research projects, and treatment experiments.

## INTRODUCTION

**Geography and Geology.** Ethiopia is a landlocked country in northeast Africa that shares borders with Kenya, South Sudan, Sudan, Eritrea, Djibouti, and Somalia (figure 2). A land of extremes with fertile grasslands, expansive deserts, tranquil lakes, and massive canyons, it hosts one of the sources of the Nile River but also the world's hottest settlement (Dallol). The largest continuous mountain range in Africa, the Simien, contrasts sharply with the barren volcanic wasteland of the Danakil Depression in northeastern Ethiopia. The highest peak of the Simien, Ras Dashen, stands over 4,500 meters (14,763 ft) above sea level, while the lowest parts of the Danakil reach 125 meters (410 ft) below.

The geology of northeast Africa is dominated by two of Africa's biggest geological structures: the African Rift Valley and the Mozambique Belt<sup>1</sup>. The African rift zone is a geologically young feature that is still active and responsible for massive basalt plateaus that make up most of Ethiopia's highland. The zone is also responsible for the low-lying volcanic depression in Afar. The Mozambique Belt is the exposed root zone of an ancient mountain range (550 Ma) that once formed the core of the Pangaea continent. It has been subjected to immense stresses, pressures, and temperatures during its long and complex formation.

Ethiopia's population of more than 105 million makes it the second most populous nation in Africa. The two largest ethnic groups are Oromo (34.4%) and Amhara (27%). While the official national language is Amharic, states also designate working languages, such as Oromo and Tigrinya for the states of Oromia and Tigray, respectively. The capital is Addis Ababa, located in the central highlands, with more than 2.7 million inhabitants. Ethiopia is regarded as one of Africa's political centers, and it hosts many important organizations in its capital. The African Union, United Nations Economic Commission for Africa,

<sup>1</sup>The Mozambique Belt is a suture zone that developed during the formation of the Gondwana supercontinent. Currently it stretches from central Mozambique up into the Arabian Peninsula. Most of the islands in the Indian Ocean (including Madagascar and Sri Lanka) and parts of southern India and eastern Antarctica are also part of the Mozambique Belt. Today it is exposed at the surface, but once it was covered by more than 10 km of rocks, which caused it to reach high temperatures and be subjected to incredible pressures. These immense natural forces created many of today's gemstone deposits in East Africa and Asia. It is believed that Mozambique's rubies and most of Madagascar's corundum are related to the Mozambique Belt. In Tanzania, it is linked to the ruby deposits in Longido and Winza, as well as the tanzanite deposits in Merelani. Kenya's most famous gemstone, tsavorite, is also related to this geological feature. On the other side of the Indian Ocean, Sri Lanka's sapphire wealth is attributed to the Mozambique Belt.

Organization of African Unity, and many others are all based in Addis Ababa (Ham and Carillet, 2017).

**Culture and Religion.** Ethiopia is known as “the land of origins,” where many important archeological and paleontological milestones have been uncovered. The earliest human ancestors were discovered in the Afar Depression in northeastern Ethiopia, with Lucy (*Australopithecus afarensis*) the most famous of them all. She was long considered the first hominid, but more recent discoveries have unearthed even older skeletal remains (*Ardipithecus*, or Ardi) that may belong to another genus.

Throughout history, Ethiopia has been an important territory in northeastern Africa. Ancient kingdoms were based there, many of which dominated trade around the Horn of Africa and thus between Asia and Europe. Probably the most famous is the Kingdom of Aksum in northern Ethiopia, which is considered to have been the equal of Rome, Persia, and China around 2,000 years ago. Other notable kingdoms were based out of Gondar (post Middle Ages), which is known for the Royal Enclosure, sometimes referred to as “Ethiopia’s Camelot.”

From about 1850 through World War II, Ethiopia was ruled by a line of emperors that ended with the most influential of all, Haile Selassie. Although Ethiopia has never been colonized, Italy occupied it

from 1936 to 1941. After World War II, Haile Selassie returned to power and tried to lead the nation into modernity. This led to civil unrest, and in 1974 the Derg communist regime took power. During the regime, hundreds of thousands were deported or died from either hunger or the “Red Terror,” a late-1970s cleansing campaign against enemies of the regime. When communist rule ended in 1991, the Federal Democratic Republic of Ethiopia was installed.

The majority of the country is traditionally Ethiopian Orthodox Christian. In 330 CE, King Ezana the Great declared Christianity the state religion, and the faith is deeply rooted in the culture. The epicenter of Ethiopian Orthodox worship is the Church of Our Lady Mary of Zion in Aksum. The original church was built in the fourth century CE and has been destroyed and rebuilt several times. Today, visitors can find the nearby Chapel of the Tablet, which is believed to hold the Ark of the Covenant. Other important locations for the Ethiopian Orthodox faith are the Holy Trinity Cathedral in Addis Ababa, which houses the tomb of emperor Haile Selassie, and the rock-hewn churches in Lalibela (figure 3; see Ham and Carillet, 2017).

Diversity is reflected in every aspect of Ethiopia, from its history to its people and languages to its landscapes.

*Figure 3. Ethiopia’s rich cultural history was evident in every locality we visited, such as the Church of Saint George in Lalibela, where this priest guards the relics. Photo by Wim Verriest.*



## ETHIOPIAN SAPPHIRE

Our field trip began at the sapphire deposits in Ethiopia’s northern Tigray Province, near the border with Eritrea, which were discovered in the last months of 2016. Rumors of the discovery reached the trade in early 2017, and the first stones were seen in the Asian markets of Chanthaburi (Thailand) and Beruwala (Sri Lanka) in April 2017. Since the initial discovery near Chila, sapphires have been found in many localities throughout Tigray Province.

**Background and History.** The sapphires are mined in the vicinity of Aksum. This town was the capital of the ancient Aksumite kingdom, which erected intriguing monuments known as *stelae*. These monoliths, measuring up to 33 meters high, are closely associated with burial tombs of local elite and royalty. Aksum’s rich heritage makes it one of Ethiopia’s main tourist hubs, so access is convenient and accommodations are readily available.

The sapphires are mined and traded north of the city, in the direction of the Eritrean border. The countries have had a tense relationship since Eritrea regained its independence from Ethiopia in 1991. This



Figure 4. A family with goods packed on their camel travels on the road to the weekly market in Chila. Photo by Wim Vertriest.

has caused many border disputes, often resulting in casualties, although steps toward peaceful resolution have been taken since mid-2018. At the time of our visit, it was nearly impossible for foreigners to travel north of Aksum toward the border, where the sapphire fields are located. Numerous military checkpoints and watch posts are set up along the main roads north from Aksum. The GIA team was only able to visit the off-limits area with special permission from the Ethiopian Ministry of Mines, Petroleum and Natural Gas. Local authorities keep a close eye on every visitor, including Ethiopians from other parts of the country.

The Tigray area is barren and sparsely vegetated. The protected valley where Aksum lies is fertile, but life in the wastelands toward the Eritrean border in the north is much tougher. Dusty, rocky roads wind through the badlands made up of granitic boulders, and only the occasional tree serves as a recognizable landmark. Since the area is remote and road access is limited, most transport is with beasts of burden such as camels and donkeys (figure 4). Despite the harsh and arid climate, people depend heavily on agriculture and their herds of animals. Rainfall is

scarce but intensely concentrated, which creates violent periodic rivers. These high-energy water flows move boulders, rocks, and soil with enough power to wash away an entire fertile soil layer in one storm.

Most people know this area as the region most affected during the great famine in the early 1980s. A perfect storm of extreme drought, raging civil war, and failed government policies amplified the devastation. Large international relief efforts were set up, most famously the 1985 Live Aid concert in London. Longer-term plans supported by the United Nations Food and Agricultural Organization aimed to provide sustainable and robust farming methods to increase local food production. This was done mainly by improving soil conditions through terracing and preserving farmlands.

**Trading.** The sapphire mines are located near the town of Chila, 25 km northwest of Aksum. There are around 250 buildings in the town and numerous services for many people and smaller communities in the surrounding desert. During the local market every Saturday, crowds gather in the main street to buy and sell goods ranging from livestock to handicrafts—and, since late 2016, Ethiopian sapphires.



Figure 5. Gem dealers gather in front of their offices during the weekly market in Chila. Photo by Wim Vertriest.

Ethiopian dealers have set up offices in Chila, where they buy gems at the Saturday market (figure 5). The trade there is limited to sapphire and the occasional red garnet. During our visit, more than 15 offices were open in the town. It is illegal for foreigners to go to Chila and the mining areas, let alone buy gemstones near the mines. Local dealers take the

goods to Addis Ababa, where foreign buyers can purchase and export the stones. Most of the foreign buyers are Sri Lankans and Thais, who will improve the stones' appearance with heat treatment.

Chila has benefited greatly from the gem trade. During our visit, we saw that many new buildings had been erected. Before the discovery, there was one small bank branch; there are now three banks with full branches in the village. The police station has also been upgraded, and law enforcement actively monitors the presence of sapphire buyers. Several foreign buyers were arrested in 2017 for attempting to purchase in the village.

**Geology.** We visited a mining site, Godefey, located a few kilometers north of the trading town. More than 500 people were there searching for sapphires. Based on our initial observations, the geological makeup of the area is fairly straightforward. The basement (shown in figure 6) is made up of very resistant rocks that have experienced multiple episodes of metamorphism, with numerous folding and vein-forming phases. When these rocks were exposed at the surface, they weathered down to a relatively flat surface (known to geologists as a peneplain).

Later this flat land was covered in thick basalt flows (see figure 6). These basalt extrusions brought the sapphires to the surface and liberated them slowly while they eroded. The lava flows are still visible in

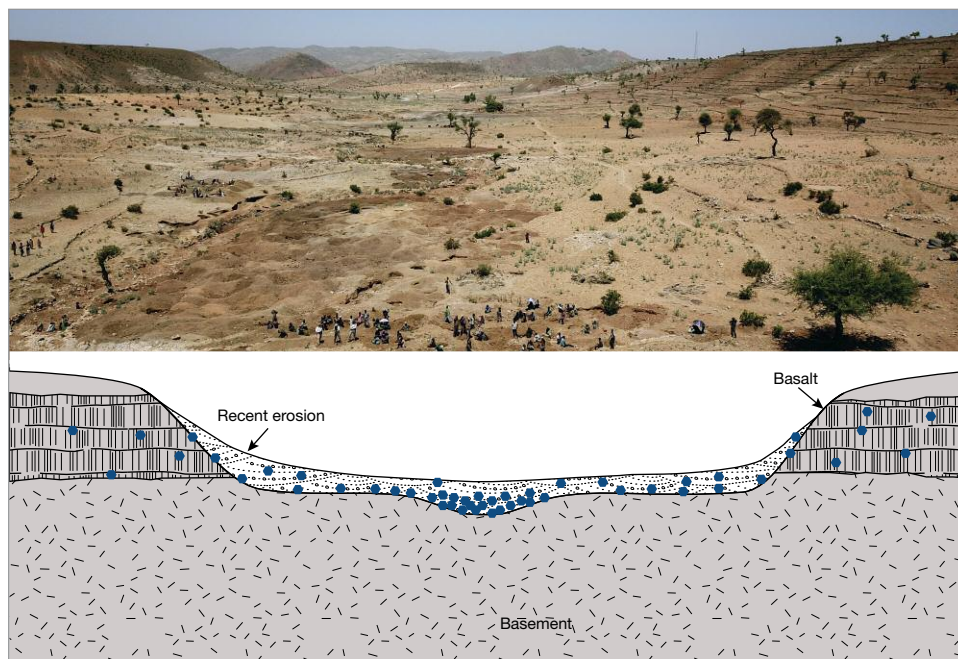


Figure 6. A schematic cross-section of the Godefey mining area (in which the blue hexagons represent sapphire) shows the basalt flows, recent erosion products, and the basement. Photo by Wim Vertriest.



Figure 7. Mining crews at Godefey sit next to their pits. The terraces on the hills are built to optimize agricultural yield. Photo by Wim Verriest.

the current topography, where all the plateaus are very flat and of uniform height. These plateaus are crosscut by multiple broad valleys, which started as “V” shapes eroding in the basalts. Once they reached the contact with the much harder basement, they started to widen to the broad valleys we see now. During weathering of the basalt, the main minerals such as pyroxene and olivine broke down very rapidly. This means that more-resistant minerals such as corundum, garnet, and zircon accumulated in the debris. These heavy minerals were then transported by water to the center of the valley and became concentrated in placer deposits such as river bends or cavities in the basement.

**Mining.** Most of the mines are situated in the center of the valley, near the exposed riverbeds. This is where the highest concentrations of minerals should be found. Some miners work higher up on the hillside, and sapphires have reportedly been found on top of the basalt plateaus. This would indicate that the entire basalt plateau is sapphire bearing. In most places, the hills are terraced in an effort to limit soil erosion from heavy rainfall (figure 7). To protect their food sources, landowners do not allow mining on land set aside for crops.

All mining activity is artisanal, with minimal equipment. Crews of five to twelve people, including many entire families, operate together (figure 8). Using simple tools such as shovels and picks, the miners dig

Figure 8. A family crew works together to extract sapphires from a pit. Photo by Wim Verriest.







Figure 9. Aerial view of mining pits in the Godefey area. Photo by Wim Vertriest.

pits until they reach a gravelly layer. This layer is typically deposited straight on the hard rock basement, at depths of one to three meters. Gem-bearing gravel is loosened and thrown to the surface or passed along in buckets. Miners dump the gravel onto the ground next to the pit, where it is searched by hand for sapphires.

This is often a completely dry process, with no washing or concentration involved due to the lack of water. Only in rare cases is the water table cut and the pit flooded. We observed one crew using a diesel pump to remove the excess water, while the rest did this manually with buckets or an ingenious wooden pedal pump. The water is not stockpiled or used for washing purposes; at most it is poured over the gravel to clear some of the finer sand.

Overall the mining techniques are very primitive, and we believe this leads to a much lower yield.

Only large stones (>1 ct) with obvious colors are picked out. Smaller goods, stones covered in dust or mud, and other potentially valuable specimens are all discarded. Yet it would be difficult to improve the situation under the circumstances. The area's remoteness makes it challenging to bring in heavier equipment, and fuel supply is irregular. Water is even more scarce (see figure 9), and there are no nearby bodies of water where communal washing efforts could be set up. The river is only seasonal, created by flash floods, making it hard to capture the water. The current mining is very strenuous and employs many hands, which means that many locals receive some portion of their income from sapphire mining.

### PROPERTIES OF ETHIOPIAN SAPPHIRE

**Visual Characteristics.** The gemstones found in northern Ethiopia are mainly blue sapphires. Since they are related to alkali basalt extrusions, they show characteristics very similar to sapphires from other magmatic deposits, such as those in Australia, Thailand, or Nigeria. These deposits are called BGY sapphire deposits because they predominantly yield blue, green, and yellow colors (figure 10). They also routinely produce black sapphires, whose dark body-color is caused by their high content of iron-rich inclusions. The majority of Ethiopian sapphires are blue, with a few pure (dark) yellows. Often one finds stones containing different colors as subtle color zones, or even as full parti-colors. Black bands may occur, caused by high concentrations of particles in certain zones. The locals describe these as "zebra sapphires." Fully black sapphires and star sapphires have not been observed.

Figure 10. Left: High-quality blue sapphires from northern Ethiopia. Right: A lower-grade parcel of sapphires with fancy-color specimens mixed in. Photos by Wim Vertriest.





Figure 11. Left: Lamellar twinning with intersecting growth tubules under fiber-optic illumination; field of view 3.6 mm. Center: Cluster of zircon; field of view 1.8 mm. Right: Angular band of minute particles under fiber-optic illumination; field of view 3.6 mm. Photomicrographs by Charuwan Khowpong.

The color of the blue sapphires ranges from dark greenish blue to a pleasing light blue. Dichroism is often very strong. In the milkier stones with fine rutile clouds, a yellowish cast is often observed when put to the torch. This is due to the Tyndall effect, the scattering of light when it interacts with the small particles. The sapphires are very large, with rough stones ranging from 1 ct to more than 100 ct.

**Inclusions.** Ethiopian sapphires are characterized by a variety of inclusions similar to those observed in sapphires from other basalt-related sources. Most notable are twinning planes (figure 11, left), in which two nonparallel sets are common. These planes show growth tubules that intersect. It is often easier to spot the tubules than the twinning planes unless the stone is being evaluated between crossed polarizers. These tubules are sometimes associated with small fingerprints.

Crystal inclusions vary: opaque ferrocolumbite crystals, large feldspar and monazite crystals, and small but well-formed zircon crystals. The zircon inclusions are often found in clusters (figure 11, center). Larger solitary inclusions often form comet tails (trails of fine particles/dislocations). One sample showed interesting inclusions of corundum crystals within the sapphire.

By far the most common inclusions are particles, and two distinct varieties are found in Ethiopian sapphires. The first is a classic rutile particle, seen as clouds, needles, or streamers or in hexagonal bands. These bands (figure 11, right) often contain a second type of particle as well. These are more iron-rich, and their composition ranges between ilmenite and hematite. Their appearance is distinct, and they are often more concentrated. The iron-rich particles have a golden brown reflection compared to the silvery white appearance of the classic titanium-rich silk.

**Spectroscopy.** Ultraviolet/visible/near-infrared (UV-Vis-NIR) spectra show a typical pattern for basalt-related blue sapphire: bands due to  $\text{Fe}^{3+}$  and  $\text{Fe}^{2+}\text{-Ti}^{4+}$  pairs that create the blue color. These chromophores are very strongly dependent on orientation, explaining the obvious dichroism in these stones. The broad band outside the visible range at 880 nm is typical for basalt-related blue sapphires.

**Trace-Element Chemistry.** We analyzed 50 sapphires from Tigray using laser ablation-inductively coupled plasma-mass spectrometry (LA-ICP-MS) to determine their trace-element concentrations. We analyzed three to fifteen points on each sample, often in different zones of the stone. This gave us a total of 718 data points, of which 194 were in blue zones without visible particles, 193 in zones with visible particles, and 331 in zones with very distinct particles, such as dense milky clouds or iron-rich silk.

Table 1 provides some insight into the chemical analyses of these samples. Beryllium was detected in several stones, in both clean and visibly included areas. Higher concentrations were found in the heavily included zones. Other elements such as niobium, tantalum, tungsten, and zircon followed similar trends. Titanium was clearly enriched in the most included zones but was also present at lower quantities in non-included zones. All of these elements probably exist in particles of various sizes that might be too small to observe with a conventional microscope. Only one heavily included sample showed the presence of chromium, probably due to particles as well. Iron concentrations were always very high, with an absolute minimum of 750 ppma and a maximum near 5000 ppma.

## ETHIOPIAN OPAL

**Background and History.** Opal has been recovered from Ethiopia's Wollo region since the 1990s, al-

though production volume and quality were initially very low (Koivula and Fritsch, 1994). In 2008, production increased when deposits of white precious opal were found near Wegel Tena (Rondeau et al., 2009). In 2013, a deposit of black opals was found 30 km away (Kiefert et al., 2014). During the past decade, Ethiopian opals have reached the market in large quantities. Most of the material is processed in Jaipur and serves the Indian market.

The opal deposits occur in a remote area of Ethiopia, between the towns of Dessie and Lalibela. The terrain consists of high plateaus (approximately

3,000 meters) crosscut by wide, steep valleys about 1,000 meters deep (figure 12). The fertile highlands are well suited for agriculture. Teff, the native grain and the staple of the Ethiopian diet, is grown here. The yearly precipitation is only 20% less than that of Seattle, Washington, but 95% of this rain falls in the span of a few weeks. These huge volumes of water move across the valleys with enormous power, cutting them deeper every year. When the riverbed is completely dry, the base of a valley is strewn with house-sized boulders that are transported by the seasonal torrents.

**TABLE 1.** Concentrations (in ppma) of selected trace elements in Ethiopian sapphires (718 analyses total).

	<sup>9</sup> Be	<sup>24</sup> Mg	<sup>47</sup> Ti	<sup>51</sup> V	<sup>53</sup> Cr	<sup>57</sup> Fe	<sup>69</sup> Ga	<sup>90</sup> Zr	<sup>93</sup> Nb	<sup>178</sup> Hf	<sup>181</sup> Ta	<sup>182</sup> W	<sup>232</sup> Th
<b>Blue zones<sup>a</sup></b> (194 analyses)													
% of samples above detection limit	17%	100%	100%	100%	0%	100%	100%	11%	26%	8%	28%	7%	13%
Average	4	5	57	4	—	1291	47	0.0109	1.5826	0.0018	2.1317	0.1013	0.0059
Max	17	24	852	12	bdl <sup>d</sup>	3797	119	0.0492	13.8718	0.0048	14.9883	0.2884	0.0316
Min	1	1	4	0	bdl	748	28	0.0009	0.0014	0.0003	0.0007	0.0017	0.0001
Standard deviation	5	4	137	3	—	485	17	0.0107	2.9783	0.0013	4.2765	0.1237	0.0087
<b>Particles<sup>b</sup></b> (193 analyses)													
% of samples above detection limit	15%	99%	100%	100%	0%	100%	100%	10%	28%	5%	41%	3%	13%
Average	4	6	47	6	—	1326	41	0.0464	3.9063	0.0158	1.2840	0.0529	0.0468
Max	70	20	371	15	bdl	3907	80	0.6371	161.984	0.1200	67.8419	0.1852	1.0018
Min	1	0	12	0	bdl	752	26	0.0015	0.0014	0.0006	0.0004	0.0021	0.0000
Standard deviation	13	5	46	4	—	637	11	0.1423	22.1774	0.0354	7.8879	0.0733	0.1945
<b>Heavy particles<sup>c</sup></b> (331 analyses)													
% of samples above detection limit	12%	100%	100%	100%	2%	100%	100%	14%	30%	7%	47%	10%	11%
Average	13	6	125	7	2	1264	43	0.1166	5.1534	0.0483	2.0515	0.0576	0.1125
Max	91	27	1486	17	4	4966	114	1.0686	73.5294	0.2513	42.4857	0.3039	0.4605
Min	0	1	16	0	1	803	27	0.0007	0.0014	0.0007	0.0004	0.0016	0.0003
Standard deviation	22	4	211	4	1	597	16	0.2424	13.0648	0.0708	6.2452	0.0813	0.1435
Detection limit	0.19	0.18	0.59	0.04	0.45	0.77	0.02	0.0007	0.0009	0.0001	0.0001	0.0001	0.0013
<sup>a</sup> Blue zones: blue bodycolor without visible particles													
<sup>b</sup> Particles: blue bodycolor with fine particles													
<sup>c</sup> Heavy particles: blue or greenish bodycolor with many large and irregular particles, usually with a higher Fe component													
<sup>d</sup> bdl: below detection limit													

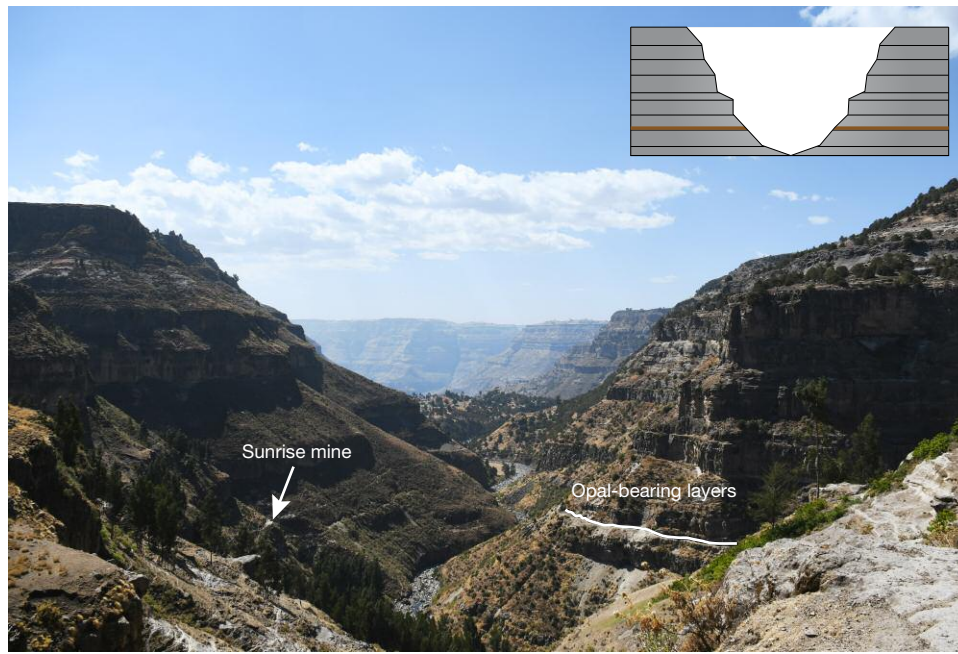


Figure 12. Cross-section of a valley where Ethiopian opal is mined. The opal-bearing layers indicated on the photo are marked in brown in the inset. The arrow points to the Sunrise mine. Photo by Wim Vertriest.

This topography makes travel very difficult since the canyons take several hours to cross even with all-terrain vehicles. The direct distance between Lalibela and Wegel Tena is around 50 km. Because we had to cross the Bashilo canyon, the trip took nearly seven hours. Yet the views were magnificent as we wound down the canyon on dusty roads. Indigenous wildlife such as ibex, birds of prey, and gelada monkeys inhabit the cliffs and valleys, often foraging in the fields near the plateau edge. This perilous journey requires a very skilled driver and a vehicle in excellent condition.

**Geology.** The geology of the opal mining areas is dominated by stacked horizontal layers of volcanic origin. The sequence is over 3,000 meters thick and consists of alternating layers of varying composition ranging from basalt to rhyolite. Some of the individual layers are more than 100 meters thick. These were deposited during extreme volcanic events related to opening of the East African rift zone about 30 million years ago. Opal mineralization is restricted to a single thin layer with a rhyolite (silica-saturated) composition. No other opal-bearing layers have been found to date.

Traditionally, Ethiopian opal has been considered a volcanic opal, similar to Mexican opal. Australian opal is believed to have a sedimentary origin. However, recent studies suggest that Ethiopian opal has a strong sedimentary component. According to Rondeau et al. (2012), these opals might have formed in soil conditions (pedogenic). This is based on micro-

scopic observations of plant fossils in the opals, as well as several features that are typical for soils: desiccation cracks, presence of clay minerals, and grain sorting.

It is assumed that Ethiopian opal formed during a calmer period, without new volcanic deposits, where soils could develop and support plant life. During this period, volcanic glass would disintegrate and dissolve in fluids, and feldspar would be altered to clay. The silica-enriched fluids deposited the opal in voids throughout the soil horizon. They often preserved the soil textures, which we see today as inclusions or opal textures (Rondeau et al., 2012).

**Mining.** Because the opal is found in a single thin horizontal layer, all of the mines are located at the same level in the valleys. The opal-bearing layers are about 350 m below the top plateau. The only way to reach it is by trails. No animals other than goats and sheep can traverse the steep paths. This means that the miners must carry down all supplies and equipment, and all opal-bearing rocks must be carried up.

Crews of 10 to 20 miners work together to extract the opal. First, they dig a narrow tunnel into the horizontal layer and remove the host rock and opal with simple hand tools (figure 13). The tunnels can reach lengths of more than 70 meters and are sometimes only 40 centimeters wide. It is relatively easy to carve through the rocks since they are fairly soft and not well solidified. There is no need for explosives in these mines. While the temperatures inside the tunnels are relatively cool, the humidity is high and oxy-

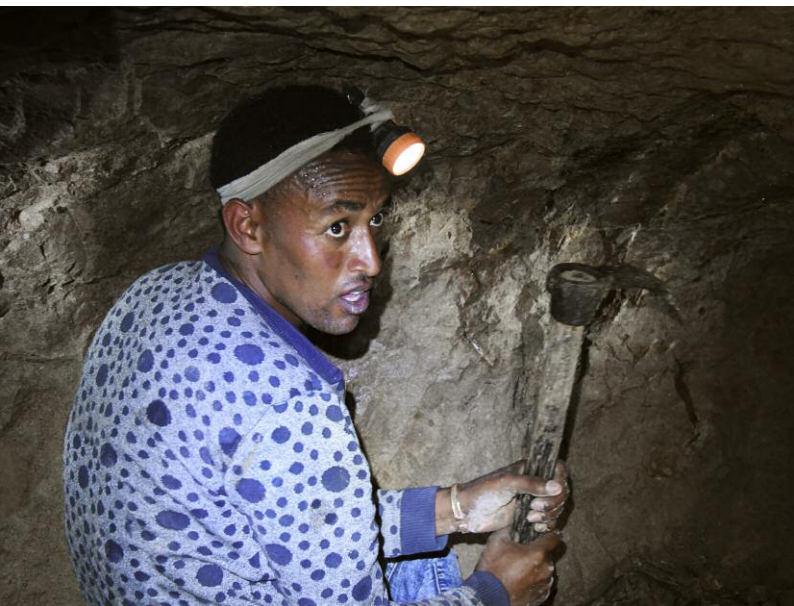


Figure 13. An opal miner works in the tunnel using simple hand tools. Photo by Wim Vertriest.

gen levels are more depleted, which makes the work very difficult. Miners only remove opal-bearing rocks, since the others are not profitable. Once the opal-bearing rocks are loosened, miners carry them by hand toward the exit for further processing.

According to a mining association representative, more than 20 tunnels are active in the valley, and each produces 50–100 kg of opal on a weekly basis.

### PROPERTIES OF ETHIOPIAN OPAL

Ethiopian opal has been mined in various qualities. Bodycolors include white, chocolate brown, reddish



Figure 15. Parcel of mixed Ethiopian opals. Photo by Wim Vertriest.

brown, black, and even colorless (figures 14 and 15). Sizes range from small grains to massive chunks, and pieces over 500 grams are routinely found.

The majority of Ethiopian opal is hydrophane, which means it absorbs water. This may affect the appearance of the stone, causing play-of-color, transparency, or crazing. There are different degrees of porosity, so not every type of Ethiopian opal reacts in the same way. While some of these effects are reversible through dyeing and impregnation, the processes and exact parameters are not yet fully understood. This has led to many controversies about the stability and treatment of Ethiopian opals.

All types of opal—precious or common, stable or requiring treatment—are found together in the same layer and the same tunnels.

Figure 14. Large rough pieces of transparent precious opal (left) and brown precious opal (right). Photos by Wim Vertriest.





Figure 16. Ethiopian emeralds from the Hallo mine (left to right): a 2.00 ct square emerald cut, a 9.72 ct cabochon, and a 4.12 ct modified cushion cut. Photo by Robert Weldon/GIA, courtesy of Mayer & Watt.

## ETHIOPIAN EMERALD

**Background and History.** News of Ethiopian emerald first reached the trade in 2011–2012, when a few smaller pieces (< 2 ct; see figure 16) reached the market (Cevallos et al., 2012). According to Farooq Hashmi (Intimate Gems, New York), they were mined near Dubuluk. Since the initial discovery, Gemfields acquired an emerald mining license in southern Ethiopia near the town of Web and started developing this in 2017 (Pardieu and Barriere-Doleac, 2018). In late 2016, the first emeralds from the Shakiso area started reaching international markets, with parcels showing up at GIA's labs in Bangkok and Carlsbad, California (Renfro et al., 2017).

Shakiso is a trading town in southern Ethiopia, located on a large highway that links Addis Ababa with northern Kenya. The city is used for trade because access is convenient and some accommodations are available.

The area around Shakiso looks very different from the opal and sapphire mining areas. Because it is closer to the equator and at medium elevation (between 1,600 and 2,000 meters), precipitation is more evenly spread throughout the year and dense vegetation covers the hills. During the trip from Hawassa to Shakiso, we drove for a few hours through the Great African Rift past Lake Hawassa before climbing out of the valley into the green highlands. Cloudy

skies and misty conditions provided a setting that was nothing like the arid, sunny conditions near the opal and sapphire mines. Dense forests alternated with grassy bogs in the shallower areas near creeks. This continuous humidity, combined with tropical temperatures and abundant vegetation, increases the weathering rate of outcropping rocks, making it very challenging to study geology in the area.

Secondary deposits where resistant minerals are concentrated are very common, but most of them are gold and coltan minerals, not gemstones. The area has a long tradition of mining, and many deposits of gold and tantalum have been mined artisanally for years. Some very large tantalum mines also operate in the region, as do several smaller cooperatives. In 2014, the Kenticha mine contributed 3% of the world's supply of tantalum (Yager, 2014).

The mines are located around the small mining village of Kenticha, more than 60 km from Shakiso, and the drive took over five hours. Recent rainfall had turned the dirt roads into muddy tracks, causing even the most rugged four-wheel-drive trucks to slip and slide all the way from Shakiso to Kenticha.

**Trading.** Emeralds near Kenticha were discovered in 2016 by local diggers looking for other precious minerals. This triggered a rush of miners, and an artisanal mining community formed in the first months of

---

2017. Because the area has been mined extensively for gold and tantalum, many residents have experience in mineral extraction and trading. They quickly set up new professional structures or adapted old ones. Many miners have grouped themselves into cooperatives. This allows them to step away from the unlicensed artisanal arrangement into one that is more regulated, where everyone still has a voice.

The cooperative we visited, Bua Obsa, had been mining gold and tantalum for more than 15 years, but it has grown from 15 members to more than 300 since the emerald discovery. All the members are active in the mining operation, either as support staff or mining personnel. While they had a clearly defined organization with people trained in finance, law, export procedures, and management, they needed to develop the specific skills required to run a colored stone mining and trading operation. The Bua Obsa cooperative quickly realized its shortcomings and partnered with foreign-trained experts. During our visit we met an experienced mining foreman from the Zambian emerald mines and a highly trained geologist with an academic career at the University of Addis Ababa.

This partnership approach allowed Bua Obsa to expand the mine quickly and in a controlled way. Instead of learning the hard way, through trial and error, they partnered with existing knowledge. At the time of our visit, more than seven cooperatives were working in the area, as well as many active small-scale or individual mines. This changed in the second half of 2018, when Bua Obsa became the dominant cooperative in the area. It now represents the lion's share of the miners. Local dealers buy the material near the mines and bring it to Shakiso, the main trading hub for emeralds mined by the small-scale artisanal miners. From there, the material goes to Addis Ababa, where it is presented to international clients. Larger cooperatives such as Bua Obsa have mining and export licenses and are able to export directly to foreign customers/wholesalers.

Because the cooperatives are formed by the local community, there is very strong local support for the emerald mining. During the artisanal rush, miners flocked to the small village of Kenticha, expanding it greatly. After the rush, many of them left to try their luck elsewhere. Kenticha is now inhabited by about 1,000 people, mostly natives of the surrounding area.

**Emeralds from God's Hand.** Large companies have been mining and exploring the Kenticha area for gold and tantalum since the 1980s, often neglecting local

communities. Now that the cooperatives have discovered this new emerald resource in one of the most extensively explored areas of Ethiopia, the situation is much different. The Bua Obsa cooperative considers this a gift from God. The wealth generated by these emeralds will directly contribute to the local communities. Within one year, the cooperative had already built roads, medical outposts, and churches with the profits from emerald mining.

**Geology.** The local geology is very well known due to the exploration for gold and tantalum. The presence of tantalum in particular provides interesting insights into the emeralds' geology. Tantalum mineralization is related to pegmatites, which are also the source for beryl. The pegmatites are related to granite intrusions. These molten rocks intruded right after the formation of the East African orogenic belt. The host rock consists of numerous mafic units, ranging from mafic schists to ultramafic serpentinite bodies. These can have magmatic origins (ophiolites) or a metasedimentary origin (pelitic schists, graphite schists, and marbles) (Küster et al., 2009; Tadesse, 2001). These host rocks are part of the Mozambique Belt, which is related to many other East African gem deposits.

When the pegmatites intruded, a reaction zone formed between the intrusion and the host rock. This zone consists predominantly of dark mica (biotite) but also hosts minerals that are a blend of both rock types. The best example is emerald, which is a beryl (pegmatite-influenced) with chromium trace elements (influenced by the host rock).

We could clearly see the dark mafic host rocks and one white pegmatite intrusion. The pegmatite ranges in thickness from five meters to a couple of centimeters. According to the mine geologist, two types of emeralds are found. One is found in the pegmatite and is much lighter and of lower quality. This is due to the abundance of silica and virtual absence of chromium in the pegmatite. The other type is found in the reaction zone, where chromium is abundant and there is a lot of space to grow in between the mica crystals. He also told us that there are multiple pegmatite intrusions close to each other and that all of them are emerald bearing. A couple of meters south of the mining pit, a pegmatite intrusion reaches the surface.

**Mining.** According to the local people, early emerald mining was strictly artisanal. Initial discoveries were made where the pegmatites reached the surface, but the mining quickly moved to deeper ground. Small crews would sink shafts vertically until they reached



Figure 17. Ethiopian emeralds, in the rough and faceted (8.03 ct, no fracture filling). The rough stones are from the GIA reference collection, and the faceted emerald is courtesy of Jeffery Bergman (Primagem). Photo by Wim Vertriest.

the emerald-bearing rocks. This was all done using hand tools, sometimes digging 20 meters deep (Schollenbruch et al., 2017). More than 10,000 miners were active in the small area at its peak in spring 2017.

With the formation of the cooperatives, mining became more professional. The Bua Obsa cooperative is currently working a large open-pit mine, exposing all the rocks and selectively extracting emeralds. The pit was about 25 meters deep and 50 by 50 meters long at the time of our visit. It is located on top of the hill where the emeralds were originally discovered. Overburden is carefully stripped away, and safe routes are created to descend into the mine. Wall stability is also monitored. This results in periods where the mine is not productive, but these steps are required to develop the mine and ensure safety. Bua Obsa uses large equipment, including bulldozers and excavators; emerald picking, sorting, and washing is still done manually. This larger-scale mining requires

coordination and experience, which is why they have hired a foreman who worked in the Zambian emerald mines for more than 20 years.

#### PROPERTIES OF ETHIOPIAN EMERALD

**Visual Characteristics.** The Ethiopian emeralds have a wide range of qualities and sizes. Material with lighter colors is usually cleaner, but clean deep green crystals have been found (figure 17). While most of the emeralds are fairly small, large crystals have been recovered, some weighing more than 600 grams. Crystals are often (sub-) euhedral with clean terminations. The roots are commonly more included. Rough emeralds are coated in mica, which is sometimes speckled throughout the entire stone. Color zoning is regularly seen. Some stones have a cloudy whitish appearance, probably due to an abundance of fine quartz inclusions. As with emeralds from all localities, some material requires enhancement by fracture filling.



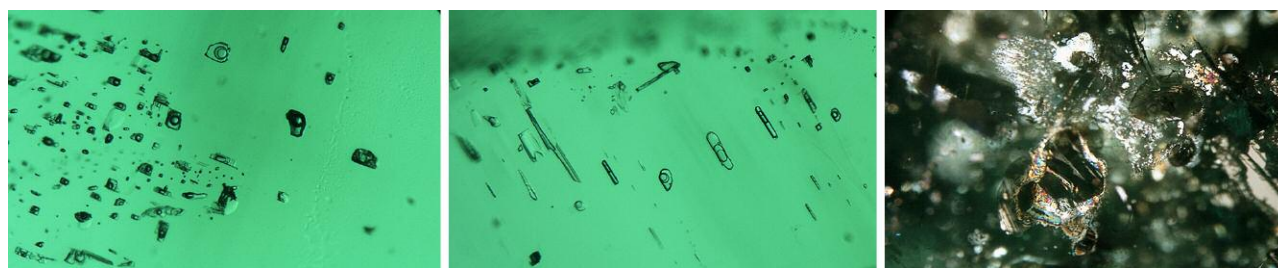


Figure 18. Left: Blocky, irregular two- and three-phase inclusions. Diffused illumination; field of view 0.8 mm. Center: Elongated three-phase inclusions with separated gas phases. Diffused illumination; field of view 0.7 mm. Right: Brownish phlogopite mica crystals surrounded by planes of thin films. Fiber-optic illumination; field of view 2.0 mm. Photomicrographs by Ungkhana Atikarnsakul.

**Standard Gemological Properties.** The Ethiopian emeralds had an average density of 2.72 g/cm<sup>3</sup>, ranging from 2.68 to 2.76 g/cm<sup>3</sup>. Refractive index ranged from 1.580 to 1.590, with an average birefringence of 0.008. None of our samples showed any reaction under long-wave or short-wave UV light or in the Chelsea filter.

**Inclusions.** The inclusions in Ethiopian emerald can be divided into three groups. The first consists of variously shaped fluid inclusions that are often blocky (figure 18, left). Depending on the viewing angle, they appear more irregular or elongated (figure 18, center). It is estimated that the gas phase takes up 40–50% of the crystal's volume at room temperature. Some inclusions exhibit two separate gas phases at room temperature but quickly homogenize when they are held over the well light in the microscope. This indicates a large CO<sub>2</sub> component in the inclusion. In some elongated two-phase inclusions, the tip is tapered, resembling a nailhead spicule inclusion. Under high magnification, small crystals can be seen within the fluid inclusions. Fingerprints with more rounded, smaller secondary fluid inclusions are very common.

Growth patterns such as color zoning, hexagonal growth zones, or even roiled growth features are frequently observed. New generations of emerald form-

ing are often associated with these growth zones.

Common crystal inclusions in the emerald are brownish mica identified by Raman spectroscopy as biotite and phlogopite, which form in various sizes and shapes. A phlogopite mica plate was often found together with a granular flake of iridescent thin films (figure 18 right). Colorless quartz crystal can also be observed in Ethiopian emerald. Rarer inclusions, identified as calcite, talc, bertrandite, magnetite spinel, and chlorite, are found in some samples.

**Spectroscopy.** UV-Vis-NIR spectroscopy showed two broad bands related to Cr<sup>3+</sup>, at around 430 and 600 nm for the ordinary ray (o-ray) and 420 and 630 nm for the extraordinary ray (e-ray). Fe causes the narrow band around 372 nm related to Fe<sup>3+</sup> and the strong broad band around 810 nm related to Fe<sup>2+</sup>, which is most clearly expressed in the o-ray spectrum.

No spectroscopic features indicate that V<sup>3+</sup> contributes significantly to the color of these stones.

**Trace-Element Chemistry.** We selected 25 samples for trace-element analysis using LA-ICP-MS (table 2) and analyzed three to eight spots per sample, resulting in 134 total measurements. Ethiopian emeralds are characterized by a relatively high content of

**TABLE 2.** LA-ICP-MS trace-element concentrations in Ethiopian emeralds (ppmw).

	<sup>7</sup> Li	<sup>23</sup> Na	<sup>24</sup> Mg	<sup>39</sup> K	<sup>45</sup> Sc	<sup>51</sup> V	<sup>53</sup> Cr	<sup>57</sup> Fe	<sup>60</sup> Ni	<sup>66</sup> Zn	<sup>69</sup> Ga	<sup>85</sup> Rb	<sup>133</sup> Cs
Min.	183	7830	9140	99	31	75	95	1970	5	21	14	15	151
Max.	446	16700	16800	889	111	129	3760	5320	21	146	25	166	544
Avg.	309	11175	12690	310	74	103	1441	3890	11	53	20	57	355
Stand. dev.	59	1760	1215	98	19	10	1045	463	4	15	2	17	79
Det. limit	0.42	21.54	0.59	11.09	0.87	0.28	4.50	21.12	0.77	1.17	0.21	0.15	0.05

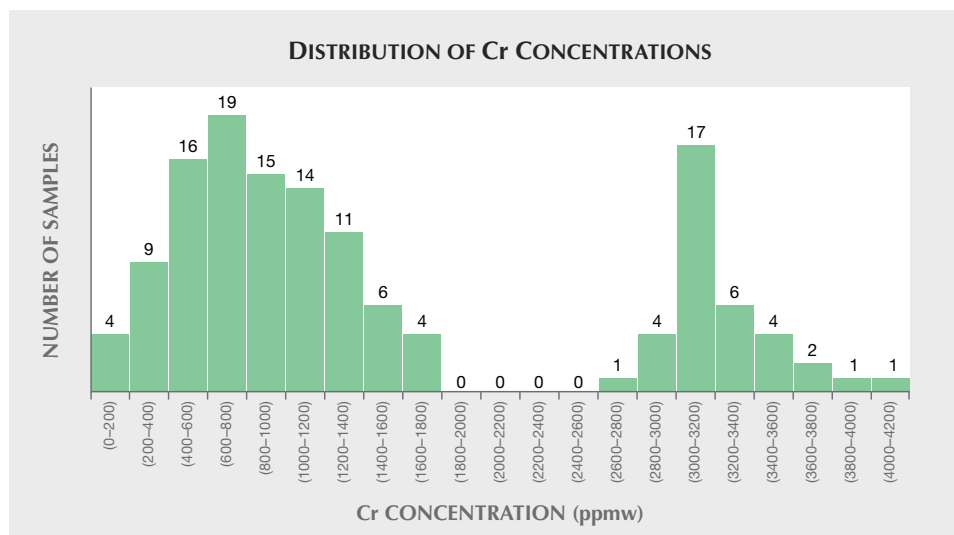


Figure 19. The distribution of Cr concentrations (ppmw) clearly shows that there are two types of Ethiopian emerald: one that is Cr-rich and one with lower Cr concentrations. This is probably closely related to their formation mechanism.

alkaline ions (Li, Na, K, Rb, and Cs). Vanadium is found in the emerald but does not influence the color. It is noteworthy that Cr and Fe values show a large range and the Cr values have a very large standard deviation. Cr values ranged from 95 ppmw to more than 3700 ppmw. Examining this data more closely, we see two groups of emeralds with different Cr concentrations, as shown in figure 19, that are under 1800 ppmw and over 2500 ppmw. These groups seem to be defined only by their Cr values and not by other chemical concentrations of trivalent ions such as Fe and V. This difference can be related to initial geological observations. According to the mine's geologist, emeralds are found in two different rock types: in the pegmatite and in the reaction zone. This geological model would explain the difference in color and in Cr content, where the emeralds from the reaction zone are richer in chromium and have a deeper color than the beryl formed in the pegmatite.

Since emerald inclusions are very similar for most pegmatite-related emerald deposits, trace-element analysis is a critical technique for origin determination. Emeralds from Zambia, Russia, Brazil, Pakistan, and Madagascar can be separated from Ethiopian material based on chemical composition, although some overlap can occur.

## CONCLUSIONS

Ethiopia has an incredibly rich history spanning several millennia, but gemstones were not a part of this history until a decade ago. Opal was the first Ethiopian gemstone that rose to fame, emerging from the northern province of Wollo in large volume and various

qualities. This colorful gemstone has faced scrutiny over its stability. Our visit to the mining area granted us insight into the grueling work to retrieve opal from the hard rock tunnels in the highlands.

The Ethiopian sapphire fields of Tigray Province, also in the northern part of the country, have only recently been discovered and are being worked in very rudimentary fashion. The secondary deposits supply dark to light blue sapphires that often require heat treatment. Few qualify as high-end material, but they are finding a strong market as commercial grade. The area has no sapphire mining history, but the local miners are learning quickly. The future will tell whether more sapphire-bearing areas will be discovered and mining processes can be improved. Both are equally important to sustain Ethiopia as a sapphire-producing region.

At the moment, Ethiopia's most sought-after gemstones are the emeralds from the southern part of the country. Since their discovery in the Shakiso area in late 2016, the growth of the deposit has been remarkable. The mining quickly shifted from a chaotic artisanal rush to a well-organized larger-scale operation aiming to cover the entire mine-to-market line. The emeralds can reach impressive sizes, and high-quality material has gone on the market. Based on their inclusions, these could be confused with emeralds from other pegmatite-related sources such as Zambia, Brazil, or Russia, but trace-element chemistry can often separate Ethiopian origin.

Since 2017, Ethiopia has proven to be one of the most interesting gem-producing countries, with large reserves of sapphire and emerald coming onto the market. During our expedition we could see that the

local gemstone industry was still in its infancy but growing at breathtaking speed. Ethiopian dealers, exporters, and governments are gathering knowledge

about new deposits, other gem varieties, and gemstone manufacturing to make the most of these immense gemstone resources.

#### ABOUT THE AUTHORS

Mr. Vertriest is supervisor of field gemology, Ms. Wongrawang is a staff gemologist for colored stones, and Ms. Atikamsakul is a colored stone analyst, at GIA in Bangkok. Mr. Girma is an analytics technician for colored stones at GIA in New York. Mr. Schumacher is a photo and video producer for Gems & Gemology at GIA in Carlsbad, California.

#### ACKNOWLEDGMENTS

This expedition was made possible through the support of the Ethiopian Ministry of Mines, Petroleum and Natural Gas. Specifically, Mr. Teweldbrahn Abay, Mr. Getachew Addis, and Mr. Biniyam Bekele helped with administration and on-ground support. This expedition was successful only because of the great

team that traveled to the mines with us: Andy Lucas (former GIA field gemologist) and external consultants Steve Curtis and Alessandro Martello. We are thankful to the Bua Obsa cooperative for hosting us at their mine site, especially to Mr. Adisse Mekonnen (chief geologist) and Mr. Wodessa Yachisi Bululta (association president). The data in this article was collected by GIA's colored stone teams and in particular Charuwan Khowpong, Vararut Weeramonkhonlert, Sasithorn Engniwat, and Suwasan Wongchacree. Thank you to Pedro Padua and Betsy Winans, both of GIA, for assistance with video editing.

Of course, this article would not have been possible without the support and effort of the people and gem mining communities throughout Ethiopia.

#### REFERENCES

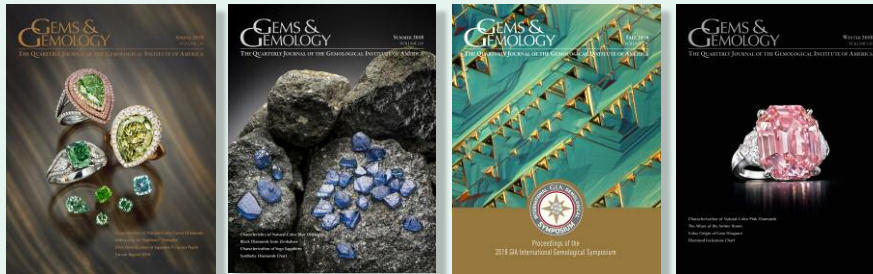
- Cevallos P., Simmons W.B., Falster A.U. (2012) Gem News International: Emerald from Ethiopia. *G&G*, Vol. 48, No. 3, pp. 219–221.
- Ham A., Carillet J.-B. (2017) *Lonely Planet Ethiopia @ Djibouti*. Lonely Planet Global Limited.
- Kiefert L., Hardy P., Sintayehu T., Abate B., Woldetinsae G. (2014) Gem News International: New deposit of black opal from Ethiopia. *G&G*, Vol. 50, No. 4, pp. 303–305.
- Koivula J.L., Fritsch E., Eds. (1994) Gem News: Opal from Ethiopia. *G&G*, Vol. 30, No. 1, pp. 52–53.
- Küster D., Romer R.L., Tolessa D., Zerihun D., Bheemalingeswara K., Melcher F., Oberthür T. (2009) The Kenticha rare-element pegmatite, Ethiopia: Internal differentiation, U-Pb age and Ta mineralization. *Mineralium Deposita*, Vol. 44, No. 7, pp. 723–750, <http://dx.doi.org/10.1007/s00126-009-0240-8>
- Pardieu V., Barriere-Doleac D. (2018) Ethiopia, land of origins part I: Emeralds from southern Ethiopia. <https://www.youtube.com/watch?v=9eKiYe1LRbc>
- Renfro N., Sun Z., Nemeth M., Vertriest W., Raynaud V., Weeramonkhonlert V. (2017) Gem News International: A new discovery of emeralds from Ethiopia. *G&G*, Vol. 53, No. 1, pp. 114–116.
- Rondeau B., Cenki-Tok B., Fritsch E., Mazzero F., Gauthier J.-P., Bodeur Y., Bekele E., Gaillou E., Ayalew D. (2012) Geochemical and petrological characterization of gem opals from Wegel Tena, Wollo, Ethiopia: Opal formation in an Oligocene soil. *Geochemistry: Exploration, Environment, Analysis*, Vol. 12, No. 2, pp. 93–104, <http://dx.doi.org/10.1144/1467-7873/10-MINDEP-058>.
- Rondeau B., Fritsch E., Gauthier J.-P., Mazzero F., Bekele E. (2009) A new source of play-of-color opal at Wegel Tena, Welo Province, Ethiopia. *31st International Gemmological Congress—Abstracts*, Arusha, Tanzania, pp. 43–44.
- Rondeau B., Fritsch E., Mazzero F., Gauthier J.-P., Cenki-Tok B., Bekele E., Gaillou, E. (2010) Play-of-color opal from Wegel Tena, Wollo Province, Ethiopia. *G&G*, Vol. 46, No. 2, pp. 90–105, <http://dx.doi.org/10.5741/GEMS.46.2.90>
- Schollenbruch K., Link K., Sintayehu T. (2017) Gem quality emeralds from southern Ethiopia. *InColor*, Vol. 35, pp. 48–54.
- Tadesse S. (2001) Geochemistry of the pegmatitic rocks and minerals in the Kenticha Belt, southern Ethiopia: Implication to geological setting. *Gondwana Research*, Vol. 4, No. 1, pp. 97–104, [http://dx.doi.org/10.1016/S1342-937X\(05\)70658-4](http://dx.doi.org/10.1016/S1342-937X(05)70658-4)
- Vertriest W., Weeramonkhonlert V., Raynaud V., Bruce-Lockhart S. (2017) Gem News International: Sapphires from northern Ethiopia. *G&G*, Vol. 53, No. 2, pp. 247–248.
- Yager T. (2014) The mineral industry of Ethiopia. In *2014 Minerals Yearbook*, U.S. Geological Survey, Reston, Virginia.

## For More on the Ethiopian Gem Industry

View the diverse Ethiopian landscapes and deposits, watch interviews with gem miners and dealers, and get insights from field gemologists. Visit [www.gia.edu/gems-gemology/spring-2019-land-origins-gemological-expedition-ethiopia](http://www.gia.edu/gems-gemology/spring-2019-land-origins-gemological-expedition-ethiopia)



TAKE THE 2019 **GEMS & GEMOLOGY**  
**CHALLENGE**



The following 25 questions are from the Spring, Summer, and Winter 2018 issues of *G&G*. (The Fall 2018 issue, which contained the proceedings of GIA's International Gemological Symposium, is not included.) Please refer to the articles in those issues to find the single best answer for each question.

Mark your choice on the response card provided in this issue or visit [gia.edu/gems-gemology](http://gia.edu/gems-gemology) to take the Challenge online. Entries must be received no later than **Friday, August 12, 2019**. All entries will be acknowledged with an e-mail, so please remember to include your name and e-mail address (and write clearly).

Score 75% or better, and you will receive a certificate of completion (PDF file). Earn a perfect score, and your name also will be listed in the Fall 2019 issue of *Gems & Gemology*.

- |   |  |  |
|---|--|--|
| <p>1. The 550 nm absorption band in pink diamonds results from which defect?</p> <p>A. One that has not been identified<br/>           B. The <math>NV^{0-}</math> center<br/>           C. GR1<br/>           D. N3</p> <p>2. Which of the following statements about DNA testing of pearls is false?</p> <p>A. It is minimally destructive.<br/>           B. A minute amount of pearl powder is required.<br/>           C. It involves extraction, amplification, and sequencing of the DNA.<br/>           D. This type of testing is not currently performed in gemological laboratories.</p> | <p>3. Amber production from primary deposits in Russia dates back to</p> <p>A. 1700.<br/>           B. 3000 CE.<br/>           C. 37–68 CE.<br/>           D. before recorded history.</p> <p>4. Radiation damage in natural green diamonds</p> <p>A. is the most common cause of the green color.<br/>           B. tends to quench fluorescence.<br/>           C. creates vacancies.<br/>           D. All of the above</p> <p>5. Almandine garnets from the Garibpet deposit in India</p> <p>A. are generally inclusion-free.<br/>           B. have no chemical zoning.<br/>           C. contain sillimanite fibers.<br/>           D. are calcium-rich.</p> | <p>6. Where is rainbow hematite found?</p> <p>A. United States<br/>           B. Brazil<br/>           C. Italy<br/>           D. All of the above</p> <p>7. The chromophores in color-change diaspore include all of the following except:</p> <p>A. <math>Cr^{3+}</math><br/>           B. <math>V^{3+}</math><br/>           C. <math>Co^{2+}</math><br/>           D. <math>Fe^{2+}-Ti^{4+}</math> pairs</p> <p>8. Most fancy red diamonds show _____ fluorescence to long-wave UV.</p> <p>A. orange<br/>           B. yellow<br/>           C. green<br/>           D. blue</p> |
|---|--|--|

9. The trace-element chemistry of Yogo sapphires most closely matches that of ruby from which origin?  
 A. Sri Lanka  
 B. Kashmir  
 C. Madagascar  
 D. Thailand/Cambodia
10. The pearls currently produced in Lake Kasumiguara  
 A. have thinner nacre than akoya pearls.  
 B. are all brown or yellow.  
 C. are between 5 and 10 mm in size.  
 D. are all beaded.
11. Black diamonds from the Marange deposits in Zimbabwe  
 A. show no evidence of natural irradiation.  
 B. are typically less than 1 ct in size.  
 C. were discovered by De Beers.  
 D. contain only cuboid sectors.
12. Pipi pearls  
 A. are from Australia.  
 B. are almost all cultured.  
 C. are generally over 1 cm in diameter.  
 D. are typically yellow or golden in color.
13. The iridescence of rainbow hematite  
 A. is dependent upon the aluminum and phosphorous impurities.  
 B. changes color with respect to the light source.  
 C. is present due to stacked sheets of nanorods.  
 D. All of the above
14. Which statement about Lake Kasumiguara pearls is false?  
 A. Culturing usually takes 3–4 years.  
 B. The pearls grow the fastest in the winter.  
 C. The bead nuclei are from the United States.  
 D. A metal pin is used in the culturing process.
15. Pearls from *Pinctada maculata* mollusks  
 A. are easy to distinguish from other mollusk species using spectroscopy.  
 B. are commonly cultured.  
 C. do not come in a desirable range of colors.  
 D. are generally less than 6 mm.
16. A boron-containing blue diamond will display distinctive  
 A. IR absorption features.  
 B. PL spectroscopy features.  
 C. visible phosphorescence.  
 D. All of the above
17. The ancient term \_\_\_\_\_ is thought to have been used to refer to garnet.  
 A. *upala*  
 B. *adamas*  
 C. *smargados*  
 D. *alabandenum*
18. Diaspore and corundum share which properties?  
 A. Both are composed strictly of  $AlO_6$  octahedra.  
 B. Both contain edge-shared octahedra.  
 C. Both contain face-shared octahedra.  
 D. They are both uniaxial.
19. Natural black diamonds  
 A. are hard to distinguish from diamonds that have been irradiated or heat-treated.  
 B. generally receive high clarity grades.  
 C. can have brown radiation stains.  
 D. are rarely larger than 0.50 ct.
20. Which statement about blue Yogo sapphire is false?  
 A. The color is dependent upon silicon.  
 B. They generally have a tabular habit.  
 C. They exhibit color zoning.  
 D. They have high clarity.
21. Natural violet diamonds  
 A. generally owe their color to hydrogen defects.  
 B. have been found in the Argyle mine.  
 C. tend to show a gray component.  
 D. All of the above
22. Nickel in natural green diamond  
 A. works with other defects that absorb the blue end of the spectrum to create a green color.  
 B. is the major defect associated with producing a green color.  
 C. causes color through emission of light.  
 D. Both B and C
23. The adhesives used to hold amber pieces in place in the original amber room  
 A. contained a substance used in ship caulking.  
 B. were considered permanent.  
 C. were resistant to melting.  
 D. would crack over time.
24. What minerals can react with corundum to form a spinel coating?  
 A. Dolomite  
 B. Garnet  
 C. Biotite  
 D. All of the above
25. Which of the following pearls is expected to have the thinnest nacreous layer?  
 A. *Koshi-mono*  
 B. *Tonen-mono*  
 C. Natural pearl formed over a period of three years  
 D. None of the above

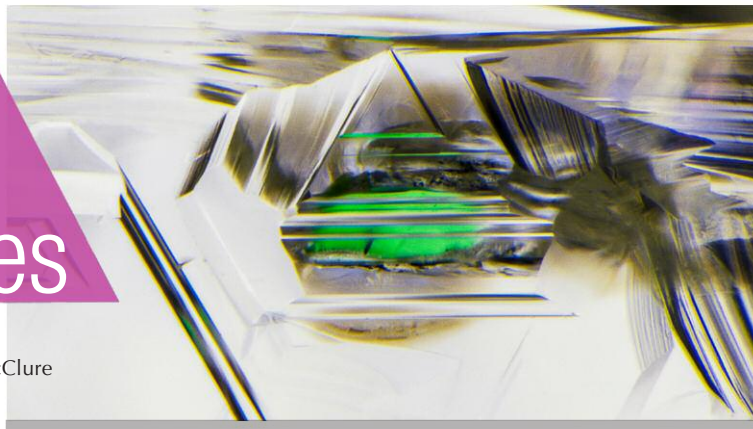
To take the Challenge online please scan the QR code to the right.



# Lab Notes

## Editors

Thomas M. Moses | Shane F. McClure



## The Largest DIAMOND Ever Discovered in North America

In October 2018, a diamond weighing a remarkable 552.7 ct was recovered from the Diavik mine in Canada. This is by far the largest known gem diamond found to date in North America. It is nearly three times larger than the 187.63 ct Diavik Foxfire which was unearthed from the same mine in August 2015, and about twice the size of a 271 ct white diamond mined from the Victor mine in Canada. GIA's New York laboratory had the opportunity to examine this notable diamond in late January 2019, before it went on public display at Phillips auction house in New York.

This large diamond (54.5 × 34.9 × 31.8 mm) has a striking yellow bodycolor and a rounded irregular ovoid shape (figure 1). The markedly rounded overall shape is due to strong resorption of the crystal surface, leaving a coarse surface texture of complex terraces and hillocks. Negative trigons were sparsely distributed. A fracture oriented perpendicular to the length divides a portion of the diamond, about a quarter of the way in from the smaller end (the left side in figure 1). In and around the fracture there are a few small black inclusions, possibly graphitic or sulfide. At high magnification, a portion of the frac-



Figure 1. This 552.7 ct yellow diamond (54.5 × 34.9 × 31.8 mm) from the Diavik mine in Canada is by far the largest diamond found to date in North America.

ture is slightly resorbed, suggesting that at least part of the fracture developed during ascent in the kimberlite. Patches of surface abrasion up to 7 mm across, but limited to a very shallow depth, are spread widely over the surface. According to a statement by Dominion, these markings are thought to be the result of abrasion during the recovery process, and the fact that the diamond remains unbroken is remarkable.

Infrared absorption spectroscopy reveals that the diamond is type Ia, with a very high concentration of aggregated nitrogen. A very weak absorption at 3107 cm<sup>-1</sup> from the N3VH lattice defect was also recorded. UV-visible absorption spectroscopy reveals strong absorption from N3 (415 nm) and N2 (478 nm), a typical feature of “cape” diamonds. No other ab-

sorption features were detected in the UV-Vis spectrum, consistent with the pure yellow bodycolor visible to the eye. Under long-wave UV radiation, this diamond has strong blue fluorescence and weak but long-lasting yellow phosphorescence. Moderate whitish blue fluorescence and very weak orange phosphorescence were observed under short-wave UV radiation. All these gemological and spectroscopic features are very similar to those observed in the Diavik Foxfire. Photoluminescence analysis at liquid nitrogen temperature with varying laser excitations from the UV to the infrared region revealed additional features of a typical “cape” diamond. Main emission peaks included very strong N3 at 415 nm and weak H3 at 503 nm. In addition, weak emissions at 489, 535, 604, 612, 640, 700, 741,

*Editors' note: All items were written by staff members of GIA laboratories.*

GEMS & GEMOLOGY, Vol. 55, No. 1, pp. 91–101.

© 2019 Gemological Institute of America



Figure 2. This 4.86 ct cabochon displays unusual yellowish chatoyancy against a predominantly purple bodycolor.

787, and 910 nm were recorded. No emission from H4 (496 nm) or H2 (986 nm) was observed.

This diamond has a combination of size, color, and top gem quality that is extremely rare. It will be exciting to see this special diamond crafted into polished form. The Diavik mine is jointly owned by mining companies Rio Tinto and Dominion Diamond Mines.

*Wuyi Wang and Evan M. Smith*

### Chatoyant Quartz/Tourmaline DOUBLET

Doublets are assemblages of two different materials, often joined with cement. Historically they were composed of inexpensive materials used to imitate precious stones. Recently new combinations have been reported, such as a beryl/topaz doublet (Winter 2014 GNI, pp. 306–307), synthetic sapphire/synthetic spinel doublets (Winter 2016 Lab Notes, pp. 418–419), and a beryl/glass complex assemblage (Summer 2018 Lab Notes, pp. 206–208).

GIA's Tokyo laboratory had the chance to examine a unique doublet. The 4.86 ct purplish cabochon, measuring  $11.07 \times 10.00 \times 5.94$  mm, appeared to display chatoyancy with a yellowish sheen (figure 2). The hydrostatic specific gravity (SG) and spot refractive index (RI) readings were 2.66 and 1.54, respectively. Assembled fea-



Figure 3. Viewed from the side, the assemblage was obvious. Trapped bubbles in the cemented plane can also be seen.

tures with a cemented plane were easily recognized when viewed from the side, as shown in figure 3. Standard gemological testing, microscopic observation, and infrared spectra revealed that the cabochon segment was a natural amethyst. There were no parallel inclusions that might have caused chatoyancy in this segment. On the other hand, the semitransparent yellowish base had

parallel striations and tube-like inclusions throughout (figure 4). Raman spectroscopy identified the base as tourmaline.

Parallel inclusions located near the bottom of a cabochon can create a chatoyant phenomenon (Winter 2017 Lab Notes, pp. 459–460). This assembled item displayed a similar effect due to the flat tourmaline base with parallel structures. When light was reflected through the amethyst by the tourmaline base, the parallel striations and tube-like inclusions in the tourmaline created the band of reflected light that appeared on the cabochon. Transparent amethyst and semitransparent yellow tourmaline are an uncommon combination. This doublet is an example that assemblages are not always aimed to imitate precious stones but can be creative artworks.

*Yusuke Katsurada*

### Large Faceted GAHNOSPINEL

Gahnospinel is a rare dark greenish blue gemstone that belongs to the spinel group. Its properties result from

Figure 4. Cavities on the base show the parallel striations and columnar or tube-like inclusions. Field of view 1.88 mm.

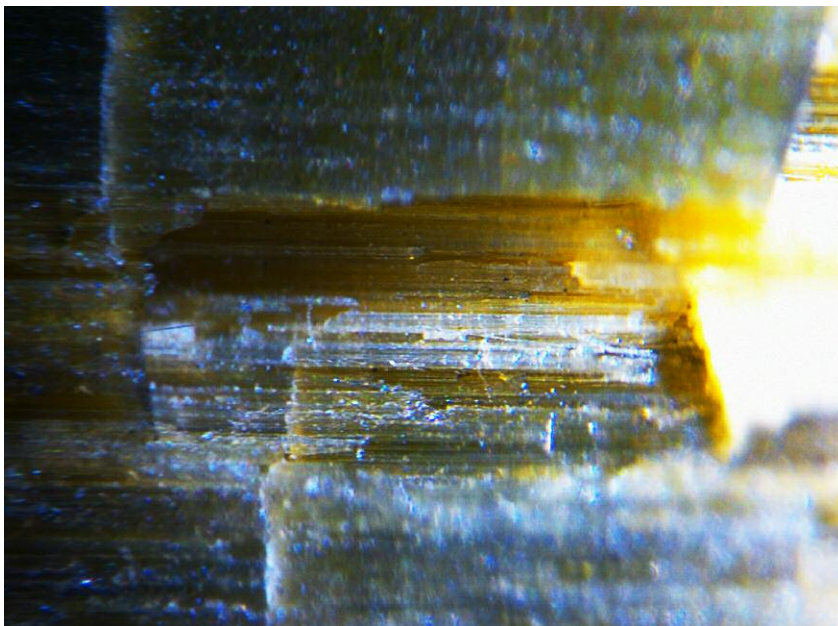




Figure 5. This 11.34 ct gahnospinel was the largest identified by GIA.

being part of a solid solution series with the end members gahnite ( $ZnAl_2O_4$ ) and spinel ( $MgAl_2O_4$ ). Because of the high amount of zinc in the mineral, the RI and SG shift from lower values for the spinel end member to higher values as the amount of Zn substituting for Mg increases, which may lead to confusion when trying to identify it. Spinel has an SG of 3.06 and an RI of 1.718, while gahnite has an SG of 4.55 and an RI of 1.800. As a combination of the two, gahnospinel's SG can fall anywhere in between.

An 11.34 ct transparent faceted oval mixed cut (figure 5) was recently submitted to the Carlsbad lab for an identification report. Despite the

stone's large size, the only inclusions were tiny crystals. To date, this is the largest gahnospinel seen at any GIA laboratory worldwide. The previous stones submitted were 1.95 ct and below.

Standard gemological testing revealed an RI of 1.754 and an SG of 4.10. These results are not typical for spinel. Inductively coupled plasma-mass spectrometry (ICP-MS) data revealed a very high zinc content and the stoichiometry of the sample was calculated to be the following:  $(Mg_{0.485}Zn_{0.385}Fe^{2+}_{0.043})_{0.913}(Al_{2.049}Si_{0.004})_{2.053}O_4$ . The atomic mass of zinc is 65.38, far greater than the 24.31 atomic mass of Mg. As the amount of zinc substitution for Mg in gahnospinel increases, it tends to have a higher RI and specific gravity than spinel. This variety of spinel may bring identification challenges without advanced testing techniques to identify the presence of Zn.

Jessa Rizzo

#### GLASS Bangles

Recently, the Carlsbad laboratory was sent two bangles for identification: a 343.94 ct translucent white bangle and a 355.52 ct translucent mottled light purplish gray and green bangle (figure 6). The white bangle could have easily been given a sight identi-



Figure 7. An elongated gas bubble seen below the surface of the white bangle. Field of view 3.57 mm.

fication of nephrite due to its color and dullness. But its RI of about 1.500 eliminated the possibility of nephrite, which has an RI of 1.62. Further observation showed an even color and no natural inclusions. Gas bubbles of various sizes could be seen just below the surface (figure 7). The RI in combination with the gas bubbles indicated that this bangle was a manufactured product.

The mottled bangle had a color very similar to that of jadeite. An RI of 1.610, rather than the typical jadeite RI of 1.66, indicated that this piece was also not what it appeared to be. Gas bubbles were identified throughout the bangle (figure 8), further confirming that this was a manufactured product. Strings of gas bubbles were observed without mag-

Figure 6. The 343.94 ct translucent white bangle on the left and the 355.52 ct translucent mottled purplish gray and green bangle on the right were carved from manmade glass.





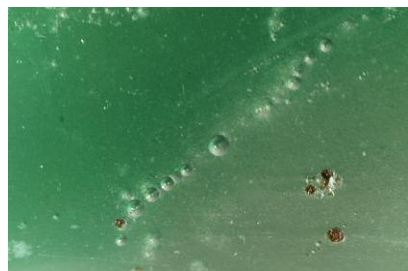


Figure 8. Gas bubbles of various sizes could easily be seen throughout the mottled purplish gray and green bangle. Field of view 3.57 mm.



Figure 9. Clusters of gas bubbles with a string-like structure in the mottled purplish gray and green bangle. Field of view 3.57 mm.



Figure 10. This 1.33 ct brownish orange pear-shaped brilliant cut is the first faceted parisite GIA has examined.

nification, an arrangement that could have easily been mistaken for a natural jadeite structure (figure 9).

These gemological properties and observations identified these bangles as manmade glass and not the nephrite and jadeite they resembled. With nephrite and jadeite having such a rich cultural history, it is common for imitations to show up on the market. Items like these demonstrate the need to always be cautious when purchasing jewelry.

Nicole Ahline

### Rare Faceted PARISITE

Recently the Carlsbad laboratory received a 1.33 ct transparent brownish orange pear brilliant for identification service (figure 10). Standard gemological testing revealed a refractive index from 1.670–1.750 with a birefringence of 0.080 and an SG (obtained hydrostatically) of 4.40. There was no fluorescence observed with exposure to long- or short-wave UV light. The stone also appeared doubly refractive when examined with polarized light. Microscopic examination with a fiber-optic light source showed strong doubling, two-phase fingerprints with trapped liquid and gas, and crystal inclusions. Raman and mid-IR spectroscopy conclusively identified the stone as parisite-Ce. The Raman spectrum displayed the strongest vibrational band at 1083  $\text{cm}^{-1}$ , and subsequent peaks at 1740, 1567, 1431,

741, 398, and 269  $\text{cm}^{-1}$ , which positively identified the mineral. The mid-IR spectrum revealed areas of rare earth element (REE) absorption. Energy-dispersive X-ray fluorescence (EDXRF) analysis detected Ce, La, and Ca, supporting this identification.

Parasite is one of the rare-earth carbonite minerals found in the bastnäsite group, with a chemical formula of  $\text{Ca}(\text{Ce,La,Nd})_2(\text{CO}_3)_{3/2}\text{F}_2$ . Parasite crystals are found in carbonatites, granite pegmatites, alkaline syenites, and hydrothermal deposits associated with these environments. Normally the crystals of parisite are too small and cloudy to produce decent gemstones. They are usually found as mineral inclusions in emerald from

the Muzo mine in Colombia and in quartz from Zagi Mountain, Pakistan. This is the first time a faceted parisite gem has been examined by GIA.

Maxwell Hain

### Freshwater Bead-Cultured PEARLS with Multiple Features of Interest

GIA's Hong Kong laboratory recently examined a necklace consisting of 24 white baroque-shaped nacreous pearls ranging in size from 21.92 × 15.24 mm

Figure 11. Eleven of the 24 pearls in this necklace exhibited a shape like a dumbbell or peanut shell, which corresponded with the internal twin bead structure revealed by subsequent microradiography.



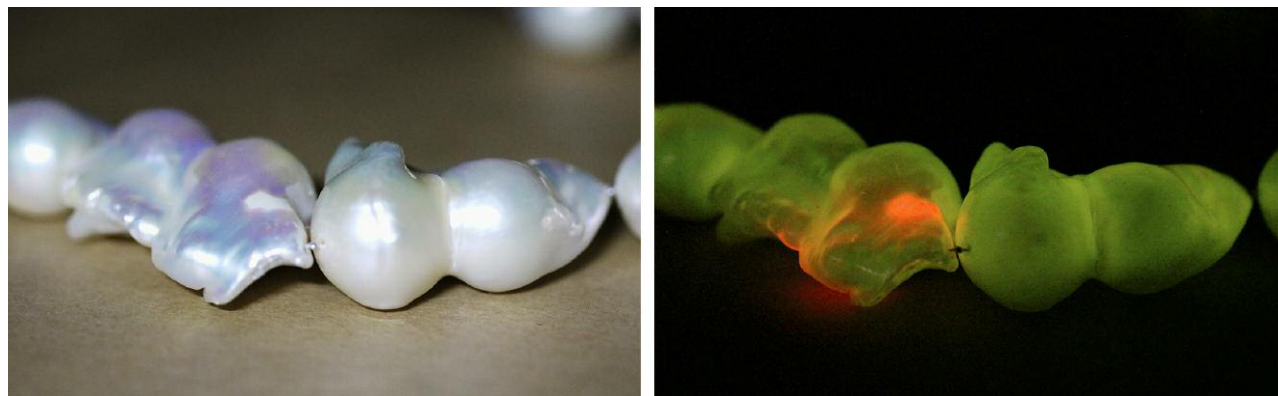


Figure 12. A small whitish non-nacreous region was observed on one pearl under white light (left). The optical X-ray fluorescence image (right) revealed a strong green fluorescence reaction, as expected for freshwater pearls. An atypical reddish orange reaction was observed on the whitish non-nacreous portion.

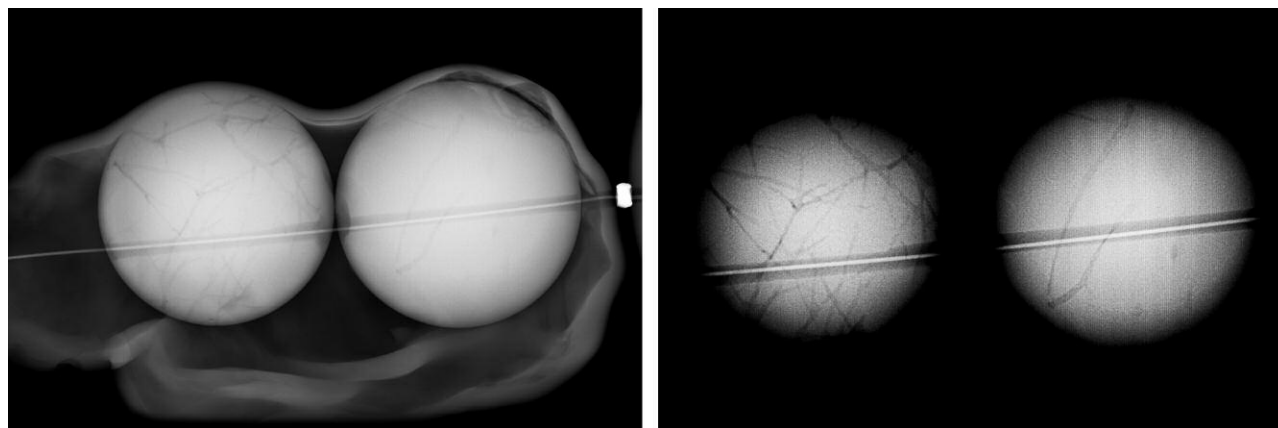
to 24.95 × 15.12 mm (figure 11). Their external appearance, high luster, and strong orient hinted at a freshwater origin. Detailed examination revealed additional features of interest.

While their appearance was indicative of freshwater pearls, energy-dispersive X-ray fluorescence analysis was performed on a random selection to confirm their formation environment. The high manganese concentrations of 751–1728 ppm were consistent with freshwater pearls. In keeping with the reactions seen in freshwater pearls with such levels of Mn, the samples exhibited strong

green fluorescence when exposed to X-rays. However, one in particular displayed moderate to strong reddish orange fluorescence on some areas of its surface (figure 12), associated with whitish non-nacreous regions on the pearl. Similar reddish fluorescence reactions had previously been observed around damaged areas of nacre on pearls examined in GIA's New York laboratory (Summer 2013 Lab Notes, pp. 113–114). The exact reason for this reaction, which GIA gemologists have seen in cultured and natural freshwater pearls from time to time, is unknown.

Eleven of these pearls had a shape resembling a dumbbell or peanut shell, indicating the possible presence of two nuclei in each. Real-time microradiography confirmed the presence of two round bead nuclei in these pearls (figure 13). The remaining 13 contained only a single round bead, consistent with the majority of bead-cultured pearls on the market. In addition, a network of tubules was observed within most of the bead nuclei. Such tubules resembled those observed in saltwater shells, which result from the burrowing actions of parasites. Thus, the bead nuclei were

Figure 13. Microradiographs revealed two round bead nuclei in one of the dumbbell-like pearls (left) and a network of tubules in the beads, resembling the parasite tubes commonly associated with saltwater shells (right). X-ray contrast permits the observation of structures near the surface and nearer the center of the pearls.



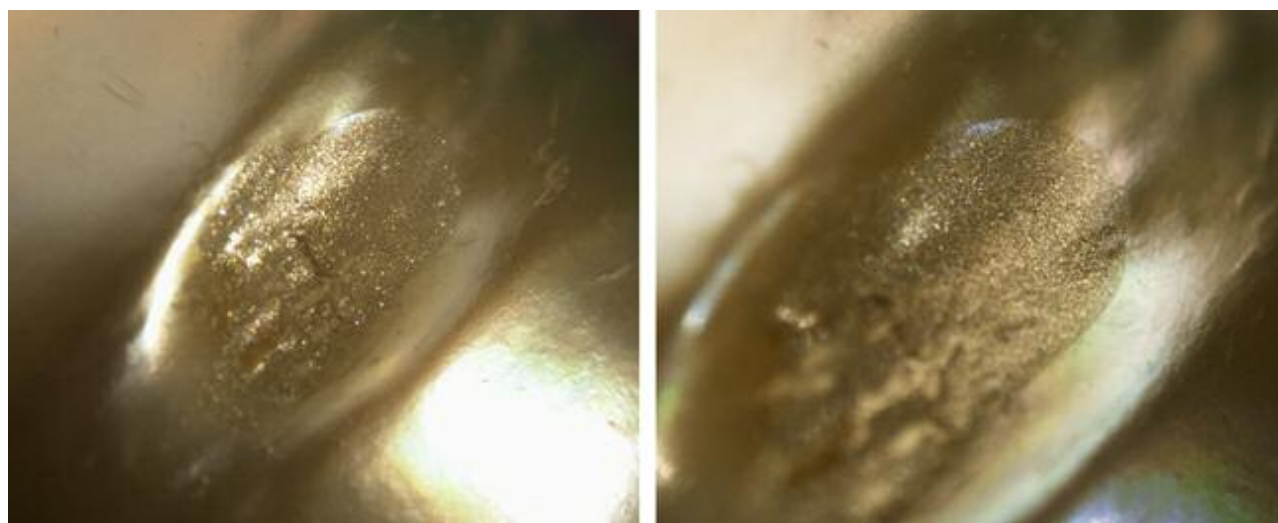


Figure 14. Artificial material was observed filling and masking surface blemishes on some of the pearls in the necklace. Fields of view 5.68 mm (left) and 3.74 mm (right).

likely fashioned from saltwater shells rather than the usual freshwater nuclei employed. Nonetheless, it was impossible to determine the nature of the shell beads without destructive testing. Microradiography examination proved the bead nuclei were not pre-drilled, a characteristic often observed in freshwater nuclei used to culture freshwater pearls (H.A. Hänni, "Ming pearls: A new type of cultured pearl from China," *Journal of the Gemmological Association of Hong Kong*, Vol. 32, 2011, pp. 23–25) and typically encountered by GIA during testing. While pearls cultured with two bead nuclei are relatively uncommon, their existence has been acknowledged in the literature (Fall 1993 Lab Notes, pp. 202–203). The twin bead structure clearly influenced the appearance of these pearls and resulted in some pleasing baroque shapes.

Finally, upon closer examination, a "glittery" grainy material was observed on the pits and blemishes of several pearls (figure 14). This resembled the *essence d'orient* applied on the surface of some imitation pearls. Raman analysis of this material yielded a number of peaks (e.g., 634–639  $\text{cm}^{-1}$  and 1604  $\text{cm}^{-1}$ ) that matched, to some degree, the peaks of the filling material described in an earlier reference (Winter 2017 GNI, pp. 482–484).

While the GIA laboratory examines pearl strands on a daily basis, we seldom encounter one submission possessing several interesting features such as the twin bead structure, reddish orange optical X-ray fluorescence, and filled surface blemishes. It is important for gemologists to always stay alert to the surprises they might find when examining pearls.

Bona Hiu Yan Chow

#### Low-Fe, High-V Color-Change Burmese SAPPHIRE

A color-change sapphire was recently submitted to the GIA lab in Carlsbad

for an origin determination report. The 5.68 ct transparent cushion mixed cut displayed a strong color change from grayish violet in fluorescent light to purple-pink in incandescent light (figure 15). Color-change sapphires generally range from blue to violet in daylight-equivalent (fluorescent) light and from purplish pink to pinkish purple in incandescent light. Stones displaying a strong color-change phenomenon are highly desirable.

Standard gemological testing proved that this stone was corundum with an RI of 1.760 to 1.768. Its weak ruby spectrum displayed absorption lines in the red area between 660 and

Figure 15. This 5.68 ct cushion mixed-cut sapphire showed a strong color change from grayish violet in fluorescent light to purple-pink in incandescent light.



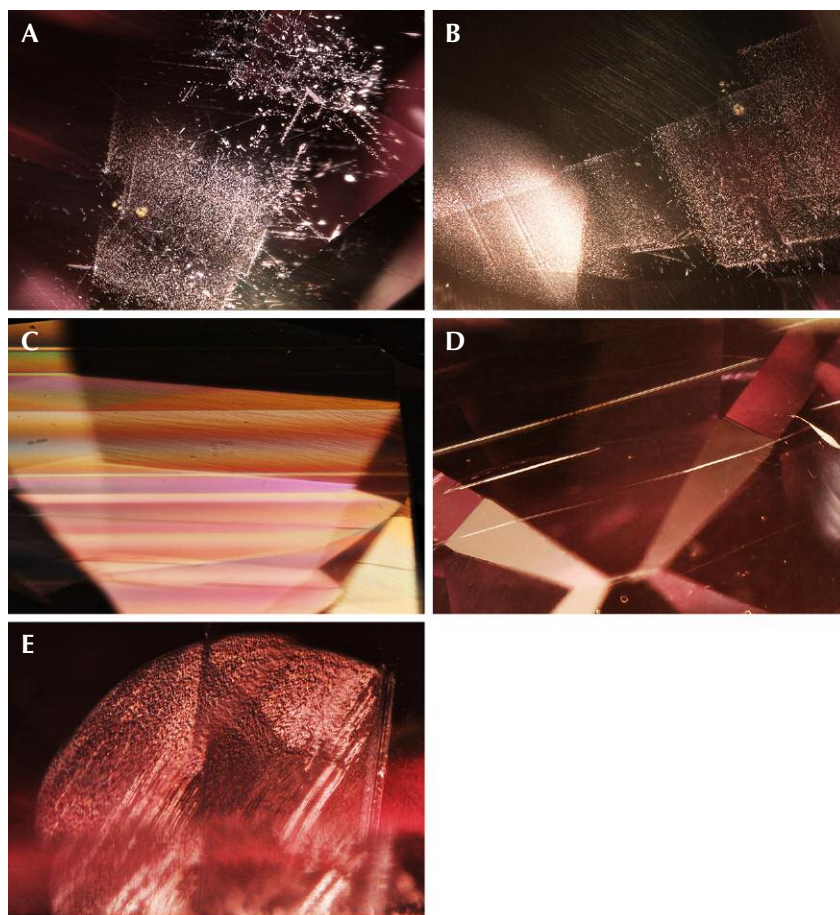


Figure 16. A: Exsolved rutile as reflective platelets, arrowheads, particles, and needles in sapphire; field of view 6.42 mm. B: Loose white particle clouds arranged in a geometric pattern and in stacked planes; field of view 3.80 mm. C: Twinning lamellae are commonly observed in Burmese sapphires; field of view 4.79 mm. D: Boehmite needles or tubules often occur with polysynthetic twinning; field of view 4.79 mm. E: Reflective fingerprints with iridescence in sapphire; field of view 1.37 mm.

695 nm, a broad absorption in the green-yellow area between 500 and 600 nm, and two fine lines in the blue area between 460 and 480 nm. It fluoresced a strong patchy orange color under long-wave UV and a weaker orange under short-wave UV. Microscopic examination revealed exsolved rutile as reflective platelets, arrowheads, particles, and needles (figure 16A); loose white particle clouds arranged in geometric and stacked patterns (figure 16B); a series of twinning lamellae (figure 16C); boehmite needles or tubules (figure 16D); and reflective fingerprints with iridescence (figure 16E). No evidence of heat treatment was observed. The

stone showed diffused pinkish purple zoning in immersion. This inclusion scene is common in but not limited to sapphires from Sri Lanka, Madagascar, and Myanmar (formerly Burma).

To help with the country of origin determination, we collected laser ablation-inductively coupled plasma-mass spectrometry (LA-ICP-MS) chemistry. The results showed very low concentrations of iron, 11–13 ppma, and an unusually high vanadium at 300 ppma.

Several years ago a parcel of color-change sapphires was documented at GIA's laboratory in Bangkok. That material, which had the same unusual chemistry of low Fe and high V,

was from Myanmar. The chemistry profile of our client-submitted stone was consistent with that of the research stones previously documented from Myanmar.

This is the first time the Carlsbad lab has encountered a color-change sapphire with such a unique chemistry profile. LA-ICP-MS again proved to be a useful tool for gemstone origin determination, especially when the inclusion scenes of different localities overlapped.

Rebecca Tsang

### SYNTHETIC DIAMOND CVD Layer Grown on Natural Diamond

A 0.64 ct Fancy grayish greenish blue cushion modified brilliant (figure 17) was recently found to be a composite of synthetically grown and natural diamond. During testing, the infrared spectrum showed both strong absorption of nitrogen and the absorption of uncompensated boron, features characteristic of type Ia and type IIb diamonds, respectively (figure 18). The UV-Vis-NIR spectrum showed “cape” peaks, which are nitrogen-related de-

Figure 17. Face-up image of the natural diamond with CVD synthetic diamond overgrowth. The blue color is due to the boron-doped CVD layer.



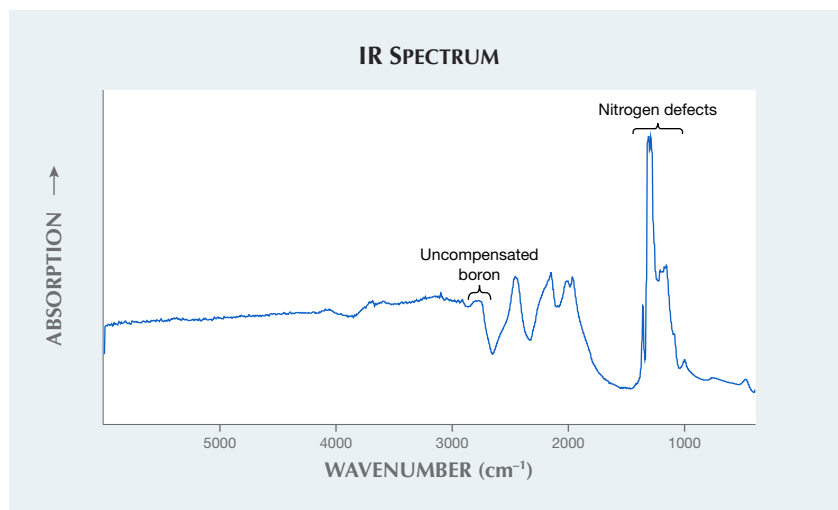


Figure 18. The infrared spectrum shows both nitrogen- and boron-related defects. This combination of defects is very unusual in natural diamonds and a cause for concern.

fects, but also a sloping absorption into the red portion of the spectrum caused by uncompensated boron. It is very unusual for boron- and nitrogen-related defects to be seen together in natural diamonds, though an example has been seen before (Spring 2009 Lab Notes, pp. 55–57). Mixed-type diamonds always call for additional scrutiny.

The DiamondView fluorescence image taken on the pavilion showed a blue hue, caused by luminescence from the N3 defect, and natural growth features. The image taken on the crown showed a greenish blue color common to boron-bearing diamonds and the dislocation patterns characteristic of CVD-grown diamonds. In the image taken from the side, a layer can be seen between the natural substrate and the CVD-grown addition (figure 19). These two distinct fluorescence patterns—the greenish blue from the CVD layer and the darker blue from the naturally grown layer—prove that a layer of CVD synthetic diamond was grown on a natural substrate. A wireframe model generated from a non-contact optical measurement device was uploaded to the DiamCalc diamond modeling program. Using the fluorescence images as a guide, we obtained a 3D section that represented only the

CVD layer. From this, we calculated an approximate layer weight of 0.10 ct and a thickness of approximately 200 microns. A similar diamond previously reported was also a type IIb CVD layer grown on a natural Ia substrate (Summer 2017 Lab Notes, pp. 237–239). That composite was Fancy blue, weighed 0.33 ct, and had a CVD layer that was 80 microns thick.

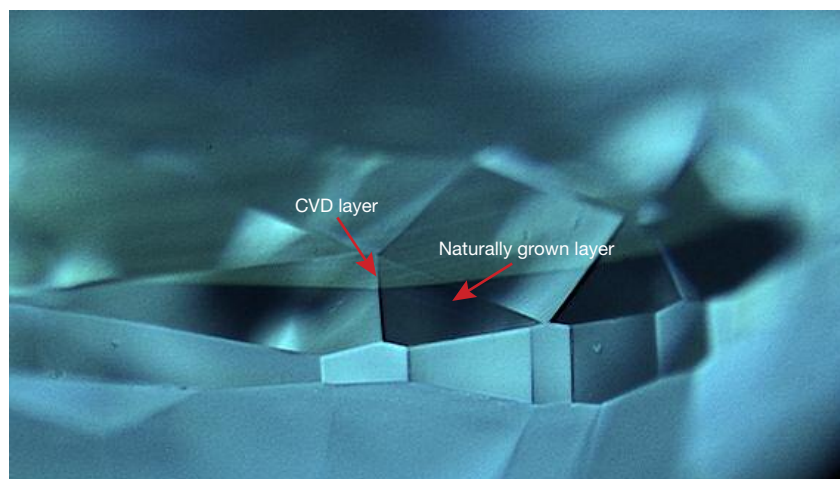
When viewed through a microscope, small pinpoint-like polish features were observed from facet to facet along with a faint line resem-

bling surface graining. These polish features were visible along the entire area of this division and correlated with the separation plane seen in the fluorescence images. Examination with an electrical conductivity tester showed that the crown was conductive but not the pavilion. This is consistent with a type IIb crown and type Ia pavilion.

In immersion, the CVD layer was grayish blue whereas the natural substrate had a yellowish bodycolor (figure 20). The blue color in the CVD layer is from the uncompensated boron, and the yellowish color in the substrate is due to the “cape lines” in the visible spectrum. The final color, Fancy grayish greenish blue, is caused by the gray and blue components from the CVD layer and the yellow from the substrate. The resulting color was likely the main motivation for growing the CVD layer on top of the natural diamond, though the extra weight gained could also be a factor. Viewing under crossed polarizers in immersion revealed dislocation bundles that started at or near the interface and grew upward and outward (figure 21). This proves that it was a thick CVD layer and not a coating of CVD overgrowth.

In CVD-grown diamonds, there is some indication in PL spectra that the diamond has been grown in a labora-

Figure 19. A DiamondView image showing the separation plane.



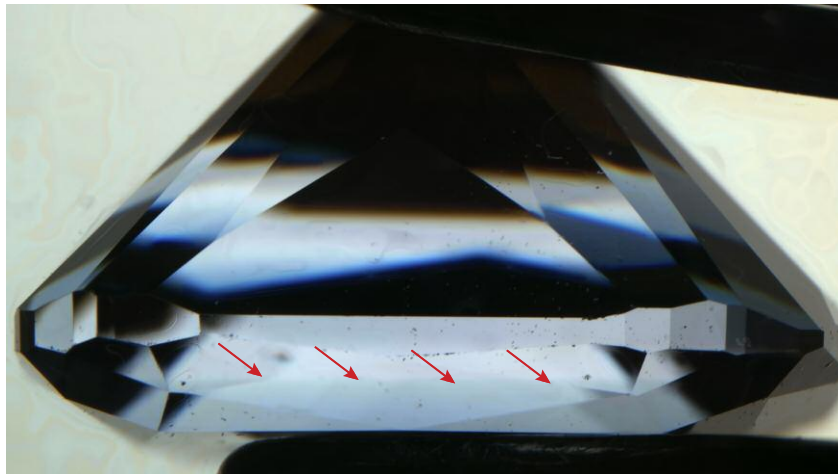


Figure 20. In immersion, the blue color of the CVD layer is clearly visible.

tory—usually the presence of the silicon doublet peak at 736.5 and 736.9 nm or the 596/597 nm defect. Numerous PL spectra were collected in standard and confocal mode on both the crown and pavilion of the diamond in search of any indication of this synthetic overgrowth. In this case, neither of these CVD features were evident, likely due to the thinness of the layer.

With the second of these composites seen at GIA, this could be a new type of product entering the market. Natural diamonds with synthetic diamond grown on the surface require extra scrutiny due to the presence of

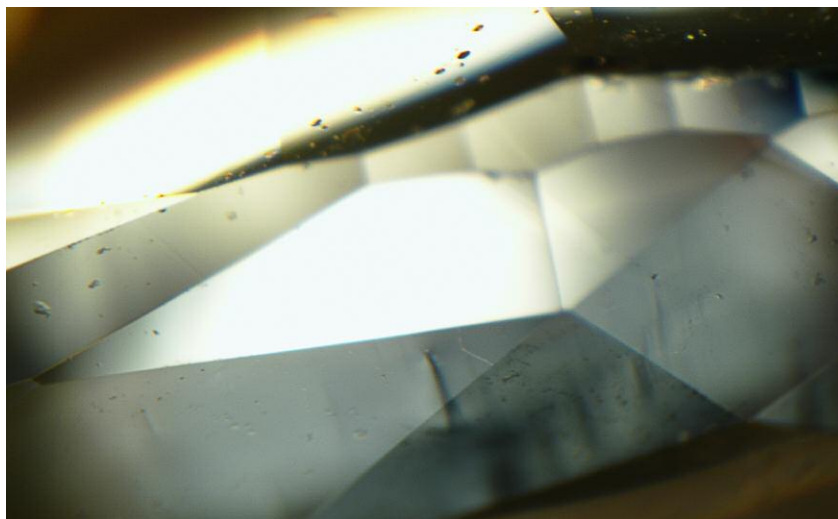
natural-looking features, both spectroscopic and gemological. Careful inspection still reveals the presence of synthetic indicators, which expose the true nature of the diamond.

*Troy Ardon and Garrett McElhenny*

#### Faint Green HPHT Synthetic Diamonds

The Carlsbad lab recently received 25 diamonds for grading reports that all proved to be undisclosed HPHT synthetics, ranging in weight from 0.46 to 0.52 ct. Of these, nine were equiva-

Figure 21. Dislocation bundles in the CVD layer are visible under crossed polarizers in methylene iodide. Field of view 1.90 mm.



lent to the colorless to near-colorless range, eight equivalent to Faint yellow-green, seven equivalent to Faint green (e.g., figure 22), and one equivalent to Very Light green. We found that the green coloration was due to high concentrations of nickel. Nickel is a common impurity in HPHT synthetics, but rarely in amounts significant enough to affect the color.

Previously, GIA gemologists described an HPHT synthetic diamond whose color was equivalent to Fancy Deep yellowish green due to massive amounts of nickel creating an absorption band at ~685 nm (Spring 2017 Lab Notes, pp. 96–98). They showed that the optically active nickel impurities were preferentially incorporated into the {111} growth sectors, as detected by the PL spectral maps and observable color zoning.

Among this set of 25 HPHT synthetic diamonds, none showed the SiV<sup>-</sup> defect at 737 nm with 633 nm PL excitation while 16 showed detectible amounts of uncompensated boron at 2800 cm<sup>-1</sup> in their IR absorption spectra. In this suite, five showed the 685 nm absorption band generally associated with strong nickel impurities while the others showed a broader,

Figure 22. This 0.50 ct HPHT synthetic diamond, color equivalent to Faint Green, owed its color to nickel impurities.



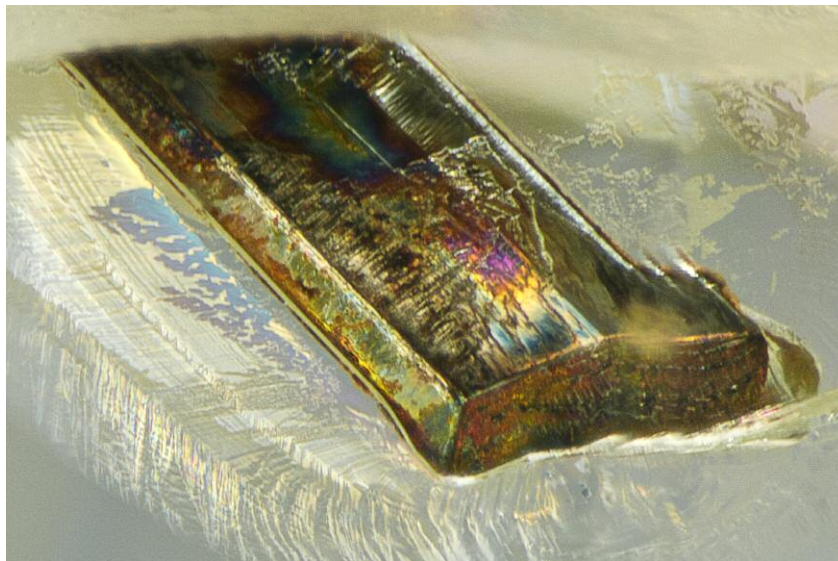


Figure 23. This 0.52 ct Faint yellow-green HPHT synthetic diamond also showed pronounced metal flux inclusions, further proof of its lab-grown origin. This view shows the pavilion facets, with the girdle at the top of the photo. Field of view 1.76 mm.

less pronounced absorption band ranging from 650 to 800 nm. The quantity of uncompensated boron was relatively low, with most containing 0.2–5.6 ppb and one near-colorless sample containing 18 ppb.

Uncompensated boron is also a common impurity in HPHT synthetics, as it is incorporated during the growth process; these low concentrations did not contribute to the coloration. Additionally, several showed distinctive

metal flux inclusions, also indicative of HPHT growth (e.g., figure 23).

Having such a large dataset of similar but unusually colored HPHT synthetic diamonds in the laboratory simultaneously also allowed us to perform additional analyses to compare them. Photoluminescence (PL) maps using 785 nm excitation were collected on the table facet of eight samples, spanning across the various graded colors (figure 24). As expected, the nickel peaks showed the highest concentration within the {111} sectors. From each of the collected maps, we could identify the {111} sectors and determine the average PL intensity of the nickel-related 883/884 nm peaks. When these were plotted according to their equivalent color, the peak intensity was seen to generally increase as the color grade went from the colorless to near-colorless range to Very Light green. Nevertheless, the nickel-related defect at 883/884 nm is not believed to be the same nickel-related defect creating visible absorption. A similar PL map, not shown, was collected on the Fancy Deep–equivalent yellow-green HPHT synthetic diamond (again, see

Figure 24. Left: This PL map, collected with 785 nm excitation, shows that the highest amounts of nickel are concentrated within {111} growth sectors of this 0.52 ct Faint yellow-green HPHT synthetic diamond. This false-color map shows the area of the 883/884 nm doublet normalized with the diamond Raman peak. Right: The average PL intensity of the nickel-related 883/884 nm peak within the {111} sectors increases as the equivalent color increases from colorless to Very Light green.

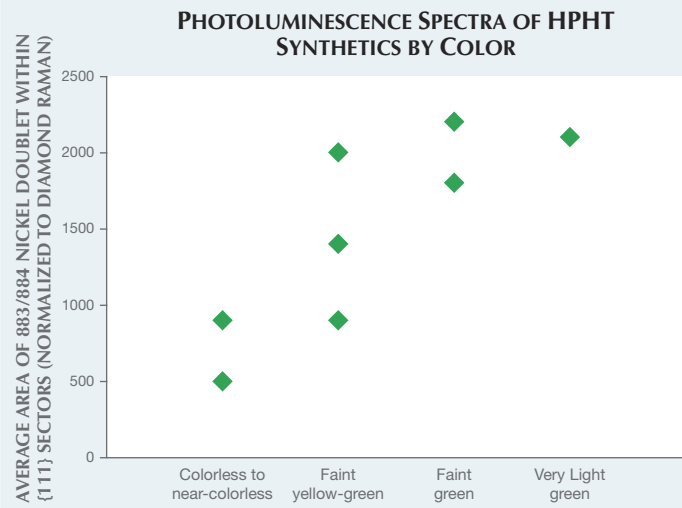
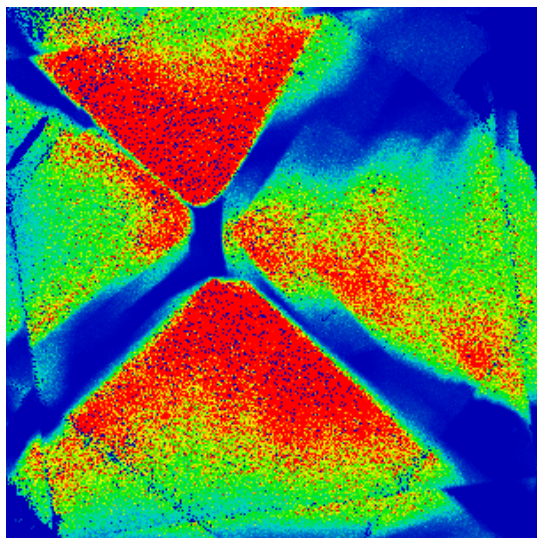




Figure 25. This 7.78 ct round brilliant and 4.90 ct cushion brilliant displayed a blue-green and green-blue color, respectively, that are reminiscent of Paraíba tourmaline.

Spring 2017 Lab Notes, pp. 96–98); the nickel intensity in that case was approximately 10× greater than the Faint green samples studied here.

As laboratory-grown diamond manufacturers continue to experiment with their recipes and the process further evolves, we will likely see greater quantities and a wider variety of color ranges.

Sally Eaton-Magaña

### Paraíba-Like SYNTHETIC SAPPHIRE

Recently GIA's Carlsbad laboratory received for identification two gemstones weighing 7.78 and 4.90 ct (fig-

ure 25) that showed a neon green-blue to blue-green color similar to that of Paraíba tourmaline. Standard gemological testing yielded an RI of 1.76–1.77 and an SG of 4.00, consistent with corundum. Microscopic examination revealed curved color banding (figure 26) when viewed with diffused light and immersed in methylene iodide. Plato lines were observed when examining the stones parallel to the optic axis using cross-polarized light. Curved color banding and Plato lines are the two most important pieces of evidence to separate natural from flame-fusion synthetic sapphire using standard gemological testing. Also observed were wavy, finely textured



Figure 26. Subtly curved color zoning was seen in this vibrant blue-green synthetic sapphire, confirming its flame-fusion origin. Field of view 5.33 mm.

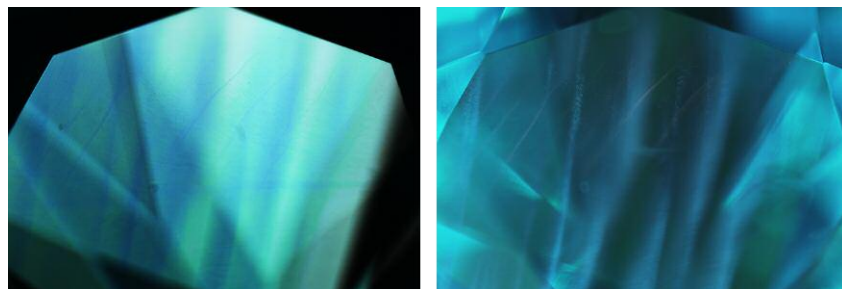
clouds associated with the blue color zones (figure 27). Pink emission caused by the presence of trace-element magnesium was seen only with fiber-optic light. This stone does not react to fluorescent light.

Trace-element chemistry measured by LA-ICP-MS showed the presence of cobalt (105–158 ppmw, with detection limit at 0.652 ppmw), which is presumably responsible for the vibrant color, and magnesium (0.52–1.05 ppmw, with detection limit at 0.044 ppmw). Other trace elements such as Ni, Fe, Cr, and Ti were under the detection limits.

This is the first time GIA's Carlsbad lab has examined flame-fusion synthetic sapphire with a color similar to Paraíba tourmaline.

Forozan Zandi

Figure 27. Blue color zones in the Paraíba-like synthetic sapphires showed wispy clouds when observed with fiber-optic illumination. Field of view 4.95 mm.



### PHOTO CREDITS

Jian Xin (Jae) Liao—1; Shunsuke Nagai—2, 3; Yusuke Katsurada—4; Diego Sanchez—5; Robison McMurtry—6, 10, 15, 17, 22; Nicole Ahline—7, 8, 9; Johnny Leung—11; Sharon Tsz Huen Wu—12, 13, 14; Jonathan Muyal—16, 20, 23; Garrett McElhenny—19; Troy Ardon—21; Nathan Renfro—25; Forozan Zandi—26, 27





# DIAMONDS FROM THE DEEP

## WINDOWS INTO SCIENTIFIC RESEARCH

Karen V. Smit and Steven B. Shirey

## How Old Are Diamonds? Are They Forever?

### Age Is Important

The age of something is fundamental. Humans, animals, wine, cars, and antiques are viewed and understood in the context of their age. So it is with rocks and minerals. A geologist needs to know the age of rocks to construct the geologic history of an area. In the field, *relative ages* can be determined by cross-cutting relationships (the younger rock “cuts” across the older rock) or superposition (the younger rock overlies the older rock). To determine the *absolute ages* of rocks and minerals such as diamond, scientists measure naturally occurring radioactively decaying elements. Absolute ages are free of any knowledge of relative age relations to any other geological material. This is known as the science of *geochronology*.

Early diamond hunters in South Africa cared little about absolute age because diamonds were found as alluvial material in riverbeds and beaches, and only where they could be found mattered. Once diamonds were discovered to be hosted in kimberlite, absolute diamond ages became important in exploring for more diamonds, as well as answering the key questions about how they form:

- Are diamonds the same age as the rock (kimberlite) in which they are found?
- Did they crystallize from the kimberlite or were they picked up from country rock during volcanic eruption?
- What are the ages of kimberlites? What are the ages of the diamonds?
- Can one mine have diamonds with multiple ages?
- Are diamond-forming events a result of specific larger-scale geologic processes?

A benefit of this quest has been to show that the oldest mineral sample you can obtain and wear as jewelry is a diamond that is often three billion years or older—this is almost three-fourths of the earth’s age. This attribute will never be matched in any synthetic diamond.

### Radioactive Decay and Mineral Age

The most robust way to determine the absolute age of any mineral or rock is through radiogenic isotope analyses.

GEMS & GEMOLOGY, VOL. 55, No. 1, pp. 102–109.

© 2019 Gemological Institute of America

Long-lived radioactively decaying elements such as uranium, samarium, rhenium, and rubidium have one or more isotopes that spontaneously decay (known as a “parent”) to the isotope of another element (or “daughter”) at a constant average rate (box A). Modern mass spectrometers can measure infinitesimally small differences in the parent and daughter isotopes that have been trapped in minerals by measuring isotopic ratios. From this data and by knowing the isotopic *decay rate*, the mineral’s age can be calculated.

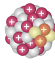


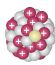
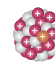

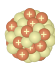
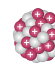

The assumption for isotopic dating is that each mineral behaves as a tiny closed system. The mineral starts with a known quantity of the parent and the accumulation of the daughter is measurable because original amounts of the daughter isotope are insignificant, and what accumulates cannot escape from the mineral structure. What occurs in nature is the equivalent of an hourglass where the mineral is the glass and the decaying parent and accumulating daughter are the sand. The neck in the glass that controls the rate at which the sand passes is the radioactive decay rate. As long as the mineral has remained a closed system from the time of its formation to its analysis in the lab today, an absolute age of the crystal is obtained.

In theory all minerals could be dated this way, but in practice only a small number of minerals can actually be dated. Limitations are due to low abundances of radioactive elements in a mineral’s structure, a decay rate of the parent isotope that is too slow, poor retention of the daughter isotope under certain geological conditions, and inadequate analytical sensitivity.

### If Diamonds Cannot Be Dated Directly, How Can They Be Dated at All?

Although diamond is composed primarily of carbon, it cannot be carbon-dated since the half-life of carbon is too short (atmospheric  $^{14}\text{C}$  decays to  $^{14}\text{N}$  with a half-life of only 5,700 years) to be useful for any geological material such as diamond that typically has ages on the order of millions to billions of years. Diamonds also do not contain sufficient amounts of any of the radioactive elements mentioned in box A. Instead, geochronologists use mineral inclusions such as iron sulfide, clinopyroxene, and garnet that are trapped within the diamond and contain sufficient Re-Os, Rb-Sr, and Sm-Nd to determine diamond ages. The simplest assumption is that the obtained age indicates how long the inclusion was trapped in the diamond, and therefore gives the time of diamond formation.

## BOX A: ISOTOPES AND RADIOACTIVE DECAY

Decay type	Radiation emitted	Model		
Alpha decay	${}^4_2\alpha$			
Beta decay	${}^0_{-1}\beta$			
Gamma emission	${}^0_0\gamma$			

Modified from scienceabc.com

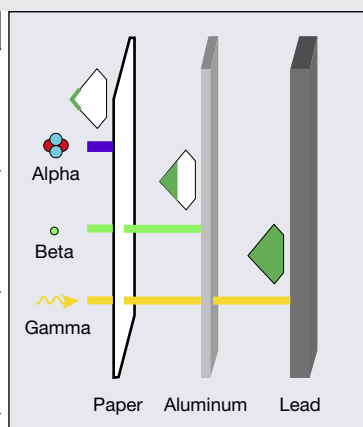


Figure A-1. Three different types of radioactive decay, and the atomic models for their radiation (from Breeding et al., 2018).

To understand basic radioactive decay, some atomic-level definitions are necessary. Each element of the periodic table is composed of atoms that have the same number of *protons* in the *nucleus* and *electrons* in a shell surrounding the nucleus. However, the number of *neutrons* in the nucleus may vary, and when it does, it will be a different *isotope* of the same element. In other words, an isotope of an element is simply the same element with a different number of neutrons. Radioactive decay is a nuclear process that affects the number of protons and neutrons and thus forces us to think in terms of isotopes.

As shown in figure A-1, there are three types of different natural radioactive decays: alpha ( $\alpha$ ), beta ( $\beta$ ), and gamma ( $\gamma$ ). For dating of geological materials, we are concerned only with alpha and beta—both of which involve the change of an isotope of one element, the *parent* isotope, into an isotope of another element, the *daughter* isotope.

Radioactive decay of parent to daughter isotopes (figure A-2) occurs randomly, but for many atoms the average decay rates over time are very constant. This constant, known as a *decay constant*, can be measured and is specific for each decay scheme. The *half-life* refers to the time it takes for half the amount of parent isotope

to decay to its daughter isotope and is an inverse function of the decay constant. Isotope systems with very long half-lives such as uranium-lead, samarium-neodymium, lutetium-hafnium, rubidium-strontium, and rhenium-osmium are employed for geological materials that can have ages anywhere from 4.6 billion years ago (the age of the earth) to the present day.

Figure A-2. Common parent-daughter isotope systems that have sufficiently long half-lives to be used for dating of geological materials. The age of the earth was determined using the U-Pb isotope system. The majority of worldwide diamonds are dated by measuring Re-Os isotopes in sulfide inclusions.

Radioactive "Parent" Isotope	"Daughter" Isotope	Half-life
${}^{238}\text{U}$	${}^{206}\text{Pb}$	4.5 billion years
${}^{235}\text{U}$	${}^{207}\text{Pb}$	710 million years
${}^{147}\text{Sm}$	${}^{143}\text{Nd}$	106 billion years
${}^{176}\text{Lu}$	${}^{176}\text{Hf}$	37 billion years
${}^{87}\text{Rb}$	${}^{87}\text{Sr}$	49 billion years
${}^{187}\text{Re}$	${}^{187}\text{Os}$	42 billion years

It should be apparent now that ages cannot be determined for diamonds that do not contain large enough or any mineral inclusions—in other words, the vast majority of gem-quality diamonds. Among members of the gem trade, mineral inclusions trapped within diamonds are not normally considered a desirable feature. However, these rare mineral inclusions are extremely valuable scientifically as they are the only direct samples that geologists have to study

Earth at depth; inclusions in some diamonds have been documented to originate from more than 660 km depths. And inclusions are the only way to determine a diamond age!

Unfortunately, diamond dating is a destructive technique. Mineral inclusions have to be broken out of the diamond so that they can be characterized, dissolved, and analyzed for their isotopic composition. It is not possible to obtain a diamond formation age from a single inclusion.

From an isochron diagram (box B), it should be clear that isotopic compositions for multiple inclusions are needed, from which a slope is determined and an age calculated. Most often, multiple inclusions of a similar paragenesis (or host rock type) are analyzed to find a formation age for a suite of diamonds from the same locality. Occasionally, scientists get lucky and are able to obtain multiple inclusions from a single diamond. In this case, the diamond's formation age can be obtained or even a long-lived growth history may be revealed.

Once the mineral has been released from its diamond host, parent and daughter elements must be removed from the mineral and purified. Since minerals are solid, removal and purification of the parent and daughter elements first requires dissolving the mineral in very strong acid solutions (such as mixtures of chromic, sulfuric, hydrochloric, nitric, and hydrofluoric acids). Once the mineral is dissolved, miniaturized purification methods—using essentially the same type of polystyrene resin beads that are found in

household water filters—are applied to separate out extremely pure parent and daughter elements. But since elements are a combination of both radioactive isotopes and so-called stable isotopes that do not decay, a further step is needed to separate out the radioactive isotopes for analyses. To separate and measure them, we turn to the mass spectrometer (box C). In this final step, the dried-down salt of the element of interest is placed onto a metallic filament that is then placed into the mass spectrometer to be slowly heated and ionized. The ions are accelerated through a curved magnetic field, and each isotope is then counted separately in a specialized detector. The detectors in a modern mass spectrometer are sensitive enough to count each and every ion that passes through its magnetic field.

## The History of Diamond Age Determination

The first diamond ages were determined by Professor Stephen Richardson of the University of Cape Town when

### BOX B: THE ISOCHRON DIAGRAM

A graphical method of evaluating the data produced by the mass spectrometer is needed to determine an age. In this example of an *isochron diagram* (figure B-1), the analyses of three different minerals (blue circles) have been plotted. The x-axis on the diagram displays the ratio of the radioactively decaying isotope to a non-decaying, stable isotope of the daughter. A ratio is necessary on this diagram because mass spectrometers measure ratios well and we need to know how much parent isotope is available for decay relative to the daughter. The minerals with higher amounts of parent plot further to the right. The higher the content of parent, the more daughter is produced. These minerals plot at a higher position on the y-axis, which is the ratio of the radiogenic daughter to the same stable daughter isotope as on the x-axis.

Radioactive decay (red dashed arrows) is a transformation of a single parent isotope of one element to a single daughter isotope of another element. This radioactive decay process preserves the slope relationship that will be generated by different amounts of parent (relative to daughter) in the different minerals. By using the slope of a line fitted through the minerals (blue line) and the independently determined decay rate (accepted by the scientific community as a constant), the true or absolute age may be calculated.

In principle this may seem complicated, but in reality the calculation is quite simple. The chief difficulties are preparing the samples in the chemistry lab for analy-

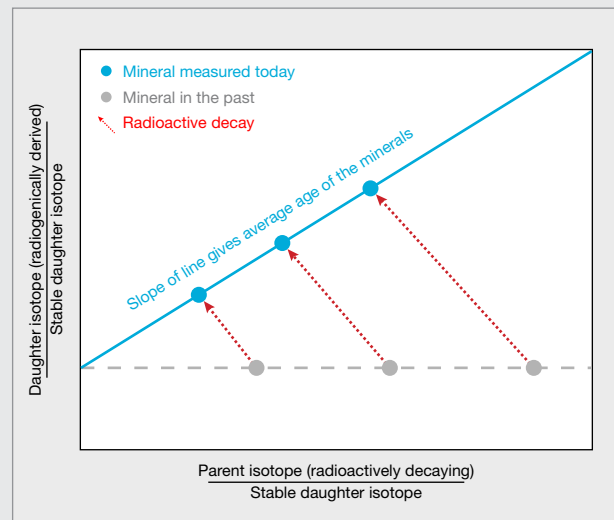
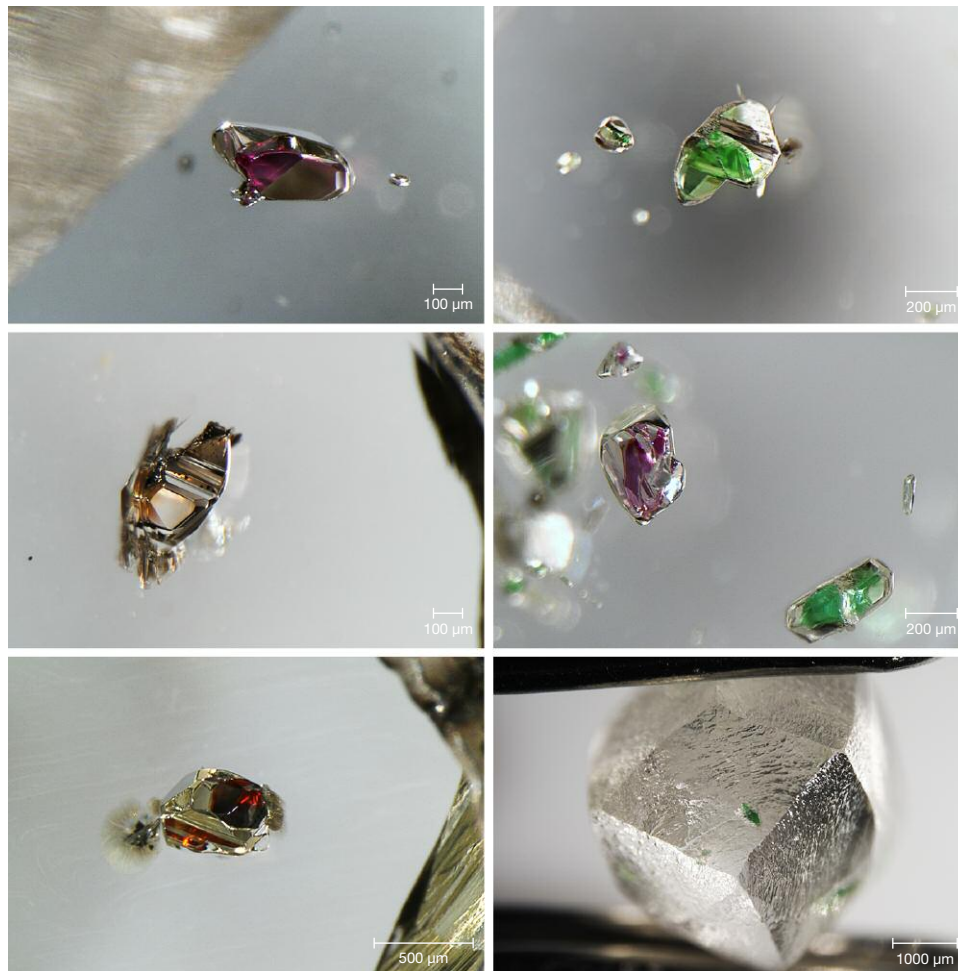


Figure B-1. The isochron diagram shown in this figure is a typical graphical way of expressing the calculation of absolute age. Minerals measured at present in the mass spectrometer fall on a line whose slope correlates directly with age.

sis and understanding the geological relationship between different minerals. For illustration purposes only, the "original" positions of the minerals are shown at the time they (re)crystallized (gray circles).



*Figure 1. Orange-red-purple garnet and green clinopyroxene minerals included in diamond can be broken out, dissolved, and analyzed for their samarium-neodymium (Sm-Nd) and rubidium-strontium (Rb-Sr) isotopes to yield ages for diamond formation. Minerals such as these provided the first-ever ages for diamonds, proving that diamonds are forever and much, much older than their host kimberlite (Richardson et al., 1984). Photos by Karen Smit.*

he was a graduate student working at the Massachusetts Institute of Technology in the early 1980s. Using samples from the Kimberley mines in South Africa (figure 1; Richardson et al., 1984), single grains of garnet or clinopyroxene from gem-quality monocrystalline diamonds needed to be grouped together with other identical grains—each broken from its own diamond host—for just one chemical analysis. Grain grouping had to be done to obtain sufficient Sm, Nd, Rb, and Sr to analyze. This technique was cutting-edge during its time, and the resulting study definitively showed that diamonds are much older than their host kimberlite. Some of the Kimberley diamonds were more than three billion years old, lending truth to the De Beers slogan “A diamond is forever.” Richardson and coauthors subsequently provided age constraints for many diamond suites from South Africa, Botswana, Australia, and Russia (e.g., Richardson, 1986; Richardson et al., 1990; Richardson and Harris, 1997) and demonstrated that there were multiple generations of diamond between one and two billion years ago in the southern African mantle.

In the mid-1990s, Professor Graham Pearson and Dr. Steven Shirey working at the Carnegie Institution for Sci-

ence miniaturized and modified the Re-Os analytical methods used on whole-rock samples so that single sulfide inclusions (typically between 2 and 10 µg but also larger, up to 30 µg; figure 2) could be analyzed rather than having to group all the inclusions together. Since the initial Re-Os study on Koffiefontein sulfide-bearing diamonds (Pearson et al., 1998), this technique has become the most widely used method to determine global diamond ages (e.g., Richardson et al., 2001; Westerlund et al., 2006; Aulbach et al., 2008; Richardson and Shirey, 2008; Aulbach et al., 2009; Smit et al., 2010; Wiggers de Vries et al., 2013; Smit et al., 2016; Aulbach et al., 2018).

Recent analytical advancements (namely even more sensitive and accurate detectors in mass spectrometry) have made it possible to measure Sm, Nd, Rb, and Sr at the extremely low concentrations in which they occur in single garnet and clinopyroxene inclusions. Researchers working with Professor Gareth Davies at the Vrije University in Amsterdam have now started using this technique to study diamond ages from Botswana and South Africa (Timmerman et al., 2017; Koornneef et al., 2017). This technique will certainly become as widely used as the Re-Os isotope system in sulfide inclusions, and for diamond suites where

both silicates and sulfides occur, the two techniques can be used in conjunction.

A new method emerging from work at the Australian National University that shows promise in this evolving field is the dating of fluid-rich fibrous diamonds using the U-Th/He isotope system. In this system, trapped microfluids contain sufficient  $^{235,238}\text{U}$  and  $^{232}\text{Th}$  that decay over time to  $^4\text{He}$  (Timmerman et al., 2019). Where mineral inclusions are used to date monocrystalline gem-quality diamonds, fluid inclusions can be used to date a separate suite of fibrous diamonds and give important constraints on whether they formed in association with kimberlite eruption.

### The Relationship of Mineral Inclusions To the Diamond

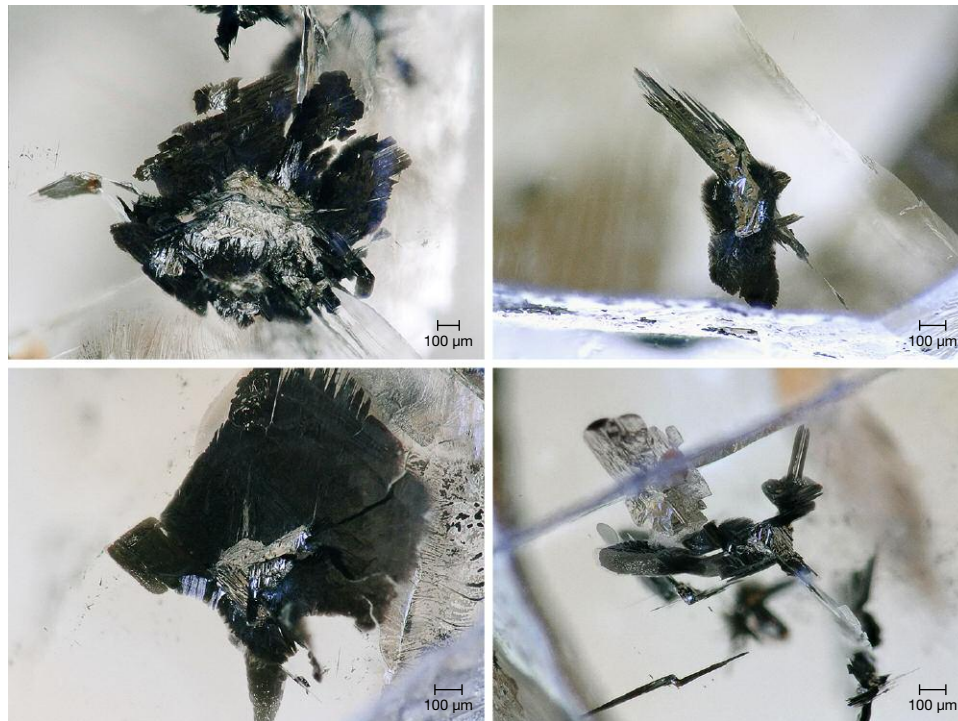
A long-standing requirement for diamond dating has been that the inclusions and the diamond co-crystallized from the same diamond-source fluid. In other words, that there is a syngenetic relationship between diamond and inclusion, as opposed to the diamond incorporating a preexisting mineral grain. The assumption of a syngenetic relationship has traditionally been based on textures observed in diamond inclusions that show that the diamond's cuboctahedral morphology has been imposed (e.g., Harris, 1968; Harris and Gurney, 1979). Epitaxial crystallographic relationships between inclusions and diamond (e.g., Mitchell and Giardini, 1953) can also be a key indicator of this syngenetic link.

However, there is now increasing evidence that inclusions in diamonds can also be preexisting rather than syngenetic (Thomassot et al., 2009; Smit et al., 2016; Milani et al., 2016; Nestola et al., 2017)—a fact that explains some long-standing compositional features of inclusions. In fact, some inclusions could have a syngenetic interface with diamond even if crystallographic evidence suggests the inclusion was preexisting (Agrosi et al., 2016).

In practice, a lack of syngenecity is not necessarily a problem for dating studies based on inclusions, since the isotopes in these older minerals are often re-equilibrated, or reset, at the time of diamond growth so that they still yield diamond formation ages (e.g., Smit et al., 2016; Smit et al., 2019). Even if isotopic equilibration did not take place, the errors on diamond ages are often sufficiently large (typically on the order of >100–200 Ma or sometimes greater; Westerlund et al., 2006; Aulbach et al., 2008, 2009; Smit et al., 2010) that if an inclusion was preexisting, it might still have formed within error of the determined age. While such large errors may seem horribly imprecise, they are more than adequate for diamond geology and in fact represent huge advances: separating out different diamond-forming events, relating the diamond-forming events to geological processes, and correlating diamond-forming events between different mines.

### What Have Diamond Ages Taught Us?

From isotope studies of inclusions in diamonds, we now know that diamonds have formed nearly throughout



*Figure 2. Sulfide inclusions in diamonds have a silver-gray appearance and are normally surrounded by graphitized (blackish) fractures. Analyses of rhenium-osmium isotopes in sulfide inclusions like these have become the most widely used method to determine diamond ages. Photos by Karen Smit/GIA.*

## BOX C: THE MASS SPECTROMETER



Figure C-1. The Thermo Scientific Triton Plus mass spectrometer used at the Carnegie Institution for Science. Photo by Steven Shirey.

The mass spectrometer is the final analytical stage for determining an absolute age. Mass spectrometers like the one shown in figure C-1 are found all over the world and used chiefly in the nuclear industry and geology.

The dried-down salt of the element of interest (e.g. lead, osmium, or strontium) is placed onto a metallic filament and heated to produce ions in the ion source at position 1. High voltage of around 10,000 volts accelerates the ions through the magnetic field created by the electromagnet at position 2. The magnetic field forces the ions into a curved trajectory; the lighter isotopes curve more (inside curve) and the heavier isotopes curve less (outside curve). In this way, the different isotopes can be separated (as shown by the diverging ion paths)

and detected individually at position 3. Although only two paths are shown for clarity, this mass spectrometer can produce and detect up to nine different isotope beams separately. Other mass spectrometers can produce and detect more than 16 isotope beams at one time!

Below the table surface is an electronics cabinet containing pumps, power supplies, circuit boards, an on-board data acquisition computer, and motor drives. Not shown is the instrument control computer that allows the scientist to control the progress of the measurement. Up to 21 samples can be loaded into the mass spectrometer at one time, and modern internet connectivity allows operation from any location.

Earth's history (figure 3). The oldest dated examples, the 3.5–3.3 billion-year-old Diavik and Ekati diamonds, were forming prior to the rise of oxygen in the earth's atmosphere (2.5 to 2.3 billion years ago). All diamonds that have

been dated so far were formed even before the dinosaurs went extinct 65 million years ago. We have no reason to believe that diamonds are not still forming right now deep in the earth's mantle. However, since they form so deep



Figure 3. Isotopic age dating of mineral inclusions shows us that diamonds have been forming through much of Earth's history. The oldest diamonds that have been studied were forming around a billion years before our atmosphere became oxygenated and life arose on Earth. This timeline is not a complete compilation of all diamond ages, but only shows some localities that illustrate the full range of ages. Many localities have multiple diamond formation events.

and do not survive the oxidizing conditions of common basaltic volcanism, we cannot access them until rare kimberlite eruptions bring them to the surface.

Aside from simply knowing a diamond's age for curiosity's sake, diamond ages have proven to be extremely valuable tools for geologists studying the deep earth. Diamond ages have told us that diamonds are much, much older than kimberlites. They did not crystallize in the kimberlite but are only passengers riding a volcanic eruption to the surface.

Diamond ages have changed our thinking about the association of diamonds with ancient continental mantle keels. Contrary to traditional thinking, diamond ages have shown that they can also form in active tectonic regions around cratons. Incorporation of such areas has expanded di-

among exploration targets and will contribute to finding new diamondiferous kimberlites.

Diamond ages have also allowed us to link their formation to known plate tectonic processes. We now know that subduction of hydrated oceanic slabs is how most of these diamond-forming fluids are supplied into the deep earth. Diamond ages have placed important time constraints on the recycling of fluid mobile compounds and elements such as water, carbon, nitrogen, boron, and sulfur into the deep earth. There is no other way to trace these so deeply and as far back in time.

Through age determinations, we have learned that diamonds are not only *forever* but they are *forever revealing* new secrets about our dynamic planet.

## REFERENCES

- Agrosi G., Nestola F., Tempesta G., Bruno M., Scandale E., Harris J.W. (2016) X-ray topographic study of a diamond from Udachnaya: Implications for the genetic nature of inclusions. *Lithos*, Vols. 248-251, pp. 153-159, <http://dx.doi.org/10.1016/j.lithos.2016.01.028>
- Aulbach S., Shirey S.B., Stachel T., Creighton S., Muehlenbachs K., Harris J.W. (2008) Diamond formation episodes at the southern margin of the Kaapvaal Craton: Re-Os systematics of sulfide inclusions from the Jagersfontein mine. *Contributions to Mineralogy and Petrology*, Vol. 157, No. 4, pp. 525-540, <http://dx.doi.org/10.1007/s00410-008-0350-9>
- Aulbach S., Stachel T., Creaser R.A., Heaman L.M., Shirey S.B., Muehlenbachs K., Eichenberg D., Harris J.W. (2009) Sulphide survival and diamond genesis during formation and evolution of Archaean subcontinental lithosphere: A comparison between the Slave and Kaapvaal cratons. *Lithos*, Vol. 112S, Proceedings of the 9th International Kimberlite Conference, pp. 747-757, <http://dx.doi.org/10.1016/j.lithos.2009.03.048>
- Aulbach S., Creaser R.A., Stachel T., Heaman L.M., Chinn I.L., Kong J. (2018) Diamond ages from Victor (Superior Craton): Intra-mantle cycling of volatiles (C, N, S) during supercontinent reorganisation. *Earth and Planetary Science Letters*, Vol. 490, pp. 77-87, <http://dx.doi.org/10.1016/j.epsl.2018.03.016>
- Breeding C.M., Eaton-Magaña S., Shigley J.E. (2018) Natural-color green diamonds: A beautiful conundrum. *G&G*, Vol. 54, No. 1, pp. 2-27, <http://dx.doi.org/10.5741/GEMS.54.1.2>
- Harris J.W. (1968) The recognition of diamond inclusions. Part I: Syngenetic inclusions. *Industrial Diamond Review*, Vol. 28, pp. 402-410.
- Harris J.W., Gurney J.J. (1979) Inclusions in diamond. In J. Field,

- Ed., *The Properties of Diamond*. Academic Press, New York, pp. 555–591.
- Koornneef J.M., Gress M.U., Chinn I.L., Jelsma H.A., Harris J.W., Davies G.R. (2017) Archaean and Proterozoic diamond growth from contrasting styles of large-scale magmatism. *Nature Communications*, Vol. 8, Article No. 648, <http://dx.doi.org/10.1038/s41467-017-00564-x>
- Milani S., Nestola F., Angel R.J., Nimis P., Harris J.W. (2016) Crystallographic orientations of olivine inclusions in diamonds. *Lithos*, Vol. 265, pp. 312–316, <http://dx.doi.org/10.1016/j.lithos.2016.06.010>
- Mitchell R.S., Giardini A.A. (1953) Oriented olivine inclusions in diamond. *American Mineralogist*, Vol. 38, No. 1-2, pp. 136–138.
- Nestola F., Jung H., Taylor L.A. (2017) Mineral inclusions in diamonds may be synchronous but not syngenetic. *Nature Communications*, Vol. 8, Article No. 14168, <http://dx.doi.org/10.1038/ncomms14168>
- Pearson D.G., Shirey S.B., Harris J.W., Carlson R.W. (1998) Sulphide inclusions in diamonds from the Koffiefontein kimberlite, S Africa: Constraints on diamond ages and mantle Re-Os systematics. *Earth and Planetary Science Letters*, Vol. 160, No. 3, pp. 311–326, [http://dx.doi.org/10.1016/S0012-821X\(98\)00092-2](http://dx.doi.org/10.1016/S0012-821X(98)00092-2)
- Richardson S.H. (1986) Latter-day origin of diamonds of eclogitic paragenesis. *Nature*, Vol. 322, No. 6080, pp. 623–626, <http://dx.doi.org/10.1038/322623a0>
- Richardson S.H., Harris J.W. (1997) Antiquity of peridotitic diamonds from the Siberian craton. *Earth and Planetary Science Letters*, Vol. 151, No. 3-4, pp. 271–277, [http://dx.doi.org/10.1016/S0012-821X\(97\)81853-5](http://dx.doi.org/10.1016/S0012-821X(97)81853-5)
- Richardson S.H., Shirey S.B. (2008) Continental mantle signature of Bushveld magmas and coeval diamonds. *Nature*, Vol. 453, No. 7197, pp. 910–913, <http://dx.doi.org/10.1038/nature07073>
- Richardson S.H., Gurney J.J., Erlank A.J., Harris J.W. (1984) Origin of diamonds in old enriched mantle. *Nature*, Vol. 310, No. 5974, pp. 198–202, <http://dx.doi.org/10.1038/310198a0>
- Richardson S.H., Erlank A.J., Harris J.W., Hart S.R. (1990) Eclogitic diamonds of Proterozoic age from Cretaceous kimberlites. *Nature*, Vol. 346, No. 6279, pp. 54–56, <http://dx.doi.org/10.1038/346054a0>
- Richardson S.H., Shirey S.B., Harris J.W., Carlson R.W. (2001) Archean subduction recorded by Re-Os isotopes in eclogitic sulfide inclusions in Kimberley diamonds. *Earth and Planetary Science Letters*, Vol. 191, No. 3-4, pp. 257–266, [http://dx.doi.org/10.1016/S0012-821X\(01\)00419-8](http://dx.doi.org/10.1016/S0012-821X(01)00419-8)
- Smit K.V., Shirey S.B., Richardson S.H., le Roex A.P., Gurney J.J. (2010) Re-Os isotopic composition of peridotitic sulphide inclusions in diamonds from Ellendale, Australia: Age constraints on Kimberley cratonic lithosphere. *Geochimica et Cosmochimica Acta*, Vol. 74, No. 11, pp. 3292–3306, <http://dx.doi.org/10.1016/j.gca.2010.03.001>
- Smit K.V., Shirey S.B., Wang W. (2016) Type Ib diamond formation and preservation in the West African lithospheric mantle: Re-Os age constraints from sulphide inclusions in Zimmi diamonds. *Precambrian Research*, Vol. 286, pp. 152–166, <http://dx.doi.org/10.1016/j.precamres.2016.09.022>
- Smit K.V., Shirey S.B., Hauri E.H., Stern R.A. (2019) Sulfur isotopes in diamonds reveal differences in continent construction. *Science*, Vol. 364, No. 6438, pp. 383–385.
- Thomassot E., Cartigny P., Harris J.W., Lorand J.P., Rollion-Bard C., Chaussidon M. (2009) Metasomatic diamond growth: A multi-isotope study ( $\delta^{13}\text{C}$ ,  $\delta^{15}\text{N}$ ,  $\delta^{33}\text{S}$ ,  $\delta^{34}\text{S}$ ) of sulphide inclusions and their host diamonds from Jwaneng (Botswana). *Earth and Planetary Science Letters*, Vol. 282, No. 1-4, pp. 79–90, <http://dx.doi.org/10.1016/j.epsl.2009.03.001>
- Timmerman S., Koornneef J.M., Chinn I.L., Davies G.R. (2017) Dated eclogitic diamond growth zones reveal variable recycling of crustal carbon through time. *Earth and Planetary Science Letters*, Vol. 463, pp. 178–188, <http://dx.doi.org/10.1016/j.epsl.2017.02.001>
- Timmerman S., Yeow H., Honda M., Howell D., Jaques A.L., Krebs M.Y., Woodland S., Pearson D.G., Avila J.N., Ireland T.R. (2019) U-Th/He systematics of fluid-rich ‘fibrous’ diamonds. *Chemical Geology*, in press.
- Westerlund K., Shirey S., Richardson S., Carlson R., Gurney J., Harris J. (2006) A subduction wedge origin for Paleoproterozoic peridotitic diamonds and harzburgites from the Panda kimberlite, Slave craton: evidence from Re-Os isotope systematics. *Contributions to Mineralogy and Petrology*, Vol. 152, No. 3, pp. 275–294, <http://dx.doi.org/10.1007/s00410-006-0101-8>
- Wiggers de Vries D.F., Bulanova G.P., de Corte K., Pearson D.G., Craven J.A., Davies G.R. (2013) Micron-scale coupled carbon isotope and nitrogen abundance variations in diamonds: Evidence for episodic diamond formation beneath the Siberian Craton. *Geochimica et Cosmochimica Acta*, Vol. 100, pp. 176–199, <http://dx.doi.org/10.1016/j.gca.2012.08.034>

For online access to all issues of GEMS & GEMOLOGY from 1934 to the present, visit:

[gia.edu/gems-gemology](http://gia.edu/gems-gemology)







G&G

# Micro-World

**Editor**

Nathan Renfro

**Contributing Editors**

Elise A. Skalwold and John I. Koivula

## Condor Agate from Argentina

“Condor” agates from the Mendoza region of Argentina are sought after by collectors for their vibrant colors and sharp banding. This variety of agate is named after the impressive Andean condor, which calls this mountainous region home. One such stone (figure 1) was recently examined for photomicrography. It displayed intense orange and yellow bands, likely colored by fine hematitic and limonitic concentrations. The banding ended abruptly at an opaque gray mineral interface that demarcated the transparent core. Contained within this lake were ghostly oolitic concretions, some of which enclosed their own hematite particles. Chalcedony is available in a dizzying selection of varieties and is a constant source of inspiring specimens.

*Tyler Smith  
GIA, New York*

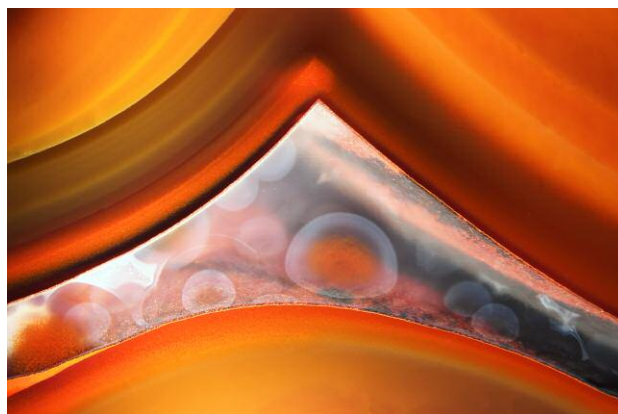


Figure 1. Core of a “condor” agate containing faint hemispheres of fibrous, white chalcedony. Photomicrograph by Tyler Smith; field of view 14.52 mm.

## “Double Bubble” Multiphase Inclusion in Beryl

Beryl often hosts multiphase inclusions consisting of all possible combinations of solid, liquid, or gas inclusions. These remnants of the growth environment become trapped within negative crystals during formation. The fluid is trapped as a homogenous liquid that separates into

component phases during cooling. Jagged three-phase inclusions commonly found in Colombian emeralds are perhaps the most well-known multiphase inclusions in beryl.

A 64.10 ct pale green rough beryl submitted by L. Allen Brown (All That Glitters, Methuen, Massachusetts) contained a plethora of prismatic three-phase negative crystals with a notable suite of gas bubbles, several species of extremely small daughter crystals, and an aqueous solution (figure 2). At room temperature, the gas phases were out of equilibrium with each other, which gave rise to a “double bubble” nested appearance: a gas bubble within a second, larger gas bubble. Over the course of about a minute, the gentle heat of the microscope well light warmed the smaller gas bubble enough to completely homogenize with the larger bubble so that only one bubble remained (figure 3).

*Hollie McBride  
GIA, Carlsbad*

*About the banner: An agate from Minas Gerais, Brazil, contains an escape-tube structure that has been polished through to reveal a yellow chalcedony interior. Photomicrograph by Nathan Renfro; field of view 23.99 mm. Courtesy of the John Koivula Inclusion Collection.*

*Editors' note: Interested contributors should contact Nathan Renfro at nrenfro@gia.edu and Jennifer-Lynn Archuleta at jennifer.archuleta@gia.edu for submission information.*

GEMS & GEMOLOGY, VOL. 55, No. 1, pp. 110–117.

© 2019 Gemological Institute of America



Figure 2. A 64.10 ct pale green rough beryl crystal containing noteworthy multiphase inclusions. Photo by Robison McMurtry.

### Native Copper Inclusions in Indonesian Purple Chalcedony

As a gem material, chalcedony can contain an array of interesting structures and mineral inclusions. This was particularly evident in one example recently examined by the authors. Purchased by author SC from gemstone dealer John Garsow (John E. Garsow Gems & Minerals, Murrieta, California), this vibrant purple chalcedony reportedly from Indonesia contained several small clusters of what appeared to be native copper (figure 4). This suspicion was confirmed by energy-dispersive X-ray fluorescence (EDXRF) testing. While the origin of the purple color is not clear, it certainly does not appear to be related to copper. In purple areas that were devoid of copper inclusions, no copper was detected by EDXRF. We did detect iron, which may be related to the purple color.

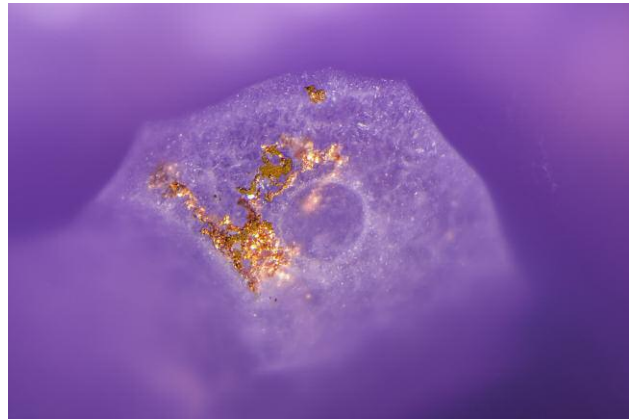


Figure 4. This purple chalcedony from Indonesia contained interesting inclusions of native copper. Photomicrograph by Nathan Renfro; field of view 5.74 mm.

While native copper inclusions have been previously reported in chalcedony (B.M. Laurs and N.D. Renfro, "Chrysocolla chalcedony with native copper inclusions," *Journal of Gemmology*, Vol. 36, No. 2, 2018, p. 92), this is the first time the authors have examined purple chalcedony from Indonesia with native copper inclusions.

Nathan Renfro  
GIA, Carlsbad

Stephen Challener  
Raleigh, North Carolina

### Grandierite Inclusions in Sapphires

Recently the authors independently encountered an inclusion that has not been previously reported in sapphire. Both stones contained colorless crystals that were identified by Raman analysis as the mineral grandierite. The sapphire

Figure 3. Photo series of a prismatic multiphase inclusion displaying a "double bubble" of gas within gas at room temperature (left). The smaller bubble shrinks by about half after approximately 45 seconds of exposure to the microscope well light (center) and completely homogenizes after about a minute (right). Photomicrographs by Hollie McBride; field of view 2.34 mm.



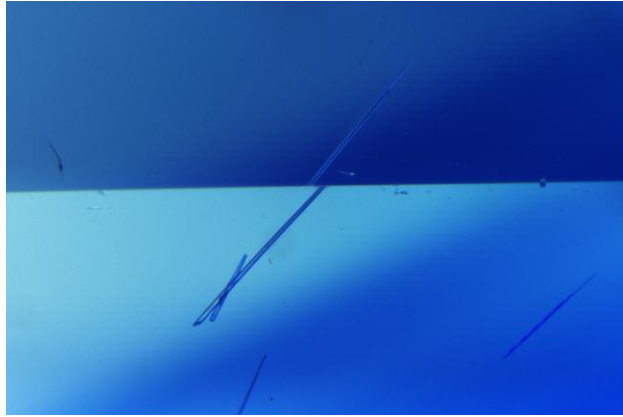


Figure 5. Lath-like mineral inclusions of grandidierite were seen in this sapphire at GIA's Carlsbad laboratory. Photomicrograph by Nathan Renfro; field of view 2.61 mm.

examined by author MH in Carlsbad, California, contained colorless lath-like inclusions (figure 5). The sapphire examined by author EBH in Bangkok contained a colorless crystal that reached the surface of the sapphire host and displayed a duller luster in reflected light, and birefringent interference colors when examined using cross-polarized light (figure 6). Both observations are consistent with what one would expect for grandidierite.

Grandidierite, named after French naturalist Alfred Grandidier (1836–1921), is an extremely rare orthorhombic Mg-Fe aluminous borosilicate with the formula  $(\text{Mg,Fe})\text{Al}_3(\text{BO}_3)(\text{SiO}_4)\text{O}_2$ . The mineral is described as bluish green to greenish blue; the blue color increases with Fe content. It is transparent to translucent with a pale yellow to colorless, greenish blue, and blue trichroism. Since its discovery, grandidierite has been found as a rare accessory mineral in aluminous boron-rich pegmatite; in aplite, gneiss, and crystalline rock associated with charnockite;

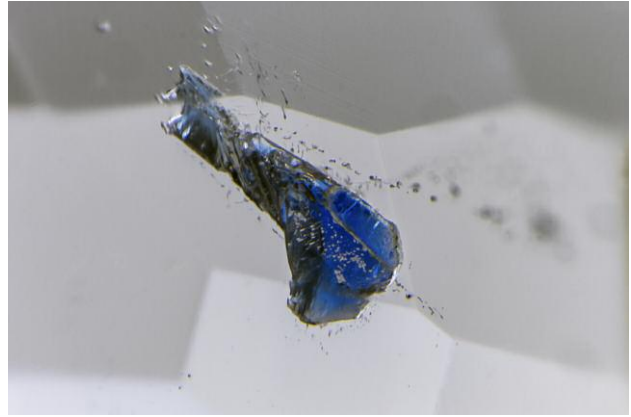


Figure 7. This light gray spinel from Mogok, Myanmar, contains a vibrant blue inclusion of lazurite. Photomicrograph by Nathan Renfro; field of view 1.59 mm. Courtesy of Mark Smith, Thai Lanka Trading Ltd.

and in rock subjected to local high-temperature, low-pressure metamorphism (contact aureoles and xenoliths). To the authors' knowledge, these are the first observations of grandidierite as an inclusion in sapphire.

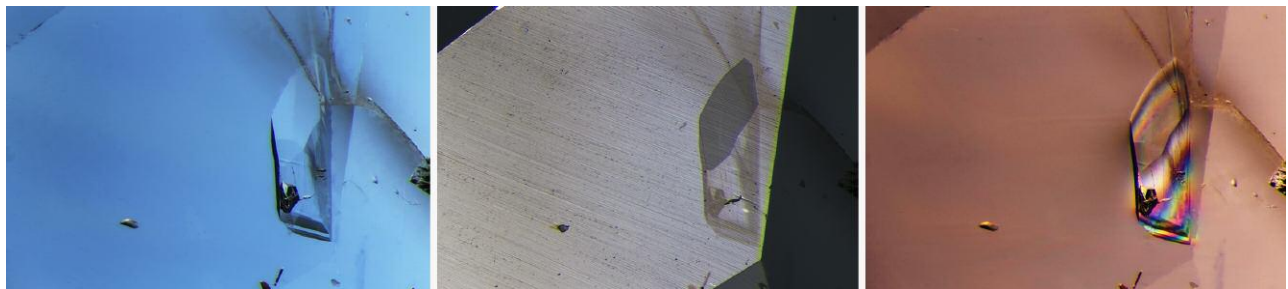
Maxwell Hain  
GIA, Carlsbad

E. Billie Hughes  
Lotus Gemology, Bangkok

### Lazurite in Spinel

Spinel is often inclusion free but occasionally showcases unusual inclusions. This was the case with a 1.02 ct light gray Burmese spinel from Mogok, courtesy of Mark Smith (Thai Lanka Trading Ltd., Bangkok), that was recently examined by the authors. A striking vibrant blue inclusion reached the surface of the pavilion, making Raman analysis straightforward (figure 7). The identity of the blue in-

Figure 6. A colorless grandidierite crystal was seen in a sapphire examined by author EBH at Lotus Gemology in Bangkok (left). In reflected light, the grandidierite inclusion showed a duller luster than the sapphire host (center) and cross-polarized light revealed birefringent interference colors (right). Photomicrographs by E. Billie Hughes; field of view 1.7 mm.



clusion was confirmed to be lazurite. The mineral has previously been found as an inclusion in Burmese ruby (Spring 2012 Lab Notes, pp. 51–52), but this is the first instance of a lazurite inclusion in spinel that we are aware of.

Nathan Renfro  
John I. Koivula  
GIA, Carlsbad

### Fossil Insect in Opal

The authors recently examined a most unusual opal. The mottled brown polished free-form stone appeared to contain a trapped insect, which one might expect to find in fossil amber or copal (figure 8). However, noticeable play-of-color made it obvious that the host material for the insect was precious opal, which was further confirmed by standard gemological testing. Its refractive index of 1.45, weak white long-wave fluorescence, and Raman spectrum were all consistent with natural opal. No microscopic evidence of any type of treatment was detected.

Play-of-color was strongest in the darker brown portions toward the base but also appeared in shallow fissures around the insect's appendages. The insect broke the surface, resulting in some of its legs and underside being cut through during polishing (figure 9, left). An apparent set of mouth parts was clearly observed, but the position of some pits on the surface partially obscured the view. Fine hairs, or setae, were found along the legs (figure 9, center). The setae closest to the surface were surrounded by a grainy white material that resembled desiccated opal. A slightly contorted abdomen was observed alongside a pair of rear legs (figure 9, right).

Precious opal formation is not fully understood, but several mechanisms have been proposed (B.Y. Lynne et al., "Diagenesis of 1900-year-old siliceous sinter (opal-A to quartz) at Opal Mound, Roosevelt Hot Springs, Utah, U.S.A.," *Sedimentary Geology*, Vol. 179, Nos. 3-4, 2005, pp. 249–278; B. Pewklian et al., "The formation of pre-

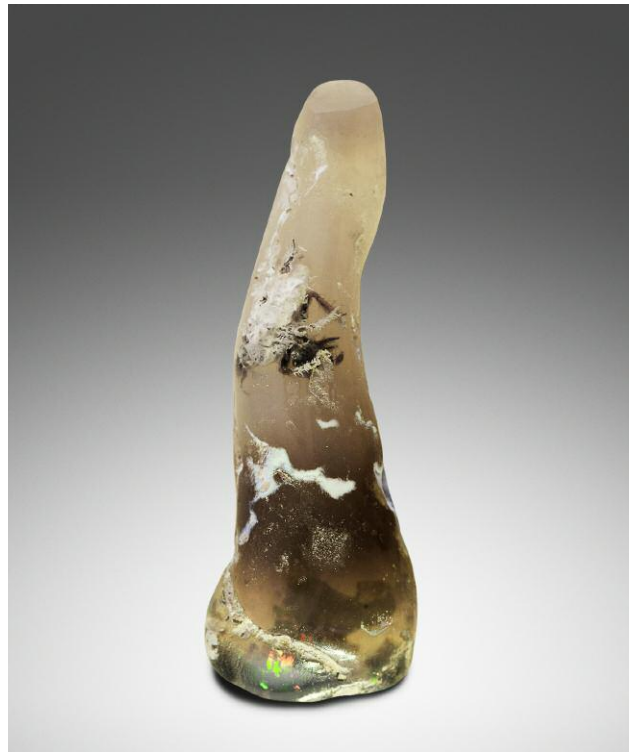


Figure 8. A polished free-form opal encapsulating an insect. Play-of-color is shown at the bottom. Photo by Jian Xin (Jae) Liao. Stone courtesy of Brian Berger.

cius opal: Clues from the opalization of bone," *The Canadian Mineralogist*, Vol. 46, No. 1, 2008, pp. 139–149). One possible explanation is that low-pH groundwater percolated through the soil, accruing colloidal silica into a silica-rich fluid. This gel then underwent polymerization within cavities and voids to form microspheres of opal-A. One could imagine a scenario where the insect was entrapped by an intrusion of this gel, rapidly enveloping the insect and allowing it to avoid decomposition.

Figure 9. An unidentified insect encapsulated in opal. Left: A head and mouth are visible along with several legs covered in fine hair-like structures, or setae. The leg in the foreground was partially cut through during polishing. Field of view 6.39 mm. Center: Setae branching from an appendage; field of view 2.57 mm. Right: The thorax of the insect is visible, though partially contorted. A grainy white layer coats and partially obscures the surface-reaching appendages and abdomen. Field of view 11.50 mm. Photomicrographs by Nathan Renfro (left and center) and Tyler Smith (right).



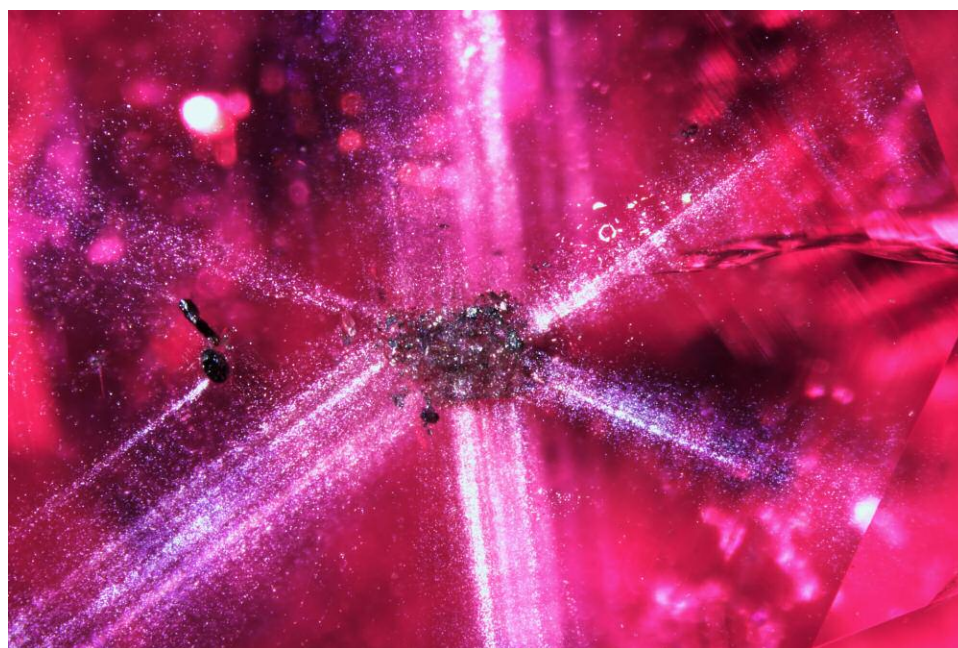


Figure 10. Each leg of the trapiche-like structure in this ruby from the Batakundi mine in Kashmir is aligned perpendicular to hexagonal growth. The center of the star consists of a hexagonal group of colorless feldspar crystals and black graphite platelets. Black rutile crystals with associated comet tails are seen near the core of the trapiche-like pattern. Photomicrograph by Patcharee Wongrawang; field of view 4.80 mm.

While fossilized organic matter in the form of roots and twigs has been found in precious opal—most notably in Virgin Valley, Nevada, and Wollo, Ethiopia—this is the first confirmed case of an opal-encased insect that the authors have examined. We were not able to find any other recorded findings, although there have been rumors of them. It is our hope that more specimens are discovered so we can more thoroughly study these exceptional rarities.

*Tyler Smith and Nathan Renfro*

### Trapiche-Like Ruby from the Batakundi Mine, Kashmir

Recently, the author examined a 5.26 ct faceted transparent oval ruby that showed a well-formed fixed six-rayed pattern under the table of the stone. Chemical analysis and gemological observation of internal features determined the origin of this stone to be the Batakundi mining area of Kashmir.

The six rays were oriented perpendicular to the sides of the hexagonal growth structure (figure 10). Each arm consisted of numerous minute particles mixed with needle-like inclusions and small thin films. The center of the star contained a group of colorless and black mineral inclusions that were identified by Raman spectroscopy as feldspar and graphite. Near the core, two black crystals with high luster were identified by Raman spectroscopy as rutile. They were also associated with a string of fine particles spreading out to form a comet tail pattern.

The pattern of this ruby from the Batakundi mine resembles that of a trapiche-type sapphire from Tasmania (Winter 2016 GNI, pp. 430–431). Trapiche-like minerals are quite different from true trapiche rubies, which have six arms that run from a core to the six corners of the hexago-

nal growth structure and show clear boundaries of six crystallographic sectors. The most renowned of the true trapiche ruby can be found in certain areas such as Mong Hsu, Myanmar (G. Giuliani and I. Pignatelli, “Trapiche’ vs ‘trapiche-like’ textures in minerals,” *InColor*, Vol. 31, 2016, pp. 45–46).

Although trapiche-like corundum specimens are not unheard of, it is unusual to find them well developed in high-quality ruby. This trapiche-like ruby from the Batakundi area shows a beautiful inclusion scene of a fixed six-rayed star standing out against the pleasing bodycolor and transparency.

*Patcharee Wongrawang  
GIA, Bangkok*

### Sapphire Inclusion with Rutile “Silk” in a Burmese Star Sapphire

GIA’s Hong Kong laboratory recently examined a remarkable sapphire inclusion inside a Burmese star sapphire. Possessing the same refractive index as its host, the sapphire guest displays extremely low relief and is nearly invisible under transmitted light. Nevertheless, its outline became distinctive under cross-polarized illumination, showing strong interference colors (figure 11, left). Closer examination using fiber-optic illumination revealed a group of oriented rutile “silk” in this sapphire inclusion (figure 11, right). Although exsolved rutile needles are a common inclusion in Burmese sapphire, it is interesting to see two sets of dense silk exsolved from both the star sapphire host and a protogenetic sapphire inclusion, each aligned with the basal plane of its own host.

*Xiaodan Jia and Mei Mei Sit  
GIA, Hong Kong*

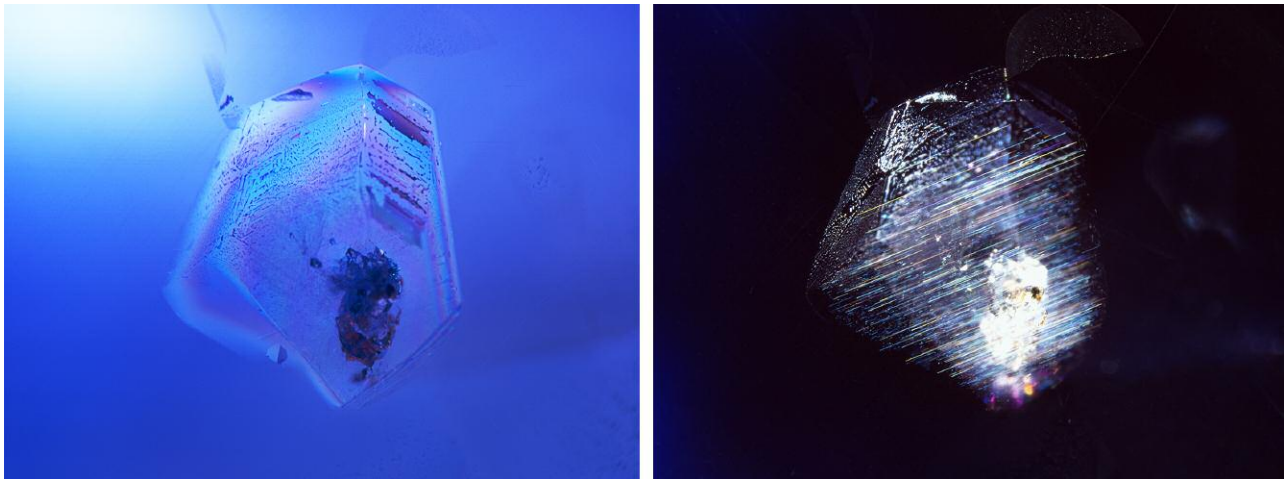


Figure 11. A guest crystal located at the back of the star sapphire stands out under cross-polarized illumination, exhibiting concentric rings of interference colors when viewed along its optic axis (left). Examination with fiber-optic light revealed a group of needle-like rutile inclusions oriented along the basal plane of the sapphire inclusion (right). Photomicrographs by Xiaodan Jia; field of view 3.83 mm.

### Star-Like Growth in Natural Yellow Sapphire

Internal growth structures (commonly referred to as graining) observed in transparent gemstones often reflect a gem's crystallography. Graining can assist in distinguishing natural from synthetic gem materials. For example, a synthetic flame-fusion corundum commonly shows curved growth lines, while natural and flux-grown corundum usually shows straight, angular, or hexagonal growth patterns.

Recently, the author examined an 8.01 ct faceted yellow

stone that had gemological properties consistent with sapphire. The most distinctive feature found in this stone was internal graining displaying as six-rayed stars (figure 12). It is interesting to note that the angle of each ray was 60 degrees, consistent with corundum's trigonal crystal structure. This is the first time the author has encountered a star-like graining pattern in natural sapphire.

Ungkhana Atikarnsakul  
GIA, Bangkok

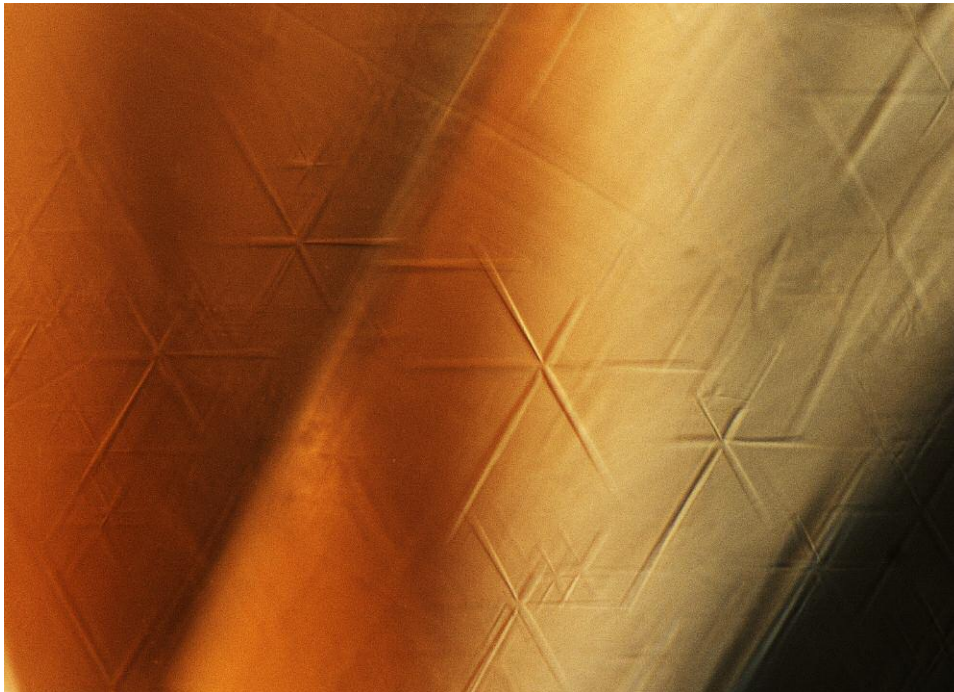


Figure 12. A group of six-rayed stars in a faceted yellow sapphire. Photomicrograph by Ungkhana Atikarnsakul; field of view 1.5 mm.



*Figure 13. Numerous bright yellow crystals dominate the interior of this 74.31 ct barite cluster from Nevada. Photo by Nathan Renfro.*



### Quarterly Crystal: Orpiment in Barite

The 74.31 ct crystal cluster of transparent to translucent colorless barite columns shown in figure 13 measures  $37.89 \times 20.83 \times 15.27$  mm. It plays host to numerous small yellow crystals and radial sprays, which together give the cluster a light yellow color. The barite specimen is from the Regent mine in the Rawhide District of Mineral County, Nevada. The Regent mine was known to produce barite crystals with yellow orpiment inclusions in the mid-1990s. The pure yellow bodycolor of these numerous inclusions suggested they might be orpiment. Laser Raman microspectrometry was able to confirm our suspicions. Focused EDXRF analysis was used in an attempt to examine the chemical makeup of the inclusions, since orpiment contains arsenic as a main constituent. The EDXRF analysis showed the presence of arsenic. Based on chemistry, we determined that the yellow inclusions shown in figure 14 are indeed the arsenic sulfide mineral orpiment.

*John I. Koivula*

*Figure 14. A combination of Raman and EDXRF analysis identified the inclusions as orpiment, a yellow arsenic sulfide. Photomicrograph by Nathan Renfro; field of view 3.83 mm.*

For online access to all issues of GEMS & GEMOLOGY from 1934 to the present, visit:

[gia.edu/gems-gemology](http://gia.edu/gems-gemology)







# Gem News International

## Contributing Editors

Emmanuel Fritsch, *University of Nantes, CNRS, Team 6502, Institut des Matériaux Jean Rouxel (IMN), Nantes, France* (fritsch@cnsr-immn.fr)

Gagan Choudhary, *Gem Testing Laboratory, Jaipur, India* (gagan@gjepcindia.com)

Christopher M. Breeding, *GIA, Carlsbad* (christopher.breeding@gia.edu)

## TUCSON 2019

The 2019 gem shows came to Tucson with a wealth of material, both new and old, as eager buyers descended on exhibitors to take in the latest trends. While traffic was not as heavy as in recent years, several vendors noticed an influx of young people looking for natural, untreated gemstones. Spectacular color in gems and stunning jewelry designs were on view, while many pointed to sustainable and ethical practices as a major consideration in their colored gemstone and jewelry purchases.

The Asian market has slowed, according to Edward Boehm of RareSource (Chattanooga, Tennessee), and as a result, gems that have been popular in Asia, particularly China, are starting to gain traction in the United States. Boehm indicated that the growth of the Asian market is still driving production in African countries, particularly Nigeria, and Americans are the primary consumer of this increased production. Improving exchange rates have also worked in the American market's favor. Dave Bindra (B&B Fine Gems, Los Angeles) said that while higher-end gemstones are still difficult to come by, they are as much in demand as ever. Commercial-grade gems, Bindra noted, have become more accessible. Like Boehm, he attributes this in large part to activity in the Chinese market in recent years. Shahin Aboosalih of SR Trading's Hong Kong office talked to us about material that remains popular in the Chinese and Japanese markets (pp. 136–138).

*Editors' note: Interested contributors should send information and illustrations to Stuart Overlin at [soverlin@gia.edu](mailto:soverlin@gia.edu) or GIA, The Robert Mouawad Campus, 5345 Armada Drive, Carlsbad, CA 92008.*

GEMS & GEMOLOGY, VOL. 55, NO. 1, pp. 118–160.

© 2019 Gemological Institute of America

Opal, particularly black opal, has seen a resurgence among high-end jewelers. Boehm believes there could be a growing appreciation for the gem due to the discovery of opal in Ethiopia, which has brought opal to different price points and different audiences in the past decade. Rod Griffin (Rod Griffin Boulder Opals) discussed his experiences in Australian opal mining and the new technology he is using to exploit deposits once thought to be depleted (pp. 122–123).

Color, of course, continues to reign, and dealers are seeing what Boehm called “an increased appreciation for the unusual.” Beyond the classic “Big Three,” vendors stocked gemstones such as sphene, grandidierite, and various colors of sapphire. Color-change stones seen in previous shows, such as pyrope garnet and alexandrites, were also on display and drawing new attention. Cutters, he noted, are making strides in recognizing and using to different effect specific phenomena in gemstones, such as the trichroism of tanzanite. Spinel remains the most popular “new” gem, according to Boehm, especially in nontraditional colors such as lavender and violet, which would have been cut too dark (or not at all) in the past. Gray spinel in particular made a splash at this year's show, with several exhibitors stocking the material in a variety of cuts.

Brian Cook of Nature's Geometry (Tucson) noticed a cross-pollination between the mineral and jewelry industries, with more designers and jewelers using raw euhedral stones to create unique looks. He also noted that several new mineral shows, developed out of dealers' collectives rather than sponsored by one promoter, have come to the city and seem to be here to stay. The popularity of the Granada Gallery (pp. 128–129), which prides itself on its dedication to “fine natural design,” is one such indicator.

American gemstones were also in heavy rotation at the shows. Eric Braunwart of Columbia Gem House, who has long stocked American production in his inventory, said that sales of these products were good. Designer Derek Katzenbach discussed his use of American gemstones such as Maine tourmaline (pp. 143–144). And among the material seen was Montana sapphire, nephrite from Washington State, Oregon sunstone, and hyalite opals from Oregon.



Buyers browse the selection of goods available at the 2019 AGTA GemFair in Tucson. Photo courtesy of AGTA.

Bindra noted that many of his company's rare gems came out of the ground 20–30 years ago, and that he relies heavily on the secondary market to procure such material. In this way, he is able to provide his clients with the high-end material they have come to expect. This sentiment was echoed by Jared Holstein of Perpetuum Jewels (pp. 146–147), a wholesaler working with antique diamonds and colored stones in historical cuts for the bridal market. Holstein also finds the secondary market to be a good way to source gemstones in an ethical and environmentally sustainable fashion.

Responsibly sourced material continues to be heavily sought after. Braunwart said this might have been his most successful show in his 41 years at Tucson (pp. 135–136). He credits this in large part to his commitment to providing fair trade, responsibly sourced gemstones. Susi Smither,

who founded The Rock Hound specifically to create an ethical jewelry line (pp. 149–150), delighted in showing us her Molten Muzo collection, which used responsibly sourced Colombian emeralds and recycled gold. And gem dealer and jewelry designer Roger Dery told us about Gem Legacy, the nonprofit he founded to benefit East African mining communities (pp. 147–148).

We hope you enjoy our coverage of the 2019 Tucson gem shows!

*Jennifer-Lynn Archuleta  
GIA, Carlsbad*

*The following contributed to this report: Erin Hogarth, Tao Hsu, Jonathan Muyal, Lisa Neely, Aaron Palke, Duncan Pay, Albert Salvato, Kevin Schumacher, Jennifer Stone-Sundberg, Wim Vertriest, and Robert Weldon.*

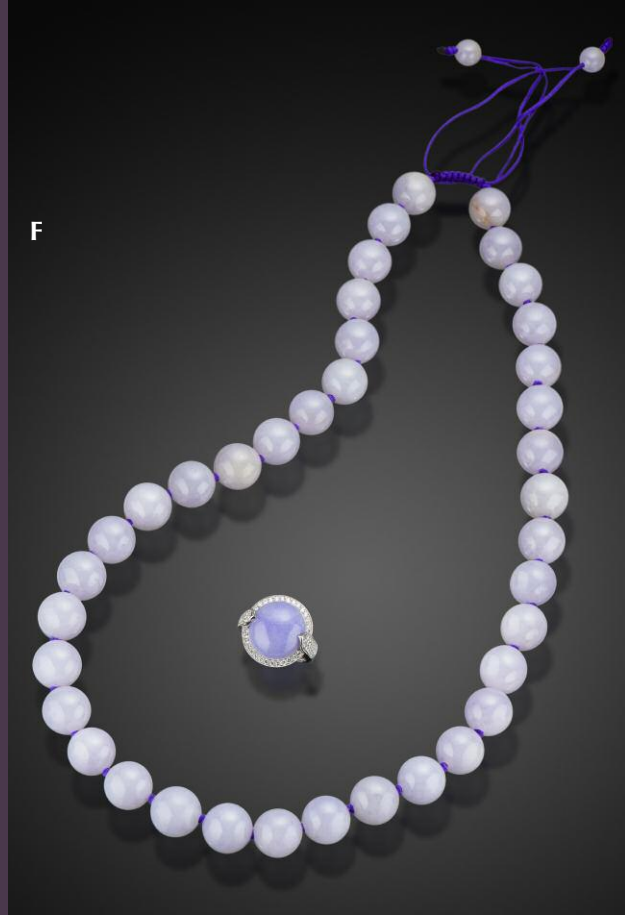
*Left: Opals like “The Chief,” a 14.41 ct Australian black specimen, were in demand this year. Photo by Kevin Schumacher, courtesy of 100% Natural Ltd. Center: Fancy-color sapphires, including this 50.08 ct color-change gem, were also popular. Photo by Robert Weldon/GIA, courtesy of Edward Boehm. Right: The secondary market is an excellent source for material, such as this 115.13 ct golden sapphire. Photo by Kevin Schumacher, courtesy of B&B Fine Gems.*



# 2019 Tucson Photo Gallery



A: 8.50 ct black opal and diamond necklace. Photo by Emily Lane, courtesy of Lightning Ridge Collection by John Ford. B: Gold butterfly with Tanzanian sapphires, spinels, and garnets, accompanied by loose purple spinel, pink spinel, and yellow sapphire. Photo by Robert Weldon/GIA, courtesy of Akiva Gil Co. C: 8.61 ct unheated purple sapphire and diamond ring. Photo by Emily Lane, courtesy of Jardin Jewels by Beacab. D: 33.36 ct Colombian emerald. Photo by Kevin Schumacher, courtesy of Karin Tremonti. E: Victorian spider pin with ruby, old mine cut diamonds, and natural pearl. Photo by Robert Weldon/GIA, courtesy of Pioneer Gems.



F



G



H



I



J

F: Burmese lavender jadeite cabochon ring and bead strand. Photo by Emily Lane, courtesy of Jade by Nikolai. G: Burmese white jadeite baby fu lion cuff. Photo by Emily Lane, courtesy of Jade by Nikolai. H: 661 ct unheated aquamarine and diamond necklace. Photo by Emily Lane, courtesy of Jardin Jewels by Beacab. I: 640 ct kunzite faceted by Victor Tuzlukov in his signature "Lotus" cut, containing 108 facets. Photo by Robert Weldon/GIA, courtesy of Victor Tuzlukov. J: Vintage oval-cut and engraved Imperial topaz, 41.30 ct. Photo by Robert Weldon/GIA, courtesy of Fei.

## COLORED STONES AND ORGANIC MATERIALS

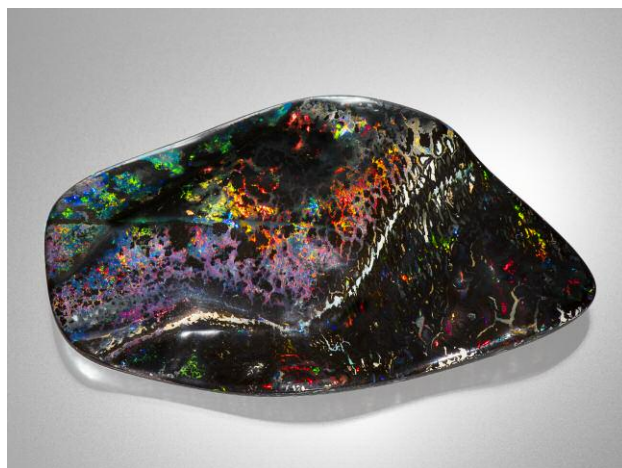
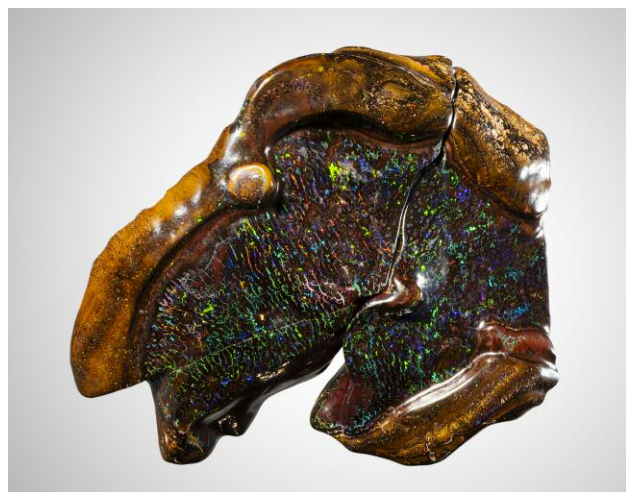
**Boulder opal mining with Rod Griffin.** At the AGTA show, Rod Griffin (Rod Griffin Boulder Opals, Silverado, California, and Queensland, Australia) told us that the world market for all types of opals continues to be strong, but Australia's opal industry is shrinking due to the costs, challenges, and changing regulations of mining. He also cited recent flooding in Queensland as a challenge; opal mining in Australia has traditionally been difficult due to severe weather and rugged terrain. At the 2018 show, we heard that production of Australian boulder opal (figure 1) was low, with fewer than 30 people mining it in Queensland.

Griffin began mining opal in 1960 with a borrowed jackhammer and a lighting plant, in Andamooka, South Australia, 600 km (~372 miles) north of Adelaide. His methods have evolved considerably in the decades since. Along with standard equipment such as bulldozers, drills, and excavators, he recently began using gamma-ray logging for prospecting, and he will add drone magnetometer surveys and subsurface radar this year.

Mining is in Griffin's blood. His great-great grandfather worked in South Australia's Burra copper mines in the 1800s. Griffin's own introduction to mining was at his uncle's opal operation in northern South Australia. His uncle, who began with six camels and a scraper, eventually had one of the first bulldozers used in opal mining.

Griffin's first find, at Andamooka, was black opal matrix in the bulldozer ramps. In 1970 he found more, in the 17 Mile Field in Coober Pedy. In 1976 he sold \$400 (~\$1,800 in 2019) worth of white Coober Pedy opal and boulder opal, bought a squareback Volkswagen, and traveled around the

*Figure 1. The Elusive mine in Koroit, Queensland, is known for boulder opal with the light pattern of color seen here. This stone fits in two hands (its weight is unknown). Photo by Kevin Schumacher, courtesy of Rod Griffin Boulder Opals.*



*Figure 2. This 245 ct boulder opal came from an open cut in the Elusive mine. The flame-like pattern is unique to Elusive. Photo by Kevin Schumacher, courtesy of Rod Griffin Boulder Opals.*

United States selling opal. He first exhibited in Tucson in 1977, at the Pueblo Inn (now the Riverpark Inn). "From that day on, I've been working all my life in opal," he said.

Since then Griffin has mined in New South Wales—where he was the first to bring a tumbling machine to White Cliffs and to use a drill in the Sheepyard field at Lightning Ridge—and South West Queensland, where he and a friend found success using an excavator for the first time. His current operations are in South West Queensland, where he owns the 40-acre Elusive mine in Koroit and will be prospecting west of Quilpie this year.

People thought Griffin was crazy when he bought the Elusive mine in 2013—it was said to be depleted after more than a hundred years of mining. But he found opal 22 feet below ground and has been finding it at 22 to 25 feet for the last several years. The mine is known for boulder opal with the light pattern of color seen in figure 1. Elusive also produces boulder opals with a flame-like pattern (figure 2), which Griffin said is unique to this mine. He added that because the stones were found at a shallow depth and the area is dry, they are stable and will not craze or crack.

In 2017 Griffin worked with two geologists to explore the Elusive mine using gamma-ray logging, which measures naturally occurring radiation in the ground to determine the potential presence of opal. According to Senior and Chaderton, microscopic lattices of silica spheres that produce precious opal's play-of-color contain radioactive elements ("Natural gamma radioactivity and exploration for precious opal in Australia," *The Australian Gemmologist*, No. 23, 2007, pp. 160–176). Gamma-ray logging of drill holes and open-cut mines has detected slightly higher radioactivity around opal deposits and led to new discoveries of opal in Queensland and New South Wales. At Elusive, it was determined that at the current rate of mining, at least seven years' worth of reserves remains. Later in 2017, in several areas of the mine that had previously been explored without success,

gamma-ray logging led to the detection of 1,230 opalized specimens, 30 of which were gem quality.

Griffin said this year he will use gamma-ray logging in prospecting 200 miles west of Quilpie; he will also use drones and subsurface radar for the first time. The drones will be fitted with magnetometers and flown a few feet above ground to measure magnetism and locate ironstone anomalies. Subsurface radar will determine the composition below the ground. Regulatory agency permitting has been secured for the property, and an indigenous land use agreement is in place. But Griffin said there has been a delay in the landowner acknowledging a standing agreement with the miners; he has seen more challenges in obtaining the agreement of all involved parties in recent years.

"There are easier ways to make money," Griffin said. "But I actually feel that I'm in heaven at the moment, doing what I want to do, because I think I found my peace in life."

*Duncan Pay and Erin Hogarth  
GIA, Carlsbad*

**Brazilian alexandrite update.** Gil International's booth at the AGTA show featured something out of the ordinary: a display case with lighting selected to reveal the color change of their Brazilian alexandrites, from blue-green in daylight to reddish purple in incandescent light. Goel "Gil" Gul built the case himself, and he said it has drawn traffic to the booth over the years. Based in New York, Gil International began exhibiting in Tucson 30 years ago; 2019 was their 19th year at the AGTA show.

Gil International specializes in natural Brazilian alexandrite (figure 3), which exhibits a strong color change. Alexandrite was first found in Russia's Ural Mountains in the 1830s. It wasn't until the discovery of Brazilian sources in the late 1980s, most notably Lavra de Hematita (also called Nova Era or Itabira), that greater quantities became available, though alexandrite is still considered rare.

Alexandrite has been in greater demand over the last 15 years, Gul said, but business has been slow the last two. In the past decade, his sales to a company that caters to cruise ships have been particularly strong. He attributes this to people "always looking for something unusual" and having

more time to look at jewelry while on vacation. When Gul entered the industry, aquamarine, tourmaline, and zircon were big. Sapphire has always been very strong, he said, but ruby has come down in the last five years. The demand for stones rises and falls over the decades based on jewelry house promotion, he said, citing Tiffany & Co.'s marketing campaign after the discovery of tanzanite in 1967. He added that more people are buying brown diamonds, previously considered undesirable, because of Le Vian's branding and heavy advertising of "chocolate diamonds."

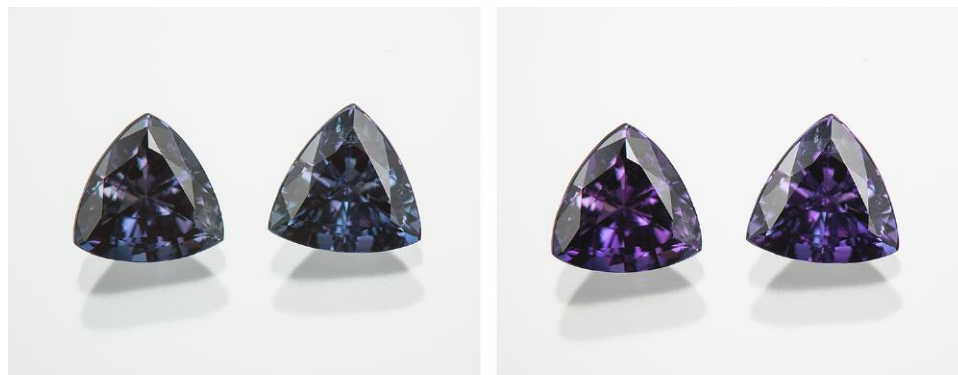
Gul said that every source has different color; for example, Sri Lankan alexandrite is typically an olive green in daylight, while Brazilian stones are more blue-green. He acknowledged that only laboratory testing can definitively determine country of origin, but he can often make an educated guess based on color. He noted that alexandrites from India are sometimes reported as Brazilian, but he can tell that they are from India because the color change is not as strong and the green tends to be lighter.

Born in Afghanistan and educated in Israel and New York, Gul worked in accounting for a decade before being introduced to the gem and jewelry industry by his four older brothers. They were already selling ruby and sapphire, so they sent him to Brazil. On his first trip to Teófilo Otoni, Minas Gerais, in 1990, Gul bought emerald. He saw some alexandrite but didn't buy any until his next visit. He later found out that the stones were from Lavra de Hematita.

"You buy one stone, but you've got three stones," he said, referring to alexandrite's color change. "I felt I could improve my life with this stone."

Gul bought alexandrite from a broker in Teófilo Otoni for several years and contacted the miner directly about 15 years ago. The miner didn't sell the rough; he had the stones cut in Hong Kong and Thailand, so he controlled the production entirely. Gul began to buy directly from him in Hong Kong.

Gul found that unlike many in the industry, the miner did not like to bargain. So he accepted the miner's prices, and as Gul bought more stones, the miner gave him better deals. As Gil International became stronger in alexandrite, Gul and the miner became good friends. Gul has bought almost all of his alexandrite from him.



*Figure 3. This pair of Brazilian alexandrites (2.41 ct and 6.7 mm each) is photographed in daylight (left) and incandescent light (right). Photos by Kevin Schumacher, courtesy of Gil International.*

"The way to make a better business is to find a relationship with the miner," Gul said. "If you have a good relationship, he can trust you; you can trust him. Sometimes even big companies with big money try to bargain, so they don't find a relationship with the miner and can't buy from him."

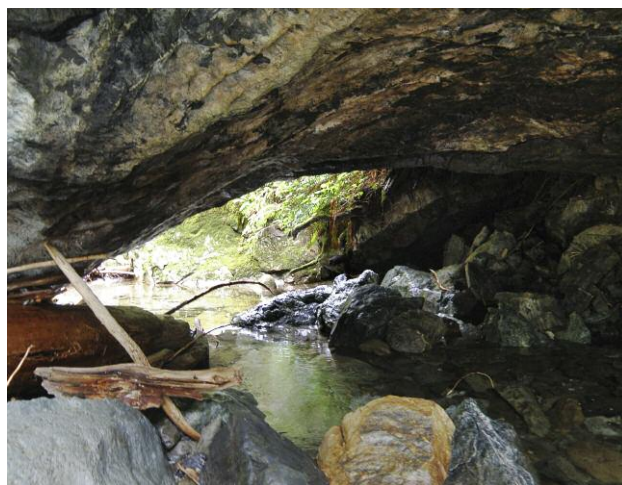
Gul spoke of turning down the miner's repeated offers to buy goods on memo—including an offer of \$12 million of goods in 2010, when the miner closed seven stores in Greece after the 2008 market crash. "I buy what I can," he said. "And he feels that I'm different [than other dealers] and gives me a chance to do more business."

*Erin Hogarth*

**Cat's-eye nephrite jade from Washington State.** Washington Jade (Edmonds, Washington) made its Tucson debut at the AGTA show with nephrite jade from Washington State. They offered a selection of cabochons with and without chatoyancy, along with carvings and rough collectors' stones. The cat's-eye nephrite (figure 4) was the most popular by a wide margin, according to Washington Jade's Nathaniel Cook. Rod Cook, his father and business partner, said that according to many at the show the chatoyancy was reminiscent of the Siberian nephrite that dominates the mid- to high-end Chinese nephrite market.

Cat's-eye nephrite is found only in Washington and Russia; a deposit in Taiwan has been mostly depleted. While nephrite has been found in northwest Washington since the early 1900s, formal production was limited to an operation west of Darrington, near Everett, that ended in the 1970s. Chatoyant nephrite was documented there in 1974. Since then there has been an artisanal "gray market" for nephrite, with people collecting illegally from streams and state lands, but no formal production. This changed in 2012 when Washington Jade began staking claims. Most of their production comes from a deposit northwest of Darrington.

*Figure 4. This 1.71 ct cat's-eye nephrite marquise (11 × 5.5 mm) was mined in Washington State. Photo courtesy of Washington Jade.*



*Figure 5. View from inside the "jade cave" on one of Washington Jade's mining claims. The ceiling appears to be a vein of chatoyant nephrite. Near the opening is another vein, the first couple feet of which provided the rough for many of the stones at the AGTA show. Photo courtesy of Washington Jade.*

Washington Jade uses innovative small-footprint mining methods instead of more invasive traditional methods. To identify a jade seam, they use pattern recognition to look at geologic models of the area, along with biological indicators such as tree species and lichen growth. Magnetic and conductivity surveys are used to locate the high-grade portion of the seam. With these methods they can develop a 3D model of the subsurface and focus on the high-grade deposits, in contrast to the traditional model of core drilling, digging up an area with heavy equipment, and taking out all the jade to be sorted by grade. They take only the high-value materials, leaving the rest in the ground. Rod Cook said they backfill and replace the plants after extracting the jade, leaving a very small footprint.

British Columbia is the leading supplier of nephrite, but Washington's deposits, part of the same geological formation, have yet to be developed. The domestic jade market is much smaller than the Asian market, where jade has been part of Chinese culture for thousands of years. Nathaniel Cook said the nephrite market overall has tightened recently and prices have come down after steady growth the past two decades, but people were still surprised by what they saw as a low price point for the cat's-eye material.

Rod Cook said there has been an explosion of artisanal jewelers using nephrite. The cat's-eye nephrite is popular with them, though market acceptance is still in the early stage. He noted that Washington Jade's output is large enough to meet domestic demand and could be scaled up to the level needed for a jeweler with a few hundred stores. He sees a trend toward jewelry with "less bling" and said that millennials seem to prefer carved material over faceted.

The Cooks also discovered a "jade cave" (figure 5) in a 200-foot canyon cut by a stream. The jade exposed there in-

forms their geologic models by allowing them to see what a similar structure looks like deep in the ground. The cave formed when a piece of the main chatoyant seam broke loose, slid down the hill, and fell into the stream along one side, creating a tunnel underneath. During the spring melt, water flowed through and created a hydraulic plume, which washed away the overburden on one side and revealed a 2-foot-wide seam of chatoyant jade traveling up into the mountains. Rod Cook estimates there are 30 to 100 tons of chatoyant jade in the cave's immediate vicinity, and they have confirmed outcrops of the main nephrite lode containing the chatoyant seam for 1,500 feet over two of their 23 claims. Based on their discoveries so far, he estimates that the main lode is 150 to 300 feet wide and "goes for miles."

See more about Washington Jade's mining methods and cat's-eye nephrite jade at <https://www.gia.edu/gems-gemology/spring-2019-gemnews-cats-eye-nephrite-from-washington>.

*Erin Hogarth*

**Color-change pink pyrope garnet update.** Jewels from the Woods (Blanco, Texas) displayed color-change pink pyrope garnets (figure 6) at the AGTA show. Their color changes from purple in daylight-equivalent light to pink in incandescent light. This was the first time there had been such a large selection of the stones at AGTA, according to independent gem cutter Desmond Chan, who was assisting Jewels from the Woods. He said the material had been very well received.

The stone had been slow to come onto the market, Chan said, because not much rough was available, and the deposit—believed to be in Morogoro, Tanzania—has been depleted. The garnets are said to have been mined in 1988. Initially assumed to be rhodolite, they were put in a safe deposit box until 2014, when they were acquired by cutters Meg Berry, Todd Wacks, and Jason Doubrava. Wacks (Tucson Todd's Gems, Tucson and Vista, California) was the

*Figure 6. This 20.00 ct oval color-change pyrope garnet was cut by Victor Tuzlukov. Photo by Kevin Schumacher, courtesy of Jewels from the Woods.*



first to detect the color change, and he introduced the garnets in 2015 at the Riverpark Inn (Pueblo) show (Spring 2015 GNI, pp. 88–89). GIA performed a gemological study of the material (Z. Sun et al., "Vanadium- and chromium-bearing pink pyrope garnet," Winter 2015 *G&G*, Vol. 51, No. 4, p. 348–369). One interesting finding was that two of the larger stones had the strongest color change.

Garnets have been "on fire" the last four or five years, according to Doubrava (Jason Doubrava Gems & Minerals, Poway, California). He said the public is more aware of garnets and more appreciative of their varied colors than in the past. "These just absolutely glow," he said of the color-change pink pyrope garnets at the booth.

*Erin Hogarth*

**Colombian emeralds and Mozambican rubies from Fura Gems.** We had the opportunity to talk with Rupak Sen, vice president of sales and marketing for Fura Gems in Dubai. Founded in January 2017, Fura holds mining assets in Colombia (emerald) and Mozambique (ruby).

In Colombia, Fura Gems owns and operates the iconic Coscuez mine (D. Fortaleché et al., "The Colombian emerald industry: Winds of change," Fall 2017 *G&G*, pp. 332–358). During its long history, this mine has produced some of the finest gem-quality emeralds, such as the 1750 ct Guinness emerald crystal. In the 1970s, Coscuez accounted for nearly 90% of the world's emerald production, but mining virtually halted during the civil war in the 1980s. In the 1990s, artisanal mining picked up and small licenses were issued by the government. Each license consisted of one tunnel, and many were dug. The approach was very basic, with no scientific exploration or use of engineering to construct the tunnels. People knew that emeralds were associated with white calcite veins, but they had no way of knowing how rich or extensive these veins would be. In the 2000s, Hernando Sanchez acquired and combined all of the small licenses. He has partnered with Fura Gems, which is doing large-scale studies and surveys at Coscuez.

Since work began at the mine in January 2018, Fura has sought to improve the existing infrastructure. The company has done test sampling by washing 3,000 metric tons of emerald-bearing rock, retrieving about 6 carats of gem-grade emerald per ton (figure 7). These numbers will likely drop to 2–3 carats/ton once the mine is in production, since much more rock has to be processed. According to recent resource estimations, around 60 million carats are still unrecovered, representing 30 years of mining. If the mines are expanded deeper underground, those numbers could double or even triple, although geologic exploration is still underway via a drilling program to determine the deposit's depth.

Around 300 people are employed at the site, mainly in bulk sampling; 280 of them are from the local community. They have experience with most aspects of emeralds, including grading and local geology, but they lack knowledge of modern mining techniques and safety measures. Large companies such as Fura are able to instruct their employ-





*Figure 7. Colombia's Coscuez mine, worked by Fura Gems since early 2018, produced the stunning emerald rough shown here. These specimens range in weight from 0.089 to 1.279 g (0.445 to 6.397 ct). Photo by Kevin Schumacher.*

ees on these matters, which they focused on in the months prior to the production stage. Workers also receive formal contracts and monthly wages rather than being given a part of the production as their wages.

Fura also focuses on social responsibility, including gender issues and environmental reclamation. Fura will be opening a women-only washing plant, where emeralds will be handpicked from the processed host rock. They also understand that while mining is an important part of the community, the entire community cannot work in the mine. Fura has looked at alternative employment opportunities, such as a bakery and a sewing workshop to create uniforms and mining gear. While Colombia has strict environmental regulations that must be addressed every time a license is renewed, Sen says that Fura goes beyond what is required, since environmental issues are becoming more important for shareholders. These efforts are part of the larger concept of responsible mining: respect for the environment, safety, employees, and local communities. One example is setting up a football academy as an after-school activity for kids.

Emeralds will be presorted at the mine and taken to company headquarters in Dubai for final sorting and grading before auction. The plan is to bring these rough emeralds to auction in summer 2019 and invite 25–30 companies from Colombia, New York, Hong Kong, and Jaipur. Fura plans to hold two or three auctions per year and will sell only rough. This will provide a regular flow of emerald to the market while allowing for continuous upgrading of the mine and expansion of community programs.

Fura also has interests in Mozambique, where they own the largest ruby mining licenses in terms of area. Demand for rubies is huge and growing, so a consistent ruby

supply is highly valued. According to Sen, Myanmar produced about US\$1 billion of rough rubies per year at its peak. This has slowed to around US\$120 million annually, leaving an enormous demand for other producers to satisfy.

Since rubies were discovered in Montepuez only a decade ago, the deposit is still developing. The rubies are found there in very shallow gravel layers (figure 8); mining is very easy compared to Colombian emerald extraction. Fura has experience with this deposit and the material, as they helped develop the area's largest ruby mine. They have also acquired Mustang Resources' ruby licenses and assets

*Figure 8. These rough rubies were collected from Fura Gems' claims near Montepuez, Mozambique. Photo courtesy of Fura Gems.*



and produced there for more than a year. Sen feels that illegal mining is no longer a major problem, which will make it easier to work with the local population.

Fura is exploring the huge license with a drilling campaign to locate the ruby deposits, the extent of which will be determined by more detailed surveys. Once the deposits are identified, bulk sampling will establish the grade. Bulk sampling was scheduled to start in March 2019. They are aiming for a workforce of 400 to 500 by the end of 2019, consisting of 90% local people. Fura is working on social initiatives in Mozambique but did not disclose specifics because the company is still identifying the communities' needs.

Fura hopes to bring the first rough rubies to auction by the end of 2019, in a system similar to their planned emerald auctions. Using this system, a company can learn the pricing of these highly specialized goods and find out which type of buyer prefers certain material. This will allow for better presentation of goods at later auctions (e.g., creating matching sets of rough in the same lot). They also want to set up a ruby treatment facility in Dubai, where rubies can be enhanced by heating prior to auction for clients who do not have these skills. Most of the buyers are expected to be from Thailand, with others from India, Sri Lanka, and Hong Kong.

Sen sees changes in the jewelry market. The 1990s were heavily focused on gold, with diamonds taking the main focus in the 2000s. He believes we are entering the "decade of color," and consumers will move toward colored stones. Since retail margins on colored stones are also higher than on diamonds and gold, retailers are motivated to work with them, further increasing demand. Of course, this does not mean that emeralds and rubies will replace diamonds, only that they will complement each other. Fura Gems sees as its biggest competitor other luxury industries such as high-end designer fashion and accessories. Creating and advertising more attractive products in the jewelry range, Sen said, will be critical to keep customers.

*Wim Vertriest  
GIA, Bangkok*

**Conversation with Color Source Gems.** Rough emerald crystals in a black host rock (figure 9) at the Color Source Gems booth stood out against the AGTA show's variety of cut stones and jewelry. Moshe Chalchinsky, president of New York-based Color Source, first admired the specimen on a supplier's desk during a buying trip to Brazil. Later, upon receiving the shipment of emeralds he had purchased, he was surprised to find the rough among them. For more than 30 years, it has accompanied him to every show. "It's like a mascot, a good luck charm," said Rachel Chalchinsky, his wife and the company's executive vice president. Although many have wanted to buy the emerald, it is not for sale.

While the emerald rough is their mascot, Color Source Gems has traditionally specialized in ruby, sapphire, and emerald (cut stones and jewelry). Moshe said that the current trend is more affordable gems, so they are branching out into tsavorite, spinel, and rhodolite. This year spinel



*Figure 9. Moshe Chalchinsky of Color Source Gems acquired this emerald rough in matrix in Nova Era, Brazil, in the 1980s. Since then it has accompanied him to every trade show. Photo by Kevin Schumacher, courtesy of Color Source Gems.*

was very popular—especially gray spinel, according to Rachel—and visitors were particularly drawn to the grape-like purple of their rhodolite garnets. Large pieces are harder to move, Moshe said. On a recent trip to Sri Lanka and Bangkok, he bought stones mostly between 1 and 5 carats.

Rachel said the gemstones they look for—clean, well cut, and well defined, with beautiful, consistent color—have become less available and more expensive. They stick to classic jewelry designs such as three-stone rings and tennis bracelets. Moshe said the market has changed because jewelry is often sold on memo now, which is not easy to compete with. They have begun focusing more on stones; two of their sons have joined the business and are also more interested in stones than jewelry.



Figure 10. The trend toward parti-color and fancy-color sapphires is exemplified by this 4.08 ct specimen. Photo courtesy of Color Source Gems.

Rachel sees social media, primarily Instagram, as a major force in the demand for colored stones. Instagram influencers, she said, are increasing the desire for stones people may not have been aware of, like Malaya garnet. People want something different now, a little out of the box, according to Moshe. Rachel noted that there's a big trend toward parti-color and fancy-color sapphires (figure 10) because they are different from traditional sapphire.

While Rachel is the fourth generation of a family in the industry, Moshe was new to the trade 35 years ago. After coming to the United States from Israel, he studied marketing and then sold insurance. He played soccer with peo-

ple in the jewelry industry, one of whom invited Moshe to work for him. "I was running on 47th Street, up and down, knocking on doors," he said. In the mid-1980s, he founded MCR Gems (renamed Color Source Gems in 2015). Moshe first came to Tucson more than 20 years ago.

Asked what's important to him from day to day, Moshe said, "It's about service....and trust. And I always treat my suppliers the right way." Rachel added that Color Source has had some of the same suppliers for over 30 years.

"We can't say no to anybody," one of Moshe's sons told him recently. "If it exists, tell them 'I'll find it for you.'"

Erin Hogarth

**The Granada Gallery.** Housed in a 1908 vintage Arts and Crafts building on Granada Avenue in Tucson, the Granada Gallery is replete with what its owners call "items of geologic relevance," or rare mineral and fossil specimens. These are carefully lit and displayed to accentuate their beauty and often combined with faceted and carved gem materials, one-of-a-kind *objets d'art*, and finished jewelry. For the visitor, this earth-to-jewel experience accentuates the jewelry industry's rich history.

"We want to further an exchange of ideas between artists, scientists, curators, and collectors," explained Rüdiger Pohl, who owns and curates the traveling gallery along with Alison Magovern. The gallery's Tucson space has been open during the gem and mineral shows since 2013.

The Granada Gallery collaborates with global artists and collectors, "sparked by happy coincidences, shared visions, and the passion for creating something unique," the owners said. This year's exhibit included a collection of Paraíba-type tourmalines from Mozambique (figure 11) and a stunning



Figure 11. Paraíba-type tourmalines from Mozambique. Left to right: a 29.34 ct oval, a 3.01 ct pear set in a rose gold ring, a 51.62 ct oval, and a 65.17 ct trillion cut. They were displayed with a 224.6 g gold nugget from Victoria, Australia. Photo by Robert Weldon/GIA, courtesy of the Granada Gallery.



Figure 12. Pezzottaite is carved into a coiled dragon by Patrick Dreher. The pezzottaite crystal measures  $9.6 \times 4.7 \times 2.1$  cm, while the carved pezzottaite is 201.03 ct. Photo by Robert Weldon/GIA, courtesy of the Granada Gallery.



Figure 14. "Chanting of the Stars" was created by the Kreis family of Idar-Oberstein. The "chanting" refers to the sound of a comet entering the earth's atmosphere. The rutilated quartz comet's impact with earth is denoted by the smoky quartz carving. Photo by Robert Weldon/GIA, courtesy of the Granada Gallery.

dragon—carved from the rare mineral pezzottaite, found in a single deposit in Madagascar—by Patrick Dreher (figure 12). Pakistani aquamarine was on display in rough and mounted forms (figure 13). And a year-long collaboration

with the Kreis family of Idar-Oberstein, Germany, resulted in their "Chanting of the Stars" piece (figure 14).

Robert Weldon  
GIA, Carlsbad



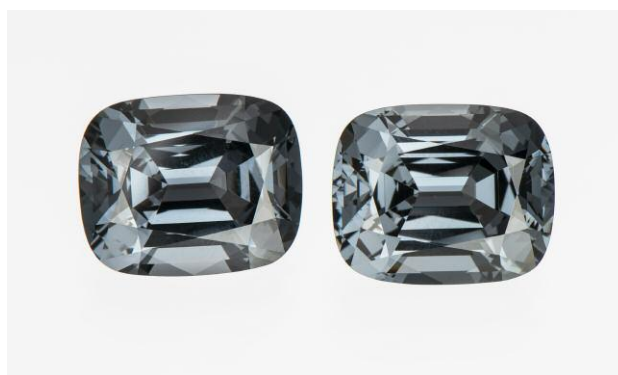
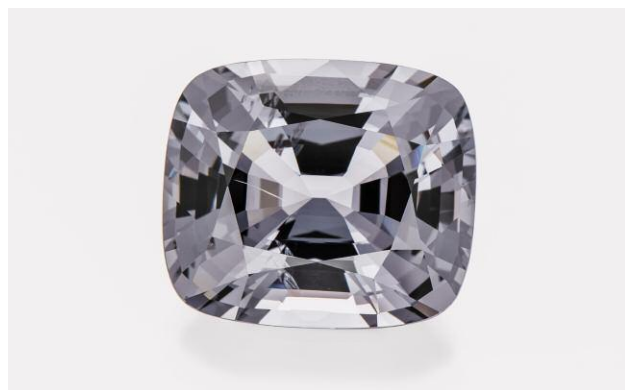
Figure 13. Left: Jochen Leën's aquamarine and gold bracelet is displayed with a  $6.1 \times 9.1 \times 8.5$  cm (369.2 g) aquamarine crystal from Pakistan. Right: This 3436 g aquamarine from the Pohl collection measures  $5.0 \times 9.4 \times 7.5$  cm, and is also from Pakistan. Aside from its quartz overgrowth, the crystal exhibits phantom growth features and iridescence. Photos by Robert Weldon/GIA, courtesy of the Granada Gallery.

**Gray spinel: A new trend in colored stones.** In recent years, the colored stone world has seen a growing appetite for unusual colors. Ruby, sapphire, and emerald with strong saturation but not overly dark tones have always been the mainstay of the colored stone market. But now there is stronger demand for stones in nontraditional colors that might have been difficult to move a decade or two ago. Especially notable is the growing popularity of lighter-toned, lower-saturation pastel stones such as garnets from East Africa or Montana sapphires.

Gray spinels were one of the obvious new trends at the Tucson shows this year. It was not hard to find exhibitors showing off their gray spinel, and everyone who had them commented on how quickly they were selling. The story is remarkable in that the colored stone market has accepted a gemstone that by definition has an unsaturated color—a gray color, no less. Most gray spinel has a minor blue or violet secondary color component. It is relatively rare to find a spinel with a perfectly neutral gray color. These stones have the most value, which increases as the depth of the gray increases. Most of the specimens on display in Tucson were under a carat. Stones larger than a few carats were relatively rare, but we were able to document some with exceptional color, such as the 5.42 ct bluish gray spinel cut by Clay Zava in figure 15 or the slightly bluish gray matched pair (10.34 carats total) from Nomad's in figure 16.

Gray spinel's success is due in large part to strong marketing. Of particular note is the influence of social media in bringing this material to the market. In the last year or so, these spinels became quite popular in gemstone circles on Facebook and Instagram. In our interview with cutter Jeff Hapeman (pp. 140–141), he noted how social media has fundamentally altered the industry by allowing gem dealers to satisfy more eclectic desires and by giving consumers power to find and purchase novel and unusual stones that were traditionally unavailable. As we continue to witness the disruptive power of social media in the industry, gray

*Figure 15. Spinel with nearly perfectly neutral gray color with only a slightly bluish tinge, 5.42 ct. Photo by Robert Weldon/GIA, courtesy of Zava Mastercuts.*



*Figure 16. Matched pair of slightly bluish gray spinels with a combined weight of 10.34 carats. Photo by Robert Weldon/GIA, courtesy of Nomad's.*

spinel will not be the last story we hear of a once unmarketable color being embraced by the colored stone world.

*Aaron C. Palke  
GIA, Carlsbad*

**Greenland ruby update.** Greenland Ruby has been mining ruby and pink sapphire in southwestern Greenland since mid-2017. The mine is located near the town of Aappaluttoq, about 150 km (93 mi) from the country's capital, Nuuk. During the AGTA show, we had the opportunity to talk to Hayley Henning, Greenland Ruby's vice president of sales and marketing. She offered updates on the development of the mine and the market for their gemstones. Over the last year, the company has refined their extraction techniques. The deposit is challenging to work, and the miners improve their skills and knowledge by mining daily. The main difficulty in working this deposit is its isolated location. The remote area, though close to the coast, is covered in ice and snow most the year. And for most of the year, the only way to reach the mine is by helicopter.

Local residents make up the majority of Greenland Ruby's staff. Around 40 people work and live on-site. The mine is highly mechanized, and heavy equipment and blasting are used to retrieve gems. The on-site sorting house is also very sophisticated. Because of this high degree of mechanization, most of the staff operates the equipment, whereas other colored stone mines often rely heavily on manual labor. Once material is mined and sorted at the plant where ruby is separated from host rock, the ruby concentrate is sent to Nuuk to be cleaned with hydrofluoric acid and sorted by color, clarity, and size. Most of the goods require treatment, which takes place in Chanthaburi, Thailand. Cutting is done in Chanthaburi and India, and then the material is sorted in Bangkok, based on the characteristics of the finished rubies. In order to apply the highest safety, environmental, human rights, and security standards at the mine and the treatment and cutting plants, Greenland Ruby works within this closed system. They feel this is the only way to guarantee the quality and disclosure of the product, and it is their main argument for not selling rough.

Greenland Ruby is experimenting with various cutting styles but sees the greatest potential in cabochons. They can produce a consistent supply of large, fine-colored cabochons. Faceted goods are much rarer. The quality of their gems varies, though most of the goods are lower-end. The material ranges in color from light pink to deep red.

In December 2018, the first collection with Greenlandic rubies was launched by Hartmann's Jewellery, a luxury brand based in Copenhagen. This strategic decision arose from the longstanding connection between Denmark and Greenland. The collection sold out in a matter of weeks. Hartmann's clientele was drawn to the combination of the traditional ruby with an exciting new source that speaks to the imagination. Another aspect that appeals to consumers is the transparent supply chain. Greenlandic rubies are controlled by one company from the moment they leave the ground until the gemstones are finished. This ensures a level of traceability that is rarely seen in the colored stone industry.

Greenland Ruby works with preferred partners rather than selling goods directly to the public. These partners are jewelry brands that want access to a reliable supplier operating with a transparent supply chain, something many clients currently demand.

The Pink Polar Bear Foundation is Greenland Ruby's corporate social responsibility project, which is involved in various research in the Arctic region covering the impact of climate change on local communities and wildlife. The foundation is currently educating locals and supporting the local community.

The mine currently has a projected life of 10 years. At least two other ruby deposits have been identified and studied, though many more can be found in southwestern Greenland.

Wim Vertriest

**Hand-carved cameos from Italy.** Vincenzo Imposimato (Naples) brought his hand-carved shell cameos and his carving tools to the GJX show to demonstrate the making of these exquisite pieces.

This was Imposimato's sixth visit to Tucson. As a child, he was fascinated by the shell carvings he watched his grandfather make at home. He has also been passionate about drawing since his early childhood, so a career in cameo carving was a natural choice.

Imposimato mainly uses two types of helmet shell. One has a dark brownish background color and originates from the Caribbean Sea; the other, with lighter orange or reddish background, is from the coast of Madagascar. Consumers prefer the darker background because it displays the carved image in greater contrast (figure 17). The Caribbean shell also has a more curved shape, allowing greater complexity in its carving, while the African shell tends to be flat. The Caribbean shell is more expensive, so consumers pay more for these finished cameos.

With a shell in hand, carvers have two possible plans: They can either make a whole-shell cameo or a small piece with different shapes. The general process for both types includes a rough shaping by machine and then detailed carving by hand. For whole-shell cameos, carvers need to hold the shell very gently. Since the shell is empty, carvers must pay extra attention when applying force to avoid damage. As for small cameos, the shell needs to be sliced into small pieces and then shaped by machine. Carvers then attach the small piece to one end of a wood stick with fish glue. Fine hand carving is done by holding the stick next to a hard surface (figure 18).

Detailed carving by hand is done with the *bulino*, a traditional tool for carving and engraving. There are bulinos of different sizes and shapes for different carving purposes. For shell cameos, carvers remove the top whitish layer to



Figure 17. Shells harvested from the Caribbean have a dark brownish background color (left), while shells from Africa—especially Madagascar—show a much lighter background color (right). Photos by Vincenzo Imposimato.



Figure 18. A carver holds the stick attached to the small cameo piece next to a hard surface, which provides support. Photo by Kevin Schumacher.

form a carving against the contrasting background color. The character or theme depicted depends on the shell's natural condition. Factors such as the curvature of the piece, the thickness of the white surface layer, and the color contrast will determine what can be carved. A whole-shell cameo typically takes about two months to finish, while a small piece takes a few days.

Japan was once the biggest market for these handcrafted shell cameos. Imposimato first visited Japan in 1993 to show local consumers how to make cameos. After that, he was invited back more than 20 times. However, the

market has slowed down over the past five years, perhaps due to changing styles. Women used to wear woolen coats that were perfectly paired with cameos. Now that they have more fashion options, many choose other accessories. Even at their height of popularity, cameos were typically purchased by women over the age of 30. Imposimato feels that the themes carved onto cameos need to be updated to appeal to young consumers and expand the market share.

Whereas cameos carved by machines tend to be flat, handmade versions tend to keep the natural curvature of the materials used. While manufactured cameos of all different types of materials are readily available these days, handcrafted shell cameos still hold a unique position in the fine jewelry world.

Tao Hsu  
GIA, Carlsbad

**Moonstone jewelry.** Blue moonstone, an orthoclase species of the feldspar group, is composed of two feldspar minerals, albite and orthoclase, that stack in alternating layers. Adularescence, the optical phenomenon resulting from the scattering of light as it interacts with these two different feldspar layers, occurs below the stone's surface. When the stone is moved, the glow produced by the scattered light appears to float like the moon in the sky. Rainbow moonstone, which shows flashes of multiple colors including blue, is also part of the feldspar group but falls under the labradorite species.

Exceptional blue and rainbow moonstone were both prevalent at this year's Tucson shows, and top designers had fashioned beautiful pieces with them. Paula Crevoshay created a bracelet with 121 moonstones flanked by 495 tiny blue sapphires (figure 19) that was as flexible and soft as a piece of fabric, allowing it to artfully showcase the move-

Figure 19. Paula Crevoshay's "Moon Dance" bracelet contains 121 moonstones totaling 133.19 carats and 495 sapphires totaling 38.61 carats, set in 18K gold. Photo by Kevin Schumacher.

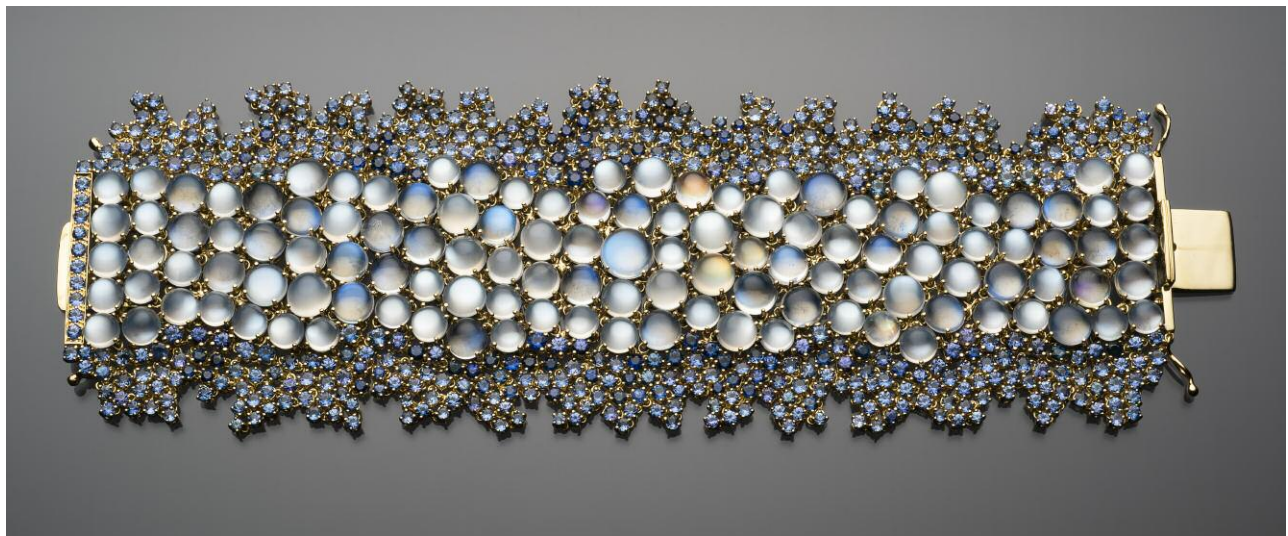




Figure 20. Erica Courtney's moonstone pendant and earrings. The mandala flower cross pendant features 20 carats of moonstones with Paraiba-type tourmaline accents. The chain contains 3.02 carats of diamonds. The double-drop moonstone earrings also have Paraiba-type tourmaline accents. Photo by Robert Weldon/GIA.

ment of the adularescent glow. Erica Courtney, winner of three 2019 AGTA Spectrum Awards, exhibited a stunning moonstone necklace and pair of earrings, both featuring African Paraiba-type tourmalines (figure 20). The intense adularescence of the moonstones in these jewelry pieces is truly captivating.

Jennifer Stone-Sundberg  
GIA, New York

**Ponderosa sunstone update.** John Woodmark, president of Desert Sun Mining and Gems (Depoe Bay, Oregon), updated us on the Ponderosa mine, which he calls the most productive source of Oregon sunstone (figure 21). Demand has increased annually over their 17 years of production, he said. With the larger excavator and high-capacity screen they brought on in 2015, they now mine about 4,300 kg (4.8 tons) of sunstone rough per year, up from about 2,000 kg (2.2 tons) in 2014. About 3% of this material is facet grade. Pon-



Figure 21. Two Oregon sunstones weighing 7.07 and 2.48 ct. The stone on the right, faceted by Larry Woods, has a very rare deep red color. Photo by Robert Weldon/GIA, courtesy of John Woodmark, Desert Sun Mining.

derosa now produces 4,000 to 5,000 cubic yards of concentrate in seven days—more than enough to process in one season (which only lasts five or six months due to snow at the high elevation). Desert Sun was once limited to mining at about 50 feet deep, but the excavator has allowed them to go a few hundred feet deep into the source. Woodmark said the sunstones at that depth are larger and less fractured, and there are some excellent red stones of good size.

Woodmark said demand is especially strong from American and European customers age 45 and under because they want natural, untreated gemstones such as sunstone, opal, and jade. They also love Oregon sunstone's schiller effect, a sparkle caused by reflective copper platelets that makes the stone "different from what their friends have." Desert Sun will be using social media this year for the first time to reach customers looking for unique gemstones.

Jewelers are excited about Oregon sunstone because of the potential high markup, according to Woodmark. He noted that sunstone isn't competing with diamond, ruby, sapphire, and emerald, for which a jeweler might see a 10% or 15% profit margin. Oregon sunstone can yield a triple or quadruple markup, yet it is still relatively affordable: Woodmark said the yellow sunstones sell for about \$30 per carat while the reds can go for \$300 to \$4,000 per carat. Sunstone's affordability, profit margin, and appeal to young consumers make it attractive to jewelers.

Woodmark said the jewelry industry's demand for calibrated sunstones continues to grow, and Desert Sun now receives significant orders from large companies. A typical order might be a thousand 5 mm rounds of orange sunstone. Every color sells well, he told us, but it is difficult to get a specific band of color in natural, untreated gemstones, so



they are trying to grade more consistently. Desert Sun has seven colors, each graded with and without schiller, so overall there are 14. He tries to educate jewelers, manufacturers, and designers on the fact that color in natural stones is more variable—and that many have unique color—to encourage them to use more than one color in their pieces.

Woodmark sees a bright future for Oregon sunstone as more consumers become aware of it. He acknowledged that there will come a time when he and Bruce Moore, Desert Sun's executive vice president, will have to step away from the deposit. "We're barely scratching the surface of what people could do with this mine," he said. Desert Sun only exhibits at the AGTA show in Tucson, but Woodmark said if someone were to take over the mine, they could do 10 shows a year across the United States. At that point, he said, sunstone would "take off."

*Duncan Pay and Erin Hogarth*

**Potentate's Montana sapphire mine: An interview with Warren Boyd.** The history of the American West is told in stories of frontiersmen seeking fortune in gold and other precious metals. It was serendipity when these intrepid adventurers arrived in western Montana and discovered strange, shiny pebbles—sapphires—while looking for gold. Little did they know the gem wealth they had uncovered with the sapphires, which were simply a nuisance to the gold miners at first. More than 100 years later, this legacy of mining is carried on by several small-scale miners across Montana, and with the arrival of Potentate Mining at the Rock Creek sapphire deposit. We had the chance to sit down in Tucson with Potentate's director of marketing, Warren Boyd, for an update on their mining activities and their plans to find a place for Montana sapphires in the market.

Sapphire mining can be challenging in the rugged Montana terrain. Harsh winters limit the mining season to about six months a year, and even then water shortages can make mining difficult. The year 2017 saw extreme wildfires that forced the mine to be evacuated several times. Despite these challenges, 2018 was Potentate's third year at full production, yielding more than 100 kg of rough sapphire each mining season. In 2018, the mine commissioned a new processing facility with a larger throughput, which will allow Potentate to process more gravel and produce more sapphires each year. The facility features a gold recovery circuit to recover the fine gold that is produced along with the sapphires. Potentate has also devoted significant resources to protect the beautiful wild areas in which they mine, and a strict rehabilitation program is in place. They are only allowed to disturb five acres at a time, and after rehabilitation there will be little evidence of their mining activities. A water clarifier has also been implemented to purify their processing waters. This is important to protect the pristine trout fishing streams in the area.

The sapphires come in a range of colors (figure 22), from fine deep blues to fancy yellows, oranges, and pinks, and there are very rare Montana rubies. Some stones come out



*Figure 22. Rough Montana sapphires in a range of colors. Photo by Albert Salvato, courtesy of Potentate Mining.*

of the ground with a fine natural color, but the bulk of the production requires heat treatment to bring out these colors. Less than 1% of the sapphires recovered will end up as faceted stones in the 2–6 ct range, with most of the production cutting stones from 0.25 to 0.99 ct. Some extremely large stones have been produced, however. In the last mining season, Potentate recovered a 64.14 ct rough sapphire, the largest gem-quality sapphire ever found in Montana.

Potentate first exhibited at the Tucson shows in 2018, with a booth in the AGTA GemFair. With mining activities proceeding at full speed, Potentate's focus now is to create market awareness of their commercial-scale production of sapphires, which represents a reliable supply of stones. Their big challenge is not finding a market for their rare large stones, but moving large quantities of small and mid-sized stones. Potentate is building relationships with jewelry manufacturers that have the capacity to find a market for Montana sapphires in the 0.5 ct range. The main markets are in the United States and Canada, but Boyd has seen interest growing internationally as well. Social media has been an important tool for Potentate, and they have started exporting stones to clients in India, Hong Kong, Sri Lanka, and Europe. Montana sapphires have even found a substantial market in sapphire-producing countries such as Australia, where consumers might be looking for their unique pastel colors that are different from those sourced domestically. With their significant investments in mining infrastructure and a clear strategy for getting stones to the market, Potentate Mining could make a substantial impact in the story of Montana sapphires.

For a bird's-eye view of the Potentate mining site, visit <https://www.gia.edu/gems-gemology/spring-2019-gem-news-potentate-mine-warren-boyd>.

*Aaron C. Palke*



Figure 23. These “rainbow lattice” specimens, a 4.14 g rough stone and a 2.18 ct kite-shaped cabochon, are from Harts Range in central Australia. Photo by Robert Weldon/GIA, courtesy of Rainbow Lattice.

**“Rainbow lattice” from Australia.** One of the most striking materials encountered in the Riverpark Inn (Pueblo) Gem Show was “rainbow lattice.” This rare phenomenal gem is a variety of feldspar exhibiting aventurescence from exsolution hematite crystals and a rainbow lattice effect from oriented exsolution magnetite crystals. Supply is extremely limited, and the only source is the tiny Utnerengatye mine in Harts Range, Northern Territory, Australia. Rainbow lattice was discovered in 1985 and acknowledged as a new gem material in 1989. One of the original discoverers, Darren Arthur, showed us all-new material he mined in 2018 and

subsequently sorted and cut (figure 23). With its scarcity and unique appearance, rainbow lattice is a must for any serious rare gem collection.

*Jennifer Stone-Sundberg*

**Sourcing stones with Columbia Gem House.** Eric Braunwart (Columbia Gem House, Vancouver, Washington) spoke to us on how the industry has evolved since he opened his doors in 1976. Columbia Gem House has been a pioneer in the responsible sourcing of gemstones.

Braunwart traces his commitment to ethically sourced gems, those that he can track and trace and align with the company’s fair trade protocols, to a project he worked on with the World Bank in Madagascar about 20 years ago. His involvement with this project led him to set up fair trade standards for his own business—no small feat, as there were no such procedures for the gem and jewelry industry at the time. To create policies, Braunwart and his staff turned to industries such as food and agriculture. The company has remained open to public feedback; this is how Braunwart became passionate about prevention of silicosis in cutting communities. They have collaborated with different entities to create projects to benefit miners and their communities (read about one such project in J.-L. Archuleta, “The color of responsibility: Ethical issues and solutions in colored gemstones,” Summer 2016 *G&G*, pp. 144–160). The company continues to seek out projects in regions where they can make a difference by setting up schools, medical facilities, and other community needs.

Growing up in the American West led to Braunwart’s interest in the region’s nontraditional gem materials, such as agates, garnets, and petrified wood. Even though his business was involved in more traditional gem materials, he was drawn to the chalcedony, variscite, and turquoise that were not featured in classic jewelry. Today, Columbia Gem House sources and cuts about 150 different varieties of gemstones. American gemstones, such as the faceted blue hyalite opal from Oregon (figure 24, left), are one of their specialties. Much of their current business comes from small designers



Figure 24. Left: These trillion-cut blue hyalite opals from Oregon, weighing about 2.25 ct each, are reminiscent of moonstone. Right: Five Montana sapphires, ranging from 0.60 to 1.20 ct, showcase Columbia Gem House’s “GeoCut,” which follows the crystal’s natural shape. Photo by Robert Weldon/GIA.



Figure 25. This 21.33 ct blue and green unheated sapphire is from Tanzania. Photo by Robert Weldon/GIA.

rather than large corporate interests. They have run their cutting facility in China for 35 years, with a trusted team that can quickly respond to orders.

While the company was in business before millennials were even born, this generation has clearly influenced the company's sales; many of this year's buyers in Tucson were people in their twenties representing small designer firms making modest purchases. Braunwart has been able to capitalize on social media (particularly Instagram) to make decisions on materials, colors, and cuts, allowing followers to vote on what types of material to promote. He believes that social media will continue to drive consumers toward ethical and sustainable choices in jewelry, with the full impact being felt within the next five years.

The 2019 AGTA show brought many new and established buyers to the Columbia Gem House booth. In fact, Braunwart said that this Tucson show, the company's 41st, was their most successful ever. He attributes that to a growing interest in sustainably and ethically mined gemstones. Popular items included small baguettes in a variety of colors and materials, unheated Montana sapphire, Cortez pearls, and fossilized coral from Utah. The company's "GeoCut," a simple cut that follows the natural shape of the crystal, is used in materials such as Montana sapphire (figure 24, right). One remarkable stone from outside the United States was a 21.33 ct unheated sapphire from Tanzania showing distinct blue and green colors (figure 25).

*Jennifer-Lynn Archuleta and Jennifer Stone-Sundberg*

**Thoughts on the Chinese and Japanese gem markets.** At the Tucson shows, Shahin Aboosalih, director of SR Trading, spoke to us about his path to the gemstone and jewelry industry and his company's gemstone business in Japan and China.

Shahin, as he prefers to be called, comes from four generations of Sri Lankan gem merchants, but initially he took another career path. He spent seven years in the Sri Lankan

banking industry and then decided to go to school in Japan to study the language, with no intention of entering the gem industry. In fact, his father always encouraged him to pursue a career outside the gem business. In 1993, after completing his Japanese language studies and gaining experience in computer graphics, Shahin returned to Sri Lanka and joined Dilmah, a major tea exporting company, as a packaging designer. In 1996, he was offered an opportunity to work in Kofu, Japan, by STS Gems Japan Ltd., an Indian multinational colored gemstone and jewelry company. This was his stepping stone to the world of gems. "At that time, I didn't know what a tanzanite or sapphire was, even though my family had huge knowledge in corundum from Sri Lanka for several generations," he explained.

When Shahin started in the industry during the 1990s, Japan's economy was in recession, yet fine gemstones like Paraíba tourmaline (figure 26) were still in demand. As the recession continued, gemstones that were once rare and more difficult to source—such as fine blue star sapphires, emeralds, and Paraíba tourmaline—kept momentum and held their prices.

Sunil Agrawal, CEO of STS and one of Shahin's early mentors in Japan, taught him everything "from scratch." The company sent Shahin to Jaipur, India, for several months to learn colored stone identification. Then he traveled to Brazil, India, South Africa, Thailand, and Sri Lanka to find new material to meet the heavy demand from his Japanese clients for a wide range of stones, including fine corundum, spinel, tourmaline of all kinds, and aquamarine. He also learned finer cutting techniques in Sri Lanka from his father-in-law, Naji Sammoon (founder and chairman of

Figure 26. Paraíba tourmaline, such as this 3.71 ct pear-shaped stone, was popular in Japan when Shahin entered the gem trade. Photo courtesy of SR Trading.





Figure 27. This rare blue-green beryl from Madagascar, weighing 10.19 ct, contains iron, chromium, and vanadium. Photo by Kevin Schumacher, courtesy of SR Trading.

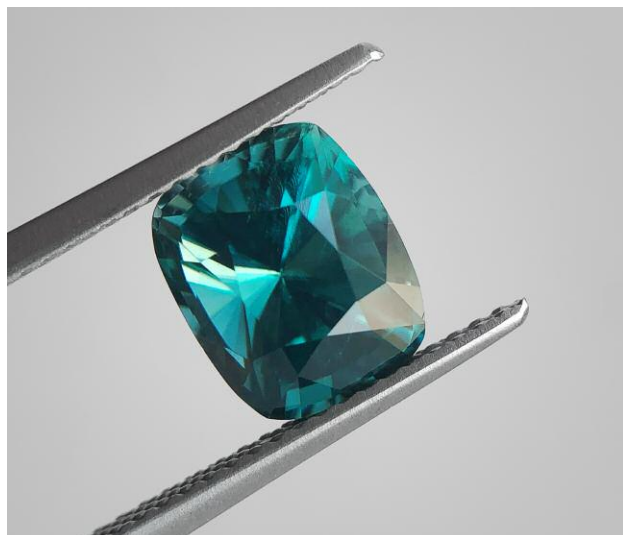


Figure 28. A 2.95 ct grandidierite from Madagascar. Photo courtesy of SR Trading.

Sapphire Cutters (Pvt) Ltd. in Colombo). He used these skills, along with his computer graphics background, to perfect gem cuts and meet the high standards for faceted stones in the Japanese market. "The trade is looking for nice material, precision, and perfection," Shahin said.

At the height of the global recession in 2008, Shahin became managing director of SR Trading, his older brother's company. Japanese clients were looking for unusual and rare material that had become more popular in recent years, including grandidierite and benitoite. In 2012, Shahin transitioned to the Chinese market. His brother Ruzaik Aboosalih runs the business in Japan, specializing in padparadscha sapphire, Paraíba tourmaline, and other rare stones. Shahin sees great opportunity in China and Hong Kong. He has developed a very strong client base along with Cindy Xin Hao, who started out as his Chinese translator and has become a gem expert and managing partner of the Chinese business.

Shahin thinks of China as a "young" market with consumers who are curious to see variety, more so than their traditional Japanese, European, and American counterparts. Here he targets almost every colored gemstone. His Chinese clients look for a wide variety of colored stones: corundum, emerald, and aquamarine and other beryls (see figure 27), as well as precious opal and tourmaline in its many colors. This gives Shahin opportunities to look for more stone varieties every day. Despite this market's demand for a wide variety of gem material, gemological education is relatively new in China. Therefore, Shahin and Cindy conduct mini-seminars to groups of 10–15 people to teach them about gemology and the supply, demand, and value of colored stones. They also conduct gem mining and leisure tours in Sri Lanka for small groups from China. They educate the tourists about the process, from mining and cutting to the finished product.

Shahin said that historically some of the finest corundum has come from Sri Lanka, but currently most sapphire is sourced from Madagascar. For other colored stones—such as grandidierite (figure 28), spinel, and Paraíba and other tourmalines—the main producers are mainly Brazil, Tanzania, Kenya, Congo, and India. Shahin buys stones from Hong Kong and Bangkok as well; such gems include spinel, rubies, mint-green garnets, and tanzanite (figure 29). Most of the time he buys faceted mate-

Figure 29. A 22.6 ct precision cushion-cut deep blue tanzanite. Photo by Kevin Schumacher, courtesy of SR Trading.





Figure 30. A pink 173.22 ct fluorite, measuring 35 × 33 mm, from Uri, Switzerland. This stone is representative of minerals discovered by strahlers, mineral hunters from the Swiss Alps. Photo by Kevin Schumacher, courtesy of Gravier & Gemmes.

rial, but as a perfectionist, he will recut 90% of his stones in Sri Lanka. He purchases all his stones, and they all undergo his personal inspection and quality control. His passion for his stones is what makes them easy to sell, because they are all very special to him. "I love them all," he said.

Shahin sees plenty of opportunity for those who can bring value-added merchandise to the market. The global industry is looking for attractive, ethical, value-added gems. While it can be a struggle to find quality material—be it corundum, Paraíba tourmaline, spinel, or any other colored stone—it is worth it to work hard and be patient enough to find the right opportunity and source. Shahin notes, "With the experience and connections and what I've learned in the past 20 years, it helps to meet the right people and prod-

uct to satisfy the demand. This demand will continue, and I see that as an opportunity to make business in the future."

Jonathan Muyal  
GIA, Carlsbad

**Unusual faceted gemstones.** Denis Gravier of Gravier & Gemmes (Poncin, France) exclusively sells rare and unusual faceted stones, such as the pink fluorite from Switzerland shown in figure 30. During the GJX show, he shared insights about the market for such gems.

Gravier developed a passion for colored stones and minerals while growing up in the French countryside. He studied mineralogy, crystallography, and petrology before traveling to the Republic of the Congo, Pakistan, Mexico, the former Yugoslavia, and Morocco a few decades ago to collect mineral specimens. He also learned gemstone cutting techniques. With the knowledge and experience he gained, he decided to open a company specializing in faceted stones of unusual varieties. Some of these gems, he explained, are rarely if ever used in jewelry. The challenge is finding them, but after decades of traveling and visiting the mines, he knows many people in the trade. Now the stones come to him during major shows, so it is no longer necessary to go to the sources. He still travels occasionally to Sri Lanka and Madagascar, where he buys rough that he will have cut in France or overseas. Gravier says Tucson "is a great show...you can almost see all that is available in the world at that time during the show." In Tucson he meets with clients from the U.S., Japan and other parts of Asia, and European countries.

In terms of novelty and rarity, Madagascar offers the largest variety and supply. New gemstones are always emerging, Gravier explained. Among his stones from Madagascar were the dumortierite and green sphene in figure 31.

He also described the market for unusual faceted gems. Collectors, not the jewelry industry, are the clientele for rare stones in France and around Europe, which is dominated by



Figure 31. Unusual stones from Madagascar. Left: A 0.51 ct dumortierite (5.4 × 4.5 mm). This mineral, commonly known as an inclusion, is now available in very limited quantities as a gem. Right: A 19.65 ct round-cut green sphene. Photos by Kevin Schumacher, courtesy of Gravier & Gemmes.



Figure 32. A 1.21 ct intense yellow legrandite, a rare zinc arsenate mineral from Mexico. Since the last discovery of this mineral in the 1970s, it has appeared on the market only sporadically. Photo by Kevin Schumacher, courtesy of Gravier & Gemmes.

the “Big Three” and diamond. Faceted legrandite (figure 32), grandidierite, and dumortierite, for example, are generally not used in jewelry pieces. On the other hand, in Asia, especially Japan, people are attracted by rarity and there is a demand for “exotic” quality material, even in small sizes, for use in jewelry. Gravier feels that more people there have a general knowledge of and interest in gemology and colored stones. The Chinese market is becoming increasingly important for his business. One benefit of the rare stone market is that treatments are not common among these gems, making it a good source for people seeking untreated material.

Even though there is growing competition, with goods at all price points available on the Internet and aggressive marketing through the web and social media activity, Gravier chooses not to sell on the Internet. He invests in improving the quality and variety of his stock, relying on his long-term relationships with clients and suppliers.

Gravier sees a rising interest in rare stones. He believes he is helping to create more appreciation for a wide range of colored stone varieties. He hunts for rare treasures and, as an ambassador for unusual stones, gives them a chance for public exposure and recognition.

*Jonathan Moyal*

**A variety of colored stones from Mayer & Watt.** Mother-and-son team Laurie and Geoffrey Watt (Mayer & Watt, Maysville, Kentucky) noted that while there were plenty of customers at the AGTA show this year, the formula for success was a wide selection of materials and competitive pricing. Their booth had a selection of what was hot this year: the highly sought-after gray zircon, as well as pink and blue zircon; fancy colors of Montana sapphire;



Figure 33. An 8 mm 2.01 ct trillion-cut gray spinel from Myanmar. Photo courtesy of Mayer & Watt.

Ethiopian emerald from Shakiso; electric pink spinel from the Mahenge deposit in Tanzania; and a wide variety of garnet colors, such as true purple garnet from Mozambique. Gray spinel was one of the most popular stones this year for a wide variety of jewelry applications, including engagement rings. Mayer & Watt had one of the best selections of actual achromatic gray spinel, with no stray hues of blue, green, or purple (figure 33). The true purple garnet offered by Mayer & Watt and a handful of other vendors at AGTA and GJX comes from a single small source discovered in 2015 in Mozambique (figure 34). This garnet lacks a pinkish cast, unlike less expensive pinkish purple material coming from Tanzania.

*Jennifer Stone-Sundberg*

Figure 34. This purple garnet from Mozambique is a 1.25 ct hexagon measuring 6.1 mm. Photo courtesy of Mayer & Watt.



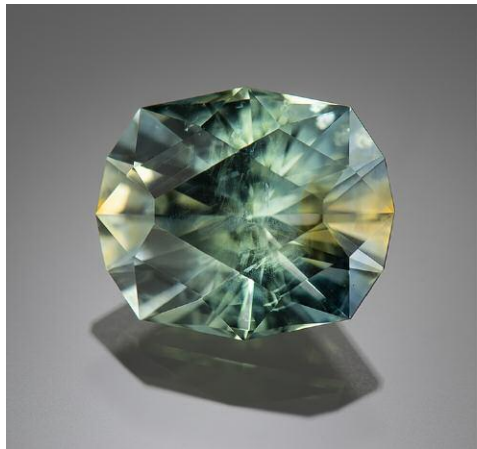


Figure 35. Left: This 4.37 ct unheated bi-color sapphire from the Potentate mine in Montana features Jeff Hapeman's signature Helena cut. Courtesy of Jeffrey R. Hapeman, *Earth's Treasury*. Right: A 4.57 ct heated blue sapphire from Potentate. Photo by Kevin Schumacher.

## CUTS AND CUTTING

**Jeff Hapeman: Stories from a gem cutter.** Jeff Hapeman of *Earth's Treasury* (Westtown, Pennsylvania) loves a gemstone with a good story. Whether it's the story of a young couple buying one of his Montana sapphires for an engagement ring or the amethyst he dug out of the ground on an Amish farm in rural Pennsylvania, Hapeman feels that every gemstone needs a story. His own story starts with a boy reading old rock and mineral magazines, staring in fascination at the new find of blue-cap tourmalines coming out of Pala, California, in the early 1970s. These images were fresh in Hapeman's mind when he took a break from his career in finance technology in Southern California to work at the Oceanview pegmatite mine. One of the miners thought he might have the talent for cutting stones and pushed him to take up faceting.

Since cutting his first gemstone in 2013, Hapeman has developed his own style, creating designs he describes as "somewhat modern and somewhat classic at the same time." The modern elements are seen in the elegant but slightly angular and geometric appearance of many of the stones he cuts. At the same time, Hapeman claims there is a simplicity to his designs, even though "simple" is certainly not a term that comes to mind when you see his work. His designs are often born out of necessity as he fits the cut to work with a piece of rough that would not work with his previous designs. One of his more recognizable designs is the Helena cut, named in honor of Montana's state capital. Rough Montana sapphires are often found in flattened, slightly oval shapes. Ovals are among the least rewarding stones for many lapidary artists. Even when skillfully executed, the results can be boring. And yet, through a fine balance between rigorous mathematical modeling and his own gut feeling and intuition, Hapeman has managed to produce a visually interesting oval cut that is well suited for Montana sapphires, deepening the color of these typically pastel-hued gemstones (figure 35).

Montana sapphires have become particularly important in Hapeman's career. He became involved with the Potentate Mining operation at Rock Creek (p. 134) as they were

developing their mine. Montana sapphires can be trickier to cut than blue sapphires from Asia and Africa. While they often have exceptional clarity, fine cutting can greatly benefit Montana sapphires due to their sometimes lighter pastel colors and pleochroism. Early on, Hapeman cut many Montana sapphires in order to demonstrate this to Potentate Mining. Since then he has become one of the most prominent cutters working with Potentate's production, and he often collaborates with them to cut and market some of their larger and finer stones.

When sourcing material, Hapeman seeks out the unusual. His involvement with Potentate gave him the opportunity to cut several exceptionally rare Montana rubies from the Rock Creek deposit (figure 36). Unlike some lapidary artists, he actually likes cutting round brilliants, as he appreciates the beauty and symmetry of a perfectly executed cut. He especially seeks out materials with high lus-

Figure 36. A collection of eight Montana rubies from Rock Creek, mined by Potentate, ranging in weight from 0.172 to 0.578 ct. Photo by Kevin Schumacher, courtesy of Jeffrey R. Hapeman, *Earth's Treasury*.





Figure 37. This rare faceted scheelite weighs 6.08 ct. Photo by Kevin Schumacher, courtesy of Jeffrey R. Hapeman, *Earth's Treasury*.

ter and dispersion for his experiments with round brilliants, such as the scheelite from China in figure 37.

Hapeman also discussed the use of social media in the gem and jewelry industry. Social media has helped cutters like him who deal largely in nontraditional stones by allowing them to reach clients with eclectic tastes. It has profoundly reshaped the gem industry by giving more control to end consumers to purchase exactly what they want. Hapeman said that those in the gem and jewelry trade who can harness social media will gain a competitive edge. This is especially true for the younger generation of cutters and designers, who are using social media to find a market for gems and jewelry that could have been hard to move 10 or 20 years ago.

Aaron C. Palke

**Largest square cushion-cut tsavorite.** At the AGTA show, Bridges Tsavorite unveiled the largest known square cushion-cut tsavorite, weighing 116.76 ct (figure 38). The 283.74 ct rough stone was mined by the company in Merelani, Tanzania, in September 2017. Bangkok-based gem cutter Victor Tuzlukov cut the stone at Bridges Tsavorite's Arizona office over the course of a month in 2018.

The tsavorite could be a once-in-a-lifetime stone, said Bruce Bridges, the company's CEO and son of the late Campbell Bridges. Despite seeing most of the finest tsavorites in the world above 20 carats, he had never seen one comparable to this size in a square cushion cut. The square cushion and round cuts are the rarest shapes for tsavorite because the rough typically lends itself to other shapes.

Size and cut were not the only factors contributing to this tsavorite's rarity. The rough was extremely clean for its size. It had several very well-terminated euhedral faces, unusual for tsavorite, which typically has more fragmented face formation. The tsavorite also has the distinction of being the largest gemstone cut in the United States.

Bridges said that the public is much more concerned about ethical sourcing than in the past and wants to know where a gemstone came from; in keeping with Bridges Tsavorite's mine-to-market tradition, the stone's process from mining to finished product was completely documented. "My father would be very happy that we're doing this and that we're carrying on his legacy," he said.

In March 2018, a GIA team traveled to Arizona to document the cutting of the stone. Find out more about this rare tsavorite, and how Victor Tuzlukov approaches the cutting process, at <https://www.gia.edu/gems-gemology/spring-2019-gemnews-largest-square-cushion-cut-tsavorite>.

Duncan Pay and Erin Hogarth

Figure 38. This 283.74 ct rough tsavorite (left) was mined in Merelani, Tanzania, by Bridges Tsavorite and yielded a 116.76 ct square cushion cut (right). Photos by Robert Weldon/GIA, courtesy of Bruce Bridges.







Figure 39. This cuprian tourmaline from Mozambique measures  $37 \times 26.5$  mm and weighs 109.62 ct. Photo by Kevin Schumacher, courtesy of Wild & Petsch.

**Wild & Petsch: Sourcing rough and cutting in Idar-Oberstein.** Wild & Petsch (Idar-Oberstein, Germany) was formed when two established companies, headed by brothers-in-law Alexander Wild and Thomas Petsch, joined forces. The roots of the merged company go back to 1901. Today the firm is still sourcing rough and faceting stones in their 15-cutter workshop in Idar-Oberstein. Over the last few years they have increased their quality levels, embracing the slogan “Nothing leaves our offices that is not perfect.” While most of their work involves freeform hand faceting, machine-assisted techniques are used during preforming to achieve optimal results. They supply other businesses mainly through trade shows and an international network of distributors.

According to Alexander Wild, high-quality material is not limited to facet-grade rough. Wild & Petsch produces faceted stones, cabochons, and beads, but all must be of the highest quality. To guarantee high standards of their craftsmanship, the firm has started an apprenticeship program. During this three-year period, enrollees learn high-level lapidary skills in the company’s professional workshop while attending school. After this period, they are certified as gem cutters, and after a few more years they can receive the distinction of Master Gem Cutter. The region has seen a renewed interest in lapidary work among young men and women.

All the material cut in the workshop is sourced by Wild & Petsch. They travel to the producing areas and buy as close to the mines as possible. In some cases, this means buying at the source, which requires a strong relationship with the mine owners. Wild & Petsch has such relationships with tourmaline miners in East Africa. Elsewhere, they collect stones in the local markets (e.g., Arusha, Tanzania) where material from a wide area comes together.

Wild said the rough trade has not changed much in the last few decades. As new sources are found, it remains extremely important to maintain contact with the source and the end client to strike the best deals. Flexibility is key, as they must be able to check out new finds right away. For example, the majority of beryl is sourced from Africa, but

in the mid-1990s the most amazing materials came from Ukraine and other former Soviet states. Without an extensive international network that covers nontraditional mining areas, such opportunities would be missed.

The biggest change in recent years is likely the speed at which information travels. Today a single social media post about a new find can alert the whole world, but simply having that information is not sufficient. Rough buying is clearly more complex than traveling to mining areas with sufficient funds. Being able to judge parcels quickly in terms of quality and value—and having the confidence to invest in the material—requires years of experience. This is not a skill that can be learned in school. In this area, established companies like Wild & Petsch have an enormous advantage.

For Wild & Petsch, the most exciting material in the last five years has been Mozambican cuprian tourmaline (figure 39), which satisfies a market demand created by the original Paraíba tourmalines from Brazil. Another exciting find is green non-cuprian tourmaline from Mozambique (figure 40), with its fresh, minty colors and blue-green tones. Apart from tourmaline, the company works with a wide range of colored gemstones, including different beryls, fine tanzanite, and African garnets.

Wild acknowledged that regional trends strongly impact rough buying and finished goods sales, using the interest in bicolor tourmaline from Asia about 10 years ago as an example. Many dealers had those stones in stock for decades already, with prices established. Clients paid a premium for these tourmalines, and everyone was happy to sell their old stock for an additional profit; this also raised prices at the source. This unusual market behavior did not last, and prices quickly collapsed. As a result, many people are now sitting on very expensive rough material that does not conform to current market prices. Even though those trends

Figure 40. A non-cuprian green tourmaline from Mozambique, weighing 37.01 ct and measuring  $22 \times 17.5$  mm. Photo by Kevin Schumacher, courtesy of Wild & Petsch.





Figure 41. Katzenbach's "Colors of Maine" kaleidoscope features 71.74 carats of Maine tourmaline and 66.05 carats of Maine quartz between three lenses. Photo by Brian Moghadam, courtesy of AGTA.



Figure 42. Katzenbach created this top, which uses 18K gold, sapphire, alexandrite, tourmaline, tsavorite, and other garnets, to resemble a "spinning rainbow." Photo by Derek Katzenbach.

impact the trade on different levels, Alexander Wild stands by the motto "Good taste is international."

Responsible practices have become increasingly important in the gem trade, and Wild & Petsch is working on its own set of standards to provide to customers. Wild said that his larger clients have already requested such information. He noted, "This is a rocky road with many challenges and obstacles. We will have to take a realistic approach and acknowledge that there will be limits to what we can do and not everything is within reach. Unfortunately, you can't control the world." Wild does believe that everyone in the trade should see how they can apply responsible practices in sorting, cutting, manufacturing, and exporting.

Wim Vertriest

## JEWELRY DESIGN

**Derek Katzenbach: Faceter, gem artist, custom jeweler.** Derek Katzenbach, winner of multiple AGTA Spectrum Awards, was once a marine biology student visiting a local gem show. Until then, the thought of working in a creative industry had never crossed his mind. He spent much of his savings at that show, leaving with a bag full of stones but no idea what to do with them. He decided to take jewelry manufacturing classes and learn more as an apprentice in a jewelry store. The owner convinced Katzenbach to attend GIA, where he completed the Graduate Gemologist and Graduate Jeweler programs. There he honed his skills and learned new techniques.

He also saw a lot of gems, triggering an interest in lapidary and how brilliance and scintillation can influence appearance. A friend taught Katzenbach the basics of faceting, and he kept practicing and experimenting with different patterns. He started working with concave faceting, inspired by the work of Dalan Hargrave and Richard Homer. Eventually he spent a week with them to refine his technique. After

graduating from GIA, he went back to work at the same store for five years before starting his own business.

In his experience, gem cutters and metalworkers look at stones very differently. Having a background in both fields gave him a unique advantage in pushing boundaries and experimenting even further.

One of Katzenbach's most celebrated pieces is a kaleidoscope, shown in figure 41, called "Colors of Maine." For this he chose Maine tourmaline (the official gem of his home state) and Maine quartz. Most of the gems in the kaleidoscope come from Plumbago Mountain, where about a ton of gem tourmaline was recovered between 1972 and 1974. The green tourmalines are from the Havey mine. Apart from the cutting of melee and very small stones, Katzenbach did most of the work himself.

"Colors of Maine" won first place in the Objects of Art category at the 2017 AGTA Spectrum Awards. Afterward, the piece was bought and donated to GIA, where it is on display at the Carlsbad campus with other Maine tourmalines. Creating the kaleidoscope sparked Katzenbach's interest in *objets d'art*. He had always been fascinated by such pieces but found most of them boring and restricted because you cannot touch them. Katzenbach wanted to do something different. This gave him the idea to create a spinning top (figure 42) reminiscent of a rainbow. He used a variety of gemstones—including sapphire, alexandrite, tourmaline, tsavorite, and other garnets—to create this 18K gold toy that no one can resist spinning. The top can be seen in motion at <https://www.gia.edu/gems-gemology/spring-2019-gemnews-derek-katzenbach>.

Katzenbach also creates traditional jewelry. He has always been drawn to a mix of modern pieces with micro-pavé and the lacy textures of Victorian and Edwardian jewelry, but he loves to add color to them. He works mostly with locally sourced Maine minerals, which he finds through miners, collectors, and even museums. Tourmaline (figure 43) is the most common, but he also uses garnet,

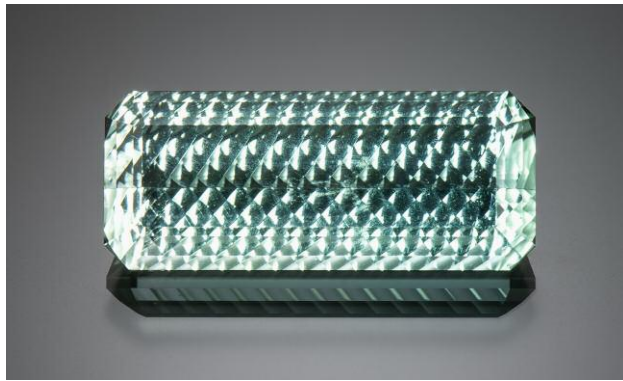


Figure 43. This 7.48 ct cuprian tourmaline uses what Katzenbach calls his “fantasy cut.” Photo by Kevin Schumacher.



Figure 44. This exceptional 10.02 ct 15.4 × 12.0 mm cushion-cut dark blue cobalt spinel is unheated. Photo by Robert Weldon/GIA, courtesy of Jeffrey Bilgore and John Bachman.

aquamarine, smoky quartz, and rare minerals. He occasionally sources internationally, but his favorite gems are Oregon sunstone and Montana sapphire.

Katzenbach would like to get back into engraving, something he enjoyed during his time as a gemology student. He feels that many great gemstone and jewelry artists, including carvers, metalsmiths, and gem setters, are embracing each other’s work and actively looking for collaborations. This will inevitably lead to new and exciting jewelry creations in the coming years.

*Wim Vertriest*

**Jeffrey Bilgore gems and jewelry designs.** Jeffrey Bilgore is both a prominent gem dealer and an award-winning jewelry designer, and at his AGTA booth we found examples of exotic gems and exquisite jewelry. Among these was one of the most notable cobalt spinel gems we have encountered (figure 44). Displayed between two similarly sized

blue sapphires, the unheated spinel was almost indistinguishable from them. A stunning fire opal and Russian demantoid garnet pin with tsavorite garnets and yellow diamonds (figure 45) also caught our attention, a testament to the artistry of Bilgore’s work.

*Jennifer Stone-Sundberg*

**New designs from Paula Crevoshay.** Paula Crevoshay continues to delight with whimsical designs and masterful control of color and light. At the AGTA show, she introduced several new pieces in her collection of threatened and extinct species, such as the charming penguin shown in figure 46. Crevoshay currently has a one-woman exhibition at the Natural History Museum of Los Angeles County entitled *Art of the Jewel: The Crevoshay Collection*, which explores her exhaustive process for creating jewels depicting nature all the way back to the uncut gem materials. A collaboration with lapidary intarsia master Nicolai Medvedev



Figure 45. A fire opal and Russian demantoid garnet pin designed and produced by Jeffrey Bilgore. The piece contains five carved fire opal leaves (18.74 carats total), four demantoid garnets (0.40 carats total), seven tsavorite garnets (0.17 carats total), a 0.20 ct pear-shaped Fancy Intense yellow diamond, and five additional yellow round diamonds (0.03 carats total), set in platinum. Photo by Robert Weldon/GIA.



Figure 46. Paula Crevoshay's "Penguin" pendant features 120 white moonstones, 10.09 carats total. It also contains 152 black diamonds with a total weight of 4.22 carats, 14 yellow diamonds (0.43 carats total), and eight orange opals (0.27 carats total), set in 18K gold. Photo by Robert Weldon/GIA.



Figure 48. Crevoshay's "Anemone" features a 10.86 ct center sapphire surrounded by 16 opals with a total weight of 5.37 carats: four pears, four marquise cuts, and eight rounds. The outer layer contains blue zircon, sapphire, tsavorite, and apatite. Photo by Robert Weldon/GIA.

yielded the breathtaking "Garden of Delight" mystery box (figure 47), replete with a blue columbine on top, gold insects on each corner, mating hummingbirds that arise when the box is opened, and a delicate string of ladybugs making their way up the hinge. Another piece that demonstrates

Crevoshay's artistry is the "Anemone" pendant/brooch, which mixes greens and blues from a variety of gems, including sapphire, opal, zircon, sapphire, garnet, and apatite (figure 48).

Jennifer Stone-Sundberg

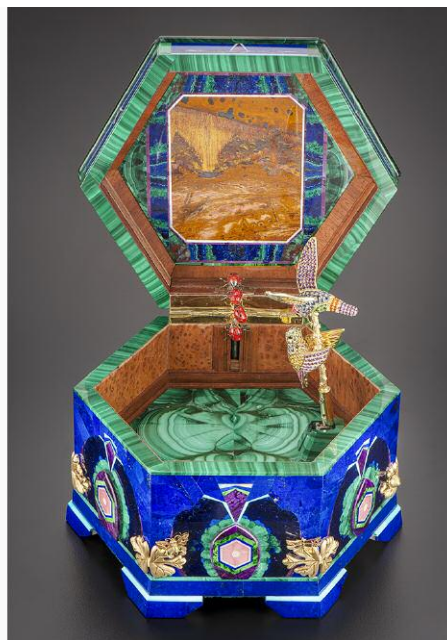


Figure 47. The "Garden of Delight" mystery box (165 × 188 mm) contains lapis lazuli, opal, sugilite, malachite, turquoise, azurite-malachite, rhodochrosite stalactites, and maw-sit-sit. The hummingbirds and branch inside the box feature amethyst, spinel, sapphire, tsavorite, opal, and black diamond. The removable columbine brooch on the lid is set with 13.89 carats of Yogo sapphire along with yellow sapphire and diamond in 18K yellow and white gold. Photos by Robert Weldon/GIA.



Figure 49. This 2 ct Old European cut diamond has a color grade of N and a clarity grade of VS<sub>1</sub>. The faceted girdle is not original to the stone; originally this would have had a bruted girdle. Photo by Albert Salvato, courtesy of Perpetuum Jewels.

## RESPONSIBLE PRACTICES

**Recycled gemstones from Perpetuum Jewels.** The Tucson shows were busy for Perpetuum Jewels (New York and San Francisco), a wholesaler specializing in post-consumer recycled diamonds and colored stones in original, antique cuts. They also work with mine-to-market gemstones and estate jewelry. Co-founder Jared Holstein spoke to us about the importance of recycled gems to the industry (figure 49).

Perpetuum works mainly with designers and jewelry stores in the bridal market. The company originally sought to provide alternatives to newly mined material, focusing on stones cut before 1940. They are active on social media and with organizations such as the Women's Jewelry Association and Ethical Metalsmiths, which drives traffic their way. Holstein and his partner, Jay Moncada, enjoy working with antique stones because each one is different. Rather than achieving a "mathematical ideal of what a stone should look like," each is cut to different proportions and has a history and character all of its own. Holstein teaches his clients the progression from the first point cut (with eight facets) to today's multifaceted cuts. While they have a good deal of stock for center stones, they also have antique melee for eternity bands and other pieces.

Their clients seek the smallest possible environmental footprint—as Holstein points out, "Diamonds are the ultimate recyclable material, because they are so hard," allowing them to be used in jewelry again and again—or choose, for other reasons, to avoid newly mined gems. Many simply love the appearance and mystique of large antique-cut diamonds. The oldest one in stock was a Peruzzi-cut diamond with a double-cut bottom and a triple-cut top; the diamond came from a Victorian ring that it clearly predated. Diamond's hardness allows a long journey through many cuts and several mountings. Holstein explained, "I like to think that there is probably a modern brilliant, which was a transitional cut, which was an Old European cut, which was an



Figure 50. This 3.74 ct unheated sapphire was removed from a vintage 1960s platinum pendant. The sapphire was refaceted by Jean-Noel Soni of Top Notch Faceting. Photo by Albert Salvato, courtesy of Perpetuum Jewels.

old cushion, which was a Peruzzi, which was a Mazarin, which was a table cut, and which was a point cut."

With the emergence of the "alternative bridal market," Holstein and Moncada see designers choosing to work with colored stones instead of diamonds. In these cases, they work with a large supply of corundum. While they carry fine classic and antique blue sapphire (figure 50), their clientele gravitates toward softer blues, teals, and greens (figure 51); Montana and Australian bi- and parti-color sapphire are also popular. Holstein would like to see a move toward spinel and garnets by their bridal clients.

Perpetuum is the only company to achieve the SCS Recycled Gemstone Standard, a third-party certification for 100% post-consumer recycled diamonds and gemstones. The SCS annually audits all aspects of a business to ensure it is a responsible source before awarding this certification. A company must prove, for instance, that its environmental footprint decreases every year while recycled inventory increases annually. The latter has become difficult for Perpetuum, as

Figure 51. This 1.28 ct blue-green sapphire is from Montana's Eldorado Bar deposit. Photo by Kevin Schumacher, courtesy of Perpetuum Jewels.





Figure 52. Sourcing gem rough from East Africa led Roger Dery to seek ways to benefit the communities. These pink and green tourmalines are from the Democratic Republic of the Congo. Photo by Rachel Dery.

they now carry recently mined Montana and Australian sapphire to meet their clients' needs. Doing so has lowered their level of recycled gemstones to below 100%.

Holstein said he has never been able to separate the jewelry pieces he loves from the issues endemic to the industry. He has always been aware that the makings are

"from someone else's backyard." He considers it his responsibility to engage in ethical, environmentally sustainable and responsible practices because they are better for the communities that mine and cut the metals and stones that help him make a living; this is at the core of his business practices. Perpetuum's booth in Tucson allows him to meet with new and existing clients and educate them on these matters that are close to his heart.

*Jennifer-Lynn Archuleta*

**Gem Legacy: A nonprofit for East African communities.** The launch party for Gem Legacy, a nonprofit organization benefiting East African mining communities, was held in Tucson on February 8. This author sat down with founder Roger Dery (Roger Dery Gem Design, Royal Oak, Michigan) to discuss the organization's mission and projects.

Dery entered the trade in 1981, supplying gems from Brazil, India, and East African countries to jewelry stores in the Midwest before becoming a cutter. He took his first trip to Africa in 2008, visiting a dozen mines in Madagascar over 17 days and purchasing rough from the communities (see figure 52). Over the course of several more trips, also visiting mines and gem dealers in Tanzania and Kenya, Dery realized that he did not just want to purchase goods and leave, nor did he want to conflict with local customs. Through 2017, he and his fellow travelers brought food to mining villages to build trust and contribute to each community.

After consulting with his wife and daughter about the best way to contribute to these communities, in 2018 Dery formed Gem Legacy, a nonprofit that supports specific projects in the areas of education, vocational training, and entrepreneurship. Gem Legacy has provided three sessions of gemological training in Malawi (in conjunction with the country's Ministry of Mines), paid school fees for orphans in Malawi (figure 53), provided beds to orphaned children



Figure 53. Through the work of Gem Legacy, orphans in the Mwatate Children's Home in Mwatate, Kenya, had their school fees covered. Photo by Rachel Dery.

---

in Kenya, and delivered equipment to women miners in southern Kenya. They are now raising funds to update the machines at Tanzania's Arusha Gem Faceting School.

There are many ways to give through Gem Legacy. Retailers may choose to stock souvenirs made in communities that benefit from the nonprofit and donate all proceeds back to the communities. Other options include event hosting and donating a percentage from sales of a given collection. Gem Legacy also encourages pajama, toy, and book drives; grassroots fundraising through platforms such as GoFundMe; and direct donations to the nonprofit itself. For more on Gem Legacy, go to <https://www.gemlegacy.org>.

*Jennifer-Lynn Archuleta*

**Jewelry Development Impact Index.** The Jewelry Development Impact Index (JDI), one of the initiatives from the second Jewelry Industry Summit in January 2017, has become the flagship project of the Minerals, Materials and Society (MMS) program at the University of Delaware. Patricia Syvrud, development manager of MMS, discussed the program, which she calls a "road map to responsibility."

The index is a work in progress; it has been part of the MMS curriculum since the fall 2018 semester. Rather than comparing products from various areas, the index analyzes the impact of sourcing on a given country. Graduate students are given two countries and asked to compare them using the seven UN Indicators of Human Security as a framework. From there, they devise a methodology for measurement. In fall 2018, students looking at sapphire mining in Madagascar and platinum mining in South Africa drafted a binary quantitative approach that created scores and rankings based on answers to closed-ended questions. Such questions included "Is this country a signatory to the Extractive Industries Transparency Initiative?" (Zero points are assessed for a yes, one point for a no.) After the total risk has been calculated on a scale from 0 to 10 for each category, recommendations for risk reduction are proposed. The fall 2018 assessment is being used and enhanced by the spring 2019 students. At the same time, students in the university's Energy and Environmental Policy program are developing a methodology to compile existing indices in order to help MMS students leverage this published knowledge.

Syvrud, who has worked in many areas of the gem and jewelry industry, became involved with the JDI on a volunteer basis. She advised the U.S. Department of State on how to measure a gemstone supply chain's impact on the welfare of a country, particularly since the sale of gemstones might fund terrorism and other illegal activities. It was decided that the best way to collect and compile this information was through academic research and case studies. During this time Syvrud met Dr. Saleem Ali, who had received a grant to create the Gemstones and Sustainable Development Knowledge Hub (GemHub; see Summer 2018 GNI, pp. 243–245). Shortly thereafter, Ali was awarded a grant from the Unidel Foundation to create an interdisciplinary program at the University of Delaware to study all extractable mineral

resources and the science, politics, and socioeconomics surrounding them. He and Syvrud identified the JDI as the project that would anchor the MMS program and the graduate certificate that students would earn upon completion.

Response to the JDI has been positive. The Organisation for Economic Co-operation and Development, among others, has taken notice, and invited the MMS program to participate in their responsible minerals forum in April 2019. Syvrud is hopeful that the JDI can help members of the industry understand and answer questions about supply chains; it will also help companies understand and adhere to the numerous supply chain certifications and standards to become more transparent themselves.

*Jennifer-Lynn Archuleta*

**Reinvesting in Cartagena: Jewelry School of the Caribbean.** Alfredo Diaz (Caribe Jewelry, Cartagena, Colombia) spoke to the authors about the Jewelry School of the Caribbean (FEJOCAR), a nonprofit organization that teaches at-risk youth the art of jewelry making.

Working as a tour guide in his native Colombia, Diaz was frequently asked by tourists where to buy jewelry. He and his brothers opened a small jewelry repair workshop in 1983, catering to both tourists and locals. They expanded into selling their own small jewelry pieces, often featuring Colombian emerald. They sold through other businesses at first but eventually began selling pieces directly to the public. As they made more money, the brothers realized it was important to generate more employment in Cartagena. In 2009 they formed FEJOCAR and began outreach to poverty-stricken areas of the city, focusing on young people from neighborhoods with heavy gang and criminal activity.

The school accepts 75 students per year. Once enrolled, the students may choose between the jewelry design, manufacturing, gemstone polishing, and goldsmithing tracks. Caribe hires the most promising students for their own business. The education at FEJOCAR involves knowledge of jewelry techniques and training in software so that the students can use CAD/CAM and create prototypes. The gem polishing and jewelry design programs take four to six months to complete, while the jewelry manufacturing and goldsmithing tracks take one year.

The Diaz brothers faced challenges at the outset of the program. Some found it hard to believe that the brothers would trust their new employees, some of whom had criminal backgrounds. In fact, Diaz said, trust is essential to their working relationships. Employees appreciate this trust and respond in kind. While investigating student absences, they found out that many did not have the money for transportation or meals, so they started providing transportation fees and breakfast and lunch on-site. Today, FEJOCAR provides 30 full scholarships to help students in need enroll and complete their programs. Of the 120 employees at Caribe Jewelry's stores, about 40 were recipients of scholarships.

About 60% of their students are women, a dramatic shift from when the program began; at the start, all of the

goldsmithing students were men. Diaz also intends to set up home workshops for employees who are mothers, to reduce their need for childcare while maintaining production. They have plans for one employee to polish emeralds at home; the other will have a goldsmithing station.

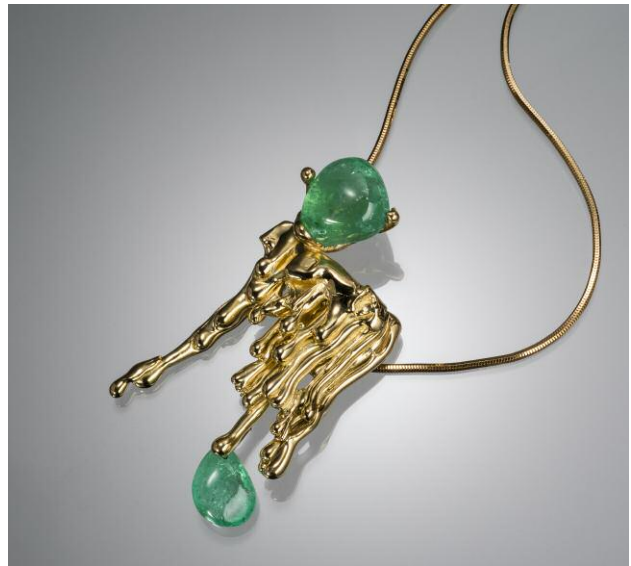
Emeralds are very important to Colombia and to Caribe Jewelry; to that end, the Diazes have set up the Emerald Museum at their store on Bocagrande Calle in Cartagena. The highlight of the museum is "Petra," the largest emerald in matrix ever to emerge from Colombia. They also have space dedicated to other varieties of beryl, including heliodor, aquamarine, red beryl, and goshenite.

The success of the school led the Diazes to move to a larger building to accommodate their students; they have also been able to increase their in-house production. Diaz said their long-term goal is to produce 90% of their own jewelry and buy 10% of their goods from wholesalers; at this point they produce 60% of their own pieces (up from last year's 30%). One of the benefits of local craftsmanship is the ability to maintain a distinctive look that incorporates pre-Columbian indigenous imagery, separating it from Chinese or European designs. Another is the interaction between employees and tourists. The school offers a class for tourists wherein each visitor is paired with a FEJOCAR student. Visitors tour the museum before sitting down to make a piece of jewelry and getting to know a Cartagena local, a wonderful experience for both tourist and student. The Diaz brothers look forward to expanding their business, the school, and their students' horizons in the years to come.

To watch video of the FEJOCAR students, go to <https://www.gia.edu/gems-gemology/spring-2019-gem-news-jewelry-school-of-caribbean-cartagena>.

*Jennifer-Lynn Archuleta*

**The Rock Hound: Muzo emeralds and ethical practices.** At the JCK Tucson show, Susi Smither (The Rock Hound, London) displayed pieces that showcase her love of gemstones and her passion for color. Combining technical knowledge with aesthetics to create unique lines, Smither refers to her business as "the gemologist jeweler," and re-



*Figure 54. The centerpiece of the Molten Muzo collection, the "Candelabra" necklace features 20.63 carats of responsibly sourced Colombian emeralds. Photo by Kevin Schumacher, courtesy of The Rock Hound.*

ceives a number of commissions from gemologists. She offers jewelry at multiple price points, ranging from \$400 to \$11,000. A major point of pride for Smither is Molten Muzo, a five-piece fine jewelry collection launched in December 2018. One of 25 international jewelry designers selected by Muzo Emerald Colombia for collaboration, Smither combined ethically sourced emeralds in tumbled form with Fairtrade 18K yellow gold. The "Candelabra" necklace, the collection's lead piece, is shown in figure 54. The collection also features two pairs of earrings and two rings, one of which is shown in figure 55. Smither allows the emeralds to steal the show; the gold "dripping" from the gemstones complements, rather than overtakes, the simplicity of the tumbled stones.

The daughter of mineral collectors, Smither entered the industry as a jewelry designer and maker about 10 years ago.



*Figure 55. Left: The "Drip" earrings from the Molten Muzo collection use 16.22 carats total of emerald, catching the light as the wearer moves. Photo courtesy of The Rock Hound. Right: An inner world is visible in this 11.05 ct emerald, from one of two rings in the collection. Photo by Kevin Schumacher, courtesy of The Rock Hound.*





Figure 56. Pieces from The Rock Hound's Chromanteq line. Left: This pendant features a 6.48 ct Brazilian heliodor in an 18K recycled white gold setting and an 18K yellow gold chain. The pendant's blue color comes from a signature ceramic coating. Right: The rings in this line also use the ceramic coating. The ring on the left uses 18K recycled white gold and is set with a 9.95 ct Afghani peridot. The ring on the right has a 2.38 ct Tanzanian spessartine set in 18K recycled yellow gold. Photos by Kevin Schumacher, courtesy of The Rock Hound.

As she took on more commissioned work, she earned her FGA diploma from Gem-A, immersing herself in the world of "science and beauty." During a field trip to Sri Lanka with the Scottish Gemmological Association in 2012, she was struck by the disparity between the luxuriously appointed jewelry shops of Hatton Garden and Bond Street and the gritty, often dangerous reality of mining. Thus, at the core of Smither's brand are her ethical practices. The Rock Hound has been a Fairtrade licensee since its inception in 2015, using only recycled gold and Fairtrade Gold from Peru.

Smither noted that the industry has evolved even since The Rock Hound began. Last year she found a casting house in the UK that creates three different alloys of 18K gold three times a week, opening the doors for a fully Fairtrade Gold collection called RockStars, inspired by the shape of a natural tourmaline crystal. To ensure the integrity of her supply chain, she works with artisanal lapidaries who go into the field to work with mining communities. Stones sourced in this way are used in her Chromanteq line, which sets colored gemstones in ceramic-coated recycled 18K gold (figure 56).

Smither's commitment to responsible standards extends to her packaging, made from the perch leather that is a byproduct of the fishing industry. She has sometimes had to choose from a limited selection of materials due to her commitment to responsible sourcing. As a result she would design once she procured her materials rather than designing solely with good in mind. However, she feels that as a young designer starting out, she was better positioned to put sustainable practices in place. Trying to replace longstanding protocols would have been far more difficult for an established business. As this type of sourcing becomes more widespread, she feels that she can expand the design side of The Rock Hound—these days,

Smither is "dreaming bigger." She is eager to create new lines for the next wave of consumers who are equally passionate about sustainable jewelry.

*Jennifer-Lynn Archuleta*

## CONFERENCE REPORTS

**Accredited Gemologists Association (AGA) conference.** The AGA conference, held February 6 in Tucson, was attended by 138 participants from 11 countries. The program was diverse and engaging, as evidenced by the audience questions after each presentation. During the break, participants were invited to a hands-on demonstration of traditional gemological and advanced spectroscopy equipment.

The first talk was by **Jeffery Bergman** of Primagem, who detailed the mine-to-market effort for emeralds from the Shakiso mine in southern Ethiopia. He described some of the material as similar to Muzo's in color, and some as having a "Paraíba-like glow." To ensure that the finest material can receive grades of "no clarity enhancement," mineral oil is never used on the rough. For material that warrants clarity enhancement, only high-grade cedarwood oil is used. A variety of inclusions have been identified, most commonly biotite mica. Other inclusions are growth tubes, blocky two- and three-phase inclusions, horsetails, dendritic magnesium oxide, chromite, and tourmaline. Color zoning in this material can be very strong.

**Gina Latendresse** of the American Pearl Company gave a fascinating overview of natural pearls from the Western Hemisphere. She described the vast quantities collected by Native Americans from the coast of Venezuela that made their way to Spain in the 1500s, establishing the New

World as a source. She then covered the pearl rush between 1850 and 1900 in New Jersey and the Tennessee Valley following the discovery of many impressive specimens. David Howell found the largest American freshwater pearl, 400 grains (100 ct) in size, in New Jersey in 1857. Shortly after, an attractive 93 grain (13 ct) pink pearl was found nearby and sold to Charles Tiffany. Unable to find a U.S. customer, he sold it to Empress Eugenie, resulting in the name “Queen Pearl.” By 1901, the lakes and rivers in the Tennessee Valley had developed pearl fisheries, with production peaking in 1904. Latendresse introduced U.S. natural pearls of many shapes and colors originating from a variety of mollusk species.

**Claudio Milisenda** presented an overview of tourmaline, including Idar-Oberstein’s efforts to promote the material, localities, and the roles of chemistry and heat treatment in tourmaline color. He walked the audience through the varieties verdalite, indicolite, chrome tourmaline, rubellite, red tourmaline, canary tourmaline, and Paraíba tourmaline. The talk also reviewed various tourmaline treatments and imitations encountered today.

To complement the Gübelin Gem Lab’s launch of “Provenance Proof Blockchain” by Gübelin Labs at Tucson this year, managing director **Daniel Nyfeler** gave a presentation on the traceability of gemstones. The talk addressed the lack of transparency in the gemstone supply chain and Gübelin’s solutions for this issue. Reasons cited for the lack of transparency included the mines’ remoteness and restricted access, the informal nature of mining, frequent changes of custody, trading based on relationships and trust, a complex and fragmented value chain, and the lack of an established method for traceability. The problems arising from this lack of transparency include unreliable information provided to consumers (gem labs try to fill this gap with provenance determination), the dilemma for ethically conscious consumers—particularly millennials—who are willing to pay for sustainably sourced products, and the lack of independent audits within the industry. Stakeholders who would benefit from greater transparency are governments (for legal and tax purposes), insurance agencies, financial institutions, and consumers.

Two solutions that would work in tandem were presented: a physical tracer embedded in the stone at the mine, and a digital tracker. The physical tracer would involve Gübelin embedding 100 nm silica spheres that hold synthetic DNA programmed to include information such as the mine location. These permanently implanted spheres, which require openings of at least 400 nm, are designed to survive all cutting and cleaning processes. Gübelin would have the ability to later extract the DNA, sequence it, and verify the stone’s origin. This tracer is designed for emerald, and the present design would not survive the more physically punishing corundum processing. The digital tracker, meanwhile, would allow a stone to be tagged all the way back to the mine using blockchain so that each time the stone changed hands, a logbook entry would be made, allowing

for permanent storage of encrypted information at each step of the journey from mine to market. The Provenance Proof Blockchain system was released February 8 at the AGTA show. It is free and open to the industry for all gemstone types. The benefits touted for this tracking included new avenues of storytelling for retailers, reduced costs as gem reports would not be needed, and less inflated prices as non-value transactions would be eliminated. And with the ability to audit the supply chain, more aspects of the business could be properly insured. Following the presentation, a spirited question-and-answer session touched on privacy for dealers and consumers, the impact on artisanal miners, the logistics of implanting the encapsulated DNA, and resistance from gem dealers over security concerns.

The last scheduled talk, an overview of the new FTC rules, was canceled due to the recent U.S. government shutdown. A substitute talk graciously given by **Jon Phillips** (Corona Jewellery Company, Ltd.) covered Canadian diamonds. He noted Canada’s place as the world’s second-leading producer of diamonds and reported on the significant mines, the types of material coming from them, and notable stones found. The Ekati mine has both surface and underground components, and has produced numerous vivid and intense yellows as well as pinks and colorless. Within the mine, 53-million-year-old wood that had been perfectly preserved in the oxygen-free environment was found and brought to the surface. The Renard mine was plagued by the hardness of the kimberlite, making diamond separation extremely difficult. De Beers is showcasing its “Future Smart” mining process with the Chidliak project in Nunavut, Baffin Island, where there are no roads, environmental impact is minimal, and power is supplied by wind energy. Notable stones from the Diavik mine include the 177.71 ct Vega, the 24.82 ct Capella, the Fancy Vivid yellow 30.54 ct Arctic Sun, and a recently discovered 552.74 ct yellow diamond that is likely the largest diamond ever found in North America.

Following the conference, the AGA presented its 20th annual Bonanno Awards. For the first time, three categories were recognized in the same year: education, gemological instrumentation, and gemological research. The award for gemological education went to **Donna Hawrelko**, a gemology and jewelry educator at Vancouver Community College. Hawrelko’s 27 years of teaching has touched thousands of individuals, and she was key in developing the educational program offered by the Canadian Gemmological Association. The award for gemological instrumentation was given to the cofounders of Magilabs, **Alberto Scarani** and **Mikko Aström**. Scarani and Aström have made advanced spectroscopy accessible and affordable to a wide range of gemologists by developing portable tools such as the GemmoRaman system. These allow appraisers and gemologists access to technology that was recently available only through major laboratories. The award for gemological research went to **Karl Schmetzer**, a renowned researcher and author, for his more than 50 years of gemological and mineralogical work documented in over 400

publications, two books, and 12 new mineral discoveries. Dr. Schmetzer has shared his research with the community and strived to improve professional standards in the industry through work with CIBJO and other organizations.

*Jennifer Stone-Sundberg*

**2019 Jewelry Industry Summit.** The third Jewelry Industry Summit, held in Tucson February 2–3, revealed the successful implementation of several initiatives mapped out since the conference's inception in 2016.

Opening remarks by summit chair **Cecilia Gardner** and AGTA's **Doug Hucker** were followed by a session on mining communities. In a presentation on sustainable mining, **Assheton Stewart Carter** (The Dragonfly Initiative) discussed incentivizing improvements while managing environmental, social, and governance risks and needs at artisanal and small-scale mines. He explained how the Dragonfly Initiative creates partnerships with other organizations that can provide research, funding, and other assistance on the local level. This was followed by the Dragonfly Initiative's **Vivien Johnston**, **Fiona Wellington** of Myne, and **Mahmood Alam Mahsud** (Fine Cut Lapidary)—all by video chat—describing their efforts to create an emerald cutting and polishing center to employ and empower Pakistani women. **Tom Cushman** (Richfield Investor Services) recounted issues with sourcing gold in Madagascar, while **Toby Pomeroy** provided insights into the Mercury Free Mining Challenge, a quest to create a safe and effective alternative to the use of mercury by artisanal and small-scale gold miners. The Initiative for Responsible Mining Assurance, or IRMA, an organization dedicated to creating and sharing financial value for mines that achieve best practices, was introduced by consultant **Christina Miller** and **Lara Kortizke** of IRMA. Two breakout sessions occupied much of the first afternoon: one on creating an industry-accepted glossary (see [www.gia.edu/gems-gemology/spring-2019-gemnews-jewelry-summit-glossary-initiative](http://www.gia.edu/gems-gemology/spring-2019-gemnews-jewelry-summit-glossary-initiative)), and the other on building a business with responsible sourcing principles. This was followed by a lively discussion on the benefits and drawbacks of blockchain between **Mike Pace** (Connected Jewelry), **Robin Gambhir** (Fair Trade Jewellery Co.), **Carrie George** (Everledger), and **Mark Hanna** (Richline).

Day two provided a synopsis of the Jewelry Development Impact Index by **Patricia Syvrud** of the University of Delaware's Minerals, Materials and Society program (p. 148), as well as a discussion with Doug Hucker and Patricia Syvrud on the silicosis abatement program sponsored by GemHub, AGTA, and the Minerals, Materials and Society program. **Steven Benson** (CIBJO) reported on the release of CIBJO's Blue Book on the responsible sourcing of gemstones and precious metals (p. 158), available as a free download from [www.cibjo.org](http://www.cibjo.org). **Brian Cook** (Nature's Geometry) provided an update on the Bahia Brazil Golden Initiative, a cooperative of rutiled quartz miners in the Chapada Diamantina region of Bahia State, Brazil. Patricia Syvrud spoke with **Charles Lawson** (Lawson Gems International)

on the outcomes from four years of gem and jewelry training for women sapphire miners in Sakaraha, Madagascar. The day ended with a screening of the gold mining documentary *River of Gold*, with a speaker panel consisting of producer **Sarah duPont**, **Torry Hoover** (Hoover and Strong), **Toby Pomeroy**, and **Tom Cushman**.

*Jennifer-Lynn Archuleta*

## ANNOUNCEMENTS

**Second annual Buccellati Award winner.** Ching-Hui Weng, a 2018 graduate of GIA's Jewelry Design program in Taiwan, received the second annual Gianmaria Buccellati Foundation Award for Excellence in Jewelry Design. One of 18 finalists from GIA's seven schools, her winning design was a bird brooch (figure 57) featuring white and yellow gold, white and yellow diamonds, opal, aquamarine, lapis lazuli, black chalcedony, and coral. "My inspiration for this piece is the *Urocissa caerulea*, a blue bird that represents Taiwan," said Weng. "The gemstones in this piece illustrate the bird's fierce temperament and flight."

Weng will travel to Italy to meet Mrs. Buccellati and view part of the foundation's collection. She will also receive a plaque recognizing her achievement.

"We are pleased to congratulate Ms. Ching-Hui Weng, and look forward to welcoming her to Italy. Together with GIA, we hope to continue to encourage and support the dreams of young jewelry designers throughout the world," said Larry French, chief officer of North America strategies for the Gianmaria Buccellati Foundation. "We know Gianmaria would have been proud to have his name on an event that celebrates, so beautifully, the art of jewelry design, the art that he loved so much."

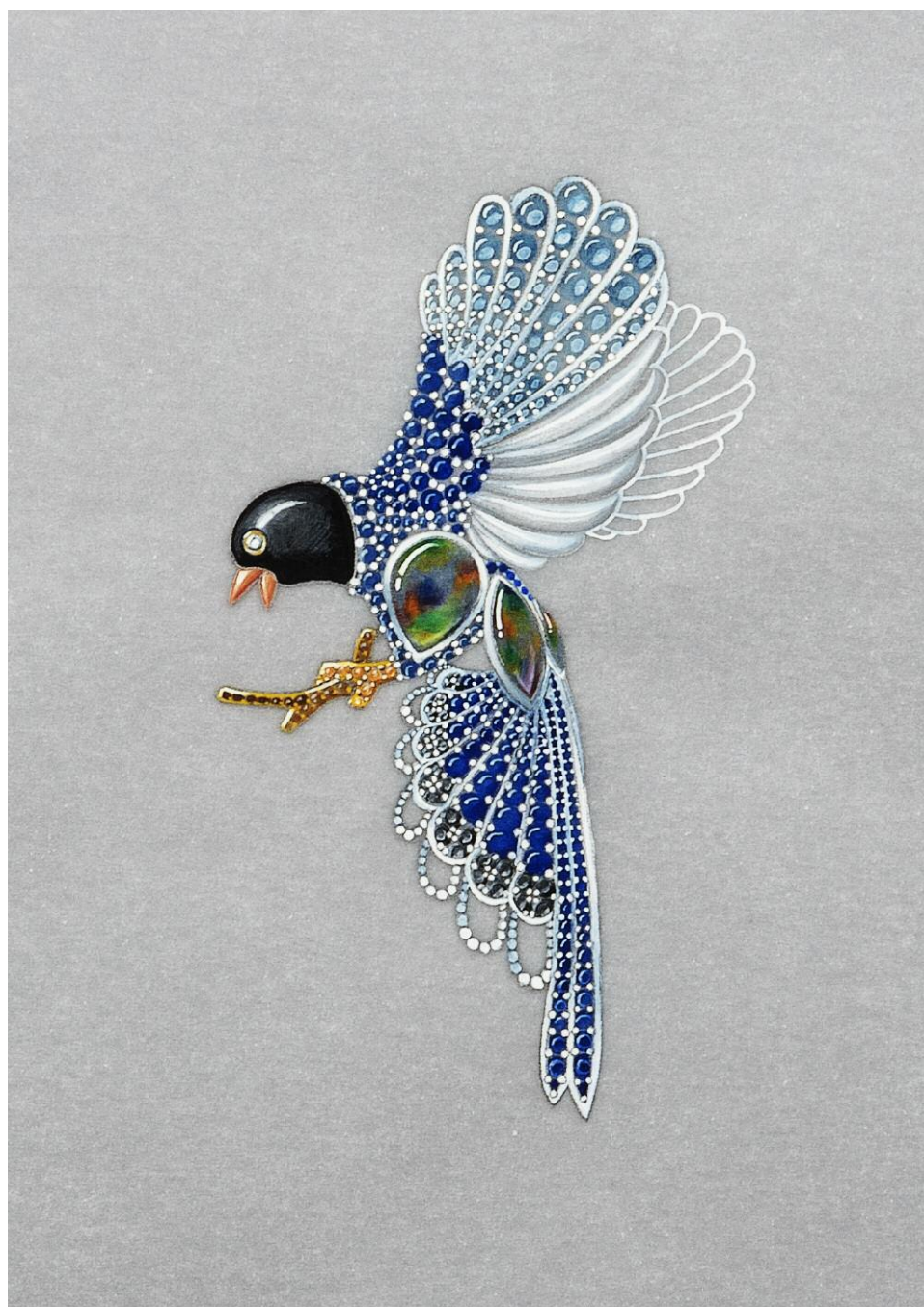
Submissions were presented as original, hand-rendered designs. Following several phases of judging, they were finally evaluated by a panel of industry experts. Weng was announced as the winner at the annual GIA alumni event held during the AGTA Gem Fair in Tucson.

The Gianmaria Buccellati Foundation sponsors the award to inspire beginning designers and honor the house's founder. The 2019 award is now open to GIA Jewelry Design students who meet the eligibility requirements.

## REGULAR FEATURES

### COLORED STONES AND ORGANIC MATERIALS

**Unique orange sapphire with golden sheen effect reportedly from Kenya.** Golden sheen sapphires from Kenya have been reported in this journal and elsewhere (e.g., T.N. Bui et al., "From exsolution to 'gold sheen': A new variety of corundum," *Journal of Gemmology*, Vol. 34, No. 8, 2015,



*Figure 57. Ching-Hui Weng's design, which won the second annual Buccellati Award, was inspired by the Urocissa caerulea bird, which is representative of her native Taiwan. The finished piece features white and yellow gold, white and yellow diamonds, opal, aquamarine, lapis lazuli, black chalcedony, and coral.*

pp. 678–691; N. Narudeesombat et al., “Golden sheen and non-sheen sapphires from Kenya,” *The Gem and Jewelry Institute of Thailand*, July-August 2016, pp. 282–288). Those sapphires, however, were the cabochon-quality blue-green-yellow stones that exhibited a shimmering golden effect caused by the light reflection from hematite platelets and needle-like inclusions. No faceted transparent stones have been mentioned in the previous literature. Recently the Gem and Jewelry Institute of Thailand’s Gem Testing Laboratory in Bangkok encountered a faceted orange sap-

phire with an attractive golden sheen effect that was reportedly from Kenya.

The sample was a transparent, 4.34 ct faceted mixed-cut stone of orange hue with attractive golden sheen effect almost throughout the crown facets (figure 58). Standard gemological testing revealed a refractive index (RI) of 1.765 to 1.775, a birefringence of 0.01 with a uniaxial negative optic sign, and a hydrostatic specific gravity (SG) of 3.98. The stone exhibited brownish orange and greenish yellow pleochroism and was inert to both long- and short-wave



Figure 58. This 4.34 ct transparent oval-cut orange sapphire displayed an attractive golden sheen effect. Photo by Tasnara Sripoonjan.

UV radiation. Microscopic observation revealed abundant metallic hematite platelets and rutile needles (figure 59, left), confirmed by Raman spectroscopy, that were situated along the basal pinacoid face. A cluster of zircon crystals, as suggested by its crystal morphology, could also be found in the specimen (figure 59, right).

In previous studies, the golden sheen sapphires from Kenya were translucent to opaque, with yellow and blue bodycolor (Bui et al., 2015; Narudeesombat et al., 2016). They contained abundant internal features, such as exsolved intergrowth Fe-Ti oxide phases of hematite platelets and short ilmenite needles that gave the sheen effect, as well as inclusions of goethite, boehmite, and diaspore needles. They also had large surface-reaching cracks. The stone in this investigation is orange, transparent, and without surface-reaching cracks, though it also possesses a significant number of hematite platelets that are in part responsible for its golden sheen effect.

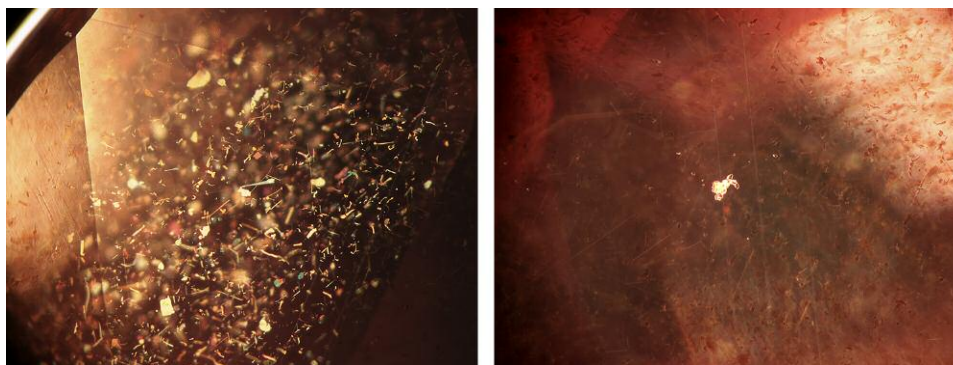


Figure 59. Internal features of the orange golden sheen sapphire: abundant metallic hematite platelets and rutile needles (left) and a cluster of zircon crystals (right). Photomicrographs by Saengthip Saengbuangamlam; field of view 3.00 mm.

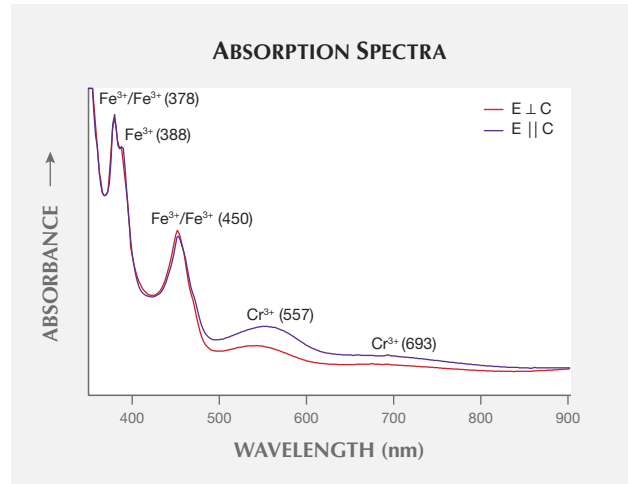


Figure 60. UV-Vis spectra of the orange golden sheen sapphire showing  $\text{Fe}^{3+}$ - and  $\text{Cr}^{3+}$ -related absorption peaks and bands.

The polarized ultraviolet-visible (UV-Vis) spectra of the specimen displayed predominantly  $\text{Fe}^{3+}$ -related absorption bands at 378, 388, and 450 nm that are responsible for its yellow hue (e.g., J. Ferguson and P.E. Fielding, "The origins of the colours of natural yellow, blue and green sapphires," *Australian Journal of Chemistry*, Vol. 25, No. 7, 1972, pp. 1371–1385), whereas the absorption band at around 557 nm (also at ~410 nm) is caused by a  $\text{Cr}^{3+}$  transition contributing to the reddish hue (figure 60). As such, the stone coloration appears orange. R-line luminescence of  $\text{Cr}^{3+}$  near 693 nm also appears in the spectra. When compared to the more common non-sheen counterparts, the UV-Vis spectra yield only  $\text{Fe}^{3+}$ - and Fe-Ti-related absorptions (Narudeesombat et al., 2016).

The energy-dispersive X-ray fluorescence (EDXRF) results of the orange sapphire showed very high content of  $\text{Fe}_2\text{O}_3$  (1.94 wt.%) with moderate content of  $\text{Cr}_2\text{O}_3$  (0.05 wt.%) and  $\text{TiO}_2$  (0.04 wt.%).  $\text{Ga}_2\text{O}_3$  and  $\text{V}_2\text{O}_5$  were equal at about 0.01 wt.%. This result (particularly the iron content)

**TABLE 1.** Comparison of chemical composition of orange golden sheen sapphire with golden sheen and non-sheen sapphires, analyzed by EDXRF.

Oxides (wt.%)	Orange golden sheen (this study)	Golden sheen (Narudeesombat et al., 2016)	Non-sheen (Narudeesombat et al., 2016)
TiO <sub>2</sub>	0.04	0.01–0.02	0.02–0.07
Cr <sub>2</sub> O <sub>3</sub>	0.05	0.00–0.01	0.01–0.03
Fe <sub>2</sub> O <sub>3</sub>	1.94	1.00–1.50	1.19–1.58
V <sub>2</sub> O <sub>5</sub>	0.01	0.00–0.01	0.01–0.04
Ga <sub>2</sub> O <sub>3</sub>	0.01	0.02–0.05	0.02–0.04

is somewhat similar to those of the common golden sheen and non-sheen stones from Kenya in the previous work (table 1), which also suggests a similar magmatic source. Nonetheless, the Cr<sub>2</sub>O<sub>3</sub> content in this orange sapphire is particularly distinctive, since such an oxide is almost undetectable in most golden sheen sapphires.

While Kenya is known to supply large amounts of golden sheen sapphires, some rare orange sapphires with sheen effect such as this one are also being supplied to the market. Sheen effect makes the stone distinctive compared to common orange sapphire from other sources, for example, from Songea in Tanzania (cf., originating from a metamorphic source and having somewhat lower iron content). However, the owner informed us that this specimen might eventually be subjected to heat treatment at a relatively low temperature to remove some silk-like inclusions and make it more transparent. Nevertheless, careful examination yielded no indication that this stone was heated. Its unique characteristics—heavily included hematite platelets and rutile needles that give rise to the golden sheen effect plus its high iron content—suggest a Kenyan origin.

*Tasnara Sripoonjan (stasnara@git.or.th), Saengthip Saengbuangamlam, and Marisa Maneekrajangsaeng  
The Gem and Jewelry Institute of Thailand, Bangkok*

**Sapphires from Colombia.** Colombian sapphires were first reported in *G&G* nearly 35 years ago and are still circulating in the market today (see P.C. Keller et al., “Sapphire from the Mercaderes–Río Mayo area, Cauca, Colombia,” Spring 1985 *G&G*, pp. 20–25). The deposit is located in southern Colombia in the Cauca Valley, in the small town of Mercaderes. This location is notorious for being politically unstable and dangerous. This deposit continues to produce in small quantities, with most material extracted from riverbeds using picks and shovels. Independent miners collect year-round and go to Bogotá to sell the material. Vanessa Van Horssen (Carlsbad, California) recently purchased several unheated Colombian sapphires and learned about the active mines from a third-generation miner in Bogotá. She loaned GIA’s Carlsbad laboratory five samples (figure 61) for scientific examination.

Colombian sapphires occur in a variety of colors, such as blue, pink, and violet, and there have been past reports of color-change sapphire from this deposit. The five samples



*Figure 61. Five unheated Colombian sapphires, ranging from 0.41 to 3.65 ct. Photo by Diego Sanchez.*

consisted of a 0.41 ct pink faceted pear, a 0.92 ct color-change (blue to violet) faceted oval, a 1.66 ct pink rough, a 2.26 ct blue faceted octagon, and a 3.65 ct blue rough. All five had gemological characteristics consistent with corundum. They exhibited a refractive index of 1.762 to 1.770 and a specific gravity of around 4. Laser ablation–inductively coupled plasma–mass spectrometry (LA-ICP-MS) was performed to identify their chemical compositions. A high concentration of Fe ranging from 1515 to 1749 ppm suggested a magmatic source. Infrared spectroscopy showed no indications of treatment.

The internal features (figure 62) were color zoning, particle clouds, angular milky clouds, and twinning. The sap-

*Figure 62. Zircon crystals scattered throughout angular milky clouds were more prominent in these sapphires compared to other high-Fe sapphires. Photomicrograph by Jessa Rizzo; field of view 4.7 mm.*



phires contained transparent colorless and red crystals that showed no sign of heat treatment. Using Raman spectroscopy, the inclusions were identified as unaltered zircon and rutile crystals, consistent with the inclusions reported in Keller et al. (1985). Sapphires transported to the surface by hot magma tend to show characteristics similar to those of artificially heated sapphires, such as tension fractures around crystals and altered fingerprints. The suite of inclusions in these high-temperature-formed sapphires confirmed that no heat treatment was performed.

These stones provided useful data for ongoing origin determination studies. Although Colombian sapphires are rare, they are on the market, and the deposit continues to show great promise.

Jessa Rizzo  
GIA, Carlsbad

**Trapiche emerald from Colombia.** Colombian trapiche emeralds, in general, consist of a transparent or nontransparent tapered core and six transparent prismatic growth sectors, which are separated by nontransparent boundaries. These boundaries form the arms of a six-rayed fixed star and radiate from a central point or a central area within the conical core. The tapered core is also designated a basal or pinacoidal growth sector. The boundaries consist of emerald, various minerals (e.g., calcite and albite), and trapped fluid phases.

In the gem trade, trapiche emeralds are mostly cut as slices or cabochons with an orientation perpendicular to the sixfold axis of the emerald to show the hexagonal growth pattern of the gemstone and especially to display the six-rayed fixed star. The conical shape of the core is derived from the different diameters of the core on both sides of such a cabochon. Slices of trapiche emeralds with an orientation parallel to the *c*-axis clearly show a tapered core, representing the basal growth sector, and a rim on both sides of the core formed by two prismatic growth sectors. However, because rough trapiche emerald specimens are mostly broken on both ends, the complete trapiche pattern parallel to the *c*-axis is not observed, and even textbooks dealing with Colombian emeralds show only sketches or photos of crystal fragments.

Recently, a complete outline of a trapiche emerald pattern consisting of two pinacoidal (basal) and six prismatic growth sectors was presented by I. Pignatelli et al. ("Colombian trapiche emeralds: Recent advances in understanding their formation," Fall 2015 *G&G*, pp. 222–259), but only fragments of trapiche crystals sliced parallel to the *c*-axis were available for that study. Consequently, the present author took the opportunity to examine the pattern in a transparent sample which, on a first view, seemed to be a complete or almost complete trapiche emerald crystal. The emerald was submitted by collector Georg Sellmaier (Kranzberg, Germany), who purchased the sample about 10 years ago from a local dealer while traveling in the Muzo area of Colombia.

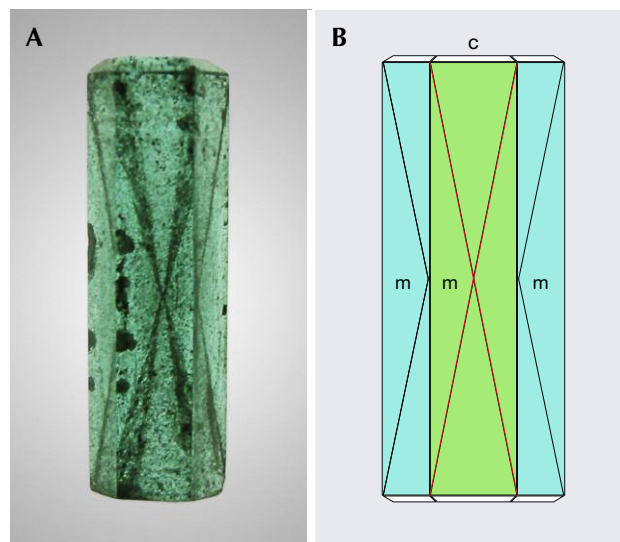


Figure 63. Colombian emerald crystal with prismatic habit; in the orientation shown, the sample measures 15.4 × 5.2 mm. A: View perpendicular to one of the six prism faces, transmitted light. B: Schematic drawing of the crystal in the same orientation. Three prism faces *m* are observed. In a view through the central face (green), a cross formed by four boundaries is seen (red lines); in a view through the two adjacent faces (blue), two boundaries are observed (black lines). Photo by K. Schmetzer.

The 3.49 ct emerald crystal (figure 63A) shows a prismatic habit with six elongated prism faces *m* (10 $\bar{1}$ 0) and is terminated on one end by a basal pinacoid *c* (0001) and six small hexagonal dipyramids *p* (1012). Most likely, at the second termination of the crystal a facet approximately in the direction of a basal pinacoid was cut because the sample was slightly broken or did not show a plane face. The length of the crystal is 15.4 mm, while the diameter between the prism faces is 4.6 mm and the diameter between the crystal edges is 5.2 mm. Its pleochroism is blue-green parallel to the *c*-axis and yellow-green perpendicular to the *c*-axis.

In an orientation where the crystal is resting on one of the six prism faces (i.e., in a view perpendicular to this face), three different prisms are seen. In a view through the central prism, a cross in the form of an X was observed, with a pattern described as part of such a cross seen also in views through the two other adjacent prism faces (again, see figure 63A). A schematic drawing of this situation is presented in figure 63B. In the immersion microscope, upon rotation of the emerald crystal along its hexagonal axis, in each view parallel to two of the six prism faces (i.e., rotated by 30° versus the view perpendicular to a prism as described above and depicted in figure 63), a pattern consisting of a sharp cross is seen, with a vertical line dividing the cross into two parts (figure 64, A and B). The schematic

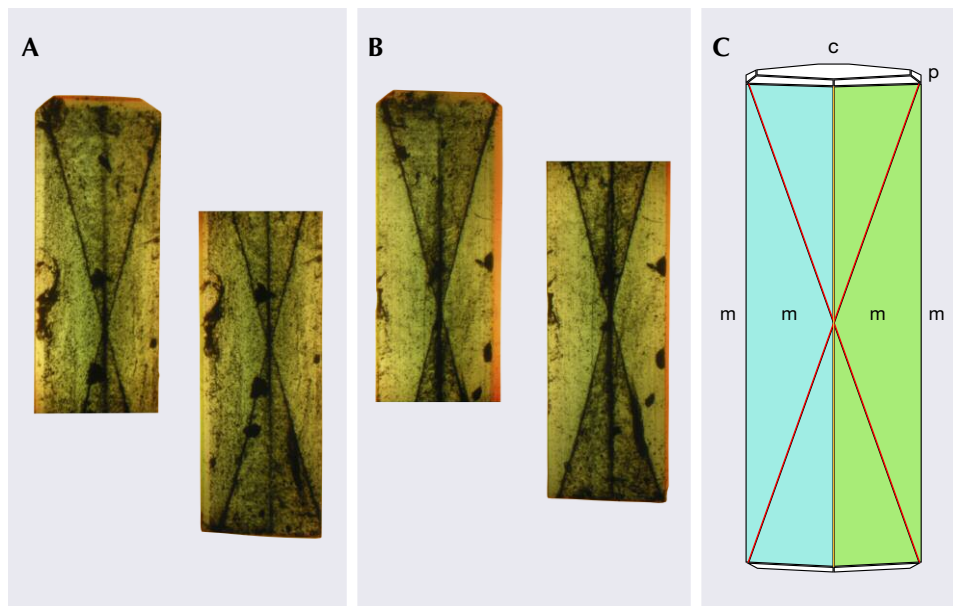
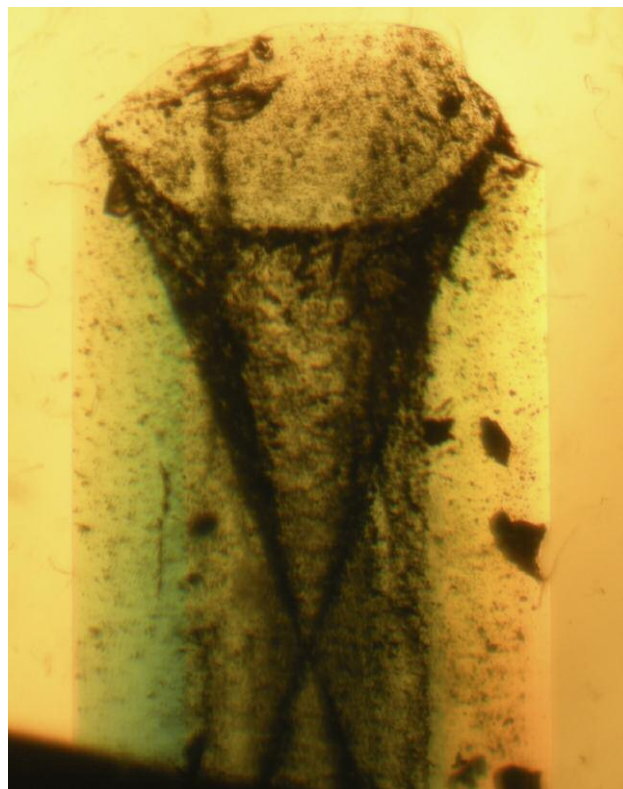


Figure 64. A and B: View in immersion through the emerald crystal in two orientations related by a rotation of  $60^\circ$  along the c-axis; two prism faces are parallel to the direction of view. The pattern observed consists of a cross subdivided by a vertical line. C: Diagram of the crystal; a view through each of two prism faces m (blue and green) shows two boundaries (red lines). These boundaries form an X, also subdivided by a vertical boundary (yellow line). Photos by K. Schmetzer.

drawing in figure 64C reflects this situation. In a view oblique to the c-axis, a tapered cone formed by six plane boundaries is seen at both ends of the crystal (figure 65). In a view parallel to the c-axis, due to the length of the crystal and the various layers covered with inclusions present throughout the crystal, the sample is only translucent, but a pattern of a six-rayed fixed star is observed.



It is evident that the various lines forming crosses in the form of an X are the traces of plane boundaries between the two pinacoidal and the six prismatic growth sectors. The vertical lines that subdivide these crosses in the second orientation described here represent boundaries between the six prismatic growth sectors (see figures 63B, 64C, and 66A). The cone-shaped outline of each pinacoidal growth sector is formed by boundaries between the tapered core and six prismatic growth sectors (figure 66B). The different patterns depend only upon the orientation of the crystal in the direction of view and the orientation of the various boundaries between the six prismatic and two basal growth sectors within the emerald.

The crystal described represents an almost complete emerald with prismatic habit and trapiche pattern. In the present case, the trapiche pattern is similar to an hourglass structure. However, the trapiche emerald shows numerous inclusions that are trapped at the boundaries between different growth sectors, forming thin layers. As described in the literature, these layers between the individual emerald growth sectors consist of a mixture of emerald with other minerals and fluid phases trapped in cavities. In contrast to most trapiche emeralds from Colombia, the layers in the emerald described in this paper are thinner and translucent, which allows an observation of the complete three-dimensional trapiche pattern, especially in views perpendicular to the c-axis. This observation is consistent with the conclusion made by several authors about the cone-shaped

Figure 65. View in immersion of the emerald crystal in a direction oblique to the c-axis. A tapered central core is seen, formed by six plane boundaries between a basal and six prismatic growth sectors; the diameter of the crystal in this view measures 5.2 mm. Photo by K. Schmetzer.



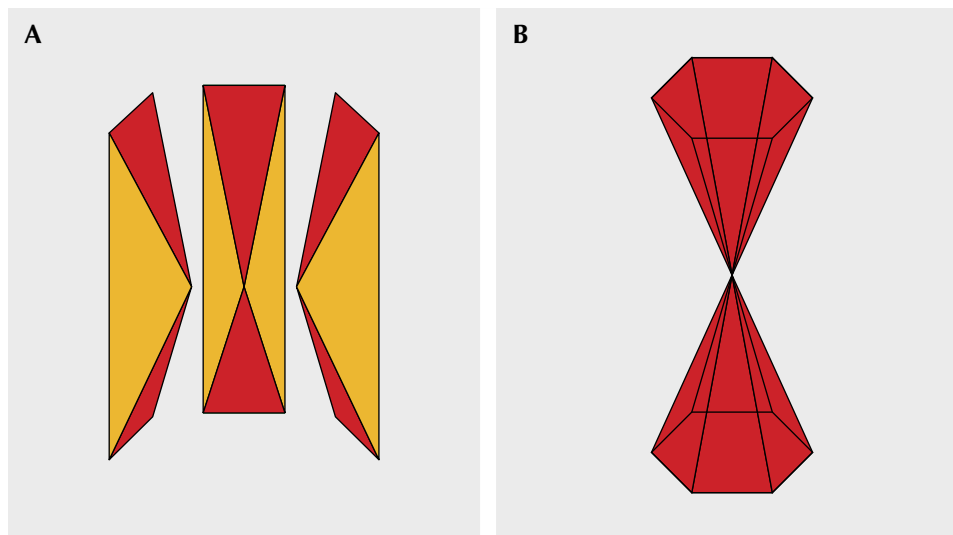


Figure 66. A: The patterns seen through the prism faces in different orientations of the emerald crystal are formed by boundaries between six different prismatic growth sectors (red, only three growth sectors are shown) and the two pinacoidal growth sectors, and boundaries between adjacent prismatic growth sectors (yellow). B: The outline of the tapered core is formed by the boundaries between six prismatic growth sectors (red) and two pinacoidal growth sectors.

cores of trapiche emeralds and confirms the three-dimensional model of the trapiche pattern presented by Pignatelli et al. (2015).

Karl Schmetzer  
Petershausen, Germany

## RESPONSIBLE PRACTICES

**CIBJO Blue Book and “Do’s and Don’ts” guide on responsible sourcing.** The World Jewellery Confederation (CIBJO) released the first edition of the *Responsible Sourcing Book* in January 2019. The latest in CIBJO’s series of Blue Books, it provides a framework and guidance for due diligence related to the responsible sourcing of gemstones and precious metals in the jewelry sector. In March, the organization also approved a simplified “Do’s and Don’ts” guide.

The new Blue Book is the result of a yearlong effort, during which a responsible sourcing commission was formed and a policy document introduced at CIBJO’s 2018 congress in Bogotá. The book, which was thoroughly reviewed by external members of the trade, advises all industry members to have a responsible sourcing policy in place and to perform due diligence on their supply chains “to the best of their ability.” It also recommends that industry members check for and mitigate risks related to human rights, labor practices, or criminal activity. The Blue Book aligns with the OECD’s *Due Diligence Guidance for Responsible Supply Chains of Minerals from Conflict-Affected and High-Risk Areas*, and it requires compliance with both the Kimberley Process Certification Scheme and the United Nations Guiding Principles on Business and Human Rights.

The “Do’s and Don’ts” document, at 11 pages, does not replace the Blue Book released in January. It is intended as a reference tool for business owners and their staff to ensure best practices and promote consumer confidence. As of March 2019, the simplified guide can be downloaded in English, Arabic, Dutch, French, Hebrew, Italian, and Por-

tuguese. Additional language versions are being prepared.

Both the Blue Book and the “Do’s and Don’ts” document are available, free of charge, at [www.cibjo.org](http://www.cibjo.org).

Jennifer-Lynn Archuleta  
GIA, Carlsbad

## CONFERENCE REPORTS

**“The Ethics of Jewelry” at MetFridays.** “The Ethics of Jewelry” panel (figure 67) was held on January 25, in conjunction with the New York Metropolitan Museum of Art’s temporary exhibit, “Jewelry: The Body Transformed,” which ran from November 2018 to February 2019. The exhibit featured an array of headaddresses and ear ornaments, brooches and belts, and necklaces and rings, along with sculptures, paintings, prints, and photographs that amplify the many stories of transformation that jewelry tells. The 230 objects were drawn almost exclusively from the Met’s own collection and displayed the museum’s jewelry artifacts from ancient to contemporary times. “The Ethics of Jewelry” panel was part of the museum’s MetFridays evening series of concerts, classes, and presentations open to the public. The purpose was to discuss timely issues facing the world of jewelry today, including urgent questions about mined, lab-produced, and sustainable materials.

Panelists were Monique Péan, a New York-based jewelry designer who prides herself on using sustainable materials in her one-of-a-kind pieces that are sourced globally through fair trade initiatives; Karen Smit, a GIA research scientist who holds a PhD in diamond geology; and Patricia Syvrud, program development manager for the Minerals, Materials and Society program at the University of Delaware, and immediate past executive director of the World Diamond Council. The panel was moderated by Ben Smithee, CEO and founder of The Smithee Group, a digital strategy, content, and advertising firm.

The panel opened with introductions, where each speaker described a bit of his or her background and rele-



Figure 67. Left to right: “Ethics of Jewelry” panelists Monique Péan, Karen Smit, and Patricia Syvrud joined moderator Ben Smithee at the New York Metropolitan Museum of Art. Photo by Stephen G. Strickland.

vance to the event. Péan shared her travels to the far reaches of the globe, where she gets the inspiration and many unusual materials for her pieces, such as pyritized dinosaur bone, Peruvian opaline, and Scandinavian meteorite. Smit gave a scientific overview of natural versus synthetic diamonds, and Syvrud shared the progress of the Minerals, Materials and Society education and training program and related research projects (see p. 148).

Smithee asked the panelists for clarification of some terms that are frequently used but little understood when speaking of “ethical jewelry,” such as “responsible sourcing,” “sustainability,” and “conflict-free” diamonds and gold. Although the terms “ethical jewelry” and “responsible sourcing” can mean different things to different people, the term “sustainability” has a globally recognized definition that basically means “meeting the needs of today without compromising the needs of future generations.” The current definition of the term “conflict diamonds” is also globally recognized, according to a United Nations resolution, to mean “Diamonds that originate from areas controlled by forces or factions opposed to legitimate and internationally recognized governments...” However, this definition does not address the human rights issues of artisanal and small-scale mining. The conversation then moved to a comparison of responsibly sourced gold vs. gemstones and how technology such as blockchain can be

integrated into supply chains to enhance transparency and sustainability in the jewelry sector.

The session concluded with a focus on the artisanal and small-scale mining (ASM) that takes place in the diamond, colored gemstone, and gold mining sectors. Although challenges related to human rights and environmental and social impacts remain, the benefits from ASM to local stakeholders and communities should be more widely shared.

*Patricia Syvrud*  
University of Delaware, Newark  
Minerals, Materials and Society Program

## IN MEMORIAM

**E. Alan Jobbins (1923–2019).** Alan, as he was known to his friends and colleagues, passed away February 2 at the age of 95. He was internationally respected for his lasting achievements in the fields of mineralogy and gemology. He started down his lifelong career path at the age of 13, when his geography professor showed him some attractive crystal specimens of the mineral mimetite from the Cumberland area of England. This immediately sparked his interest and led to a lifetime devoted to mineralogical and gemological studies, and his career appointment from 1950 to 1983 as curator of minerals and gemstones at the Institute

of Geological Sciences in London. There he was responsible for organizing the extensive gemstone and mineral collection and exhibitions.

Over his 33 years at the museum, Alan conducted numerous important gemological and mineralogical research projects, such as a major study of East African garnets, research into the characteristics of synthetic opals, the discovery and description of the mineral magnesioaxinite, and the geological field study of the meteorite in Barwell Parish, England.

Alan's work took him on many assignments for the United Nations and the British government. These included gemological and geological surveys of gem deposits in Brazil, Cambodia, Guyana, India, and Sri Lanka for the United Nations and the British Overseas Development Administration.

In the late 1960s, Alan set up a mineralogical and gemological training and research laboratory in Burma, guiding that country's first gemologists to FGA diplomas. Some students went on to obtain doctorates at English universities. Alan led a study of Pailin ruby and sapphire deposits in Cambodia, resulting in a detailed monograph and important recommendations for improved recovery methods. He also spearheaded an assessment of diamond and opal deposits in Piauí State, Brazil, and a survey of the Sri Lankan gemstone industry in which he recommended improved mining methods and cutting techniques.

In 1988 and 1989, he initiated gemological training with new laboratory facilities at the China University of Geosciences in Wuhan. In the UK, his record includes 32 years as a gemological lecturer at the Sir John Cass College

(now London Metropolitan University), 20 years as chief examiner for the Gemmological Association of Great Britain (now Gem-A) gemology examinations, and eight years as editor of *The Journal of Gemmology* (1985–1993). He was also president of Gem-A from 2004 to 2008, and vice president from 2009 until his death.



Alan held various posts throughout his career, including executive member of the International Gemmological Conference (IGC) and past president of the Society of Jewellery Historians. He was also part of the team that conducted the first comprehensive gemological examination of the British Crown Jewels from 1986 to 1989, which led to the publication of an important illustrated catalogue. Among Alan's major literary contributions were very thorough revisions of B.W. Anderson's *Gem Testing* and Robert Webster's *Gemmologists' Compendium*.

In 1984, Alan became a founding member of the ICA (International Colored Gemstone Association). In 2005 the Accredited Gemologists Association (AGA) awarded him its sixth annual Antonio C. Bonanno Award for Excellence in Gemology. He served as a member of *G&G's* editorial review

board from 1994 on.

In addition to gemology and mineralogy, our dear friend Alan was an avid bird-watcher, an explorer of churches and cathedrals, and a wine aficionado. He was a devoted and loving husband to his wife, Mary. In his honor I will carry the moniker he bestowed upon me many years ago, "Young Buzzard." Alan passed away peacefully with Mary by his side. Rest in peace, dear friend.

*John I. Koivula  
GIA, Carlsbad*

## For More Coverage of Tucson 2019

Watch exclusive videos from the gem shows, featuring interviews and insider insight. Visit [www.gia.edu/gems-gemology/spring-2019-gemnews-tucson-overview](http://www.gia.edu/gems-gemology/spring-2019-gemnews-tucson-overview) or scan the QR code on the right.

